Reconstructing Holocene East Asian climate and oceanographic history of the northern South China Sea: high-resolution records of pollen, spores, and dinoflagellate cysts

by

Zhen Li
B.Eng., Chang'an University, 1994
M.Sc., Tongji University, 1998

A Dissertation Submitted in Partial Fulfillment
of the Requirements for the Degree of

DOCTOR OF PHILOSOPHY

in the School of Earth and Ocean Sciences

Supervisory Committee

Reconstructing Holocene East Asian climate and oceanographic history of the northern South China Sea: high-resolution records of pollen, spores, and dinoflagellate cysts

by

Zhen Li
B.Eng., Chang'an University, 1994
M.Sc., Tongji University, 1998

Supervisory Committee

Dr. Vera Pospelova, (School of Earth and Ocean Sciences)
Supervisor

Dr. Eileen Van der Flier-Keller, (School of Earth and Ocean Sciences)
Departmental Member

Dr. Richard Hebda, (School of Earth and Ocean Sciences)
Departmental Member

Dr. Sophia Johannessen, (Department of Geography)
Outside Member

Abstract

Supervisory Committee
Dr. Vera Pospelova, (School of Earth and Ocean Sciences)
Supervisor
Dr. Eileen Van der Flier-Keller, (School of Earth and Ocean Sciences)
Departmental Member
Dr. Richard Hebda, (School of Earth and Ocean Sciences)
Departmental Member
Dr. Sophia Johannessen, (Department of Geography)
Outside Member

Abstract

This study contributes to developing terrestrial and marine palynological indicators of winter or summer monsoon signals as well as oceanographic environments of the South China Sea (SCS). The high-resolution reconstructions of Holocene East Asian Monsoon (EAM) climate and oceanographic condition of the northern SCS provide insights into regional climate events in the western low-latitude Pacific Ocean and their impacts on local oceanography and ecology.

Sediment trap samples from the southwest Taiwan waters of the SCS in winter monsoon (March-April) and summer monsoon (July-August) seasons identify abundances of *Pinus* and *Ulmus* pollen as indicators of the winter monsoon whereas fern spores appeared to be indicators of the summer monsoon. The increased fluxes of dinoflagellate cyst (DC) taxa during summer are correlated with decreased sea-surface salinity (SSS) associated with nutrient-rich river inputs.

DC distributions across the SCS show that some taxa are good indicators of changes in sea-surface temperature (SST), SSS, water depth and chlorophyll-*a* (chl-*a*) concentrations associated with EAM and oceanographic conditions. In particular, the

concenrations of *Brigantedinium* spp. and cysts of *Protoperidinium* together with *Echinidinium* spp. are positively correlatd with SST in January and SST in July, and chl-a concentrations, respectively, which are linked to past monsoon strength and primary productivity. In total, four high cyst concentration regions have been observed off southern Vietnam, Borneo, Hainan, and South China.

High-resolution palynological records from a sediment core in the northern SCS reflect several EAM climatic and oceanographic events over the last 12.5 kyr. A short-term *Impagidinium* decrease implied that the Taiwan Strait opened at ~11.7–11.0 cal kyr BP, with reduced Kuroshio Current influence when the East China Sea waters entered through the strait. Three Holocene relative sea-level stages were identified in the palynomorph records. The highest herb pollen abundances were observed before ~10.4 cal kyr BP, reflecting the shortest distance from the grassland sources on the exposed shelf at the low sea-level stand. High *Brigantedinium* and cysts of *Protoperidinium* abundances also indicate a near-shore environment. During ~10.4- ~6.8-6.0 cal kyr BP at the rising sea-level stage, fern spore abundances increased and DC abundances decreased. Consistently low total DC concentrations and high fern spore abundance were observed after ~6.8-6.0 cal kyr BP when the present oceanographic conditions were formed. Increased abundances of *Pinus* pollen reflected three strengthened winter monsoon intervals at ~5.5, 4.0 and 2.5 cal kyr BP under the present oceanographic conditions. The highest *Dapsilidinium pastielsii* abundances reflected the warmest interval at ~6.8-5.5 cal kyr BP of the northern SCS.

Table of Contents

List of Tables

List of Figures

List of Plates

Acknowledgments

At this moment, I am so happy to calm down for the acknowledgments. The thesis research would not be completed without so many people's help. First of all, I would like to express my deepest appreciation to my supervisor, Dr. Vera Pospelova, who gave me endless input and care, encouragements, detailed instructions and suggestions throughout the course of thesis research. To me, Vera is not only a supervisor but also a mentor and a friend in my life. She keeps encouraging me and sharing her passions when I feel frustrated or puzzled due to the different cultural background. I am so lucky to have Vera as my supervisor.

I am also grateful to my committee members, Drs. Eileen Van der Flier-Keller, Sophia Johannessen and Richard Hebda for their time, guidance and support throughout this research. Their constructive comments and critical thinking led me to consider different perspectives and broaden my knowledge.

I want to thank L. Liu for his support from collecting the sediment core, sharing surface sediments, providing age measurement to the final paperwork. I am so grateful to K.N. Mertens for giving me a chance and pleasure of working with him and learning taxonomy and nomenclature of dinoflagellate cysts as well as techniques of using scanning electron microscopy and transmission electron microscopy, micromanipulation of single cells and incubation.

I also wish to thank our additional collaborators on this thesis researches for providing samples, information on field investigation and environmental observation data and discussing thoroughly to improve the manuscripts. They are C. Luo, I. Hernandez-Almeida, H.-L. Lin, W. Gong, K. Yin, B. Song, Y. Wu, H. Wu, and R. Zhou.

I would like to thank all the members of the School of Earth and Ocean Sciences (SEOS), and particularly in the Paleoenvironmental/Marine Palynology Laboratory, for their contribution to a dynamic and motivating working environment. My special thanks go to Allison Rose, Kalisa Valenzuela, Kimberly Smith-Jones, Terry Russell and Jody Spence for their support and assistance throughout the course of the study, thesis research and lab work. I am so grateful to Manuel Bringue, Carl Jonsson, and Sandy McLachlan, who guided me to the new work environment and provided lots of help and information about scientific serves and living on campus. I also thank Maximilien Genest, Curtis Evans, Weiming Jiang, Jin-Si Over, Guy Hoffman, Erinn Raftery, Alison Thomas, Iria García Moreiras, and Janset Kankus for exchanging experiences in research and daily life. I greatly appreciated Robin Connelly and Eva Maclennan for their help with sealing and labelling many microscopic slides.

Finally, I owe my sincerest gratitude to my family for their love and understanding. They have always cared, encouraged and supported me, and never trying to limit my aspirations.

I am also grateful to the financial support of the CGS D3 fellowship and CGS-MSFSS from Natural Sciences and Engineering Research Council of Canada (NSERC), President Fellowship, Montalbano Fellowship and two travel grants from University of Victoria. This work was also funded by NSERC through a Discovery grant to V. Pospelova. The national Key Project (GASIGEOGE-05) from the State Oceanography Administration of China partially supported L. Liu, in this work, the Ministry of Science and Technology Grants of Taiwan (NSC 98–3114–E–006–014 and NSC 99–2611–M–

110–006) to H.-L. Liu, and Chinese Natural Science Foundation Projects of No. 41506103 and No. 51761135021B to B. Song and W. Gong, in this work.

Chapter 1

Introduction

1.1 East Asian Monsoon (EAM) climate changes and its research significance

Climate change shows various long-term to short-term periodicities with different driving factors and mechanisms (e.g., Kutzbach, 1974; Bradley, 1999). Understanding Holocene climate cycles at various time scales could help us to identify climate mechanisms and their impacts on sedimentary and ecological systems (e.g., Jiang et al., 2005; Committee on Ecological Impacts of Climate Change, 2008), and may further help us to predict future hazards associated with abrupt climate change and reduce economic losses. The East Asian Monsoon (EAM) plays an important role in balancing moisture and heat in Asia. Reconstructions of the EAM changes on different time scales are necessary to understand variations in the moisture and heat exchange that directly influences people in the region, > 60% of the world population.

The EAM during the Holocene has been extensively studied through climate models and a number of proxy records from various environments such as pollen, geochemical elements, organic materials, silica and carbonates in lakes, loess, and marine microfossils (e.g., Xiao et al., 2002; Wang et al., 2005; Liew et al., 2006; Yancheva et al., 2007; Mather et al., 2008; Liu et al., 2013; Wang et al., 2014; Porter and Zhou, 2017). However, the reconstructed events or cycles of EAM climate are different from region to region. For example, the onset of Holocene Optimum reconstructed from the northern boundary of the EAM was ~1.5-2.0 kyr earlier than that indicated in South China (e.g., Wang et al., 2005; Liu et al., 2015). Most of studies of Holocene EAM climate

reconstruction are based on records from land environments. To have a comparison of EAM between land and marine environment is required for understanding of major mechanisms of the EAM changes. Until now, marine records of these changes are still rare.

On the other hand, different proxies for monsoon climate reconstruction perhaps also be the main factors for such difference among EAM records. In general, monsoon proxies can be divided into two categories: proxies related to monsoon winds (direction, strength and persistence), and those associated with monsoon precipitation (e.g., Wang et al., 2005, 2014). Eolian dust and wind-borne pollen associated with wind transport are common wind-based proxies (e.g., Wang et al., 2005).

The EAM records from different proxies do not show consistent results. For example, a gradual weakening of the East Asian Summer Monsoon (EASM) in the Holocene has been reported (Ruddiman, 2008), but Wang et al. (2005) inferred a general increase in the strength of the EASM in the early Holocene. A difference in sample or index resolution is one reason for such discrepancies. For example, the EAM is generally divided into the East Asian Winter Monsoon (EAWM) and the EASM in most modelling and meteorological studies that use high-resolution observational data (e.g. Wang et al., 2008; Zhou et al., 2007).

Comparatively, proxies from sediment cores cannot provide records at sufficiently high resolutions to distinguish signals of the EASM from those of the EAWM. Most research into the signals of the EASM and the EAWM has not clearly defined these phenomena, and interpretations of the proxies are based on the hypothesis that the past EAWM and EASM were in anti-phase (e.g. An, 2000; Long et al., 2010; Wang et al.,

2012; Liu et al., 2013). A stronger EAWM is characterized by intensified northeast wind with cold and dry air, whereas a stronger EASM is associated with strengthened southwest winds with humid and warm air. Therefore, cold and dry conditions reflected by proxies are often regarded as a strong EAWM, whereas warm and wet conditions are generally interpreted as the result of a strong EASM (e.g. Li et al., 2003; Huang et al., 2009).

Most terrestrial and marine records suggested that the Holocene EAWM and the EASM have not followed simple inverse relationships with glacial-interglacial cycles. Steinke et al. (2011) found that both the EAWM and EASM were strengthened in the early to mid-Holocene. This finding is also supported by the high intensity of the EAWM between 5.0 and 3.4 cal ka BP during the maximum precipitation interval of ~7.8–3.5 cal kyr BP (Xia et al., 2014). The results of the "South China Sea Monsoon Experiment (SCSMEX)" (1996–2001) indicate that a strong monsoon over the SCS usually leads to lower precipitations over the middle and lower reaches of the Yangtze River Basin, but higher precipitations in northern China (Ding et al. 2004). Observational data from 1951 to 2012 from 753 Meteorological Administration stations across China also show a significant decreasing trend in rainfall in northern China corresponding to an increasing trend of rainfall in southern China (Liu et al., 2015). Therefore, the traditional interpretation that a decline in temperature or moisture is linked to a weakened EASM or strengthened EAWM is not appropriate in the Holocene. Proxies specially associated with the EAWM or EASM parameters must be identified for high-resolution palaeo-EAM reconstructions.

1.2 EAM records in the South China Sea (SCS)

The SCS, located in the low-latitude Western Pacific Ocean in the EAM climate region, has notable seasonal variations in winds, currents, SSS, SST, and primary productivity (PP) (e.g. Fang et al., 1998; Wang and Li, 2009). However, the different regions of the SCS show various patterns. For example, a 15-year data analysis showed that the highest rain occurs from July to September in the northern SCS (20-22°N), from July to October in the middle SCS (10-20°N), and from Novenber to December in the southern SCS (<10°N south) (Jiang and Qian, 2000). Therefore the rain-related proxies are not so good for the monsoon climate study in the SCS. With its well-preserved Holocene sedimentary strata and relatively high sedimentation rates, the northern SCS is considered to be one of the best areas for high-resolution reconstructions of Holocene climatic and oceanographic changes. Some efforts have been invested in reconstructing the Holocene monsoon climatic variability and hydrographic conditions, including the SST and SSS, using a number of sediment cores from the northern SCS (e.g. Huang et al., 1997; Wang et al., 1999; Yu et al., 2005; He et al., 2008; Jiang et al., 2014; Dai and Weng, 2015). Most of these studies have shown similar general trends throughout the Holocene. However, EAM events reconstructed by different proxies from various environments display spatial and temporal differences. For example, Kong et al. (2014) reported paleoenvironmental reconstructions that underscore the differences in regional and local dynamics. These authors investigated differences between two sea-surface temperature (SST) records of the past 8.0 kyr that were reconstructed by using the long-chain alkenone unsaturation index at one offshore site from the Pearl River Delta as well as another one on the continental margin in the northern SCS. Their results suggested that

SST change not be synchronous between both locations, but rather a SST gradient developed in the northern SCS at that time (Kong et al., 2014). Even when different proxies were used for the same sediment core, higher-resolution events of the paleomonsoon climate record and paleoceanographic parameters appeared to be different from those of low resolution. For example, SSS reconstructed by diatom (Jiang et al., 2014) is different from that reconstructed by $\delta^{18}O$ of foraminifera (Wang et al., 1999) on the same core (core 17940) from the northern SCS. Therefore, to accurately interpret EAM climate and paleoceanographic environment information from proxies of sediment cores, sensitive indicators are needed and must be calibrated by using sediment trap and surface sediment samples.

1.3 Holocene oceanographic history of the SCS reflected by various proxies and its open questions

Influenced by Holocene EAM climate in part, oceanographic feature such as relative sea level, sediment source, currents and PP in the SCS also changed during the Holocene. With the warming climate of the Holocene, glacial melt water contributed to the global sea level rise (e.g. Lambeck, 1993). Comparatively, relative sea level (RSL) in the Holocene varied spatially and temporally because of the varying regional dominance of eustatic and glacio- and hydro-isostatic factors throughout the Holocene. Over the last two decades, several RSL curves for the SCS region since the LGM have been proposed based on a number of indicators (e.g., mangrove peat, corals, oyster beds, tubeworms, and beach rock exposures or other intertidal deposits) (e.g. Zong, 2004; Hanebuth et al., 2000; 2011; Liu et al., 2004; Tanabe et al., 2006). The RSL of the SCS was at ~ 130 m to the present sea level. The highest known rates of sea level rise (SLR) occurred during

Meltwater Pulse 1a at ~ 14.6 cal kyr BP (Fairbanks, 1989; Bard et al., 1996; Cronin, 2012). The SLR rates became slower during the Younger Dryas cold reversal in the interval of ~12.9-11.6 cal kyr BP (Bard et al., 2010). From the Younger Dryas/Holocene transition to ~7-6 cal kyr BP, the RSL rose approximately 60 m. This interval includes Meltwater Pulse 1b (MWP1b) between ~11.4 cal kyr BP and 11.1 cal kyr BP (Liu et al., 2004; Bard et al., 2010; Hanebuth et al., 2011). After a highstand of RSL at ~7–4 cal kyr BP, a nearly stable sea level, similar to that of the present, is indicated by evidence from archaeological sites, tidal marsh sediments, and geophysical modelling (e.g. Tanabe et al., 2006; Hanebuth et al., 2011).

Associated with its general rising RSL, the shorelines of the SCS migrated landward since the LGM. Some observations evidence a well-preserved palaeo-shoreline from the LGM along ~130-m isobaths in the northern shelf of the SCS (e.g., Liu and Chen, 1995; Chen, 1997). In the Younger Dryas/transitional period, the shoreline migrated to locations along the current ~50 m isobaths (e.g., Liu and Chen, 1995; Chen, 1997).

The distance to the terrestrial sources due to the shoreline migrations caused the changes in sources, pathways, and deposition conditions during the Holocene. The terrestrial sediment supplies to the northern SCS are complex with sedimentary materials coming from the Luzon region, the Pearl River, and Taiwan (e.g., Liu et al., 2008; Liu et al. 2012). The materials from these various sources are distributed differentially in the SCS, influenced by the EAM, surface currents, the Kuroshio Current, or by northern Pacific water through the Luzon (Bashi) Strait (e.g. Liu et al., 2010; 2014). Sediments derived from Taiwan are primarily transported to the southwest into the deep basin of the SCS. Materials entering the SCS via the Pearl River are transported southwestward along

the coast and deposited on the shelf between the Pearl River estuary and Hainan Island (Li et al., 2015). Sediments derived from Luzon are typically deposited to the northwest of the island (Liu et al., 2011). Mentioned above sediment sources have not been stable since the LGM. During the LGM, the Pearl River sediment supply was at its peak, and the sediment contribution from Taiwan was relatively low (Liu et al., 2016). As the RSL rose during deglaciation, the relative contribution of Taiwan-derived materials increased because of the intrusion of the Kuroshio Current into the SCS. Simultaneously, the Pearl River contribution gradually decreased (Liu et al., 2016). At the beginning of the Holocene, high precipitation and water runoff near the mouth of Pearl River resulted in a minimum $\delta^{18}O$ value at ~10 cal kyr BP (Buhringe et al., 2004). A local maximum in the contribution from the east of Pearl River occurred when the sea level was approximately 40 m below the present level (Liu et al., 2016).

The total PP of the northern SCS in the Holocene was generally lower than it was during the LGM, as indicated by biomarkers (e.g., He et al., 2008). This trend may have resulted from a decreased nutrient input to the northern SCS. The wet climate and high precipitation in the Holocene would have increased the input of river-transported nutrients into the northern SCS, but the RSL rise and landward migration of the shoreline resulted in decreased input of terrestrial materials to the continental slope region.

The surface-water circulation in the SCS is now predominantly wind-forced by the northeast winter and southwest summer monsoons (e.g., Caruso et al., 2006). During winters, this circulation is characterised by a basin-wide cyclonic gyre and southwestward coastal currents, whereas in summers, the basin-wide circulation splits into a weakened cyclonic gyre in the north and a strong anti-cyclonic gyre in the south

with northeastward coastal currents (e.g., Qu et al., 2002). The prevailing monsoon system, coupled with the Ekman effect, results in winter upwelling off islands of Borneo, Luzon and Taiwan, and summer upwelling along the Vietnamese coast, off Hainan and South China (e.g., Ndah et al., 2016). Currently, the surface waters of the SCS exchange freely with waters from the neighbouring seas, while deeper water flows into the SCS primarily from the western Philippine Sea through the Bashi (or Luzon) Strait. The water transport through the Bashi Strait influences the circulation and heat budget of the SCS. In addition the Kuroshio Current, which forms to the east of the Philippines and flows northward along the coast of the Luzon Island, branches into the SCS through the Bashi Strait (Yuan et al., 2002). Typically, the Kuroshio intrusion into the SCS occurs through the central region of the Bashi (Luzon) Strait and results in anticyclonic circulation in the northeastern SCS. The intrusion occasionally enters the SCS through the northern portion of Bashi Strait and forms a cyclonic circulation (e.g., Caruso et al., 2006). The surface and subsurface SCS waters are colder, fresher and more eutrophic than the Kuroshio Current water, and these waters mix with part of the water from Kuroshio Current before entering the Taiwan Strait. The mixed waters flow northward to the Taiwan Strait and even traverse the whole Taiwan Strait in summers (e.g., Huang et al., 2015).

Thompson and Shackleton (1980) reported that the southern and the northern limits of the Western Pacific warm pool migrated toward the equator, which led to a reduced latitudinal span of the warm pool during the LGM. Temperate waters were able to reach the Bashi Strait, the only connection between the SCS and the Pacific at that time, and entered the SCS. With climatic warming, strong freshwater discharge at the transition into and beginning of the Holocene would have weakened the water-mass exchange

between the SCS and the western Pacific Ocean (Jiang et al., 2006). When sills, which were exposed and formed barriers to adjacent seas during the glacial period, were submerged by RSL rise, the SCS water began to exchange with other seas. Most research about currents and water exchange in the SCS has been still limited to present or recent changes, and little investigation of currents during the Holocene has been conducted.

The above-mentioned changes in the oceanographic conditions including sea-level rise or fall, shoreline migrations and currents could also influence the EAM proxy records by the changes of their sources, transport way and taphonomic conditions. That means the changes of EAM proxy records may be not only because of the regional EAM climate change but also local oceanographic conditions. To avoid such problems, sedimentary proxies that reflect both terrestrial and marine conditions are ideal for reconstructing past climatic and oceanographic conditions of the northern SCS. A combined palynological proxy record of pollen, spores, and dinoflagellate cysts better reflects regional paleoclimatic and local (paleo) oceanographic conditions (e.g., Bouimetarhan et al., 2012; Shumilovskikh et al., 2016; Poliakova et al., 2017; Zhao et al., 2017). Moreover, pollen, spores, and dinoflagellate cysts can be extracted using the same laboratory techniques and be identified simultaneously under a microscope, which dramatically reduces method-related biases. Therefore, in this study, terrestrial and marine palynological records were used to document both the regional EAM and local currents in the Holocene at a higher resolution.

1.4 Palynological indicators of palaeo-climatic and oceanographic environments

1.4.1 Pollen and spores

Pollen and spores in marine sediments come from terrestrial vegetation. They are transported by winds or water (including currents and rivers) and are deposited in the sea together with other sedimentary particles. Compared to pollen and spores in terrestrial lakes or swamps, their distributions in marine environments are more significantly influenced by winds, river inputs, sea level, currents, geographic and oceanographic conditions besides surrounding vegetation (e.g. Urrego et al., 2009; Li et al., 2008; Luo et al., 2013, 2014, 2016a, 2016b). Therefore, pollen and spores from marine sediments have been used as indicators of past sea-level change (e.g. Ellison, 1996; Behling et al., 2001; Cohen et al., 2005; Engelhart et al., 2007; Li et al., 2012), sedimentary environment (Carvalho do Amaral et al., 2006; Dai et al., 2015), paleovegetation and climate change (e.g., Sun and Li, 1999; Li et al., 2006a, 2006b, 2010), geomorphological changes and post-glacial marine transgressions (e.g., Scourse et al., 2005; González et al., 2006; Méndez-Linares et al., 2007), and pathways of paleo-currents (e.g., Li et al., 2010; Zheng et al., 2011, 2013).

Far from the sources, the pollen in the deep sea of the SCS were perhaps less influenced by river inputs, and those preserved in sediment cores are commonly used to reconstruct past vegetation and climate, especially during glacial-interglacial cycles when the surrounding vegetation underwent significant changes (e.g., Sun and Li, 1999; Sun et al., 2003; Zhang et al., 2011; Dai et al., 2015). However, during the Holocene, vegetation surrounding the SCS did not change as much as the vegetation changes in glacial-interglacial cycles. Therefore, to infer climatic changes during the Holocene, a more

detailed understanding of pollen transport and taphonomic conditions needs to be developed. Pollen analysis on surface sediment samples is common for pollen and spore distribution patterns, sources, pathways and deposition conditions and relationship to environments (e.g., Heusser, 1988; Crowley et al., 1994; Moss et al., 2005; Li et al., 2008, 2012; Urrego et al., 2009; Zhao et al., 2016). The distributions of pollen and spores in surface sediments of the SCS, as well as their mechanisms and influencing factors, have been studied (e.g., Sun and Li, 1999; Zhang et al., 2002; Li et al., 2008; Luo et al., 2013, 2014, 2016a, 2016b; Dai et al., 2015).

However, in marine settings, surface sediments are typically collected by grab or box samplers, and these samples usually represent deposition over several years up to a thousand years. Surface sediment samples reflect multiyear averages rather than seasonal variations in pollen and spore distributions. Influenced by seasonal winds, river inputs, and currents in the EAM region, the distributions of pollen and spores during different seasons may provide strong evidence of winter or summer monsoon information if we know more details of their seasonal sources, transport pathways and oceanographic conditions. Deployment of sediment traps enabled continuous collection of sinking particles for studies of palynological particle sources and transport before their deposition (e.g., Winert et al., 2010; Lin et al., 2011). The distribution of pollen and spores in time-series sediment traps deployed in winter and summer monsoon seasons could help to determine seasonal differences and further refine the indicators of winter and summer monsoons as well as other environmental conditions. Until now, there were no sediment trap studies of about pollen and spores in the SCS.

1.4.2 Dinoflagellate cysts

Dinoflagellates are one of the major groups of modern marine plankton. Almost half of dinoflagellate species are heterotrophic, and the other half species are autotrophic (e.g., Dale, 2009). The life cycle of a dinoflagellate has two stages: asexual stage and sexual stage. In the sexual stage, after fusion, non-motile resting cysts will be formed (e.g., Head, 1996). Most cysts have an organic wall of which a major component is dinosporin, a complex organic compound similar to the sporopollenin of plant pollen and spores (e.g., Versteegh and Blokker, 2004). The organic-walled dinoflagellate cysts are highly resistant to physical, chemical and biological degradation (e.g., Dale, 1996; Versteegh and Blokker, 2004) and are thus well preserved in sediments. The cysts produced by heterotrophic and autotrophic dinoflagellates are named here as heterotrophic taxa and autotrophic taxa, respectively. Distributions of modern dinoflagellate cysts in marine environments are controlled by SST, SSS, PP, sea-ice cover, and other oceanographic conditions (e.g., Harland, 1983; Dale, 1996; Rochon et al., 1999; de Vernal et al., 2001, 2005; Marret and Zonneveld, 2003; Pospelova et al., 2005, 2008; Zonneveld et al., 2013). Therefore, being preserved in sediments, organic-walled dinoflagellate cysts are commonly used as indicators of past environmental conditions (e.g., Dale, 1996; Zonneveld et al., 1997, 2008, 2009; de Vernal et al., 2001, 2005; Mudie et al., 2002; Radi and de Vernal, 2004; Pospelova et al., 2006, 2015; Londeix et al., 2009; Marret et al., 2009; Penaud et al., 2010; Kim et al., 2012; Price at al., 2013; Bringué et al., 2014, 2016; Poliakova et al., 2016). Due to different local environments, dinoflagellate cyst distributions, concentrations and assemblages are controlled by a number of environmental parameters. Therefore, studies of dinoflagellate cyst distributions in local

surface sediments are essential to calibrate dinoflagellate cysts as paleoenvironmental indicators by comparing recent assemblages with modern environmental conditions. Over the past few decades, many studies on dinoflagellate cysts in surface sediments from different regions have contributed to understanding reliable indicators of environmental parameters (e.g., Dale, 1996, 2002; Marret and de Vernal, 1997; Devillers and de Vernal, 2000; Godhe et al., 2003; Pospelova et al., 2004, 2005, 2008, 2010; Radi et al., 2007; Bouimetarhan et al., 2009; Aydin et al., 2011; Bonnet et al., 2012; Candel et al., 2012; Kim et al., 2012; Heikkilä et al., 2014). These studies have now firmly established that the distributions of dinoflagellate cysts in sediments are determined primarily by the ecology of dinoflagellates, and may be influenced by transport or deposition conditions. Dinoflagellate cysts in surface sediments of the SCS have been investigated by Wu and Sun (2000), Kawamura (2004), and Wang et al. (2004, 2011). However, their work was primarily focused on dinoflagellate cyst taxa and distributions in very limited parts of the SCS. Lacking environmental information and data across the SCS, the factors controlling dinoflagellate cyst distribution and production in the SCS are still unknown.

For more detailed relationships between dinoflagellate cyst productions and assemblages and seasonal or shorter time interval environmental or ecological parameters, a few studies on time series sediment traps were conducted in different regions (e.g., Dale, 1992; Heiskanen, 1993; Montresor et al., 1998; Harland and Pudsey, 1999; Zonneveld and Brummer, 2000; Godhe et al., 2001; Wendler et al., 2002; Morquecho and Lechuga-Devéze, 2004; Susek et al., 2005; Fujii and Matsuoka, 2006; Pitcher and Joyce, 2009; Howe et al., 2010; Pospelova et al., 2010, 2018; Zonneveld et al., 2010; Price and Pospelova, 2011; Bringué et al., 2013, 2018; Prebble et al., 2013;

Heikkilä et al., 2016). The SCS, influenced by the tropical EAM, experiences winter monsoon and summer monsoon shifts in near-surface wind, air temperature, SST, SSS, PP, and other oceanographic conditions. These seasonal differences should result in different dinoflagellate cyst fluxes and assemblages between winter monsoon and summer monsoon. However, no such sediment trap research has been previously conducted on the seasonal dynamics of dinoflagellate cysts in the SCS.

1.5 General objectives and major research contents

This thesis focuses on reconstructing the Holocene EAM climatic and oceanographic history of the northern SCS using high-resolution terrestrial (pollen and spores) and marine (dinoflagellate cysts) palynological records. The research content includes three aspects. First of all, seasonal palynological assemblages were investigated through sediment traps deployed in the southwestern waters of Taiwan in summer and winter monsoon seasons to identify seasonal dynamics in palynological distributions and to select indicators representing winter monsoon or summer monsoon (Chapter 2). Then, surface sediment samples across the SCS were used for a palynological study to establish the relationships between palynological proxies and parameters of the EAM climate and oceanographic conditions (e.g., SST, SSS, Chl-a concentrations and PP) (Chapter 3). Finally, the history of the Holocene EAM and oceanographic environment were reconstructed through palynological analysis of one sediment core using the indicators of paleoclimatic and oceanographic conditions refined through the study of sediment traps and surface sediments (Chapter 4).

1.6 Outline of the dissertation

In Chapter 2 of the dissertation, a total of 24 samples from sediment traps deployed in winter and summer monsoon seasons in the southwest Taiwan waters were analysed for palynological taxa, assemblages and absolute abundances (concentrations and fluxes). The specific objective of this work was to document the seasonal dynamic of palynological distributions and to select or assess indicators of winter and summer monsoons and oceanographic conditions. This chapter was published in Review of Paleobotany and Palynology (Li et al., 2018).

Chapter 3 focuses on the dinoflagellate cyst analysis in surface sediment samples. A total of 42 surface sediment samples from the northern and eastern SCS were used for dinoflagellate cyst analysis. Also, the cyst dataset of 34 samples of Kawamura (2002, 2004) from the southern and western SCS was compiled. The research objectives were: to investigate the distribution patterns of dinoflagellate cyst taxa; to understand their relationship with environmental parameters further; then to identify specific dinoflagellate cyst taxa or assemblages as indicators for specific oceanographic factors. The manuscript of this study has been prepared to submit for publication.

Chapter 4 presents both marine dinoflagellate cyst and terrestrial pollen and spore records of one sediment core from the northern SCS spanning the last 12,500 yr. This study aims to reconstruct Holocene EAM climate and oceanographic conditions using pollen and spore as regional EAM proxies and dinoflagellate cysts for local oceanographic information, together with high-resolution AMS ^{14}C age frame. This chapter was published in Palaeogeography, Palaeoclimatology, Palaeoecology (Li et al., 2017).

Chapter 5 concludes this dissertation with major research findings. I also include suggestions for future research that could provide possibilities for quantitative reconstruction of Holocene EAM climate and oceanographic history of the SCS.

1.7 Contribution of authors

I have written the entire thesis. I contributed to the collection of the sediment core from the northern SCS and prepared all samples from sediment traps, surface sediments and the sediment core for microscope analysis. The figures, tables, and plates of palynological data or morphological patterns presented in this thesis were done solely by me. I also performed all analysis of the data, including statistical treatment, evaluated the results, made the interpretations and formulated the conclusions. My supervisor, Dr. Pospelova guided, trained and constructed me at every stage from initiation of the study, through the processing of sediment samples and analysis of the data, to the review and editing of the manuscripts.

Dr. Hui-Ling Lin (National Sun Yat-Sen University, Taiwan) was involved in the sediment trap study (Chapter 2) and provided us with the samples collected in the Southwest Taiwan Waters and relevant information of sampling. Dr. Wenping Gong (SunYat-Sen University, China) provided the daily observation data of the Pearl River discharges, and also contributed his useful comments on the revised manuscript (Chapter 2). Drs. Lejun Liu (First Institute of Oceanography, SOA, China) and Bing Song (Korea Institute of Geoscience and Mineral Resources) were involved in Chapter 2 and Chapter 4. They contributed the air temperature, wind and sea water velocity data, and helped to transfer the data format for further analysis in Chapter 2. They also supported and participated in the field investigations for the sediment core (Chapter 4). Dr. Bing Song

and Mr. Rui Zhou (East China Normal University) also subsampled the sediment core in labs, described sediment structures and components (Chapter 4).

Dr. Chuanxiu Luo (South China Sea Institute of Oceanology, Chinese Academy of Sciences) contributed to Chapter 3 by providing surface sediment samples from the northern SCS and relevant sampling information. She also reviewed and gave useful comments on the draft manuscript. Dr. Ivan Hernandez-Almeida (University of Bremen, Germany) provided surface samples from the Eastern of SCS and off the Southwest Taiwan and information on sampling. Dr. Kenneth Neil Mertens (Ifremer, LER BO, Station de Biologie Marine, France) was involved in Chapter 3 for his contributions of determination and taxonomy of some species.

Dr. Kedong Yin (SunYat-Sen University, China) provided the SSS monthly data of the surface sample sites from 2011 to 2012 and helped to transfer into a format for further analysis, contributing to Chapter 3. Dr. Yongsheng Wu (Bedford Institute of Oceanography, Canada) provided information about vertical water velocities along the shelf-break zones. Dr. Hui Wu (East China Normal University) contributed his efforts on the mechanism of coastal upwelling off Borneo in Chapter 3 and helped to polish the part about how coastal upwelling off Borneo and Luzon could influence the shelf-slope region.

All co-authors reviewed and gave useful suggestions and comments for improving the manuscripts that they coauthored. Dr. Vera Pospelova contributed greatly to editing the manuscripts in detail.

Chapter 2

Seasonal dinoflagellate cyst production and terrestrial palynomorph deposition in the East Asian Monsoon influenced South China Sea: A sediment trap study from the Southwest Taiwan waters

Abstract

The South China Sea (SCS), influenced by the tropical East Asian Monsooon (EAM), experiences winter monsoon and summer monsoon shifts in near-surface wind, air temperature, sea-surface temperature, salinity, primary productivity, and other oceanographic conditions. To understand how monsoon seasons influence palynological dynamics and which palynological index could be a reliable indicator of winter or summer monsoons, we studied palynological records of sediment trap samples collected in March–April (winter monsoon season) and July–August (summer monsoon season). Fluxes and assemblages of terrestrial pollen and spores, as well as marine dinoflagellate cysts, were investigated using sediment traps in the southwest Taiwan waters of the SCS. The pollen and spores of 109 taxa and dinoflagellate cysts of 53 taxa were identified in 24 sediment trap samples that were collected at 3-day intervals. The average abundance of *Pinus* pollen was notably higher in March–April at ~40%, which was double that in July–August. This trend was associated with transport by the northwest wind in March–April when *Pinus* pollen are produced by the coniferous vegetation in the South China and Taiwan Island. The pollen abundances of Chenopodiaceae/Amaranthaceae and Compositae seemed to be greatly reduced in July–August, with an opposite pattern observed for Poaceae, *Artemisia*, Cyperaceae, *Typha*, and fern spores. Fluvial transport is

likely the controlling factor since river runoff intensifies in summer. High relative abundances and fluxes of Poaceae pollen are not indicators of summer monsoons but related to cultural activities.

Dinoflagellate cyst assemblages were dominated by cysts produced by heterotrophic taxa, especially *Brigantedinium* spp. at 68–91%. Proportionally higher increases of cysts produced by autotrophic dinoflagellates resulted in lower heterotrophic to autotrophic ratios in July–August. The highest total cyst fluxes occurred in late July of ~20,000 cysts m^{-2} d^{-1} together with the highest fluxes of autotrophic *Operculodinium centrocarpum*, *Spiniferites* spp., and *Lingulodinium hemicystum*. The increased fluxes of almost all dinoflagellate cyst taxa during July–August were related to the decreased SSS due to the greater river water inputs and nutrients. The high abundances of autotrophic taxa in July-August were associated with high light availability.

2.1 Introduction

The EAM has significant effects on global climate and hydrologic cycles (An, 2000; Wang et al., 2008). It seasonally switches wind direction, precipitation, river runoff, and land-sea heating between the western Pacific and the Asian continent. The East Asian Winter Monsoon (EAWM) results in cold and dry weather in winters, whereas the East Asian Summer Monsoon (EASM) leads to warm and humid weather in summers with greater precipitation and river runoff (e.g., Chen, 1992).

The SCS is located in the tropical EAM region, and it experiences contrasting seasonal changes in wind directions and currents (Figure 2-1). During the winter (October–April), the northeastern wind dominates, and it induces a basin-wide cyclonic

gyre of the surface water circulation and southwestward coastal currents. In the summer (May– September), the southwestern wind is predominant, and the basin-wide circulation

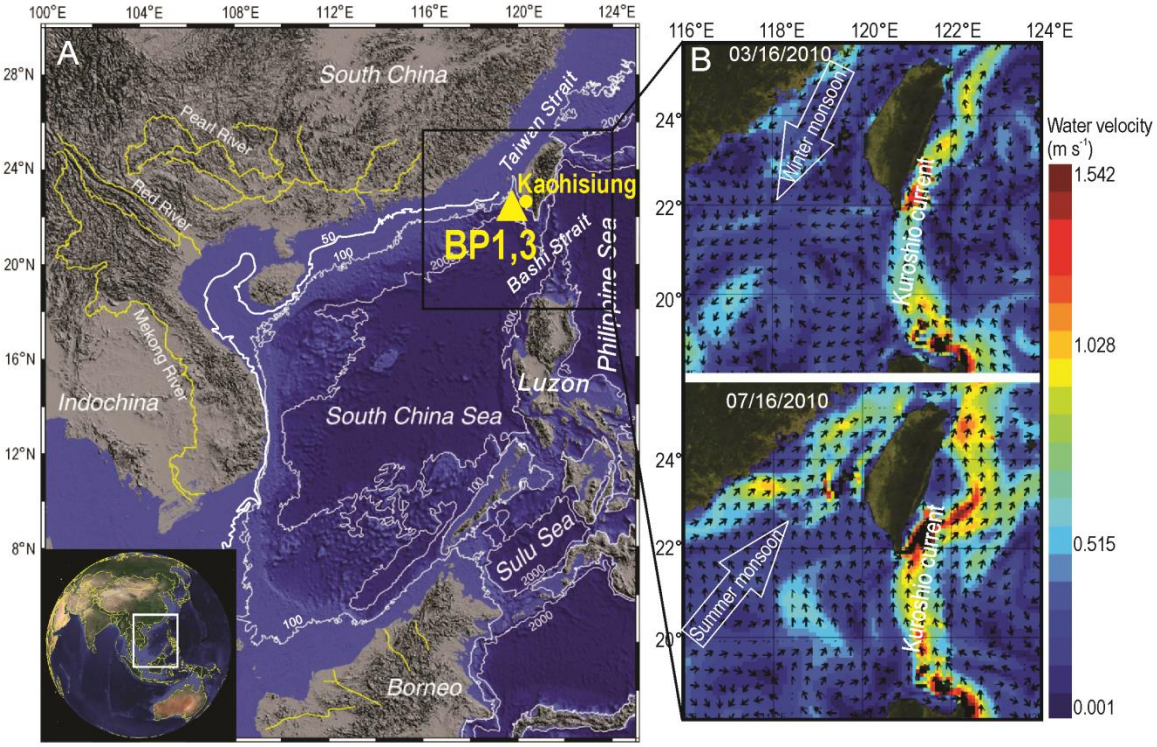

Figure 2-1. (A) Map of the study area showing the location of the sediment traps (BP1 and BP3) and bathymetry of the South China Sea (modified fromWang et al., 2008; Li et al., 2017). The yellow-filled circle on the map indicates the location of Kaohisiung station for observational data of air parameters (https://www.ncdc.noaa.gov). (B) Current velocities at -0.50mdepth on March 15 and July 15, 2010. Black arrows show current directions (from http://marine.copernicus.eu).

splits into a weakened cyclonic gyre in the north and a strong anti-cyclonic gyre in the south with northeastward coastal currents (e.g., Qu, 2000, 2002; Li et al., 2017). In addition, the Kuroshio Current flows from the western Philippines Sea and branches into the SCS through the Bashi (Luzon) Strait (e.g., Yuan, 2002; Yuan et al., 2006). The Kuroshio Current water mixes with colder and lower salinity SCS waters and flows northward towards to the Taiwan Strait (e.g., Huang et al., 2015). In winter, under the

influence of the northeasterly monsoon, the Kuroshio Current Loop appears southwest of Taiwan more frequently than in other seasons.

Influenced by EAM, seasonal water inputs from rivers in the southern China and the southwest of Taiwan Island also cause changes in major oceanographic conditions such as SST, SSS and PP. The Pearl River is the largest river that drains into the northern South China Sea, and its plume intrudes into the main channel of the Taiwan Strait in summer (Bai et al., 2015). The mean annual discharge of the Pearl River into the SCS is ~1.0×10^4 $m^3 s^{-1}$, with the minimum (~3.4×10^3 m^3 s^{-1}) in winter and the maximum (~2.1×10^4 m^3 s^{-1}) in summer (Zhao, 1990; Yin et al., 2004). Approximately 80% of annual discharge occurs during the summer monsoon season. Small rivers flowing into the SCS, such as Han River from the southern China and Tsengwen, Erhjen, Kaoping and many other rivers from the Southwest of Taiwan, show the similar seasonal trends, e.g. much higher runoff in summers (>1–10 $\times 10^3$ m^3 s^{-1}) while lower in winters (<10–50 m^3 s^{-1}) (e.g., Kao and Milliman, 2008; Wang et al., 2009).

The EAM climate and the environmental changes induce changes in the terrestrial and marine ecosystems of the SCS region. Therefore, fossils and biochemical proxies in sediment cores from the SCS have been used to reconstruct EAM climate and relevant oceanographic conditions in the past. Palynological analysis in the SCS is one of the most common methods for reconstructions of past EAM climate, shoreline migration, mangrove migration, sea-level change, and other hydrodynamic conditions (e.g., Sun and Li, 1999; Sun et al., 2003; Li et al., 2006a, 2006b, 2010, 2012; Zheng et al., 2011; Mao et al., 2012; Dai and Weng, 2015; Dai et al., 2015). Palynological records include pollen, spores, dinoflagellate cysts, acritarchs, and other microscopic organic materials (e.g.,

Traverse, 2007). Pollen and spores in marine sediments are transported there by wind or water (including currents and rivers) and deposit in the sea together with other sedimentary particles. Their distributions in marine environment are influenced by the surrounding vegetation, wind direction and strength, river water discharges, sea level fluctuations, currents, geographic and oceanographic conditions (e.g., Heusser, 1988; Sun et al., 1999; Moss et al., 2005; Li et al., 2008; Londeix et al., 2009; Crouch et al., 2010; Montade et al., 2011; Luo et al., 2013, 2014, 2016; Dai et al., 2014; Zhao et al., 2016). Therefore, determining the primary sources and transport paths of pollen and spores is a key to interpreting data for past EAM climatic and oceanographic reconstructions. For example, *Pinus* pollen grains can be transported further by winds with the aid of their air-filled sacs (e.g., Schwendemann et al., 2007), but they can also be transported farther than other pollen due to greater flotation in water (e.g., Li et al., 2010; Song et al., 2017). That means that high relative abundances of *Pinus* pollen, which is a dominant component of pollen assemblages in sediments from the SCS, may have been transported by stronger winds during winters from the mainland of China or Taiwan Island (e.g., Sun et al., 1999) or they may have been enriched by intensified river force in summers (e.g., Luo et al., 2014; Dai et al., 2015). Luo et al. (2016) compared pollen data from airborne samples with surface water samples from the SCS to determine the pollen transport modes. That work provided details on the major pollen sources, distributional patterns and effects of winds, rivers and currents in the SCS. Unfortunately, pollen grains from surface water samples were only collected at the time when the water samples were collected, which was much shorter than the depositing period (12–24 h) for pollen in each airborne sample (Luo et al., 2014, 2016).

Moreover, different pollen and spores are produced in various seasons. A comparison of the relative (percentages) and absolute (fluxes and concentrations) abundances of specific pollen or spore types from sediment trap samples in summer monsoon seasons with those samples in winter monsoon seasons can help to identify sources and pathways of these terrestrial palynomorphs, and further refine best indicators for winter or summer monsoons.

Dinoflagellate cysts are produced by dinoflagellates, one of the major groups of modern marine plankton. The distributions of modern dinoflagellate cysts in marine environments are controlled by SST, SSS, sea-ice cover, nutrient and light availability (e.g., Dale, 1996; de Vernal et al., 2001, 2005; Pospelova et al., 2008; Pospelova and Kim, 2010; Zonneveld et al., 2013; Ellegaard et al., 2017). Based on the relationship between cyst distributions and driving environmental factors, dinoflagellate cysts have also been widely used as bioindicators of past marine PP (e.g., Dale, 1996; Radi and de Vernal, 2004; Pospelova et al., 2006, 2015; Zonneveld et al., 2008; Bringué et al., 2014, 2016; Ribeiro et al., 2016). Different from pollen and spore records, which derive from terrestrial regional sources, dinoflagellate cyst records directly reflect local oceanographic conditions. A combined palynological proxy record of pollen, spores, and dinoflagellate cysts better reflect regional paleoclimatic and local (paleo)oceanographic conditions (e.g., Bouimetarhan et al., 2012; Marret et al., 2013; Pospelova et al., 2015; Shumilovskikh et al., 2016; Poliakova et al., 2017; Zhao et al., 2017). For example, considering details of sea-level changes and current influences reflected in records of dinoflagellate cysts and terrestrial pollen and spores, Li et al. (2017) reconstructed, for

the first time, the warmest period of the Holocene and three strengthened winter monsoon intervals at centennial scales in the SCS.

To provide detailed information about higher-resolution climatic or environmental changes in a monsoon region, it is necessary to refine indicators of climate and seasonal oceanographic conditions. For example, which taxa or species can be used as indicators of winter or summer monsoons, and which species are good indicators of SST, SSS, or PP. Most studies addressing these issues have been conducted by analyses of the surface sediment samples (e.g., Florin, 1963; Heusser, 1988; Marret and de Vernal, 1997; Rochon et al., 1999; Kawamura, 2004; Pospelova et al., 2008; Li et al., 2008; Richerol et al., 2008; D'Silva et al., 2013; Luo et al., 2014; Dai et al., 2014; Heikkilä et al., 2014). In marine settings, surface sediments are typically collected by grab or box samplers, and these samples represent the deposition from several to a thousand years. Therefore, such samples reflect multiannual averages rather than seasonal variations in palynological distributions.

The deployment of sediment traps enables the continuous collection of sinking particles. Palynological investigation of sediment trap samples in time series help to determine fluxes of individual taxa that may be relevant to specific sources (e.g., winter and/or summer blooming plants or dinoflagellates), atmosphere (e.g., wind direction and speed or air temperature) or oceanographic conditions (e.g., SSS, SST, and PP) (e.g., Dale, 1992, Harland and Pudsey, 1999; Godhe et al., 2001; Zonneveld et al., 2010; Pospelova et al., 2010, 2018; Bringué et al., 2013; Heikkilä et al., 2016). To date, no research has been conducted to assess seasonal patterns of pollen, spore, and dinoflagellate cysts in the SCS.

The northern SCS near Taiwan Bank is one of the best areas for high-resolution reconstructions of past EAM climatic and oceanographic changes because of its well-preserved sedimentary strata and relatively high sedimentation rates (Li et al., 2017). Palynological study of a sediment trap nearby could provide a more reliable basis for seasonal interpretation. In the southwest of the Taiwan Strait, water masses are from the East China Sea, the SCS, and the Kuroshio Current intrusion. The seasonal patterns of the wind field and the temporal variation in water current circulations have strong impacts on the plankton structures and distributions. Therefore, in this study, we analyze terrestrial pollen and spores, as well as marine dinoflagellate cysts in sediment trap samples from the southwest Taiwan waters during winter and summer monsoon seasons. Our objectives are: (i) to document characteristics of both terrestrial pollen and spores and marine dinoflagellate cysts in March–April and July–August, which are dominated by EAWM and EASM, respectively; (ii) to pinpoint differences between the two periods and determine palynological indicators of EAWM and EASM, as well as known oceanographic parameters; (iii) to identify factors and mechanisms that affect seasonal dinoflagellate cyst, pollen and spore assemblages in order to provide a basis for paleoclimatic or paleoceanographic interpretations using palynological sedimentary records.

2.2 Materials and methods

2.2.1 Sediment traps and environmental data

Sediment traps were moored at ~30 m above sea floor in the waters of western Taiwan, the SCS, in 2010. BP1 (22° 39.817′N, 119°55.342′E; 261 m water depth) and BP3 (22° 39.792′N, 119°55.246′E; 264 m water depth) sediment traps were deployed

Table 2-1. Locations of sediment trap deployment, sampling duration, collecting dates, dry weight and number of counted palynomorphs per sample (Lin, 2014).

Station information	Collecting date		Jar #	Sample code	Available fraction	Sample proportion	*Dry weight (g)	Counted number of palynomorphs per sample		
	Start	End						Terrestrial (grains)	Marine (cysts)	**_Lycopodium_ spores (grains)
BP1 Latitude: 22° 39.817' N Longitude: 119°55.342' E Trap depth: 261 m Water depth: 291 m Sampling duration: 3 days	03/16/2010	03/18/2010	1	BP1–1	<63 μm	1	0.56	333	291	10,378
	03/19/2010	03/21/2010	2	BP1–2	<63 μm	1/4	0.55	341	289	5361
	03/22/2010	03/24/2010	3	BP1–3	<63 μm	1/4	0.58	358	372	6558
	03/25/2010	03/27/2010	4	BP1–4	<63 μm	1/4	0.42	390	345	6722
	03/28/2010	03/30/2010	5	BP1–5	<63 μm	1	0.48	285	189	9488
	03/31/2010	04/02/2010	6	BP1–6	<63 μm	1/4	0.46	311	193	10,444
	04/03/2010	04/05/2010	7	BP1–7	<63 μm	1/4	0.48	462	221	13,294
	04/06/2010	04/08/2010	8	BP1–8	<63 μm	1/4	0.56	349	302	9542
	04/09/2010	04/11/2010	9	BP1–9	<63 μm	1/4	0.57	473	323	5766
	04/12/2010	04/14/2010	10	BP1–10	<63 μm	1/4	0.57	358	312	9007
	04/15/2010	04/17/2010	11	BP1–11	<63 μm	1/4	0.52	319	191	12,329
	04/18/2010	04/20/2010	12	BP1–12	<63 μm	1/4	0.44	238	125	11,546
BP3 Latitude: 22° 39.792' N Longitude: 119°55.246' E Trap depth: 264 m Water depth: 294 m Sampling duration: 3 days	07/10/2010	07/12/2010	1	BP3–1	<63 μm	1/4	0.51	300	171	9617
	07/13/2010	07/15/2010	2	BP3–2	<63 μm	1/4	2.72	365	298	4736
	07/16/2010	07/18/2010	3	BP3–3	<63 μm	1/4	3.09	384	288	3990
	07/19/2010	07/21/2010	4	BP3–4	<63 μm	1/4	2.82	452	273	2913
	07/22/2010	07/24/2010	5	BP3–5	<63 μm	1/4	2.29	391	331	3046
	07/25/2010	07/27/2010	6	BP3–6	<63 μm	1/4	2.56	342	396	6543
	07/28/2010	07/30/2010	7	BP3–7	<63 μm	1/4	2.72	300	278	2245
	07/31/2010	08/02/2010	8	BP3–8	<63 μm	1/4	2.08	380	306	2932
	08/03/2010	08/05/2010	9	BP3–9	<63 μm	1/4	1.41	316	358	9962
	08/06/2010	08/08/2010	10	BP3–10	<63 μm	1/4	0.63	308	137	9773
	08/09/2010	08/11/2010	11	BP3–11	<63 μm	1/4	2.91	643	361	7924
	08/12/2010	08/14/2010	12	BP3–12	<63 μm	1/4	3.29	326	312	9504

Note: *data from the sediments at the size <63 μm.

** 18, 584 grains *Lycopodium* spores were added into each sample.

from March 18 to April 20, and July 12 to August 14, 2010, respectively (Table 2-1) (Figure 2-1). The cylindro-conical French PPS 3/3 sediment traps with 0.125 m^2 opening were used for 3-day collection intervals of each collection cup (Lin, 2014). For in situ preservation, the cups were filled with brine solution and poisoned with HgCl. The procedures used to deploy and process the trap samples followed the description of Lin et al. (2011). Four aliquots from each collection cup were freeze-dried, suspended in deionized distilled water, and passed through 63-μm sieves (Lin, 2014). Unfortunately, for sediment trap BP1, the sediment materials larger than 63 μm were first used for the foraminifer analysis, and none remained for the palynological analysis. Thus, in this study, only palynomorphs smaller than 63 μm were used to compare palynomorphs between March–April and July–August. However, we are aware that some pollen, such as *Pinus*, could be lost because they may be larger than 63 μm. To avoid the bias, we separately prepared in the laboratory, counted pollen, spores and dinoflagellate cysts in sample fraction from 63 to150 μm (0.01–4.12 g dry weight per sample) from sediment trap BP3. Only a few pollen and spore grains or dinoflagellate cysts were found in the 63–150-μm-size residue from each BP3 samples (Table 2-2). Thus, we are confident that our results from sediments smaller than 63 μm can reflect real relative abundances and the changes in the assemblages or fluxes of palynomorphs between March–April and July–August were not much affected by the absence of palynomorphs between 63 and 150 μm.

The environmental data used in this study include SST, SSS, water current velocity (WV), current direction (CD), mean air temperature (AT), sedimentary accumulation rates (SAR), daily mean wind speed (MWS) and wind direction (WD), as well as runoff

Table 2-2. List of pollen, spores, and dinoflagellate cysts found in sediments at the range of 63-150 µm from sediment trap BP3.

Sample No.	**BP3-1**	**BP3-2**	**BP3-3**	**BP3-4**	**BP3-5**	**BP3-6**	**BP3-7**	**BP3-8**	**BP3-9**	**BP3-10**	**BP3-11**	**BP3-12**
Sample fraction	63-150 µm	63-150 µm	63-150 µm	63-150 µm	63-150 µm	63-150 µm	63-150 µm	63-150 µm	63-150 µm	63-150 µm	63-150 µm	63-150 µm
UVic ID#	2015-502	2015-503	2015-504	2015-505	2015-506	2015-507	2015-508	2015-509	2015-510	2015-511	2015-512	2015-513
Dry weight (g)	0.0119	1.1625	4.1251	0.2112	0.1303	0.7787	0.3206	0.1875	0.0552	0.0192	2.1327	3.7838
Pollen												
Pinus	1		1		1	3						
Dacrydium			1									
Quercus			1					1			1	
Castanopsis						1						
Artemisia						1						1
Spores												
Parkeriaceae		1	1									
Polypodiaceae												1
Hymenphyllum			5									
Pteridium						1						
Cyathea												1
Unidentified				1								
Reworked												
Cyperidaceae			1									
Dinoflagellate cysts												
Brigantedinium spp.		1	3		1		1					1
Lingulodinium hemicystum												1

Note: 18, 584 grains *Lycopodium* spores were added into each sample. *Lycopodium* spores were not counted since we used the entire prepared materials for counting.

Table 2-3. Environmental parameters for each sampling interval at the sediment trap site and the Pearl River runoff (from https://www.ncdc.noaa.gov; http://marine.copernicus.eu; http://www.pearlwater.gov.cn/).

Sediment trap	Last day of sampling interval (mm/dd/yyyy)	Data collected at sites BP1 or BP3				3-day PRR runoff ($m^3 s^{-1}$) [a]	SAR (g m^{-2} d^{-1}) [b]	Data collected at Kaohisiung Station		
		SSS (‰)	SST (°C)	WV (km h^{-1})	CD (°)			AT (°C)	WMD (km h^{-1})	WD (°)
BP1	3/18/2010	34.29	24.85	0.51	170	6262	1.48	32.3	19.7	280
	3/21/2010	34.24	25.24	0.51	210	6045	1.47	30	18.2	2
	3/24/2010	34.29	25.63	0.34	110	6317	1.55	31	20.4	350
	3/27/2010	34.52	24.70	0.51	345	7602	1.13	25	27.6	330
	3/30/2010	34.57	24.41	0.34	60	6830	1.27	27.3	18.2	350
	4/2/2010	34.43	24.67	0.51	180	6171	1.23	30	22.1	340
	4/5/2010	34.43	24.95	0.51	180	6432	1.27	30	27.6	360
	4/8/2010	34.43	25.11	0.34	280	8702	1.50	28	20.4	330
	4/11/2010	34.19	25.39	0.51	190	12680	1.53	29.7	35.0	330
	4/14/2010	34.14	25.31	0.6	180	10592	1.51	31	22.1	350
	4/17/2010	34.29	24.90	0.34	170	12751	1.39	27.3	16.4	2
	4/20/2010	34.43	26.04	0.43	60	17125	1.18	30	20.4	140
BP3	7/12/2010	31.10	30.67	1.26	30	33523	1.37	28.7	23.9	230
	7/15/2010	30.19	30.57	1.72	0	31733	7.25	34.3	27.6	230
	7/18/2010	29.38	30.52	1.83	350	31559	8.25	33.3	23.9	360
	7/21/2010	30.38	30.62	1.83	0	26743	7.53	33	27.6	210
	7/24/2010	31.24	30.57	2.17	0	29008	6.11	32.7	25.8	140
	7/27/2010	31.95	30.05	1.94	45	38149	6.82	29.7	22.1	362
	7/30/2010	32.76	29.62	0.91	45	53850	7.24	29.7	25.8	210
	8/2/2010	32.95	30.27	1.03	20	42403	5.55	32.7	25.8	160
	8/5/2010	32.19	30.52	0.69	0	47635	3.75	33.3	23.9	2
	8/8/2010	31.57	30.67	0.69	20	36286	1.68	33.3	18.2	230
	8/11/2010	32.43	30.57	1.03	30	31929	7.77	32.3	18.2	240
	8/14/2010	33.14	30.62	1.03	30	26647	8.77	32.7	20.4	340

Note:
SSS: Sea surface salinity, SST: Sea surface temperature, WV: water velocity, CD: current direction, PRR: the runoff of the Pearl River, SAR: Sedimentary accumulation rate, AT: Air mean temperature, MWS: daily mean wind speed, WD: wind direction.
[a] The runoff of the Pearl River in 3 days during which each sample was collected.
[b] SARs are only for <63 μm sediment fraction.

of the Pearl River (PRR) (Table 2-3). Measurements of SST and WV were obtained from the dataset of Global Ocean Physics Analysis and Forecast Updated Daily, available at COPERNICUS supported by the Marine Environment Monitoring Service of Europe Commission (http://marine.copernicus.eu). This dataset contains daily globally entire fields of SST and WV on a latitude–longitude grid of 0.083 × 0.083 degrees at a depth of 0.5 m. SSS data were acquired from the dataset of Global Ocean Physics Reanalysis GLORYS2V4 at COPERNICUS, which is on a latitude-longitude grid of 0.25 × 0.25 degrees. The observational dataset of AT, MWS and WD were from NOA Kaohsiung Station (https: //www.ncdc.noaa.gov). Only SARs of <63 um fractions were available to be calculated because we did not have the sediment weights of larger fractions (Table 2-1). Many rivers contribute fresh water to the site, and all of them have a similar seasonal discharge pattern: it is greater in summer and lowers in winter seasons. Thus, the Pearl River, the largest one, can be used as a good representation of the general pattern of river runoff to the SCS. The PRR data were obtained from the stations of Gaoyao, Shijiao and Boluo that are located at three major tributaries of the Pearl River: the West River (Xijiang), the North River (Beijiang), and the East River (Dongjiang), respectively (Zhang et al., 2012). The runoff data are at 3-day time intervals, the same as the sediment trap samples were collected (http://www.pearlwater.gov.cn). There were no strong El Nino or La Nina events in 2010. Thus we can consider this year as “normal”.

2.2.2 Palynological sample preparation and identification

Palynomorphs were extracted using a standard palynological processing technique at the Paleoenvironmental Laboratory at the University of Victoria (e.g., Pospelova et al. 2010). All samples were desalted, dried at 40 °C, and then weighed with an analytical

balance. To estimate the fluxes of palynomorphs, we added one tablet of *Lycopodium clavatum* grains (18,584 grains per tablet of batch no. 177745, University of Lund, Sweden) to each sample (e.g., Mertens et al., 2009). The samples were treated with 10% HCl to remove carbonates and 48% HF at room temperature to dissolve silicates. Then, a second 10% HCl treatment eliminated precipitated fluorosilicates. After each step, the samples were rinsed with distilled water and passed through a 10 μm Nitex nylon mesh to remove fine particles. A gentle sonication for up to 30 s was used on samples during the sieving (Mertens et al., 2012). The residues were strew-mounted in glycerin jelly between a slide and a coverslip at 95 °C. All samples and palynological slides are stored at the Paleoenvironmental Laboratory, School of Earth and Ocean Sciences, University of Victoria, Canada.

Terrestrial pollen, spores, and freshwater algae and marine dinoflagellate cysts were identified and counted using a Nikon Eclipse 80i optical microscope at 400× or higher magnification. Terrestrial and marine palynomorph concentrations, fluxes, and percentages were calculated separately on total terrestrial palynomorphs and total dinoflagellate cysts. Terrestrial palynomorphs were counted from 238 to 643 grains per sample (with an average of ~360 grains), and dinoflagellate cysts were counted from125 cysts to 396 cysts per sample (with an average of ~280 cysts) (Table 2-1), excluding cysts of *Alexandrium* spp. and *Biecheleria* spp. since their preservation or smaller than 10 μm specimens make their quantitative estimates unreliable. The identification of terrestrial palynomorphs was based on Huang (1972), Academia Sinica (1976, 1982), and Mao et al. (2012). Dinoflagellate cysts with their thecal equivalents and autotrophic (phototrophic) or heterotrophic affinity were determined according to Matsuoka (1988),

McMinn (1991), Kokinos and Anderson (1995), Head (1996), Zonneveld et al. (1997), Rochon et al. (1999), Zonneveld and Jurkschat (1999), Esper and Zonneveld (2002), Pospelova and Head (2002), Matsuoka et al. (2009), Pospelova and Kim (2010), Verleye et al. (2011), Yu and Morozova (2013) and Zonneveld and Pospelova (2015).

Cysts were identified to the species level whenever possible. However, some taxa were grouped into their genus with "spp." due to morphological similarities. Those cysts with clear morphologies but without published descriptions were designated as types (A, B,…). Folded brown cysts with obscure horns and/or granulated brown cysts were grouped as cysts of *Protoperidinium* spp. We refer to dinoflagellate cysts produced by autotrophic and heterotrophic dinoflagellates as "autotrophic taxa" and "heterotrophic taxa", respectively.

2.2.3 Statistical analysis

The relative abundances of each palynomorph type were calculated as percentages of the total counted grains of pollen and spores or the total dinoflagellate cysts. The fluxes (grains or cysts m^{-2} d^{-1}) were calculated using the following formula: $F_{total} = \frac{L_{total} \cdot P_{counted}}{L_{counted} \cdot S \cdot T}$, where F_{total} is the total flux of palynomorphs. L_{total} is the number of *Lycopodium clavatum* spores added to the sample. $L_{counted}$ and $P_{counted}$ are the numbers of counted *Lycopodium* grains counted *Lycopodium* grains and counted terrestrial or marine palynomorphs in each sample, S is the area of the sampling trap opening, and T is the number of days of sediment deposition. The individual flux of each type of pollen, spore, or dinoflagellate cyst was calculated by multiplying the total flux and the percentage of each type of total terrestrial palynomorphs or dinoflagellate cysts. According to the suitable environments of pollen and spore-producing plants, we grouped them as arboreal

pollen (AP), non-arboreal pollen (NAP), and fern spores & freshwater algae. AP was further divided into tropical conifers, non-tropical conifers, temperate broad-leaved types, tropical–subtropical broad-leaved types, and mangroves. NAP was composed of pollen from mesophytes, drought-tolerant and wetland herbs or shrubs.

The terrestrial palynomorph richness was estimated to reflect the palynological diversity, which is related to how much pollen and spores from various terrestrial vegetation types are sorted by marine currents (e.g., van der Knaap, 2009; Li et al., 2010). Rarefaction analysis was used to estimate the palynomorph richness based on the formula $E(Tn) = \sum_{i=1}^{T} 1 - \left[\frac{(N-Ni)!(N-n)!}{(N-Ni-n)!N!}\right]$, where $E(Tn)$ is the expected palynomorph richness in a standardized pollen count *Ni*, *T* is the palynomorph richness in the original pollen count, *N* is the overall palynological grain sum, and *n* is the number of grains or cysts selected for standardization in the rarefied sample (Birks and Line, 1992; Peros and Gajewski, 2008). Rarefaction calculations were performed for all types of pollen, spores, and freshwater algae using the software PAST (Hammer et al., 2001).

Detrended Correspondence Analysis (DCA) and Redundancy Analysis (RDA) were performed to quantify the relationship between the environmental parameters and patterns of the palynological distribution using CANOCO 4.5 for Windows software (ter Braak and Šmilauer, 2002). DCA was first applied to test the linear or unimodal character of assemblage variability. The length of the first DCA gradient was 1.121 standard deviations for the relative abundance dataset of terrestrial palynomorphs and 0.576 for the relative abundance dataset of dinoflagellate cysts. The standard deviations are <2, and this indicates that terrestrial palynomorphs and dinoflagellate cysts both linearly responded to environmental gradients, justifying the need for the further use of the RDA.

Forward selection was applied to reduce the set of variables that could effectively explain the greatest amount of variance in the palynological dataset. The relationship between the palynological distribution and environmental parameters was assessed by species scores and their ordination patterns. Monte Carlo testing was used to determine the significance of each environmental variable. The level of significance of the variables indicates that the environmental variables are strongly related to the species data when $P<0.05$.

2.3 Results

2.3.1 Terrestrial palynomorphs

Terrestrial palynomorphs of ~109 taxa were identified in 24 sediment trap samples (Table 2-4) (Plates 2-I, 2-II and 2-III). The richness varied from 29 to 75, with an average of 37 in March–April (BP1) and 56 in July–August (BP3) (Figure 2-2). Total fluxes of pollen and spores were 8800 grains m^{-2} d^{-1} and 16,000 grains m^{-2} d^{-1} for the averages in March–April and July–August, respectively (Figure 2-3). AP overwhelmingly dominated in assemblages in March–April with an average percentage of ~60%, which was mainly contributed by *Pinus* pollen (~37%). In July–August, AP was reduced to almost half of the average at ~36%, whereas both fern spores and NAP increased up to a level similar to AP, with average percentages of ~32 and 30%, respectively. The percentages of most types of AP were higher in March–April than in July–August, such as *Pinus*, *Quercus*, and *Myrica* (Figure 2-2). In contrast, most types of NAP and fern spores showed higher percentages in July–August than in March–April, except for the drought-tolerant types consisting of Chenopodiaceae/Amaranthaceae, Compositae and *Artemisia*. Poaceae pollen increased from ~6.2% in March–April to 9.8% in July–August, Cyperaceae from

Table 2-4. Types of pollen and spores identified in sediment traps BP1 and BP3.

Arboreal pollen		Non-arboreal pollen	Fern spores & freshwater algae
Tropical conifer		Mesophyte	Monolete
Dacrycarpus [Podacarpaceae]	Dipsacaceae	Acanthaceae	*Anisocampium* [Athyriaceae]
Dacrydium [Podacarpaceae]	*Elaeagnus* [Elaeagnaceae]	Brassicaceae	*Monogramma* [Vittariaceae]
Podocarpus [Podacarpaceae]	*Eucalyptus* [Myrtaceae]	Celastraceae	Polypodiaceae
Non-tropical conifer	*Euphorbia* [Euphorbiaceae]	Convolvulaceae	*Vittaria* [Vittariaceae]
Cupressaceae	*Ficus* [Moraceae]	Cucurbitaceae	Trilete
Cedrus [Pinaceae]	Hamamelidaceae	Daphniphyllaceae	*Athyrium* [Dryopteridaceae]
Picea [Pinaceae]	*Helicia* [Proteaceae]	Fabaceae	*Cibotium* [Dicksoniaceae]
Pinus [Pinaceae]	*Ilex* [Aquifoliaceae]	Gesneriaceae	*Cornopteris* [Athyriaceae]
Taxodiaceae	Lauraceae	*Gmelina* [Verbenaceae]	*Cyathea* [Cyatheaceae]
Tsuga [Pinaceae]	*Liquidambar* [Altingiaceae]	Orchidaceae	Gleicheniaceae
Broad-leaved	Loranthaceae	Poaceae	Hemionitidaceae
temperate	*Lonicera* [Caprifoliaceae]	Rubiaceae	*Hymenophyllum* [Hymenophyllaceae]
Alnus [Betulaceae]	*Mallotus* [Euphorbiaceae]	Valeriavaceae	*Lygodium* [Schizaeaceae]
Fagus [Fagaceae]	Meliaceae	Verbenaceae	*Lygodium microphyllum* [Schizaeaceae]
Juglans [Juglandaceae]	Moraceae	Drought-tolerant	*Lycopodium* [Lycopodiaceae]
Quercus [Fagaceae]	*Myrica* [Myricaceae]	*Artemisia* [Compositae]	Ophioglossaceae
Ulmus [Ulmaceae]	Myristicaceae	*Aster*-type [Compositae]	*Osmunda* [Osmundaceae]
Tropical-subtropical	Myrtaceae	Chenopodiaceae/Amaranthaceae	Parkeriaceae
Acacia [Fabaceae]	Oleaceae	Compositae	*Pityrogramma* [Pteridaceae]
Alchornea [Euphorbiaceae]	Palmae	Wetland	*Plagiogyria* [Plagiogyriaceae]
Aglaia [Meliaceae]	*Phyllanthus* [Euphorbiaceae]	Araceae	*Pteridium* [Dennstaedtiaceae]
Altingia [Altingiaceae]	*Rhus* [Anacardiaceae]	Cyperaceae	*Pteris* [Pteridaceae]
Anacardiaceae	Rutaceae	Lentibulariaceae	*Selaginella* [Selaginellaceae]
Arenga [Palmae]	Sapindaceae	Liliaceae	Freshwater algae
Apocynaceae	*Tilia* [Tiliaceae]	*Nymphoides* [Gentianaceae]	*Concentricystes*
Araliaceae	Mangrove	*Polygonum* [Polygonaceae]	*Zygnema*
Berberidaceae	Combretaceae	Potamogetonaceae	
Carya [Juglandaceae]	*Pandanus* [Pandanaceae]	*Thalictrum* [Ranunculaceae]	
Castanopsis [Fagaceae]	*Rhizophora apiculata* [Rhizophoraceae]	*Typha* [Typhaceae]	
Casuarina [Casuarinaceae]	*Rhizophora mucronata* [Rhizophoraceae]		
Claoxylon [Euphorbiaceae]	*Rhizophora stylosa* [Rhizophoraceae]		
Clausena [Rutaceae]			

Plate 2-I.1. *Anisocampium*, 2. *Athyriopsis*, 3. Polypodiaceae, 4. *Polypodium*, 5. *Pyrrosia*, 6–8. *Cyathea*, 9. *Hiriopteris* (*Diptopterygium*), 10. Hymenophyllaceae, 11. *Pityrogramma*, 12. *Pteris*, 13. *Pteridium*, 14. *Salvinia*, 15–16. *Selaginella*, 17. *Adiantum*? 18. Undetermined trilete spore, 19. *Concentricystes*, 20. *Dacrydium*, 21. *Picea*, 22. *Pinus*, 23–24. *Pinus*? – small type, 25. *Podocarpus*, 26–27. Taxodiaceae, 28. *Tsuga*. Scale bars are 10 μm.

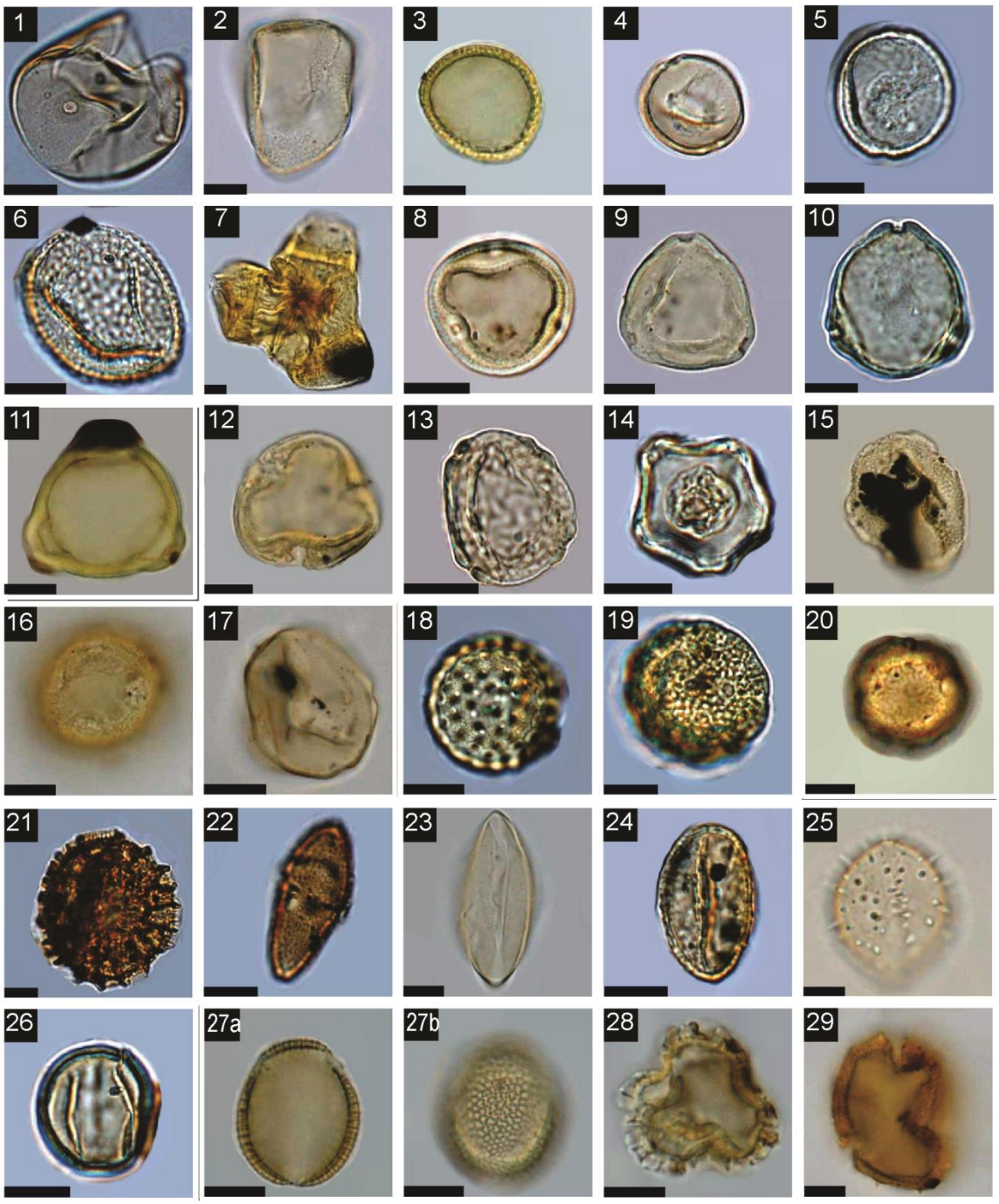

Plate 2-II. 1. Poaceae, 2. Cyperaceae, 3. *Typha*, 4. *Figus*, 5. Moraceae, 6. Potamogetonaceae, 7. *Nymphoides*, 8–9. *Carya*, 10. *Myrica*, 11. *Casuarina*, 12. *Tilia*, 13. *Ulmus*, 14. *Alnus*, 15. *Liquidambar*, 16. *Altingia*, 17. *Juglans*, 18 Chenopodiaceae/Amaranthaceae, 19. Thymelaeaceae, 20. Malpighiaceae, 21. *Polygonum*, 22. Unidentified type. 23. Magnoliaceae, 243 Palmae, 25. *Arenga*, 26. *Quercus*, 27. Cruciferae, 28. Oleaceae? 29. Clerodendron. Scale bars are 10 μm.

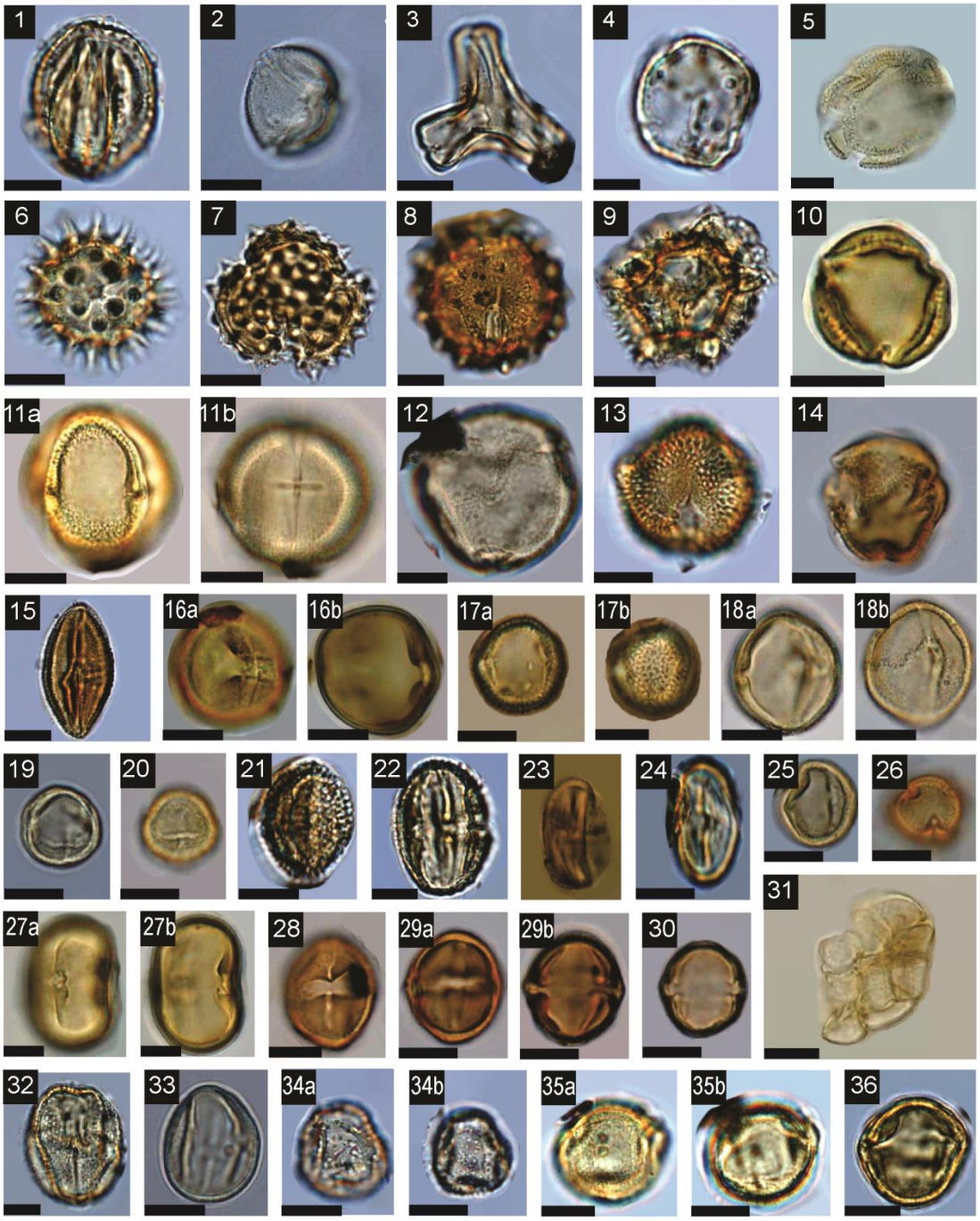

Plate 2-III. 1. Ranunculaceae, 2. Dipterocarpaceae, 3. Loranthaceae, 4. Undetermined type? 5. *Randia*, 6. Compositea, 7. *Solidago*-type, 8. *Ciraium*-type, 9. *Taraxacum*-type, 10. *Artemisia*, 11. Rutaceae, 12. *Fagus*, 13–14. Celastraceae, 15. *Euphorbia*, 16. *Mallotus*, 17. *Phyllanthus*, 18. *Crataeva*? 19–20. *Macaranga*? 21–22. *Ilex*, 23–24. *Castanopsis*/*Lithocarpus*, 25–26. Elaeocarpaceae, 27. *Planchonella*? 28–30. *Rhizophora*, 31. *Acacia*, 32. *Rhus*, 33–36. Undetermined types. The scale bars are 10 μm.

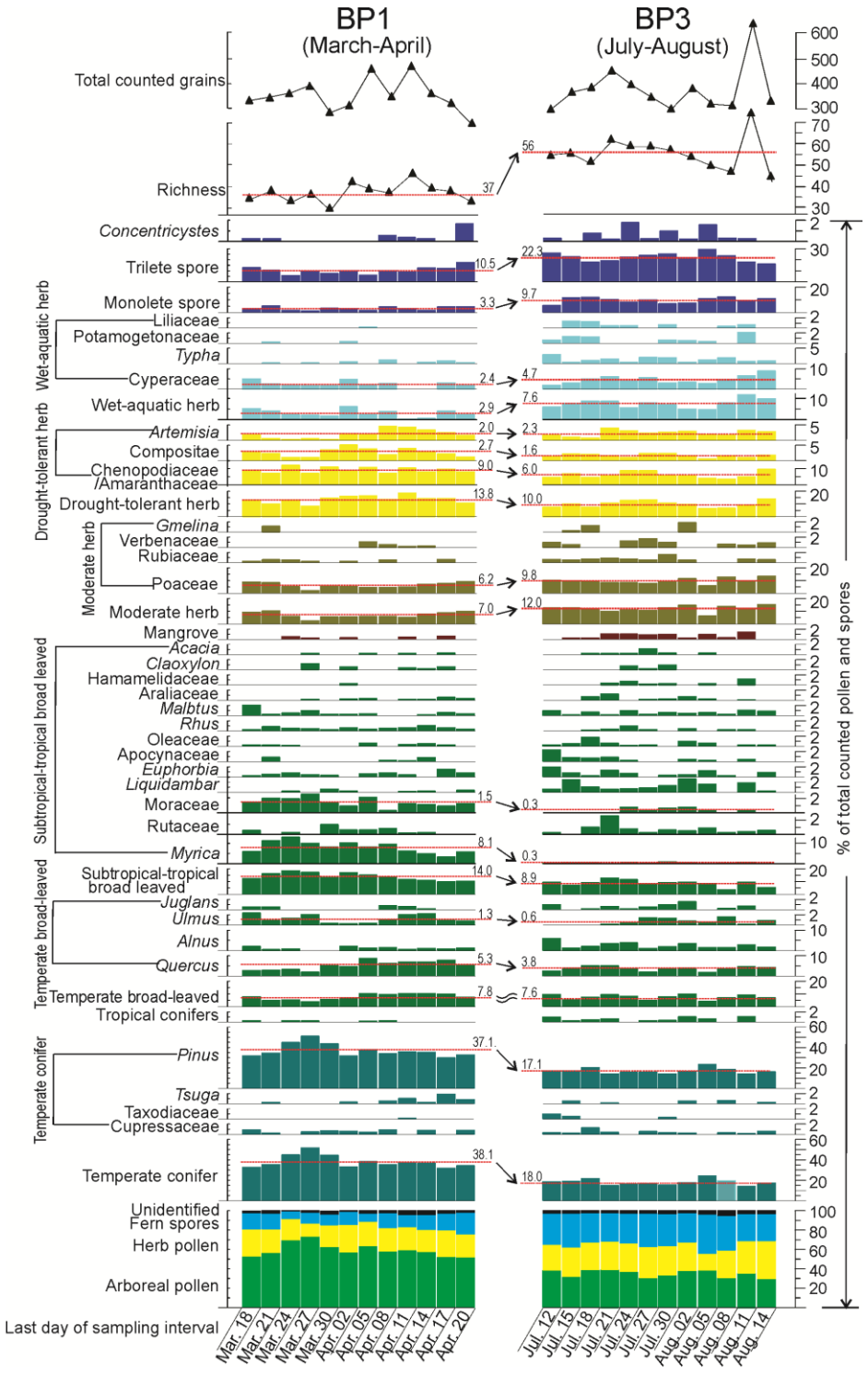

Figure 2-2. Terrestrial palynomorph assemblage composition (percentage %), total counted grains in sediment traps BP1 (March 18–April 20, 2010) and BP3 (July 12–August 14, 2010). Only major pollen and spore types (>2%) and groups are shown. The red dashed lines and numbers show average values.

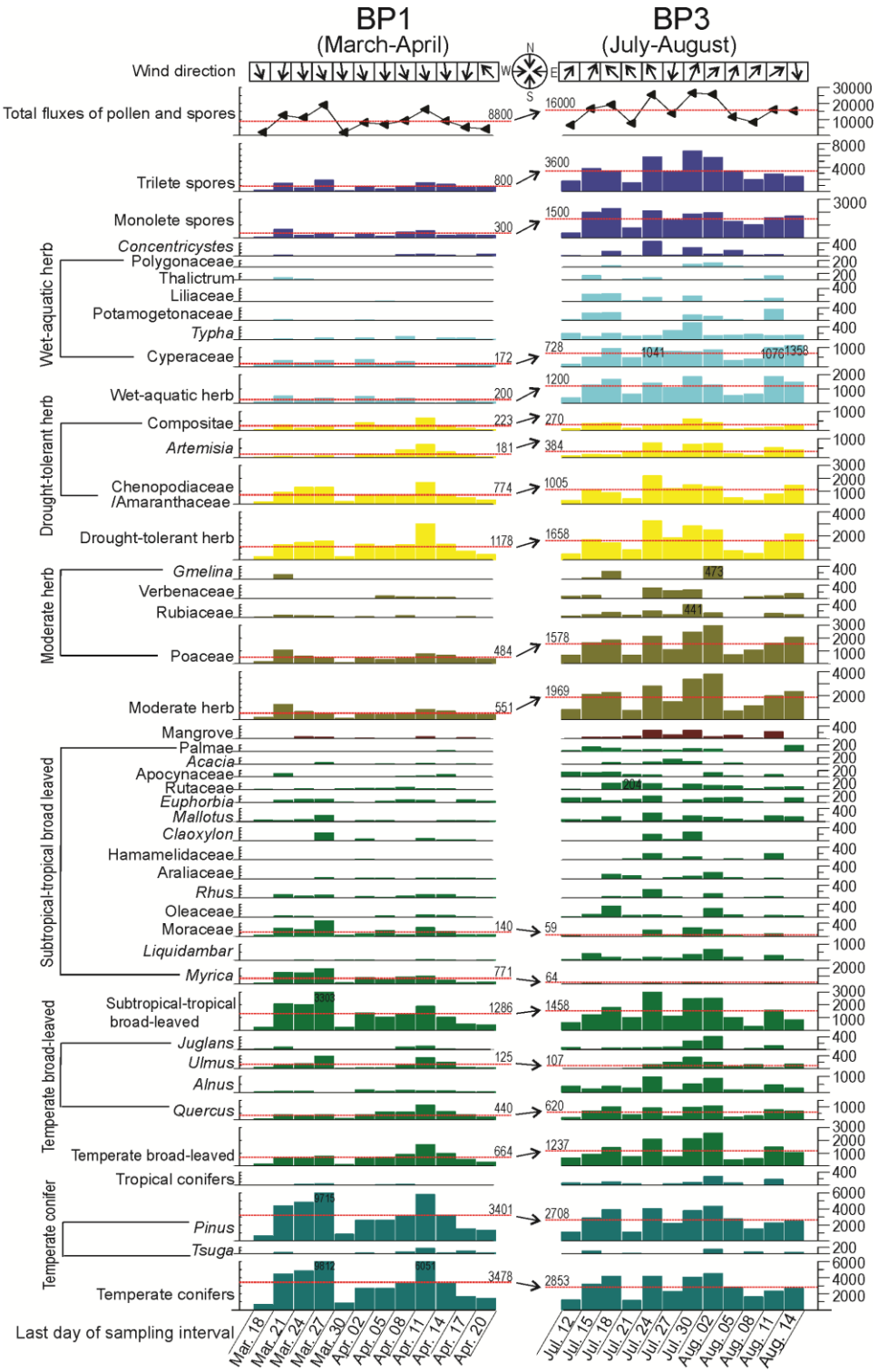

Figure 2-3. Fluxes (grains m^{-2} d^{-1}) of selected and total terrestrial palynomorph taxa/groups from sediment traps BP1 (March 18–April 20, 2010) and BP3 (July 12–August 14, 2010), as well as wind direction recorded at Kaohsiung Station. The red dashed lines and numbers show average values.

~2.4% to 4.7%, monolete spores from ~3.3% to 9.7%, and trilete spores from ~10.5% to 22.3%.

The fluxes of temperate conifer AP decreased from an average of 3478 grains m^{-2} d^{-1} in March–April to 2853 grains m^{-2} d^{-1} in July–August, mainly due to the decrease in *Pinus* flux (Figure 2-3). Other group fluxes increased in July–August. The pollen of *Myrica* and Moraceae showed high fluxes in March–April rather than in July–August (Figure 2-3).

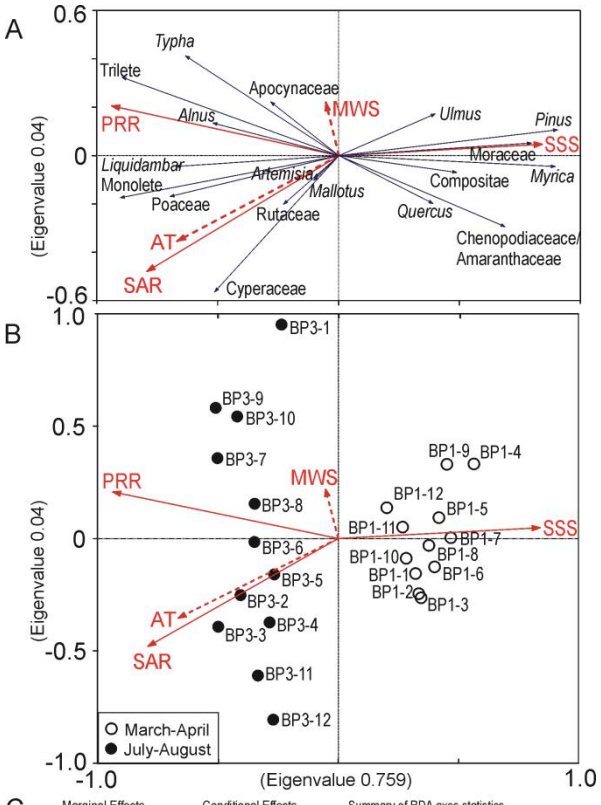

Marginal Effects

Variable	Lambda A
PRR	0.68
SSS	0.54
SAR	0.49
AT	0.35
MWS	0.01

Conditional Effects

Variable	Lambda A	P value	F value
PRR	0.68	**0.002**	46.12
SSS	0.06	**0.006**	4.98
SAR	0.03	**0.026**	3.03
MWS	0.03	0.090	2.45
AT	0.01	0.344	1.11

Summary of RDA axes statistics

	Axis 1	Axis 2	Total
Eigenvalues	0.759	0.04	1
P value	0.002		0.002
Spp.-env. correlations	0.943	0.584	
Cumulative % spp. data	75.9	79.9	
Cumulative % spp.-env.	93.7	98.6	

Figure 2-4. Redundancy analysis performed on relative abundances (%) of pollen and spores (N2%) and environmental parameters. SSS: sea-surface salinity, SAR: sedimentary accumulation rates, AT: air temperature, PRR: runoff of the Pearl River, MWS: daily mean wind speed. Ordination diagram showing species scores (4A) and sample scores (4B). 4C. Marginal effects, conditional effects and summary of RDA axes statistics. P-values <.05 are statistically significant and highlighted in bold. Lambda (Λ) is the variation explained by each environmental variable, considered independently (marginal effect), or considered after all variables already incorporated in the model (conditional effect).

The RDA was performed on the relative abundances of terrestrial palynomorphs. The ordination of species, samples, and environmental variables based on the first two axes explains 79.9% of the variance in the species data and 98.6% of the variance in the fitted species data (Figure 2-4). The first ordination axis, explaining 75.9% of the variance in the species data, is significantly and negatively correlated with

PRR (P = .002) and SAR (P = .022), but positively correlated with SSS (P = .006). AT (P=.344) and MWS (P=.090) are not significant.

Figure 2-4A shows that trilete and monolete spores have the most negative scores of axis 1. The highest scores on the positive side of axis 1 are pollen *Pinus*, *Myrica*, Moraceae, and Chenopodiaceae. The ordination of sample scores shows that all samples collected in July–August are ordinated on the negative side of axis 1, whereas the scores of samples in March–April that correspond to higher SSS are positive (Figure 2-4B).

2.3.2 Dinoflagellate cysts

A total of 49 dinoflagellate cyst taxa were identified including 27 heterotrophic and 22 autotrophic taxa (Table 2-5) (Plates 2-IV, 2-V and 2-VI). Dinoflagellate cyst assemblages were characterized by a high abundance of heterotrophic taxa, with average percentages of ~98% in March–April and ~93% in July–August (Figure 2-5). The cysts with cell content had relatively higher abundances at the end of March and end of July. A dominance of *Brigantedinium* spp. in cyst assemblages was at the percentages ranging from ~68 to ~91%, with averages of ~80% in March–April and of ~83% in July–August. Other heterotrophic taxa that contributed low abundances are cysts of *Protoperidinium* spp., *Dubridinium caperatum*, *Dubridinium cavatum*, and species belonging to *Echinidinium*, *Islandinium*, *Selenopemphix*, and *Stelladinium*. The autotrophic taxa were very low in March–April (< ~5%), resulting in the high ratio of heterotrophic to autotrophic taxa (an average of ~108). In July–August, autotrophic taxa increased to an average of ~6.2%, with main contributions of *Impagidinium* spp. (~1.2%), *Operculodinium* spp. (~2.7%), *Spiniferites* spp. (~2.2%), and *Lingulodinium hemicystum*

Table 2-5. List of dinoflagellate cyst taxa identified in sediment trap samples. Thecate equivalents are based on McMinn (1991), Kokinos and Anderson (1995), Head (1996), Zonneveld (1997), Zonneveld and Jurkschat (1999), Esper and Zonneveld (2002), Pospelova and Head (2002), Matsuoka et al. (2009), Pospelova and Kim (2010), Verleye et al. (2011), Zonneveld and Pospelova (2015).

Cyst species (paleontological name)	Dinoflagellate theca or affinity (biological name)
Autotrophic taxa	
Gonyaulacaceae	
Cyst of *Alexandrium* spp.	*Alexandrium* spp.
Achomosphaera spp.	?*Gonyaulax* sp. Indet.
Bitectatodinium spongium	*Gonyaulax* sp. indet.
Impagidinium strialatum	*Gonyaulax* sp. indet.
Impagidinium spp.	*Gonyaulax* spp.
Lingulodinium hemicystum	?*Lingulodinium polyedrum*
Operculodinium centrocarpum	*Protoceratium reticulatum*
Operculodinium israelianum	*?Protoceratium reticulatum*
Operculodinium janduchenei	Unknown
Operculodinium longispinigerum	Unknown
Operculodinium - type B	Unknown
Polysphaeridium zoharyi	*Pyrodinium bahamense*
Spiniferites bentorii	*Gonyaulax digitalis*
Spiniferites delicates	*Gonyaulax spinifera* complex
Spiniferites hyperacanthus	*Gonyaulax spinifera* complex
Spiniferites membranaceus	*Gonyaulax membranacea*
Spiniferites mirabilis	*Gonyaulax spinifera* complex
Spiniferites ramosus	*Gonyaulax spinifera* complex
Spiniferites - type A, B, C, D, E	*Gonyaulax spinifera* complex
Spiniferites spp.	*Gonyaulax spinifera* complex
Suessiaceae	
Cyst of *Biecheleria* spp.	*Biecheleria* spp.
Perdiniaceae	
Cyst of *Pentapharsodinium dalei*	*Pentapharsodinium dalei*
Heterotrophic taxa	
Diplopsalidaceae	
Dubridinium caperatum	?*Preperidinium meunieri*
Dubridinium cavatum	Diplopsalid group
Diplopsalidaceae (Or Protoperidiniaceae)	
Echinidinium aculeatum	Diplopsalid or Protoperidinioid group
Echinidinium granulatum	Diplopsalid or Protoperidinioid group
Echinidinium transparantum	Diplopsalid or Protoperidinioid group
Echinidinium - type A	Diplopsalid or Protoperidinioid group
Echinidinium - type E	Diplopsalid or Protoperidinioid group
Echinidinium spp.	Diplopsalid or Protoperidinioid group
Polykrikaceae	
Cyst of *Polykrikos* sp.	*Polykrikos* sp. indet.
Protoperidiniaceae	
Brigantedinium cariacoense	*Protoperidinium avellanum*
Brigantedinium irregulare	*Protoperidinium denticulatum*
Brigantedinium simplex	*Protoperidinium conicoides*
Brigantedinium spp.	*Protoperidinium* spp.
?Cryodinium meridianum	*Protoperidinium* spp.
Cyst of *Archaeperidinium minutum*	*Archaeperidinium minutum*
Cyst of *Protoperidinium oblongum*	*Protoperidinium oblongum*
Cyst of *Protoperidinium* -Type A.	*Protoperidinium* sp.
Cyst of *Protoperidinium* spp.	*Protoperidinium* spp.
Islandinium brevispinosum	*Protoperidinium* sp. indet.
Islandinium spp.	*Protoperidinium* spp.
Lejeunecysta sabrina	?*Protoperidinium leonis*
Quinquecuspis concreta	*Protoperidinium leonis*
Selenopemphix nephroides	*Protoperidinium subinerme*
Selenopemphix quanta	*Protoperidinium conicum*
Stelladinium reidii	*Protoperidinium compressum*
Stelladinium -Type A *(?stellatum)*	*Protoperidinium* sp.
Votadinium calvum	*Protoperidinium oblongum*

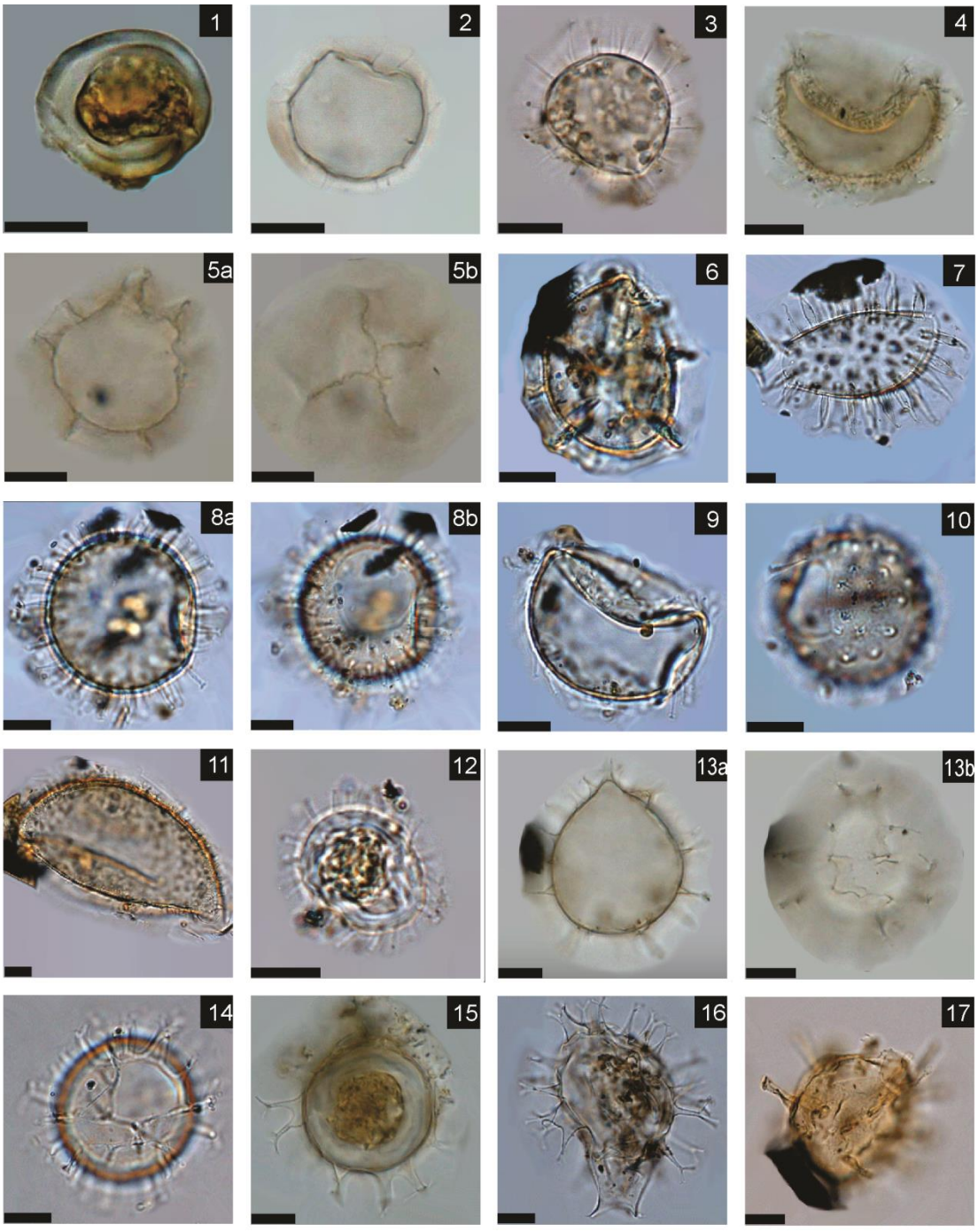

Plate 2-IV. Cyst of *Alexandrium* sp., 2–3. Cysts of cf. *Biecheleria* spp., 4. *Bitectatodinium spongium*, 5–6. *Impagidinium strialatum*, 7. *Lingulodinium hemicystum*, 8. *Operculodinium centrocarpum*, 9. *Operculodinium*-Type B, 10. *Operculodinium* cf. *janduchenei*, 11. *Operculodinium israelianum*?, 12. Cyst of *Pentapharsodinium dalei*, 13. *Spiniferites bentorii* (intergonal type), 14. *Spiniferites hyperacanthus*, 15. Spiniferites-type D-*ramosus*? 16. *Spiniferites mirabilis*, 17. *Achomosphaera* sp. The scale bars are 10 μm.

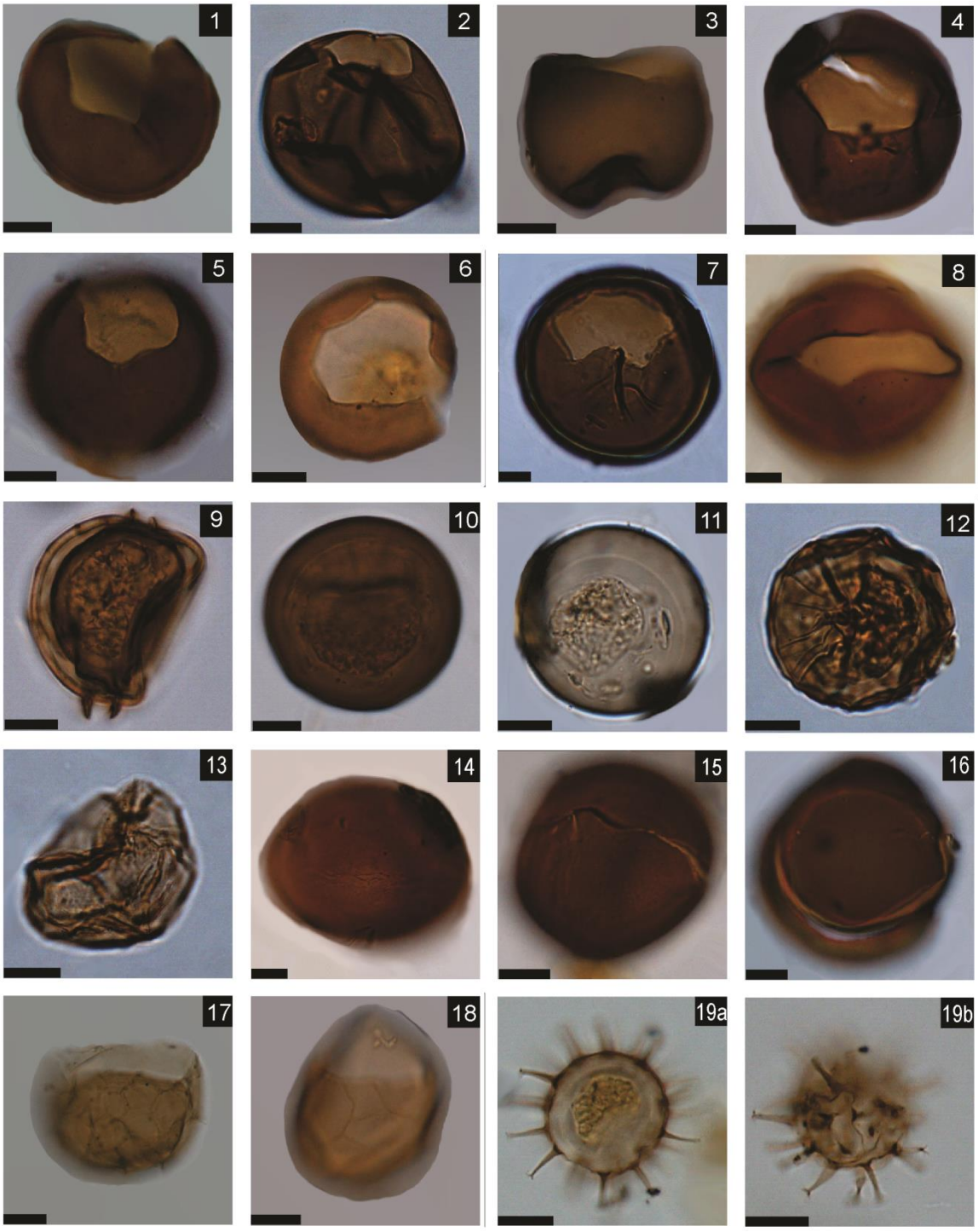

Plate 2-V. 1–2. *Brigantedinium simplex*, 3–4. *Brigantedinium*-type A, 5–6. *Brigantedinium cariacoense*, 7–8. *Brigantedinium irregulare*, 9. *Protoperidinium* sp., 10–13. *Brigantedinium*

spp., 14–16. *Dubridinium cavatum*, 17–18. *Cryodinium* cf. *meridianum*, 19. *Echinidinium aculeatum*. The Scale bars are 10 μm.

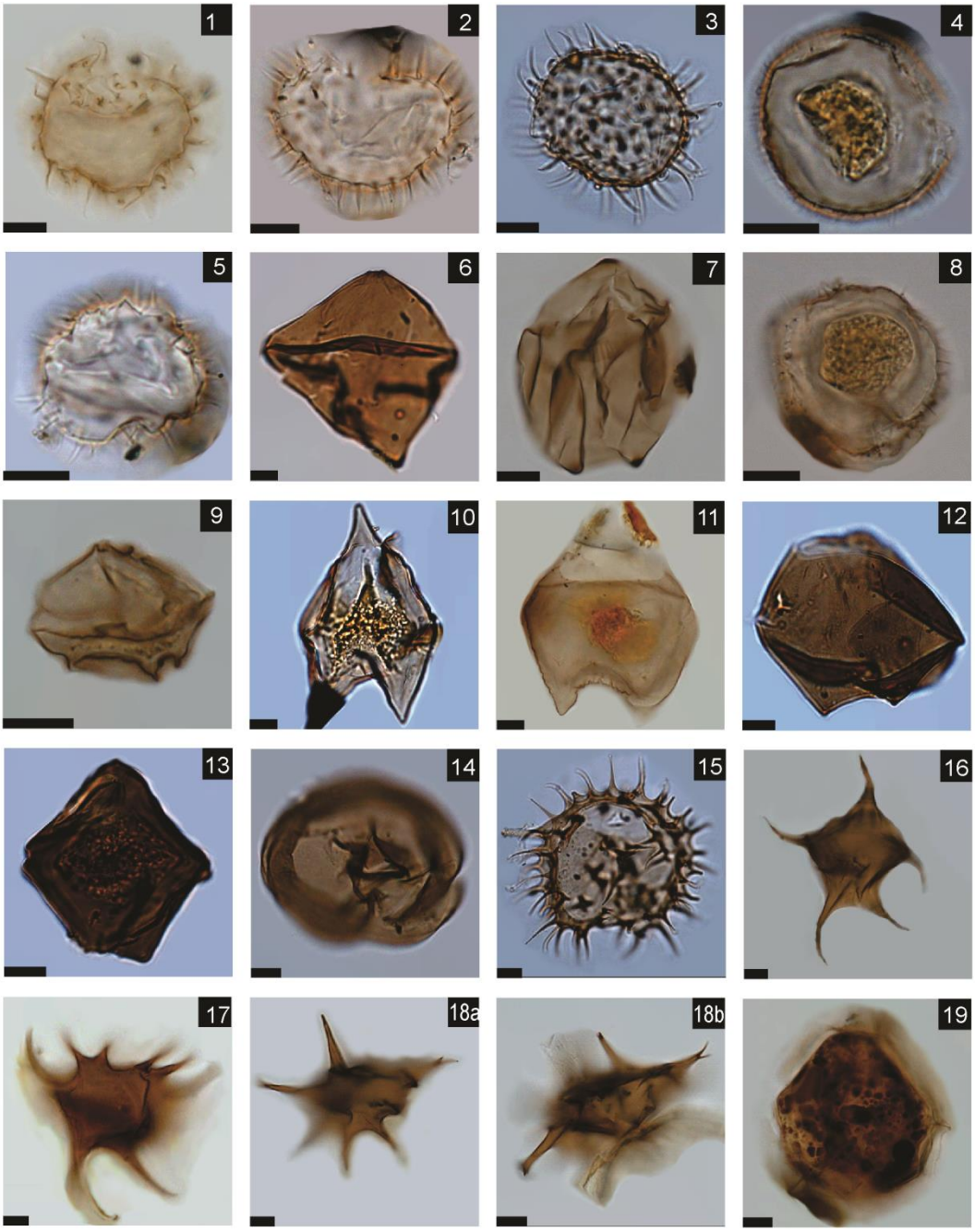

Plate 2-VI. 1–2. *Echinidinium transparantum*, 3. *Echinidinium* sp., 4. *Islandinium? brevispinosum*, 5. *Islandinium* sp., 6–7. *Lejeunecysta? sabrina*, 8. Cyst of *Protoperidinium*-type A, 9. Cyst of *Protoperidinium* sp., 10–11. Cysts of *Protoperidinium oblongum*, 12. *Quinquecuspis*? *concreta*, 13. *Quinquecuspis* sp.? 14. *Selenopemphix nephroides*, 15.

Selenopemphix quanta, 16. *Stelladinium reidii*, 17–18. *Stelladinium*-Type A, 19. *Protoperidinium* sp. The Scale bars are 10 μm.

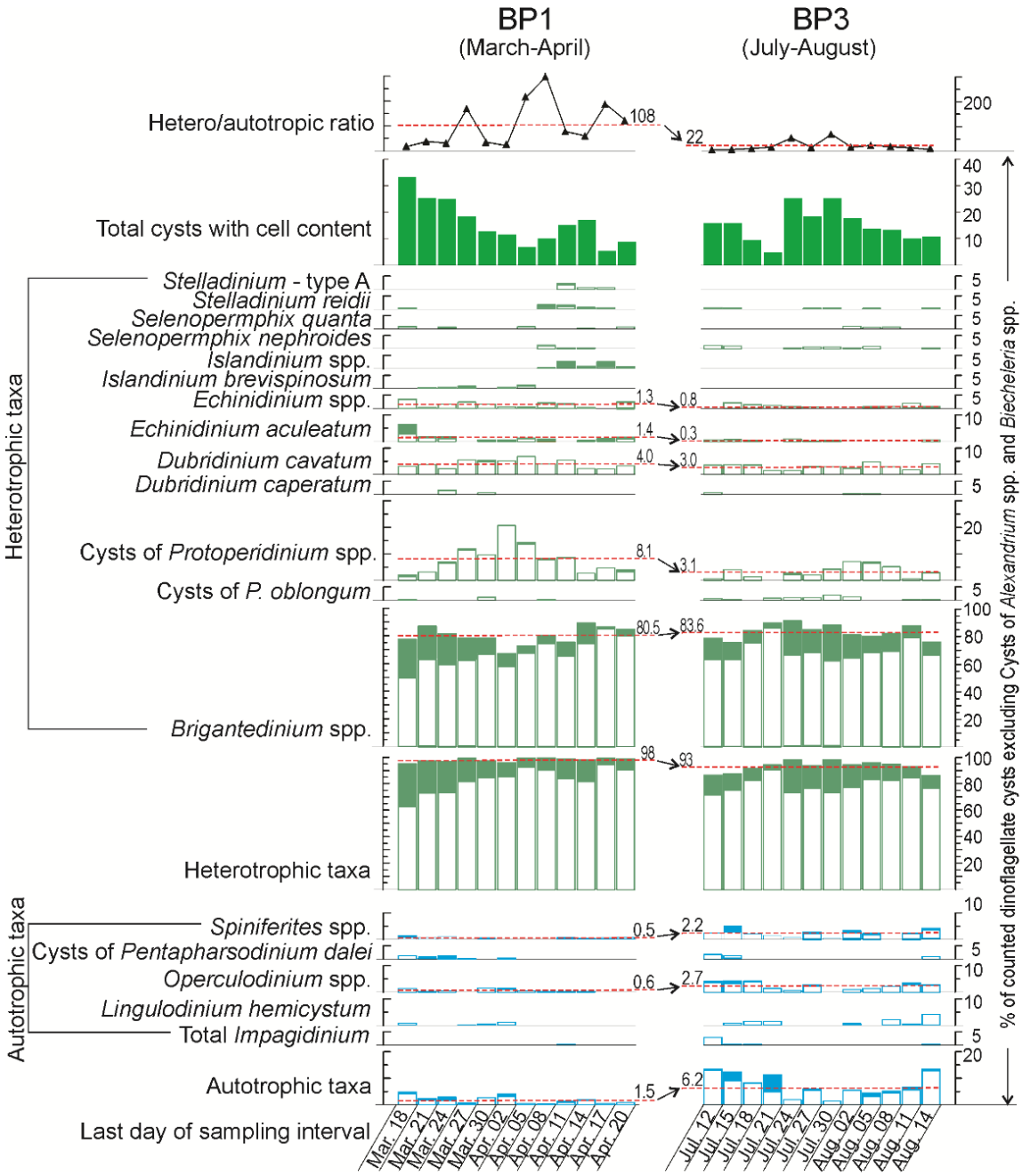

Figure 2-5. Percentages (%) of selected dinoflagellate cyst taxa and the ratio of heterotrophic to autotrophic taxa from sediment traps BP1 (March 18–April 20, 2010) and BP3 (July 12–August 14, 2010). Heterotrophic taxa are shown in green and autotrophic taxa are in blue. Filled bars show cysts with cell content. The red dashed lines and numbers show average values.

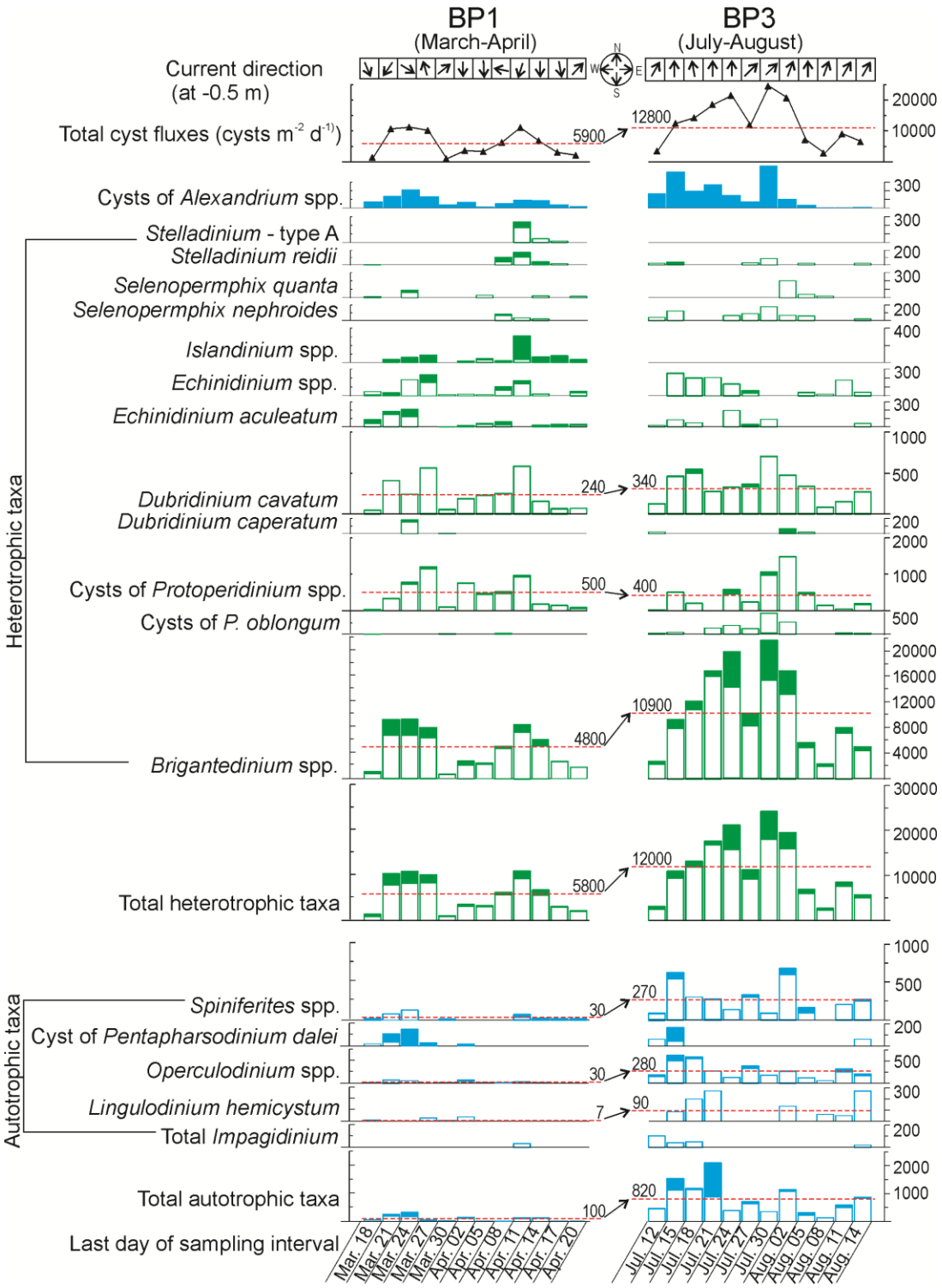

Figure 2-6. Fluxes of total and selected dinoflagellate cyst taxa from sediment traps BP1 (March 18–April 20, 2010) and BP3 (July 12 – August 14, 2010), and current direction at -0.5m depth. Heterotrophic taxa are shown in green and autotrophic taxa are in blue. Filled bars showcystswith cell content. The red dashed lines and numbers show average values.

(~ 1.8%). Other autotrophic taxa only accounted for <1% of the assemblages. The ratio of heterotrophic to autotrophic taxa decreased to ~22 in July–August (Figure 2-5).

The total fluxes of dinoflagellate cysts ranged from 990 cysts m^{-2} d^{-1} to 24,540 cysts m^{-2} d^{-1}, with averages of ~5900 cysts m^{-2} d^{-1} in March–April and ~12,800 cysts m^{-2} d^{-1} in July–August (Figure 2-6). The fluxes of total autotrophic taxa in July–August are much higher than those in March–April. The fluxes of *Spiniferites* spp., *Operculodinium* spp., and *L. hemicystum* averaged at ~30, 30, and 7 cysts m^{-2} d^{-1} in March–April, respectively, then increased to ~270, ~280, and ~90 cysts m^{-2} d^{-1} in July–August. The total fluxes of heterotrophic taxa in July–August were more than double those in March–April, mainly contributed by *Brigantedinium* spp. with average fluxes of ~10,900 cysts m^{-2} d^{-1} in July–August while ~5800 cysts m^{-2} d^{-1} in March–April. Cysts of *Alexandrium* spp. had the highest fluxes in July and the lowest in August (Figure 2-6).

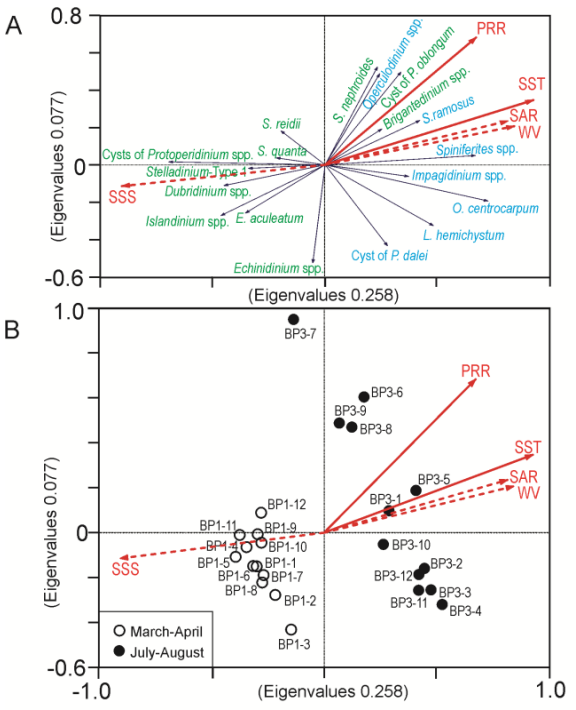

Figure 2-7. Redundancy Analysis performed on relative abundances (%) of dinoflagellate cysts (>1%) and environmental parameters. PRR: Pearl River runoff; SST: sea-surface temperature, SSS: sea-surface salinity, WV: water velocity, SAR: sedimentary accumulation rates. Ordination diagram showing species scores (7A) and sample scores (7B). 7C. Marginal effects, conditional effects and summary of RDA axes statistics. P-values <.05are statistically significant and highlighted in bold. Lambda (Λ) is the variation explained by each environmental variable, considered independently (marginal effect), or considered after all variables already incorporated in the model (conditional effect).

The first axis of RDA, using square root transformation of the relative abundances, explained 25.8% of the variance, whereas the second axis explained only 7.7% (Figure 2-7C). The first ordination axis was positively correlated with SST, PRR, WV and SAR, whereas it was negatively correlated with SSS (Figure 2-7A). Monte Carlo permutation tests indicated that SST was the most statistically significant environmental parameter (P=.002), followed by PRR (P = .002) (Figure 2-7C).

The highest scores of RDA axis 1 were found for autotrophic *O. centrocarpum* and *Spiniferites* spp. (Figure 2-7A). Most of the heterotrophic taxa were positioned on the negative side of axis 1, except for *Brigantedinium* spp., cysts of *Protoperidinium oblongum*, and *Selenopemphix nephroides* (Figure 2-7A). Samples with the positive scores on axis 1 were those collected in July–August, except for BP3–7 (Figure 2-7B). The lowest scores were obtained for samples collected in March–April (Figure 2-7B).

2.4 Interpretation and discussion

2.4.1 Seasonal factors for terrestrial palynomorph distributions

2.4.1.1 Pinus pollen

In this study, *Pinus* pollen in sediment trap samples were clearly dominant in terrestrial palynomorph assemblages, which is in line with findings from many studies examining terrestrial palynomorphs in surface sediment (e.g., Sun et al., 1999; Luo et al., 2013, 2014, 2016; Dai et al., 2014) and sediment core samples from the SCS (e.g., Sun and Li, 1999; Li et al., 2010, 2017; Dai and Weng, 2015; Dai et al., 2015). Modern plants of Pinus species surrounding the SCS (e.g., *Pinus fenzeliana*, *Pinus massoniana*, and *Pinus roxburghii*) are widely distributed in southern China, as well as highlands of

southeastern China (Figure 2-8) (Wu, 1980; Fu, 2012). *Pinus taiwanensis* occurs dominantly at high altitudes of ~1900–3600 m in the southwest of Taiwan Island, and the southernmost distribution in mainland China is Daiyun Mountain (Lin, 1990; Sheue et al., 2000, 2003; Li et al., 2013; Chen et al., 2016) (Figure 2-8). Most *Pinus* species produce pollen in March–April (Table 2-6) (Fu, 2012), when northern winter monsoons are dominant (Figure 2-3). Higher abundances of *Pinus* pollen in the SCS have been attributed to the greater *Pinus* pollen transport by northeastern winds from the mainland

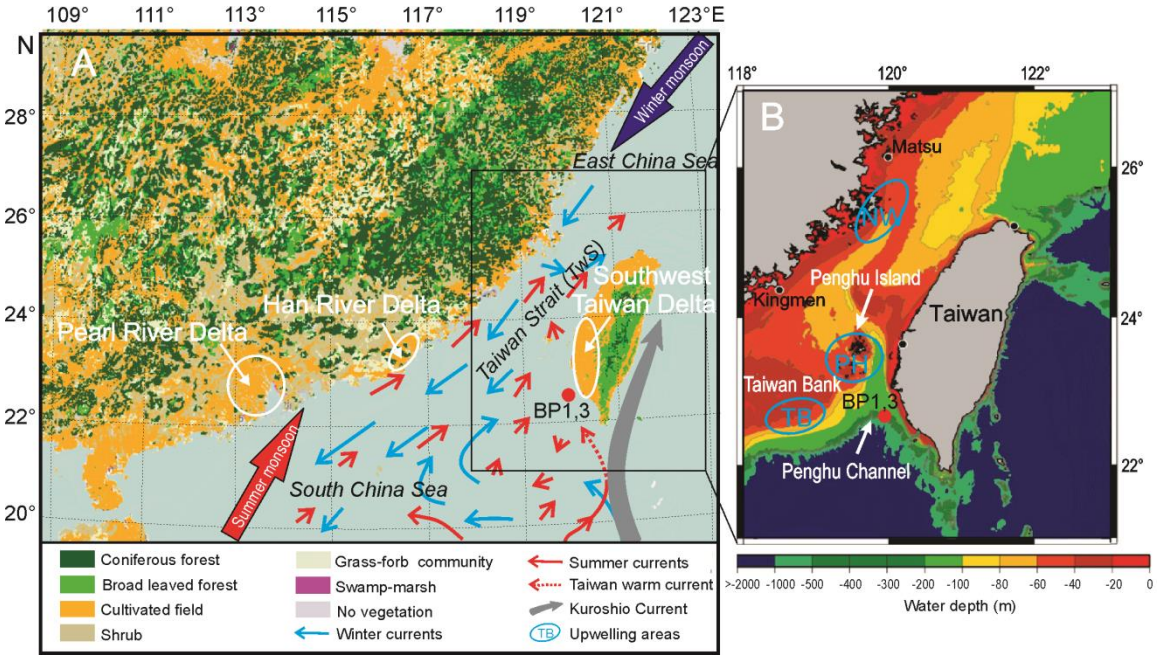

Figure 2-8. (A) Surrounding vegetation distribution of the research area and the patterns of seasonal monsoons, surface currents, and main river delta plains (modified from http://www.nsii.org.cn/ mapvege). 8B. Bathymetric patterns of the Taiwan Strait and the upwelling areas. TB: Taiwan Bank Upwelling, PH: Penghu Upwelling, NW: Northern upwelling (modified from Hong et al., 2011; Chen et al., 2016).

of China or Taiwan in winter (Sun et al., 1999; Zheng et al., 2011; Luo et al., 2016). However, *Pinus* pollen could also be concentrated to a higher relative abundance by intensified water sorting effects in summer, since they are likely transported by flotation

to much longer distances than other pollen types, and more *Pinus* pollen than other types deposit offshore (e.g., Florin, 1963; Heusser, 1988; Duplessy et al., 2001; Li et al., 2008, 2010; Dai et al., 2014). In this case, the flux would become reduced with distance from the production sources, whereas the relative abundances would increase. Luo et al. (2016) suggested that the distribution of *Pinus* was dominantly influenced by rivers near shore, but more controlled by winds offshore. Our data show that the relative abundances and fluxes of *Pinus* pollen in March–April were both higher than those in July–August (Figures 2-2 and 2-3, Table 2-6). The negative relationship with PRR and the positive relationship with SSS (Figure 2-4) reflect the dilution effect on *Pinus* pollen in sediments by fluvial inputs, rather than relative enrichment. This conclusion is supported by the negative relationship between the *Pinus* relative abundance and SAR (R2=0.602, P< .001) (Figure 2-9A), which indicates wind-dominated transportation of *Pinus* pollen with dilution effects by high sedimentation rates (e.g., Xu et al., 2005; Beaudouin et al., 2007). The greater PRR in summer can cause a decrease in SSS and an increase in SAR, reflected by a significant positive relationship between PRR and SAR, whereas a negative relationship between PRR and SSS. Therefore, the main factor underlying the *Pinus* pollen distribution patterns in the study area should be the winter monsoons, rather than the summer water transport.

2.4.1.2. Dominant broad-leaved AP

Nowadays, around the study area, broad-leaved forests grow in the uplands of Taiwan and southeast of China (Figure 2-8). Broad-leaved forests cover larger areas in Taiwan Island than coniferous forests. However, broad-leaved pollen showed under-representative among the pollen assemblages from marine sediments in both March–

Table 2-6. Potential monsoon indicators of key terrestrial palynomorph taxa, their dominant species of plants, and the relationship with environmental parameters (Wu, 1980; Fu, 2001).

Taxa	Abundance (%)		Flux (grains m^{-2} d^{-1})		Correlated to Environment					Dominant species	Flowering period	Monsoon indicator	
	Winter	Summer	Winter	Summer	SSS	SAR	AT	PRR	MWS		(Month-Month)	Winter	Summer
Pinus	H	L	H	L	+	–	–	–	–	*P. fenzeliana*	3–4	Yes	No
										P. latteri	3–4		
										P. massoniana	3–4		
										P. roxburghii	3–4		
Quercus (including *Cyclobalanopsis* spp.)	H	L	L	H	+	–	–	–	–	*C. championii*	12–3	No	No
										C. longinux	3–5		
										C. morii	4–5		
										C. sessilifolia	4–5		
										C. stenophylloides	4–5		
										Q. engleriana	4–5		
										Q. fabri	4		
										Q. Phillyraeoides	3–4		
										Q. stewardii	3–4		
Alnus	L	H	L	H	–	+	+	+	+	*A. formosana*	Autumn-Spring	No	No
										A. trabeculosa	2–4		
Ulmus	H	L	H	L	+	–	–	–	–	*U. castaneifolia*	3–4	Yes	No
										U. lanceaefolia	2–4		
										U. uyematsui	3–4		
Myrica	H	L	H	L	+	–	–	–	–	*M. adenophora*	10–11	No	No
										M. esculenta	9–10		
										*M. rubra**	3–4		
Moraceae	H	L	H	L	+	–	–	–	–	*Antiaris toxicaria*	Spring	No	No
										*Artocarpus heterophyllus**	2–3		
										A. lanceolatus	4–5		
										Ficus altissima	3–4		
										F. micrccarpa	5–6		
										F. wightianna	4–6		
										*Fructus mori**	3–5		
Poaceae	L	H	L	H	–	+	+	+	+	*Arundinella anomala*	7–10	No	No
										Apocopis paleacea	Summer-Autumn		
										Cymbopogon caesius	7–9		
										Eriachne pallescens	5–10		

(to be continued)

(to continue)

Taxa	Abundance (%)		Flux (grains m^{-2} d^{-1})		Correlated to Environment					Dominant species	Flowering perioc (Month-Month)	Monsoon indicator	
	Winter	Summer	Winter	Summer	SSS	SAR	AT	PRR	WMD			Winter	Summer
										Eragrostis ciliata	8–11		
										Eremochloa ciliaris	Summer-Autumn		
										Eulalia speciosa	8–11		
										Imperata cylindrica	7–9		
										*Ischaemum indicum**	Summer-Autumn		
										Narenga porphyrocoma	8–10		
										Miscanthus floridulus	5–10		
										Miscanthus sinensis	8–9		
										*Oryza sativa**	/		
										Panicum repens	6–11		
										*Phyllostachys spp.**	5–8		
										*Saccharum officinarum**	/		
										Sinocalamus oldhami	Summer-Autumn		
										*Triticum aestivum**	/		
										*Vetiveria nigritiana**	Autumn		
										*Zea mays**	Autumn		
										*Zoysia matrella**	7–10		
Chenopodiaceae /Amaranthaceae	H	L	L	H	+	–	–	–	–	*Suaeda heteroptera*	7–8	No	No
										S. glauca	7–8		
Compositae	H	L	L	H	+	–	–	–	–	*Eupatorium odoratum*	4–12	No	No
										Ixeris repens	5–10		
Artemisia	L	H	L	H	–	+	+	+	+	*Artemisia spp.*	8–9	No	No
Cyperaceae	L	H	L	H	–	+	+	+	+	*Carex kobomugi*	6–7	No	No
										Cyperus distans	7–10		
										C. malaccensis	Summer		
										C. scabrifolia	4–7		
										Fimbristylis sericea	8–10	No	No
Typha	L	H	L	H	–	+	+	+	+	*Typha orientali*	5–8	No	No
Monolete spores	L	H	L	H	–	+	+	+	+	/	/	No	Yes
Trilete spores	L	H	L	H	–	+	+	+	+	/	/	No	Yes

Note:
SSS: sea-surface salinity, SAR: sedimentary accumulation rate, AT: atmosphere temperature, PRR: runoff of the Pearl River, MWS: daily mean wind speed.
L: lower, H: higher, +: positive relationship, –: negative relationship.

April and July–August. Only pollen of *Quercus*, *Myrica*, *Alnus*, Moraceae, and *Ulmus* have average relative abundances greater than 1% and fluxes greater than 100 grains m^{-2} d^{-1}; others only appeared occasionally or at very low values (Figures 2-2 and 2-3). In addition to the fact that *Pinus* pollen is transported a much longer distance than the pollen of broad-leaved trees, the different flowering periods would lead to different modes of seasonal dispersal of broad-leaved plant pollen.

Similar to Pinus pollen, the relative abundances and fluxes of *Myrica*, Moraceae, and *Ulmus* are lower in the July–August (Figures 2-2 and 2-3, Table 2-6). They also have a negative relationship with PRR and SAR, as well as a positive relationship with SSS (Figure 2-4, Table 2-6). In the surrounding vegetation, *Myrica* consists dominantly of species of *Myrica adenophora*, *Myrica esculenta*, and *Myrica rubra*. Only *M. rubra* blooms in March–April (Wu, 1980; Fu, 2012), whereas other species bloom in September–November when the southwest monsoon is dominant (Table 2-5). Our sediment trap data show high relative abundances and fluxes of *Myrica* pollen in the March–April. It can be explained by spring blooms of cultivated forests of *M. rubra* that are common economic fruits in the eastern provinces of China. Their pollen can be transported to the study site by northeastern monsoons or currents. However, without *Myrica* pollen data in the autumn, when the other two main species bloom, it remains uncertain if the winter monsoon controls main patterns of *Myrica* pollen distribution.

Moraceae pollen around the study area are produced by the dominant species of *Antiaris toxicaria*, *Artocarpus heterophyllus*, *Artocarpus lanceolatus*, *Ficus altissima*, *Ficus micrccarpa*, *Ficus wightianna*, and *Fructus mori* in spring or early summer (Table 2-6) (Wu, 1980; Fu, 2012). The high content of Moraceae pollen in March–April samples

could be a result of the widely cultivated vegetation of *Artocarpus heterophyllus* and/or *Fructus mori* in the south of China and Taiwan. Our data showed that the Moraceae pollen abundance was the highest in mid-late March, which is the main flowering period of *Artocarpus heterophyllus* and *Fructus mori*. Therefore, the pollen distribution of Moraceae was predominately affected by human cultivation activity rather than by monsoon transport.

The dominant species of *Ulmus* include *Ulmus castaneifolia*, *Ulmus lanceaefolia*, and *Ulmus uyematsui* in the modern vegetation of the south or southeast of China (Table 2-6) (Wu, 1980; Fu, 2012). These plants bloom from February to April when winter monsoon is dominant. The significantly negative relationships with PRR and SAR, together with the positive correlation to SSS, possibly indicate that the distribution of *Ulmus* pollen was predominantly associated with the winter monsoons. Similar to *Pinus* pollen, the high relative abundances and fluxes of *Ulmus* pollen are consistent with the strong winter monsoon effects.

In contrast, there were lower relative abundances of *Quercus* pollen in July–August than in March–April, whereas their fluxes were higher in July–August (Figures 2-2 and 2-3, Table 2-6). The pollen of *Cyclobalanopsis* spp. are often grouped into *Quercus* pollen as evergreen types. Their pollen sources not only include species of *Cyclobalanopsis championii*, *Quercus fabri*, *Quercus phillyraeoides* and *Quercus stewardii*, which flower in winter monsoon seasons (December – the following March or March–April), but also species of *Cyclobalanopsis loninux*, *Cyclobalanopsis morii*, *Cyclobalanopsis sessilifolia*, and *Quercus engleriana* with flowering periods in March–May that extend into early summer monsoon seasons (Table 2-6) (Wu, 1980; Fu, 2012).

Thus, the *Quercus* pollen have sources that are connected with both winter and summer monsoons. Sun et al. (1999) suggested that rivers probably control the *Quercus* distribution and result in the highest quantity in marine sediments off the mouth of the Pearl River. However, Dai et al. (2014) found that evergreen *Quercus* pollen were common in marine surface sediments, but scattered in the surface sediments of the Pearl River. They proposed that the dispersal of *Quercus* pollen have occurred in more than one path. The higher relative abundances in March–April and higher fluxes in July–August in the sediment traps can be associated with winter monsoon transport and greater river discharges in summer, respectively.

2.4.1.3 Herb pollen

Cultivated field and grass communities are widely distributed in coastal and/or delta plains of the south and southeast of China, as well as the southwest of Taiwan (Figure 2-8) (http://www.nsii.org.cn/mapvege). These plants are the primary sources of herb pollen in the northern SCS. In our study, herb pollen predominantly consists of Poaceae, Cyperaceae, Compositae, *Artemisia* and *Typha* (Figure 2-2). Most dominant species of these plants flower in the summer monsoon seasons (Table 2-5) (Wu, 1980; Fu, 2012). However, they clearly exhibit one of two temporal patterns: (i) their abundances and fluxes are both lower in March–April than in July–August, together with a positive relationship to PRR, SAR, AT, and MWS; (ii) their abundances are higher, but fluxes are lower in March–April than in July–August with a negative relationship with PRR, SAR, AT and MWS (Table 2-5).

The first pattern includes the pollen of Poaceae, *Artemisia*, Cyperaceae, and *Typha*, of which high abundances and fluxes resulted from a large number of pollen sources

yielded by the dominant species in summer monsoon seasons (Table 2-5) (Wu, 1980; Fu, 2012). Rivers probably controlled the dispersal of these types of pollen. The vegetation of coastal delta plains, including the Pearl River Delta, the Han River Delta and the Southwest Taiwan Delta, are predominantly cultivated fields (Figure 2-8). The cultivated fields with Poaceae plants, including *Ischaemum indicum*, *Oryza sativa*, *Phyllostachy* spp., *Saccharum officinarum*, *Triticum aestivum*, *Vetiveria nigritiana*, *Zea mays*, and *Zoysia matrella*, are widely distributed in river catchment or delta plain areas, along with plants of wetlands, such as *Typha orientalis*, *Carex kobomugi*, *Cyperus distans*, *Cyperus malaccensis*, and *Cyperus scabrifolia* (Table 2-6) (Wu, 1980; Fu, 2012). In summer, more water discharged by rivers (Table 2-2) transports these pollen grains from their source regions to the sea, leading to abundant herb pollen deposits in the study area. Since the sediment trap mooring site is in the proximity to the Southwest Taiwan Delta, which is formed by eight small rivers (Hsiung and Saito, 2017), it is likely this region is the major herb pollen source (Figure 2-8). In summer monsoon seasons, it has been reported that ~30% annual precipitation and periodically extremely heavy rains during typhoons in July–August enhance the water and sediment discharges of rivers from Taiwan (Liu et al., 2008; Kuo et al., 2010).

The southwest wind does not deliver pollen to the study site from their primary sources. The negative relationship of these pollen abundances with SSS indicates that fluvial inputs contribute more to their dispersals in water. Dai et al. (2014) also found that the highest contents of Poaceae and Cyperaceae pollen near the shore of the Pearl River were induced by effects from river plumes or coastal currents.

The second pattern consists of the pollen of Chenopodiaceae/Amaranthaceae and Compositae. Their fluxes rather than relative abundances match with the flowering periods of their dominant species of *Suaeda heteroptera*, *Suaeda glauca*, *Eupatorium odoratum*, and *Ixeris repens*. This disagreement in seasonal changes between relative abundances and fluxes may be induced by the combined effects of wind, currents, and rivers. Thus, they cannot contain information on winter and summer monsoons.

2.4.1.4 Fern spores

Most ferns generally grow in moist or shady areas, such as under the forest canopy, along creeks or streams, and in other areas with permanent moisture. Their seasonal patterns of spore producing are not so notable as pollen producing of angiosperms. However, they are transported predominantly by rivers. In summer monsoon seasons, intensified fluvial flow can transport more fern spores from their sheltered sources and deliver them over longer distances than in winter monsoon seasons. Studies have shown that it is very common for fern spores to have relatively high relative abundances in marine sediments because of longer transport distances by flotation than non-saccate pollen types (e.g., Heusser, 1988; van Waveren 1989; Sun et al., 1999; Duplessy et al., 2001; Li et al., 2008, 2010; Dai et al., 2014; Dai and Weng, 2015). Our data reflect the seasonal differences in the fern spore distributions in marine environments (Figures 2-2 and 2-3). The higher relative abundance and fluxes in July–August than in March–April strongly support the intensified fluvial transport of fern spores (Table 2-5). The positive relationship between the abundance of fern spores and SAR (R^2 =0.436, P < .001) (Figure 2-9B) is quite different from the dilution effect on Pinus pollen (Figure 2-9A). The results that the relative abundances of spores are negatively correlated with SSS and positively

related to PRR (Figure 2-4) can be interpreted as follows: the greater amount of water discharges by the Pearl River, which is the largest river in the southern China, and its plume intrudes into the Penghu Channel (Figure 2-8) (Bai et al., 2015), together with other rivers in Southwest Taiwan. This freshwater input reduces SSS during the summer monsoon seasons and delivers more fern spores over longer distances.

2.4.2 Factors affecting marine dinoflagellate cyst distribution and PP

Dinoflagellate cyst fluxes and assemblages reflect PP, and their abundances increase in upwelling regions (e.g., Dale, 1996; Pospelova et al., 2008; Zonneveld et al., 2010, 2013; Bringué et al., 2013; Pospelova et al., 2018). Our data show that the total dinoflagellate cyst fluxes in July–August are almost twice as high as those in the March–April, and they are positively correlated with SAR (R^2 = 0.411, P = .001) (Figure 2-9C). The increases in SAR in summer are due to the greater increase of terrestrial inputs by rivers, as also seen in the increased fern spore abundances. However, along with terrigenous particles, rivers also deliver nutrients, that in turn affect marine PP. This can be supported by records of elevated values of chl-a in July (https://neo.sci.gsfc.nasa.gov/view.php?datasetId=MY1DMM_CHLORA). The higher fluxes of total and most dinoflagellate cyst taxa are likely related to the greater PP in the summer (Figure 2-6). Lin (2014) observed that chl-a (fluorescence) concentrations were higher in July than in March 2010 in our study area. It should be noted that PP varies seasonally and spatially in the Taiwan Strait. Naik and Chen (2008) documented that in the southern Taiwan Strait, high PP occurs in summer with the maximum in the upwelling areas of Penghu and the Taiwan Bank near our study area, whereas in the northern strait, the highest PP occurs near shore in March–April (Figure 2-8B). Hong et al. (2011) ascribed this pattern

to different nutrient inputs from various water masses. The elevated nutrient supply by rivers in summer (e.g., Chen and Chen, 2006; Pan et al., 2018) might be the main cause of the higher PP shown by increases in dinoflagellate cyst production. Our data showed that the SAR in July–August was nearly five times greater than those in March–April. This finding is further supported by the positive relationship of the total fluxes of terrestrial palynomorphs and dinoflagellate cysts (R^2 =0.716, P < .001) (Figure 2-9D). As discussed in Section 4.1, the increased flux and relative abundance of *Pinus* pollen is a good indicator of the winter monsoon, and the flux and abundance of fern spores are firmly associated with the summer river runoff. We found that the total dinoflagellate cyst fluxes have a stronger positive relationship with the fern spore fluxes (R^2 = 0.633, P < .001) than with the *Pinus* fluxes (R^2 =0.166, P = .048) (Figure 2-9E and F), implying that fluvial discharges in summer significantly affect dinoflagellates and their cysts at the site. Bai et al. (2015) reported that nutrients introduced by the intrusion of the Pearl River plume, together with the runoff from small rivers in Taiwan, can cause phytoplankton blooms in the area.

Upwelling also introduces nutrients from the deeper to the upper waters and results in the increase in PP in Penghu and Taiwan Bank upwelling areas (Figure 2-8). The Penghu and the Taiwan Bank upwelling systems are relatively persistent, less influenced by monsoon winds, and mainly controlled by the interaction of bottom topography and the year-round northward water flow (Hong et al., 2011). In summer, the southwest monsoon drives the SCS water flow out of the SCS basin and weakens the Kuroshio Current intrusion in the northern SCS (Figure 2-8) (e.g., Liang et al., 2008). The Kuroshio Current loop appears southwest of Taiwan less frequently than during the other

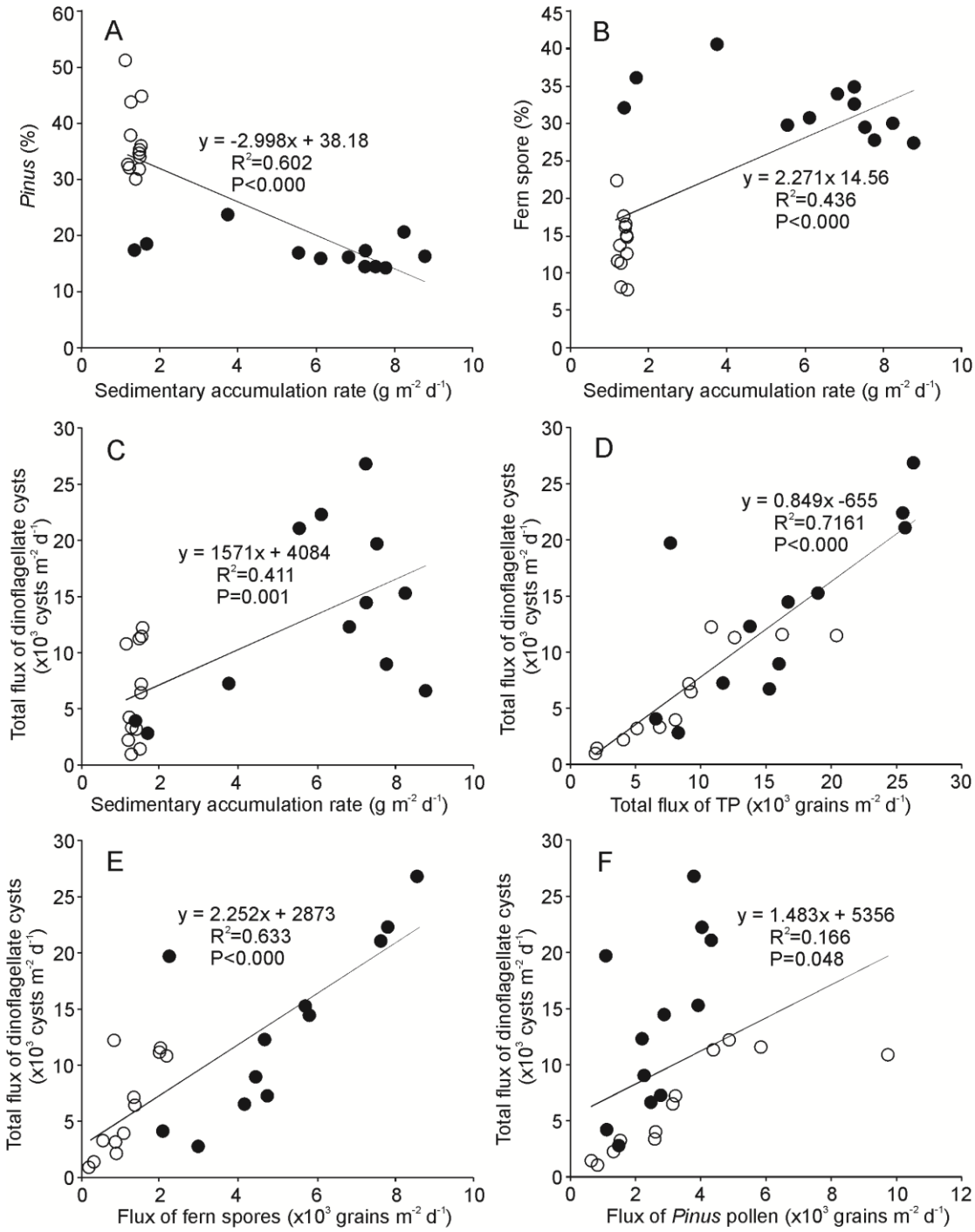

Figure 2-9. Scattered charts of (A) *Pinus* pollen (%) vs. sedimentary accumulation rate, (B) fern spore (%) vs. sedimentary accumulation rate, (C) total flux of dinoflagellate cysts vs. sedimentary accumulation rate, (D) dinoflagellate cysts vs. total flux of TP (terrestrial palynomorphs), (E) dinoflagellate cysts vs. flux of fern spores and (F) dinoflagellate cysts vs. flux of *Pinus* pollen. Circles marked the data from spring samples and black dots marked the data from summer samples.

seasons (e.g., Wyrtki 1961; Shaw 1991; Nan et al., 2011). The reduced influence of the Kuroshio Current could cause a decrease in water stratification. Therefore, it is likely that greater river discharges favor phytoplankton blooms, while the year-round stable upwelling and the weakened water stratification from the Kuroshio Current could not induce the blooms.

Heterotrophic taxa are known to be more abundant in some coastal areas of elevated PP (e.g., Dale, 1996; Zonneveld and Brummer, 2000; Marret and Zonneveld, 2003; Radi and de Vernal, 2004; Radi et al., 2007; Pospelova et al., 2008; Pospelova and Kim, 2010; Kimet al., 2012; Zonneveld et al., 2013; Heikkilä et al., 2014). The ratio between heterotrophic and autotrophic taxa is commonly considered as an indicator of coastal proximity or PP (e.g., Harland, 1983; Dale, 1996; Mudie and Rochon, 2001; Pospelova et al., 2008). An increased ratio of heterotrophic to autotrophic taxa has been commonly used as an indicator of elevated nutrients (e.g., Dale et al., 1999, Dale, 2001, 2009; Matsuoka, 2001). Our results show that is not always the case. The ratio of heterotrophic to autotrophic taxa in July–August was only one-fifth of that in March–April, although PP was much higher during that time than in March–April, as reflected by the increases in fluxes of both heterotrophic and autotrophic taxa (Figures 2-5 and 2-6). The lower ratios could be induced by the increases in the autotrophic taxa of *L. hemicystum*, *Operculodinium* spp., and *Spiniferites* spp. Their relative abundances were ~5 times greater than those in the March–April, and their fluxes reached up to ~10 times of those in March–April. The relative abundances of *Brigantedinium* spp., the dominant taxon among heterotrophic taxa, only slightly increased during July–August and it doubled in fluxes in March–April. The reason that autotrophic taxa increased more than

heterotrophic taxa is likely due to more light availability, since light reaches greater depth in summer than in winter. Lin (2014) reported that high chl-a concentration layer was at the depth from ~50 m to 90 m (with the maxima at ~60–70 m) in July, and at the depth from 60 to 70 m (with the maxima at 60m) in March in 2010.

Autotrophic taxa such as *O. centrocarpum*, *Spiniferites* spp., *L. hemicystum*, *Impagidinium* spp., and cysts of *Pentapharsodinium dalei* were recorded with higher relative abundances during July–August. However, even their highest fluxes (6–7 × 102 cysts m^{-2} d^{-1}) are generally much lower than those observed from other regions. For example, averages of 1–6 × 10^4 cysts m^{-2} d^{-1} were reported in coastal water (e.g., Omura Bay in West Japan, Fujii and Matsuoka, 2006; the Strait of Georgia, Pospelova et al., 2010; the Santa Barbara Basin of California, Bringué et al., 2013; Hudson Bay, Heikkilä et al., 2014) and 1–9 × 10^6 or ×10^7 cysts m^{-2} d^{-1} in inlets or inner seas (e.g., the Gulf of Naples of the Mediterranean Sea, Montresor et al., 1998; Gamak Bay in Korea, Shin et al., 2012). This finding can be explained by the rather low PP in many tropical regions, as shown by very low total cyst concentrations in both sediment trap samples and surface sediments from the coast of India (e.g., D'Costa et al., 2008; Narale et al., 2013; Narale and Anil, 2017; Uddandam et al., 2017) and in the SCS (Wu and Sun, 2000; Kawamura, 2004).

Our data also revealed that the relative abundances of individual autotrophic taxa have a negative relationship with SSS, whereas they were positively related to SST, PRR, WV, and SAR (Figure 2-7). However, only SST and PRR were statistically significant (P = .002). Conversely, almost all the heterotrophic taxa were negatively related to SST and PRR, except for *Brigantedinium* spp., cysts of *P. oblongum*, and *S. nephroides* (Figure 2-

7). Many sediment trap studies have documented that *Brigantedinium* spp. increases in abundance during or immediately after elevated phytoplankton production due to increased nutrient supply from upwelling or input of rivers (e.g., Zonneveld and Brummer, 2000; Godhe et al., 2001; Fujii and Matsuoka, 2006; Bouimetarhan et al., 2009; Zonneveld et al., 2010; Pospelova et al., 2010; Bringué et al., 2013). In our study area, the high discharges from the Pearl River and other small rivers from the southwest of Taiwan might play a much more important role compared with other factors. *Spiniferites* spp. and *O. centrocarpum*, the most dominant autotrophic taxa, were usually found when SSS were reduced due to the greater river discharges.

This result is in line with findings of the comparative review of *Spiniferites* spp. production in sediment traps from different geographic regions by Pospelova et al. (2018). They found that the timing of elevated total *Spiniferites* fluxes usually coincides with intervals of local seasonal environmental change at sites that are not directly affected by turbid river waters.

2.5 Conclusions

To determine seasonal abundances of terrestrial pollen and spores, as well as marine dinoflagellate cysts along with factors controlling their distributions (such as monsoons), we performed the study of March–April and July–August sediment trap samples from the southwestern waters of the Taiwan, SCS. Our study shows that both terrestrial palynomorphs and dinoflagellate cysts were much more abundant in July–August than in March–April. *Pinus* pollen were most dominant in terrestrial palynomorphs, and their highest abundance in March–April was attributed to the strong winter monsoon, which transports *Pinus* pollen from the south of China and Taiwan Island to the SCS. The

positive relationship between the *Pinus* pollen abundances and SSS, as well as the negative correlation to SAR, reflected the wind-dominated effects on the *Pinus* distribution. Therefore, *Pinus* pollen can be used as indicators of winter monsoons in the SCS area. In contrast, the fluxes and abundances of fern spores increased in July–August and were negatively correlated with SSS that decreased in summer due to the greater river runoff. The positive relationship between relative abundances of fern spores and SAR corresponds to the enriching effects of flotation, a transport mode of fern spores. Thus, it is reasonable to correlate the high content of fern spores in sediments with strong summer monsoons due to the higher river discharges.

The dispersal and depositional factors associated with broad-leaved AP varied among individual types. Pollen of *Quercus*, *Myrica*, Moraceae and *Ulmus* were dominant components of broad-leaved AP. The distribution of *Quercus* pollen did not exhibit a strongly seasonal pattern, with slightly higher relative abundances and slightly lower fluxes in March–April. This could be explained by different blooming periods of different *Quercus* species. Moreover, in association with the transport by wind and water, *Quercus* pollen appeared to be not reliable indicators of winter and summer monsoons. *Myrica* and Moraceae pollen decreased in fluxes and relative abundances in summer, and they were negatively correlated with AT. These tree species are planted widely for economically essential fruits. Thus, they are not reflective of seasonal monsoon patterns because their pollen distributions are markedly interrupted by the modern agricultural industry. The pollen distribution of *Ulmus* was mainly associated with winter monsoons. Thus, they can be used as a supplementary index for winter monsoons because they usually are rare or found at low levels in sedimentary pollen assemblages.

Pollen of Poaceae, *Artemisia*, Cyperaceae and *Typha* in the NAP all had higher individual fluxes and abundances in July–August, and they were positively correlated to PRR and negatively to SSS. Cultivated fields and river transport played major roles in their distributions.

The fluxes of dinoflagellate cysts in July–August were much higher than those in March–April with the averages of ~12,800 cysts m^{-2} d^{-1} and ~5900 cysts m^{-2} d^{-1}, respectively. In contrast to terrestrial palynomorphs transported from land, the abundances of marine dinoflagellate cysts were mainly influenced by the river discharges, as marine PP is strongly associated with the river water inputs in the SCS. This pattern was reflected by the significant positive relationship of the total dinoflagellate cyst fluxes with the fluxes of both terrestrial palynomorphs and fern spores, whereas there was no significant correlation with the *Pinus* pollen flux. The results of RDA also show that the relative abundances of *Brigantedinium* spp. and the dominant taxon of dinoflagellate cysts was significantly positively correlated with PRR and SST.

Dinoflagellate cyst assemblages were characterized by high abundances of *Brigantedinium* spp. ranging from 68% to 91%, with slightly higher averages in July–August than in March–April. The fluxes of *Brigantedinium* spp. in July–August doubled those in March–April. The abundances of the autotrophic taxa were very low in general, from the average of 1.5 to 6.2%, but the amplitude of increases in July–August was much higher than it was for heterotrophic taxa. In July–August, *Impagidinium* spp., *Operculodinium* spp., and *Spiniferites* spp., the major autotrophic taxa, increased to about five times of their relative abundances and ~10 times of their fluxes in March–April. The

higher amplitude of increases in autotrophic taxa was probably caused by greater light availability in July–August than in March–April.

This is the first sediment trap study to document seasonal terrestrial palynomorph and dinoflagellate cyst production in the SCS. Our data provide insights on the specific terrestrial palynomorph taxa relevant to the specific environmental parameters, such as winter or summer monsoons, and environmental preferences of dinoflagellate cyst taxa in the SCS. We identified that the relative abundances or fluxes of *Pinus* or *Ulmus* pollen are positive indicators of winter monsoons, and the fern spores and fluxes of dinoflagellate cysts are strongly associated with the greater river discharges during July–August. The pollen of Poaceae and *Myrica* reflect agriculture activities rather than monsoons. However, to apply EASM or EAWM palynological indicators for paleo-reconstructions, and to understand more detailed SAM influences on individual taxa of dinoflagellate cysts and their assemblages, a study of annual and/or multiannual time series at multiple sites in the SCS would be the priority for future research.

Acknowledgements

The Natural Sciences and Engineering Research Council of Canada (NSERC) CGS D3 fellowship (CGSD3-475098-2015) and Montalbano scholarship provided partial funding for this research to Z. Li. This work was also funded by NSERC through a Discovery grant (RGPIN/6388-2015) to V. Pospelova. She is the Hanse-Wissenschaftskolleg (HWK) senior research fellow in marine and climate research at the Institute for Advanced Study (Germany). H.-L. Lin was supported by the Ministry of Science and Technology Grants of Taiwan (NSC 98–3114–E–006–014 and NSC 99–2611–M–110–006). L. Liu was partially supported by the National Program on Global

Change and Air-Sea Interaction (GASIGEOGE- 05) from the State Oceanography Administration of China in this work, and B. Song and W. Gong were supported by Chinese Natural Science Foundation Projects of No. 41506103 and No. 51761135021, respectively.

Chapter 3

Dinoflagellate cyst distribution in surface sediments from the South China Sea in relation to hydrological conditions

Abstract

The geographical distribution of dinoflagellate cysts was investigated in the South China Sea (SCS) to understand environmental factors controlling their distributions in the region and to identify taxa associated with specific environmental parameters. The western SCS generally has higher total cyst concentrations (>300 cysts g^{-1}) than the eastern region (<200 cysts g^{-1}). Four high cyst concentration areas have been observed off southern Vietnam, Borneo, Hainan, and South China. The highest concentrations (>1000 cysts g^{-1}) occur off southern Vietnam, whereas the lowest cyst concentrations are found off Luzon. The ratio of heterotrophic to autotrophic taxa has distributional patterns opposite to the total cyst concentrations, induced by greater increases in autotrophic taxa than in heterotrophic cyst taxa abundances when nutrients increase.

Cysts produced by heterotrophic dinoflagellates, *Brigantedinium* spp., *Selenopemphix nephroides*, and *Selenopemphix reidii*, have similar distributional patterns and their highest relative abundances and concentrations are in the region off Borneo. Their concentrations are significantly positively correlated with sea-surface temperature in January (SST-Ja) and sea-surface salinity in July (SSS-Ju) that are associated with weak winter and summer monsoons, respectively. In contrast, concentrations of *Spiniferites* spp., *Spiniferites hyperacanthus*, *Spiniferites mirabilis*, *Spiniferites ramosus*, *Tuberculodinium vancampoae* and *Operculodinium longispinigerum* are negatively

correlated with SST-Ja and SSS-Ju. Total *Impagidinium*, *Impagidinium aculeatum*, *Impagidinium paradoxum*, *Impagidinium patulum*, *Nematosphaeropsis labyrinthus*, and *Polysphaeridium zoharyi* are positively correlated with water depth and distance to the coastlines. Their high abundances are found in the northern slope-deep basin that is under the Kuroshio Current influences, and this assemblage indicates an open-ocean environment. *Echinidinium* spp., *Selenopemphix undulata*, cysts of *Protoperidinium* spp., cysts of *Protoperidinium oblongum*, *Quinquecuspis concreta* and *Selenopemphix quanta* are positively correlated with chlorophyll-*a* (chl-*a*) concentrations and found in the regions of high primary productivity. These individual taxa are correlated with specific environmental parameters and can be used for the reconstructions of past monsoon climate events, the history of Kuroshio Current influence and paleo-primary productivity.

3.1 Introduction

Dinoflagellates are one of the major groups of modern marine plankton (e.g., Delwiche, 2007). During their life cycle, many dinoflagellates produce resting cysts that are resistant to physical, chemical, and biological degradation of organic walls (e.g., Dale, 1996). Distributions of modern dinoflagellate cysts in marine environments are controlled by the SST, SSS, marine primary productivity (PP), sea-ice cover, and other oceanographic conditions (e.g., Harland, 1983; Dale, 1996; Rochon et al., 1999; de Vernal et al., 2001, 2005; Marret and Zonneveld, 2003; Pospelova et al., 2005, 2008; Zonneveld et al., 2013). Therefore, being preserved in sediments, organic-walled dinoflagellate cysts are commonly used as indicators of past environmental conditions (e.g., Harland, 1973; Lewis et al., 1990; Edwards et al., 1991; Eshet et al., 1994; Rochon et al., 1999; Head et al., 2001; Mudie and Rochon, 2001; Mohamed et al., 2013; Olde et

al., 2015; Li et al., 2017; Uddandam et al., 2017). Many studies have used dinoflagellate cyst assemblages for quantitative reconstructions of SST, SSS, sea-ice cover, and PP in the past (e.g., de Vernal et al., 1997, 2001, 2013; Matsuoka, 1999; Rochon et al., 1998; , Mudie et al., 2002; Marret and Zonneveld, 2003; Pospelova et al., 2006, 2015; Ellegaard et al., 2006; Zonneveld et al., 2008, 2013; Ribeiro et al., 2012; Harland et al., 2013; Price et al., 2013; Bringué et al., 2014; Limoges et al., 2014; García-Moreiras et al., 2018). Studies of dinoflagellate cysts in the South China Sea (SCS), a tropical East Asian Monsoon (EAM) region in general, are rather limited. In the southern SCS, Kawamura (2002) analyzed dinoflagellate cysts and pollen in a sediment core from the Sunda Shelf and successfully reconstructed the major climatic variations and marine primary productivity variations during the last 44 kyr. In the recent work by Li et al. (2017), the warmest period of the Holocene and three strong winter monsoon intervals were identified in the northern SCS using high-resolution dinoflagellate cyst and pollen records in a sediment core.

For reconstruction on past environmental conditions in detail, it is necessary to know the relationship between individual dinoflagellate cyst species and specific environmental parameters. That requires good understanding of cyst spatial distributions in relation to environmental conditions which can be region specific (e.g., Dale, 1976, 2009; Pospelova et al., 2004; 2005; Limoges et al., 2010; Shin et al., 2011; Candel et al., 2012; Heikkilä et al., 2014; Price et al., 2016; Gurdebeke et al., 2018). For example, in the SCS, cysts can be influenced by different water masses (e.g., waters from the Kuroshio Current, the East China Sea, and rivers), broad ranges of SST, SSS, and PP variations, as well as eutrophication levels. Studies on dinoflagellate cysts in surface sediments from in this

region have been carried on in different areas: along the coast of Guangdong and Fujian (Qi et al., 1996; Wang et al., 2004a, 2004b), the northern shelf-deep basin (Wu and Sun 2000), Thailand Gulf and the eastern coast of Malaysia (Lirdwitayaprasit, 1998a), the northwestern coast of Borneo (Lirdwitayaprasit, 1998b), and offshore from Vietnam and the Sunda Shelf (Kawamura 2002; 2004). Most of the studies were focused on morphological descriptions of selected dinoflagellate cysts and areas of their presence. Wu and Sun (2000) studied dinoflagellate cysts from 38 surface sediment samples in the northern SCS. However, very low cyst counts prevented the authors from finding a relationship between cysts and factors affecting their distributions. Work by Kawamura (2002; 2004), focused on the dinoflagellate cyst distributions on the Sunda Shelf and off Vietnam (Figure 3-1), revealed first spatial maps of dinoflagellate cysts and discussed potential factors controlling cyst distributions in the study area. In this study, we investigate dinoflagellate cysts in surface sediments from the northern and the eastern SCS. Then, compiling two datasets (this study and by Kawamura, 2002; 2004), we document the major distributional patterns in dinoflagellate cysts for the entire SCS, and identify environmental parameters driving cyst distributions in the SCS.

3.2 Environmental settings of the SCS

3.2.1 Geographic setting

The SCS is one of the largest marginal seas of the western Pacific, surrounded by South China, the Indochina Peninsula (off Vietnam), and a chain of islands spanning from Luzon to Borneo (Figure 3-1). The SCS covers an area of ~ 3.5×10^6 km^2 and extends from the Tropic of Cancer to the Equator, across > 20 degrees of latitude, consisting of the deep basin (15%), the continental shelf (47%), and the continental slope

(38%) (Wang and Li, 2009). In the deep basin, the water depth averages ~4, 700 m with a maximum of 5,559 m (Wang and Li, 2009). The slope is positioned between the shelf-break zone and the deep basin, with a water depth of ~300-3700 m. There are several reef islands including Dongsha, Xisha, Zhongsha and Nansha reefs. The eastern slope is narrow and steep off Luzon (Wang et al., 2008) (Figure 3-1). The continental shelves are well developed in the northern and the southern parts of the SCS, and they tend to become narrower from the west to the east. On the northern shelf, there are numerous submarine deltas developed off the Pearl River, the Red River and other small rivers. The Sunda Shelf in the southwestern SCS is one of the largest shelves in the world, exceeding ~300 km in width (Figure 3-1) (Wang and Li, 2009).

3.2.2 Climatic and oceanographic settings

The climate of the SCS region is characterized by the tropical EAM, with the northeast wind in winter (October–April) and the southwest wind in summer (May–September) (Figure 3-2). January is the coldest month when the mean air temperature is ~15–25 °C, and July is the warmest month with the mean temperature of ~28 °C. The mean annual rainfall of the SCS is ~1000–2000 mm, and in the northern SCS, the mean annual rainfall is ~800 mm (e.g., Wang and Li, 2009).

In general, the SCS displays a pattern with high temperature, low salinity waters in the south and low temperature, high salinity waters in the north due to different water masses (e.g., Xie et al., 2003). SST in the SCS exhibits a strong seasonal cycle, and the maximum SST and minimum SST occur in July and January, respectively (e.g., Fang et al., 2006; Xie et al., 2003) (Figure 3-3). At the study sites, the SST in July ranges from ~28.5 °C to ~29.5 °C, and the highest occurring in the regions off Luzon, Borneo and

Hainan, while the lowest is in the northern coastal areas and upwelling zones (Figure 3-3, Table 3-1). The SSS varies from 31.8 to 34.1 in July and ranges from 31.9 to 34.3 in January (Figure 3-3; Table 3-1), with the highest values in January in the northern part, which is influenced by the Kuroshio Current. The lowest values in July occur near river mouths and in river plumes induced by freshwater input.

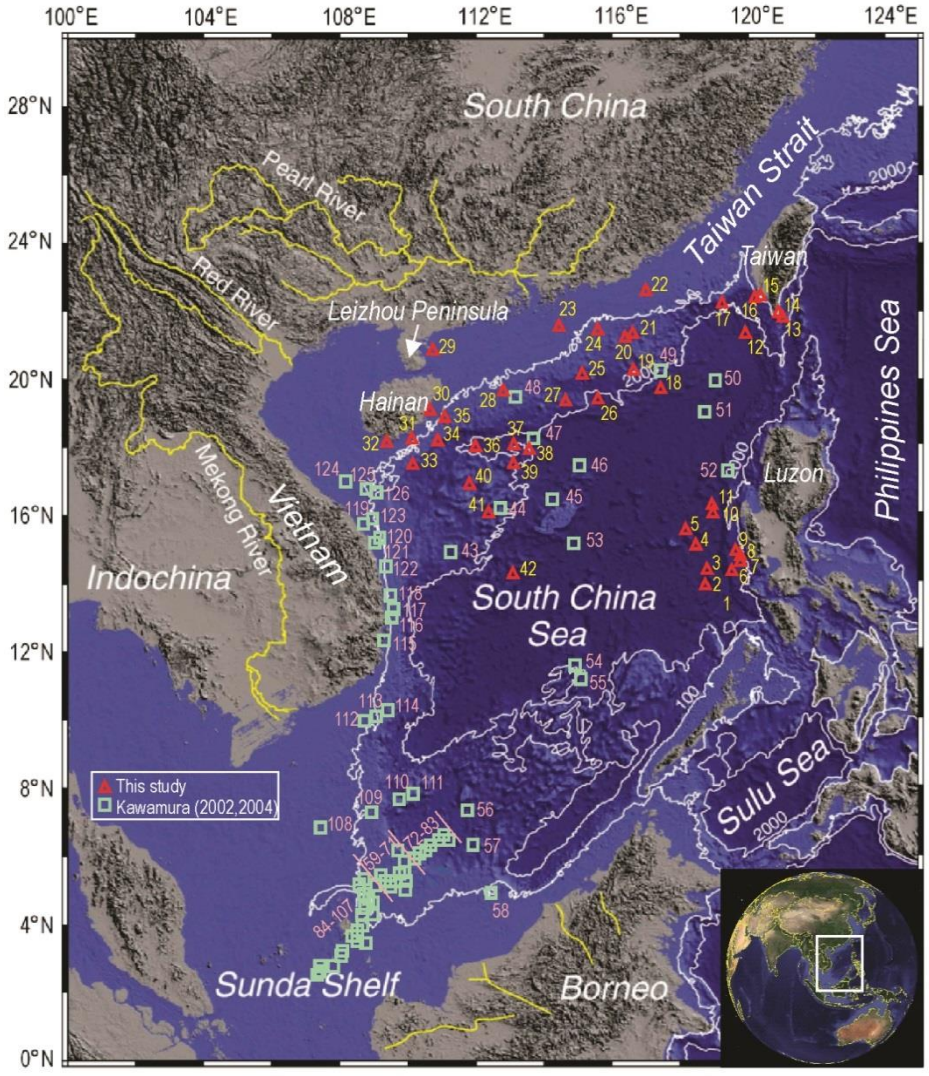

Figure 3-1. Map of the study area showing sampling sites and bathymetry of the South China Sea (modified from Wang et al., 2008; Li et al., 2017). The red triangles on the map indicate locations of samples from this study. The green squares mark locations of samples from previously published data of Kawamura (2002, 2004).

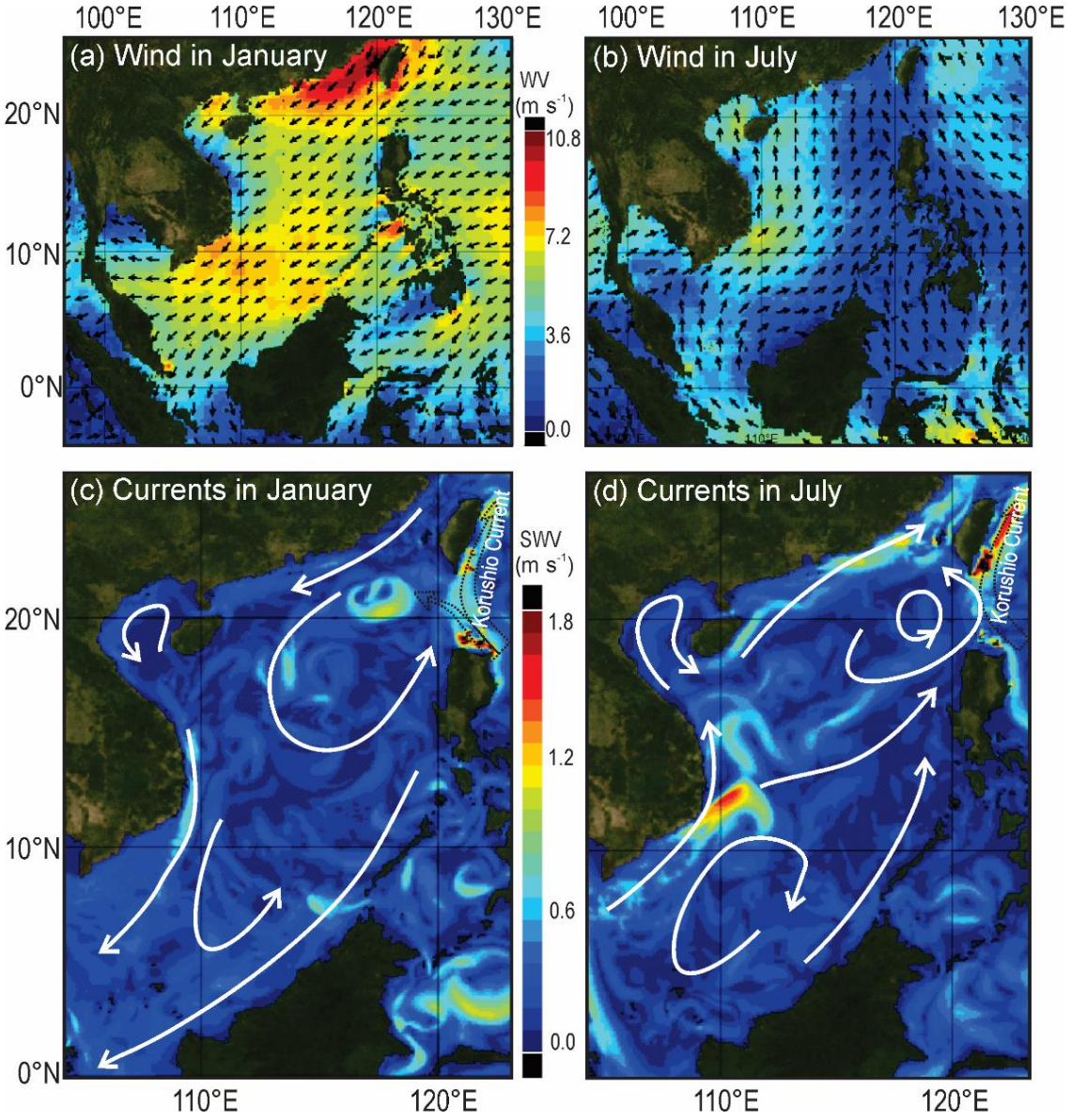

Figure 3-2. Wind velocities in January (a) and July (b), and sea water velocities in January (c) and July (d). White arrow lines are currents directions (Modified from http://marine.copernicus.eu and Fang et al., 1998).

The surface water circulation in the SCS is predominantly wind-forced by the northeast winter and southwest summer monsoons (Caruso et al., 2006). During winters, this circulation is characterized by a basin-wide cyclonic gyre and southwestward coastal currents, whereas in summers, the basin-wide circulation splits into a weakened cyclonic gyre in the north and a strong anti-cyclonic gyre in the south with northeastward coastal

currents (Figure 3-2) (Qu et al., 2002). Currently, the surface waters of the SCS exchange freely with waters from the neighbouring seas, while deeper water flows into the SCS

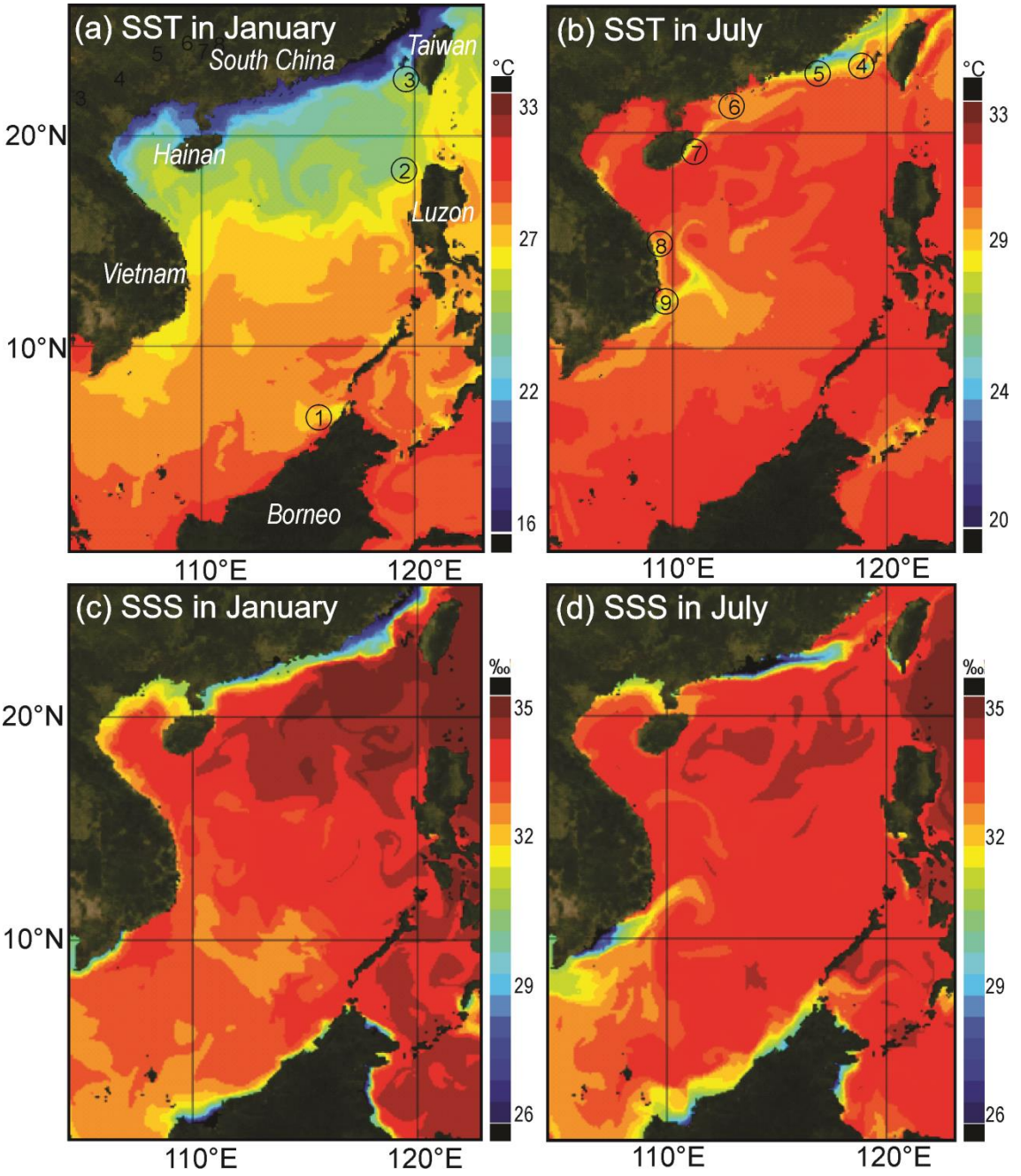

Figure 3-3. Sea-surface temperature of the South China Sea in (a) January and (b) July and sea-surface salinity in (c) January and (d) July (Modified from http://marine.copernicus. eu). Numbers of 1-3 in circles label the upwelling zones in winter off Borneo, Luzon and Taiwan, and numbers of 4-9 label the upwelling zones developing or intensifying in summer off Taiwan, South China, Hainan and the southern Vietnam.

primarily from the western Philippine Sea through the Bashi (or Luzon) Strait. The water transport through the Bashi Strait influences the circulation and heat budget of the SCS, affecting SST, SSS, circulations, and eddy generation in the northeastern SCS (e.g., Wu, 2013). Kuroshio Current forms to the east of the Philippines and flows northward along the coast of Luzon. In general, the Kuroshio tends to bypass the Bashi Strait in summer without significant westward encroachment. In winter, the Kuroshio branches into the South China Sea (SCS) because a wind stress curls off southwest Taiwan (e.g., Yuan et al., 2002; Wu and Hsin, 2012). A stronger wind stress curling off southwest Taiwan contributes to the anticyclonic circulation (Wu and Hsin, 2012). Typically, the Kuroshio intrusion into the SCS occurs through the central region of the Bashi Strait to form anticyclonic circulation in the northeastern SCS. The intrusion occasionally enters the SCS through the northern portion of Bashi Strait and forms a cyclonic circulation (e.g., Yuan et al., 2002).

Upwelling, one of the most important features of sea-surface circulation in the SCS, is induced by winds and largely affected by local topographic patterns (Woodson et al., 2007). Upwelling zones have been identified in the regions off southern Vietnam, Hainan and Leizhou Peninsula, South China, Southwest of Taiwan, Luzon and northwest of Borneo (Figure 3-3) (Hu and Wang, 2016). Influenced by monsoons, seasonal variability is a dominant feature of the upwelling in the SCS (Ndah et al., 2016). The Vietnam coastal upwelling zone is located in the shallow region along the eastern and southeastern Vietnam coast, and its cold eddy is off central Vietnam (He et al., 2002; Guo et al., 2006) (Figure 3-3). The upwelling along the northeastern coasts of the Hainan Island occurs in summer during the southwest monsoon and is the strongest from mid-July to mid-August

(e.g., Jing et al., 2009; Su et al., 2011). The upwelling off Dongshan–Shantou of South China is driven by the combined effect of wind and topography in summer and is regularly observed in June-September (e.g., Gan et al., 2009). The intrusion of the Kuroshio into the northern SCS from the Philippine Sea impinges on the outer shelf of the northern SCS and leads to the topographically induced upwelling around the Taiwan Bank and the Penghu Islands which may occur at varying strengths year-round (e.g., Hong et al., 2011). The upwelling off southwestern Taiwan usually intensifies to peak between December and March (e.g., Ndah et al., 2017). The West Luzon upwelling develops in October-November, becomes strong during the intensified northeast monsoon, and decays in February-May (Yuan et al., 2004). In the southern SCS, winter coastal upwelling has also been identified off northwest Borneo, and the winter coastal upwelling forms and strengthens between December and March (Yan et al., 2015).

3.3 Materials and methods

3.3.1 Sediment collection and environmental parameters

A total of 42 surface sediment samples were collected by grab samplers from 2008 to 2016 during various research cruises and used for dinoflagellate cyst analysis in this study. These samples cover the northern and the eastern SCS (Figure 3-1). We also used dinoflagellate cyst census data and concentrations from 34 surface samples from the southern and the western SCS (Kawamura (2002; 2004) to compile a dataset of the entire SCS (Figure 3-1 and Table 3-1). Thus, the total of 76 surface samples are from different geographic regions: sample sites 1-11 off Luzon, sites 12-16 off Taiwan, sites 17-28 in the northern shelf-deep basin off South China, sites 29-35 in the shelf-slope off Hainan, sites 36-53 in the deep basin of the SCS, sites 54-57 on the southern slope off Borneo,

sites 58-64 on the Sunda Shelf-Slope and sites 65-76 off southern Vietnam (Figure 3-1 and Table 3-1). The sediment types vary from clay to sand (see Table 3-1).

Sedimentary accumulation rates vary from region to region of the SCS, and the surface samples represent different intervals of deposition, depending on geographic locations. The accumulation rates recorded in sediment cores range from 2.5 to 111 cm kyr^{-1} in the SCS, with the highest values in the Dongsha area of the northern SCS (Huang et al., 1997; Wang et al., 1999). The lowest accumulation rates were observed in the slope-deep basin off Hainan (Huang et al., 1997; Wang et al., 1999). Therefore, the top surface sediments would at least represent the last several decades or even several hundred years of deposition.

Measured environmental parameters include: water depth (WD), distance to coastline (DC), monthly averages of chl-a concentrations, SST and SSS in January and July (chl-*a*-Ja, chl-*a*-Ju, SST-Ja, SST-Ju, SSS-Ja and SSS-Ju) from 2002 to 2016, as well as annual chl-*a* concentrations (chl-*a*-An) from 2002 to 2016 (Table 1). Concentrations of chl-*a* were obtained from the global monthly dataset on a latitude-longitude grid of 0.1×0.1 degrees (https://neo.sci.gsfc.nasa.gov /view.php?datasetId=MY1DMM CHLO RA) from July 2002 to June 2016. SST data from July 2002 to December 2006 were acquired from the monthly dataset of Advanced Very High Resolution Radiometer (AVHRR) on a grid of 0.1×0.1 degrees, and data from January 2007 to June 2016 were obtained from the monthly dataset of MicroWave Optimally Interpolated SST (MWOI) on a grid of 0.25×0.25 degrees (https://neo.sci.gsfc.nasa.gov/dataset_index.php). SSS data from May 2011 to August 2015 were acquired from the dataset of Aquarius on a grid

Table 3-1. Geographical coordinates and sediment types of studied surface sediment samples, water depth (WD), distance to the coastline (DC), Chl-*a* concentrations, sea-surface temperature (SST) and salinity (SSS), the number of counted dinoflagellate cysts and *Lycopodium* grains per sample, and sample weight used for this study and by Kawamura (2002; 2004). (https://www.ncdc.noaa.gov; http://marine.copernicus.eu; https://neo.sci.gsfc.nasa.gov).

Site	Sample	Latitude	Longitude	Sediment type	WD	DC	Chl-*a* concentrations (mg m^{-3})			SST (°C)			SSS (‰)			Counted number of:		Sample dry	Sources
No.	Code	(N)	(E)		(m)	(km)	January	July	Annual	January	July	Annual	January	July	Annual	Dinoflagellate cysts	*Lycopodium* spores	weight (g)	
1	OR1-0455-15-B	13°30.30'	118°56.64'	clayey silt	3558	131	0.18	0.12	0.13	27.54	29.49	28.87	32.97	32.81	32.89	4	3232	1.4	This study
2	OR1-0455-16-B	13°55.68'	118°39.84'	Silty clay	3447	180	0.17	0.10	0.13	27.50	29.56	28.85	32.97	32.81	32.89	0	3353	1.4	This study
3	OR1-0455-17-B	14°20.76'	118°45.18'	Silt	4060	155	0.16	0.10	0.13	27.49	29.67	28.90	32.87	32.81	32.81	0	3955	1.7	This study
4	OR1-0455-19-B	15°05.28'	118°26.70'	Silty clay	3943	158	0.16	0.08	0.12	27.10	29.50	28.66	33.25	33.32	33.24	0	3269	1.5	This study
5	OR1-0455-21-B	15°33.84'	118°10.80'	Clayey silt	3681	174	0.17	0.09	0.12	26.63	29.56	28.59	33.26	33.36	33.27	0	5163	1.6	This study
6	OR1-0455-10-B	14°18.84'	119°25.08'	Silt	2481	92	0.16	0.10	0.13	27.67	29.71	28.99	32.95	32.81	32.84	4	3953	1.6	This study
7	OR1-0455-9-B	14°34.74'	119°38.10'	Silt	2602	53	0.15	0.10	0.13	27.46	29.56	28.81	32.95	32.81	32.84	14	3164	1.9	This study
8	OR1-0455-7-B	14°45.78'	119°38.34'	Silty clay	2592	46	0.15	0.11	0.13	27.39	29.56	28.77	32.95	32.81	32.84	8	3963	1.6	This study
9	OR1-0455-6-B	14°54.60'	119°32.28'	Fine sand	2509	55	0.15	0.10	0.12	27.36	29.56	28.74	32.95	32.81	32.84	5	2353	1.5	This study
10	OR1-0455-2-B	15°57.48'	118°53.04'	Silty clay	3706	92	0.16	0.09	0.12	26.87	29.77	28.76	33.24	33.30	33.23	11	4946	1.6	This study
11	OR1-0455-1-B	16°14.16'	118°55.62'	Silty clay	3860	88	0.16	0.10	0.12	26.64	29.83	28.65	33.35	33.38	33.35	5	3788	1.9	This study
12	09-E401	21°29.78'	120°04.48'	Sandy clay	3059	85	0.28	0.10	0.15	24.62	29.60	27.36	33.57	33.15	33.38	25	4534	1.9	This study
13	OR1-0216-1-B	21°49.98'	121°01.98'	Clay	1310	20	0.32	0.10	0.16	23.93	29.09	27.00	33.57	33.15	33.38	146	5191	2.0	This study
14	OR1-0182-3-B	21°58.62'	120°54.72'	Clay	373	5	0.33	0.47	0.37	23.93	29.20	27.24	33.57	33.15	33.38	87	3304	2.9	This study
15	OR1-0299-1-B-1	22°27.72'	120°22.50'	Silty clay	24	3	0.40	0.74	0.60	23.35	28.99	26.55	33.57	33.14	33.41	117	4537	2.3	This study
16	OR1-0299-2-B-2	22°29.90'	120°15.80'	Silty clay	138	13	0.60	0.85	0.66	23.20	28.97	26.62	33.57	33.14	33.41	79	3799	2.2	This study
17	08-CF2	22°07.00'	119°17.26'	Silty clay	1320	113	0.33	0.13	0.18	23.76	29.44	26.92	33.25	32.79	33.05	141	3772	1.5	This study
18	08-E605	19°59.30'	117°32.36'	Clayey silt	2346	402	0.38	0.12	0.19	23.69	29.52	26.95	33.47	32.95	33.11	10	6680	1.3	This study
19	08-CF10	20°11.14'	116°28.51'	Sand	863	294	0.40	0.12	0.18	23.35	29.56	26.81	33.39	32.78	32.95	85	3668	0.9	This study
20	09-E108	21°17.75'	116°24.16'	medium coarse sand	318	172	0.45	0.22	0.23	22.78	29.41	26.38	32.86	32.50	32.47	18	4284	1.6	This study
21	OR1-0311-68-B	21°28.20'	116°39.78'	Coarse sand	325	163	0.40	0.21	0.23	22.91	29.32	26.35	32.86	32.50	32.47	13	4153	2.1	This study
22	OR1-0311-56-B	22°45.00'	117°06.12'	Fine sand	41	65	1.38	1.06	0.80	19.63	28.77	25.69	32.49	32.08	32.29	11	2022	1.8	This study
23	OR1-0311-90-B	21°34.14'	114°32.46'	Silty clay	72	94	0.60	0.40	0.49	21.20	29.59	25.89	32.27	31.78	31.77	344	2663	2.1	This study
24	OR1-0311-80-B	21°31.92'	115°41.04'	Clayey silt	113	127	0.51	0.42	0.29	22.08	29.61	26.05	32.46	32.20	32.15	160	2629	1.5	This study
25	79-48	19°58.00'	115°00.00'	Silty clay	1100	259	0.35	0.13	0.17	23.03	29.53	26.76	33.41	32.75	33.03	322	3509	1.3	This study
26	08-E702	19°30.24'	115°31.01'	Clayey silt	2365	311	0.34	0.13	0.17	23.28	29.55	26.92	33.41	32.75	33.03	31	5272	1.4	This study
27	08-E525	19°24.02'	114°35.83'	Clayey silt	1190	310	0.32	0.11	0.17	23.14	29.52	26.95	33.34	32.89	33.07	77	5865	1.3	This study
28	08-E524	19°39.84'	112°33.41'	medium coarse sand	150	161	0.32	0.11	0.18	22.87	29.47	26.72	33.20	32.80	32.95	282	9418*	3.7	This study
29	D15-3	20°42.00'	110°51.00'	Silty clay	25	34	3.44	1.54	2.61	20.29	29.52	26.32	31.86	32.39	32.06	98	11319*	0.7	This study
30	08-E501	18°51.78'	110°40.47'	Clayey silt	95	16	0.78	0.53	0.83	22.77	29.61	27.00	33.86	33.33	33.59	112	3279	1.8	This study
31	D21-3	18°09.85'	110°14.43'	Sandy clay	50	31	0.36	0.25	0.35	23.38	29.76	26.89	33.87	33.20	33.53	57	3705	2.9	This study
32	D22a-1	18°01.75'	109°29.91'	Silty clay	43	16	1.14	0.40	0.70	23.06	29.61	26.78	33.81	33.07	33.44	225	3686	2.1	This study
33	09-E605	17°23.37'	110°10.83'	Silty clay	768	105	0.24	0.13	0.15	23.87	29.88	27.37	33.05	32.93	33.03	329	2782	1.8	This study
34	08-E425(CF6)	18°04.30'	110°58.23'	Silty clay	1211	89	0.28	0.14	0.17	23.73	29.76	27.27	34.06	33.44	33.74	271	5136	1.3	This study
35	08-E504	18°38.21'	111°14.48'	Clayey silt	168	77	0.36	0.13	0.16	23.43	29.71	27.14	33.13	32.65	32.84	324	3069	1.6	This study
36	09-KJ16	17°59.20'	111°59.30'	Silty clay	2310	107	0.23	0.12	0.14	23.93	29.74	27.31	33.19	32.81	32.92	376	5308	1.5	This study
37	09-KJ14	18°03.57'	113°01.82'	Silty clay	2290	136	0.26	0.11	0.14	23.69	29.66	27.31	33.34	32.89	33.05	38	4064	1.3	This study
38	09-E420	18°01.15'	113°31.78'	Clayey silt	1929	159	0.29	0.11	0.15	23.65	29.66	27.27	33.34	32.89	33.05	47	4620	1.2	This study
39	09-KJ21	17°31.13'	113°01.32'	Sandy mud	1466	83	0.22	0.11	0.14	24.00	29.75	27.49	33.39	32.96	33.09	35	5555	1.2	This study

(to be continued)

(to continue)

Site No.	Sample Code	Latitude (N)	Longitude (E)	Sediment type	WD (m)	DC (km)	Chl-*a* concentrations(mg m^{-3})			SST (°C)			SSS (‰)			Counted number of:		Sample dry weight (g)	Sources
							January	July	Annual	January	July	Annual	January	July	Annual	Dinoflagellate cysts	*Lycopodium* spores		
40	09-Y01	17°04.74'	111°45.64'	Silty clay	1125	43	0.20	0.12	0.15	24.33	29.66	27.48	33.19	32.81	32.92	166	4967	1.94	This study
41	09-Y07	16°24.28'	112°10.39'	Clayey silt	955	16	0.20	0.12	0.16	24.59	29.72	27.67	32.96	32.84	32.87	129	3975	1.29	This study
42	09-KJ28	13°58.50'	113°02.35'	Sandy mud	2460	235	0.16	0.14	0.13	26.18	29.17	28.22	32.91	33.26	33.03	23	3545	1.18	This study
43	17954-1	14°45.50'	111°31.60'	Clay	1517	139	0.17	0.12	0.13	25.47	29.61	27.99	32.94	33.20	32.98	136	1466	3	Kawamura (2002,2004)
44	17950-1	16°05.60'	112°53.80'	Sandy silt	1868	50	0.19	0.11	0.13	25.06	29.67	27.91	32.96	32.84	32.87	193	3340	3	Kawamura (2002,2004)
45	17952-1	16°40.00'	114°28.40'	Clay	2340	260	0.19	0.10	0.13	24.63	29.70	27.78	33.26	33.07	33.11	121	2178	3	Kawamura (2002,2004)
46	17949-1	17°20.90'	115°10.10'	Clay	2195	332	0.24	0.10	0.14	24.02	29.71	27.50	33.41	32.90	33.04	132	1914	3	Kawamura (2002,2004)
47	17945-1	18°07.60'	113°46.60'	Clay	2404	241	0.29	0.11	0.15	23.63	29.69	27.28	33.34	32.89	33.05	98	3184	3	Kawamura (2002,2004)
48	17942-1	19°20.00'	113°12.10'	Sandy silt	329	231	0.32	0.11	0.17	23.14	29.50	26.85	33.20	32.80	32.95	243	1223	3	Kawamura (2002,2004)
49	17939-1	19°58.20'	117°27.30'	Clay	2473	344	0.39	0.11	0.18	23.63	29.51	26.92	33.47	32.95	33.11	249	2637	3	Kawamura (2002, 2004)
50	17925-1	19°51.20'	119°02.80'	Clay	2980	218	0.79	0.09	0.22	24.30	29.53	27.26	33.24	33.12	33.10	56	2110	2.95	Kawamura (2002, 2004)
51	17926-1	19°00.00'	118°44.00'	Clay	3761	199	0.44	0.10	0.20	24.20	29.59	27.32	33.46	33.06	33.15	79	1544	3.12	Kawamura (2002, 2004)
52	17927-1	17°15.00'	119°27.20'	Clay	2800	101	0.18	0.09	0.13	26.03	29.94	28.37	32.73	32.95	32.89	70	1198	3.04	Kawamura (2002, 2004)
53	17958-1	11°37.10'	115°04.90'	Clay	2581	48	0.16	0.09	0.12	27.50	29.24	28.71	32.74	32.95	32.88	112	1014	3	Kawamura (2002, 2004)
54	17959-1	11°08.30'	115°17.20'	Clay	1957	37	0.17	0.09	0.12	27.62	29.28	28.77	32.74	32.95	32.88	213	1659	3	Kawamura (2002, 2004)
55	17962-1	07°10.90'	112°04.90'	Clay	1970	68	0.21	0.11	0.14	26.98	29.29	28.75	32.83	33.11	32.98	387	1711	3	Kawamura (2002, 2004)
56	17965-1	06°09.40'	112°33.10'	Silty clay	889	59	0.19	0.11	0.14	27.30	29.43	28.86	32.69	33.13	32.93	320	1507	3	Kawamura (2002, 2004)
57	18300-1	04°21.77'	108°39.21'	Clayey sand	94	121	0.22	0.11	0.13	26.56	29.58	28.94	33.07	33.07	32.97	98	2082	3	Kawamura (2002, 2004)
58	18374-1	06°54.77'	107°39.91'	Silty sand	74	313	0.21	0.18	0.16	25.56	29.61	28.34	33.22	32.73	32.98	29	2214	3	Kawamura (2002, 2004)
59	18381-1	07°29.86'	109°07.64'	Clayey silt	214	380	0.20	0.13	0.14	26.05	29.38	28.48	32.89	32.79	32.81	130	939	3	Kawamura (2002, 2004)
60	18384-1	07°46.33'	109°48.68'	Clay	829	464	0.17	0.13	0.13	26.15	29.27	28.45	32.89	32.79	32.81	266	1196	3	Kawamura (2002, 2004)
61	18386-1	07°54.09'	110°07.85'	Sandy silt	380	386	0.18	0.13	0.14	26.22	29.30	28.52	32.85	33.00	32.86	66	1741	3	Kawamura (2002, 2004)
62	18392-1	09°37.08'	108°54.36'	Silty sand	116	163	0.24	0.16	0.21	25.28	29.29	28.02	32.82	32.57	32.67	130	1563	3	Kawamura (2002, 2004)
63	18394-1	09°47.67'	109°10.88'	Silty clay	183	152	0.22	0.15	0.18	25.37	29.27	28.03	32.82	32.57	32.67	327	1163	3	Kawamura (2002, 2004)
64	18395-1	09°59.22'	109°28.73'	Clayey silt	280	160	0.18	0.14	0.17	25.56	29.17	28.08	32.82	32.57	32.67	126	1233	3	Kawamura (2002, 2004)
65	18397-1	12°14.71'	109°19.91'	Silty clay	45	10	1.45	0.54	0.74	25.06	28.53	27.56	34.30	34.13	34.04	299	770	3	Kawamura (2002, 2004)
66	18401-1	13°30.12'	109°33.67'	Clay	134	28	0.38	0.19	0.30	24.77	28.88	27.43	32.89	33.03	32.95	206	1182	3	Kawamura (2002, 2004)
67	18404-1	13°41.11'	109°27.02'	Clayey sand	169	20	1.32	0.27	0.63	24.73	28.81	27.47	32.90	33.04	32.97	61	2304	3	Kawamura (2002, 2004)
68	18405-1	14°14.90'	109°20.20'	Clay	129	15	1.04	0.25	0.55	24.40	29.07	27.32	32.99	33.27	32.95	267	1540	3	Kawamura (2002, 2004)
69	18413-1	14°44.81'	109°17.61'	Clayey silt sand & gravel	52	23	0.91	0.22	0.50	24.40	29.21	27.42	32.99	33.27	32.95	40	1260	3	Kawamura (2002, 2004)
70	18412-1	15°12.18'	109°00.21'	Clayey silt sand & gravel	58	8	1.70	0.22	0.77	23.93	29.43	27.38	33.19	33.17	33.23	88	811	3	Kawamura (2002, 2004)
71	18409-1	15°13.35'	109°00.74'	Clay	40	7	1.23	0.20	0.60	23.93	29.43	27.38	33.19	33.17	33.23	264	606	3	Kawamura (2002, 2004)
72	18421-1	15°44.94'	108°53.33'	Sandy silty clay	83	35	1.17	0.19	0.52	23.54	29.68	27.13	33.70	32.97	33.30	22	2328	3	Kawamura (2002, 2004)
73	18408-1	15°41.21'	108°40.79'	Clay	117	40	2.54	0.25	1.19	23.57	29.14	26.45	33.70	32.97	33.30	253	1240	3	Kawamura (2002, 2004)
74	18428-1	16°23.59'	109°25.04'	Sandy silt	197	126	0.23	0.13	0.16	24.11	29.88	27.35	33.23	32.87	32.97	224	2158	3	Kawamura (2002, 2004)
75	18427-1	16°28.55'	109°11.47'	Silty clay	115	100	0.27	0.13	0.18	24.07	29.87	27.35	33.23	32.87	32.97	123	1462	3	Kawamura (2002, 2004)
76	18426-1	16°44.40'	108°27.77'	Sandy silt	93	63	0.62	0.17	0.31	23.71	29.68	26.91	33.23	32.87	32.97	135	993	3	Kawamura (2002, 2004)

Note: In this study, one *Lycopodium* tablet (9666 grains per tablet) was added into each sample, except for two tablets into samples marked with "*".
12542 grains of *Lycopodium* spores were added to each sample from Kawamura (2002; 2004).
Data of Chl-*a* concentrations, SST and SSS are the averages of January, July and Annual from 2002 to 2016.

of 0.5×0.5 degrees (https://neo.sci.gsfc.nasa.gov/view.php?datasetId=AQUARIUS_SSS), and other SSS data were obtained from the dataset of Global Observed Ocean Physics on a grid of 0.25×0.25 degrees (http://marine.copernicus.eu/services-portfolio/access-to-products/).

3.3.2 Palynological sample preparation

Dinoflagellate cysts were extracted using a standard palynological processing technique at the Paleoenvironmental Laboratory at the University of Victoria (e.g., Pospelova et al. 2010). All 42 samples from the northern and the eastern SCS were desalted and oven-dried at 40 °C, and then, they were weighed with an analytical balance. To estimate the concentrations of dinoflagellate cysts, we added one tablet of *Lycopodium clavatum* grains (9666 grains per tablet of batch no. 3862, University of Lund, Sweden) to each sample, except two tablets to samples 28 and 29. The samples were treated with 10% HCl to remove carbonates and 48% HF to dissolve silicates at room temperature. Then, a second 10% HCl treatment eliminated precipitated fluorosilicates. The samples were rinsed with distilled water and centrifuges after each step. To remove larger and finer particles than cysts, we sieved the samples with 120-μm and 15-μm Nitex nylon meshes. A gentle sonication for up to 30 s was used on samples during the sieving (Mertens et al., 2012). The residues were strew-mounted in glycerine jelly between a slide and a coverslip at 95 °C. All samples and palynological slides are stored at the Paleoenvironmental Laboratory, School of Earth and Ocean Sciences, University of Victoria, Canada. Dinoflagellate cysts were identified and counted using a Nikon Eclipse 80i optical microscope at 400 × or higher magnification. Dinoflagellate cysts were counted in each sample with an average of ~129 cysts. However, the counted

number ranges from 0 to 387 cysts due to the large differences in cyst concentrations from region to region (Table 3-1). When possible, we counted more than or at least 300 cysts, and for those samples having only a few cysts, we counted all cysts in all slides that can be made using the entire sample residue. Our counts of *Lycopodium clavatum* spike grains range from 606 to 11319 per sample.

Dinoflagellate cysts with their known thecal equivalents and autotrophic (phototrophic) or heterotrophic affinity were determined according to Matsuoka (1988), McMinn (1991), Kokinos and Anderson (1995), Head (1996), Zonneveld et al. (1997), Rochon et al. (1999), Zonneveld and Jurkschat (1999), Esper and Zonneveld (2002), Pospelova and Head (2002), Matsuoka et al. (2009), Pospelova and Kim (2010), Verleye et al. (2011), Yu and Morozova (2013) and Zonneveld and Pospelova (2015). Cysts were identified to the species level whenever possible, but some taxa were grouped into their genus with "spp." based on their morphological similarities. All smooth round brown cysts were grouped to *Brigantedinium* spp. including those with clear an archeopyle (e.g., *Brigantedinium cariacoense*, *Brigantedinium irregular*, *Brigantedinium simplex*) and those no archeopyle was observed. Folded brown cysts with obscured horns and/or granulated brown cysts were grouped as cysts of *Protoperidinium* spp. Fifty-six cyst taxa were identified (Table 3-2) (Plates 3-I, 3-II and 3-III). In this paper, dinoflagellate cysts produced by autotrophic and heterotrophic dinoflagellates are referred to as "autotrophic taxa" and "heterotrophic taxa", respectively.

Table 3-2. List of dinoflagellate cyst taxa identified in surface sediment samples in this study. The cyst-theca equivalents are based on McMinn (1991), Kokinos and Anderson (1995), Head (1996), Zonneveld (1997), Zonneveld and Jurkschat (1999), Esper and Zonneveld (2002), Pospelova and Head (2002), Matsuoka et al. (2009), Pospelova and Kim (2010), Verleye et al. (2011), Zonneveld and Pospelova (2015), Mertens et al. (2018).

Cyst species (paleontological name)	Dinoflagellate theca or affinity (biological name)
Autotrophic taxa	
Gonyaulacaceae	
Cyst of *Alexandrium* spp.	*Alexandrium* spp.
Cyst of *Pentaplacodinium saltonense*	*Pentaplacodinium saltonense*
Achomosphaera spp.	?*Gonyaulax* sp. Indet.
Bitectatodinium spongium	*Gonyaulax* sp. indet.
Dapsilidinium pastielsii	*?*
Impagidinium aculeatum	Unknown
Impagidinium paradoxum	*Gonyaulax* spp.
Impagidinium patulum	*Gonyaulax* spp.
Impagidinium sphaericum	*Gonyaulax* spp.
Impagidinium cf. *sphaericum*	*Gonyaulax* spp.
Impagidinium strialatum	*Gonyaulax* sp. indet.
Impagidinium spp.	*Gonyaulax* spp.
Lingulodinium hemicystum (machaerophorum)	?*Lingulodinium polyedrum*
Lingulodinium spp.	Lingulodinium spp.
Nematosphaeropsis labyrinthus	*Gonyaulax spinifera*
Operculodinium centrocarpum sensu Wall and Dale 1966	*Protoceratium reticulatum*
Operculodinium israelianum	*?Protoceratium reticulatum*
Operculodinium cf. *janduchenei* (*Operculodinium* sp. A of Vink 2000)	Unknown
Operculodinium longispinigerum	Unknown
Operculodinium spp.	Unknown
Polysphaeridium zoharyi	*Pyrodinium bahamense*
Spiniferites bentorii	*Gonyaulax digitalis*
Spiniferites bulloideus	*Gonyaulax spinifera* complex?
Spiniferites delicates	*Gonyaulax spinifera* complex
Spiniferites hyperacanthus	*Gonyaulax spinifera* complex
Spiniferites cf. *ludhamensis*	*Gonyaulax spinifera* complex
Spiniferites membranaceus	*Gonyaulax membranacea*
Spiniferites mirabilis	*Gonyaulax spinifera* complex
Spiniferites pacificus	*Gonyaulax spinifera* complex
Spiniferites pachyderma	*Gonyaulax spinifera* complex?
Spiniferites ramosus	*Gonyaulax spinifera* complex
Spiniferites spp.	*Gonyaulax spinifera* complex
Tuberculodinium vancampoae	*Pyrophacus steinii*
Perdiniaceae	
Cyst of *Pentapharsodinium dalei*	*Pentapharsodinium dalei*
Heterotrophic taxa	
Diplopsalidaceae	
Dubridinium caperatum	?*Preperidinium meunieri*
Dubridinium cavatum	Diplopsalid group
Diplopsalidaceae (or Protoperidiniaceae)	
Echinidinium aculeatum	Diplopsalid or Protoperidinioid group
Echinidinium granulatum	Diplopsalid or Protoperidinioid group
Echinidinium transparantum	Diplopsalid or Protoperidinioid group
Echinidinium spp.	Diplopsalid or Protoperidinioid group
Protoperidiniaceae	
Brigantedinium cariacoense	*Protoperidinium avellanum*
Brigantedinium irregulare	*Protoperidinium denticulatum*
Brigantedinium simplex	*Protoperidinium conicoides*
Brigantedinium spp.	*Protoperidinium* spp.
Cryodinium cf. *meridianum*	*Protoperidinium* spp.
Cyst of *Protoperidinium* spp.	*Protoperidinium* spp.
Cyst of *Protoperidinium oblongum*	*Protoperidinium oblongum*
Lejeunecysta sabrina	?*Protoperidinium leonis*
Leipokatium invisitatum	Unknown
Quinquecuspis concreta	*Protoperidinium leonis*
Selenopemphix nephroides	*Protoperidinium subinerme*
Selenopemphix quanta	*Protoperidinium conicum*
Selenopemphix tholus	*Protoperidinium* sp.
Selenopemphix undulata	Unknown
Stelladinium reidii	*Protoperidinium compressum*
Trinovantedinium applanatum	*Protoperidinium pentagonum*

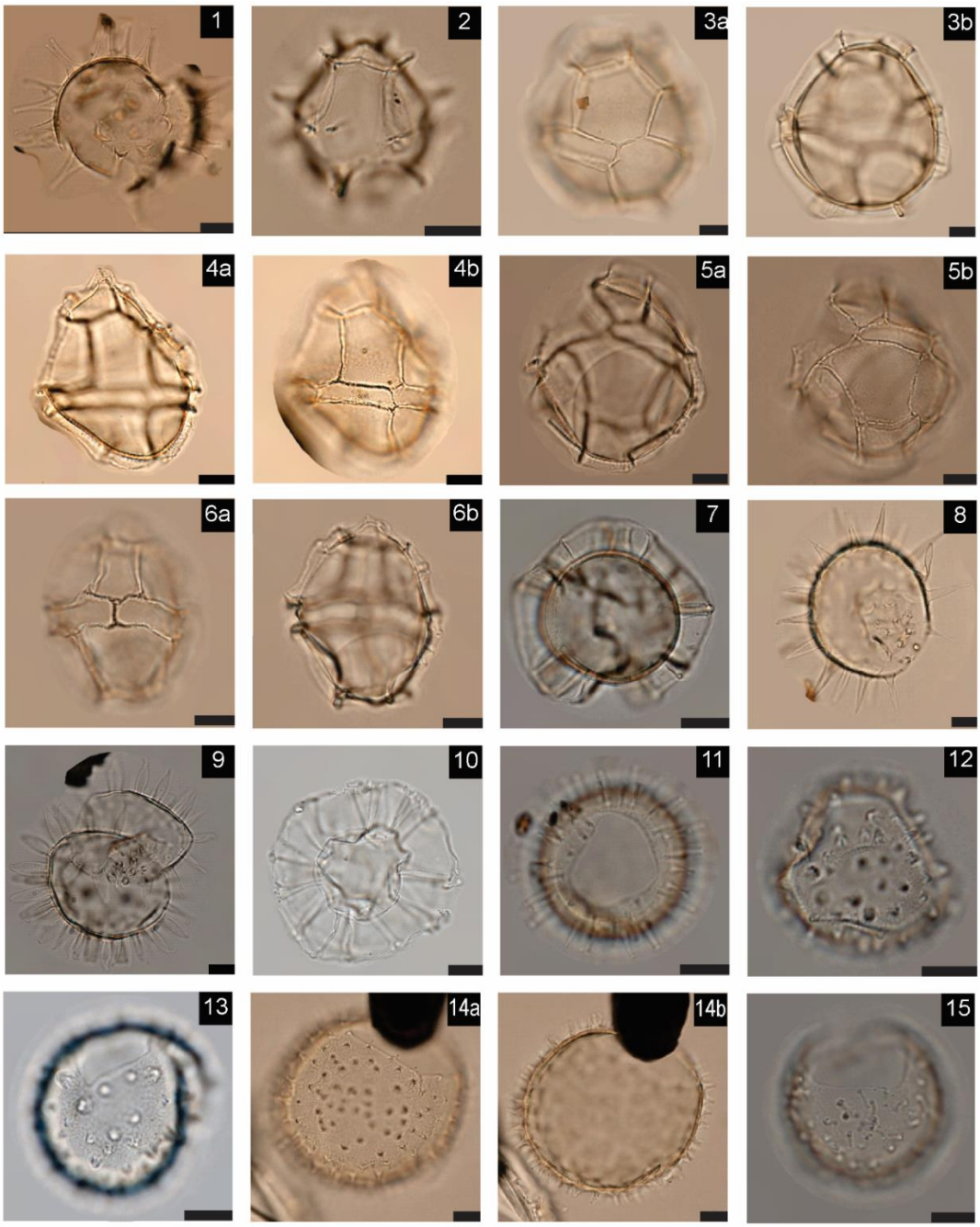

Plate 3-I. 1. *Dapsilidinium pastielsii*, 2. *Impagidinium aculeatum*, 3. *Impagidinium patulum*, 4. *Impagidinium sphaericum*, 5. *Impagidinium* cf. *sphaericum*, 6. *Impagidinium paradoxum*, 7. *Impagidinium strialatum*, 8. *Lingulodinium hemicystum*, 9. *Lingulodinium* sp., 10. *Nematosphaeropsis labyrinthus*, 11. *Operculodinium centrocarpum* sensu Wall and Dale 1966, 12-13. *Operculodinium* cf. *janduchenei* (*Operculodinium* sp. A of Vink 2000), 14. Cyst of *Pentaplacodinium saltonense*, 15. *Operculodinium* cf. *israelianum*. The Scale bars are 10 μm.

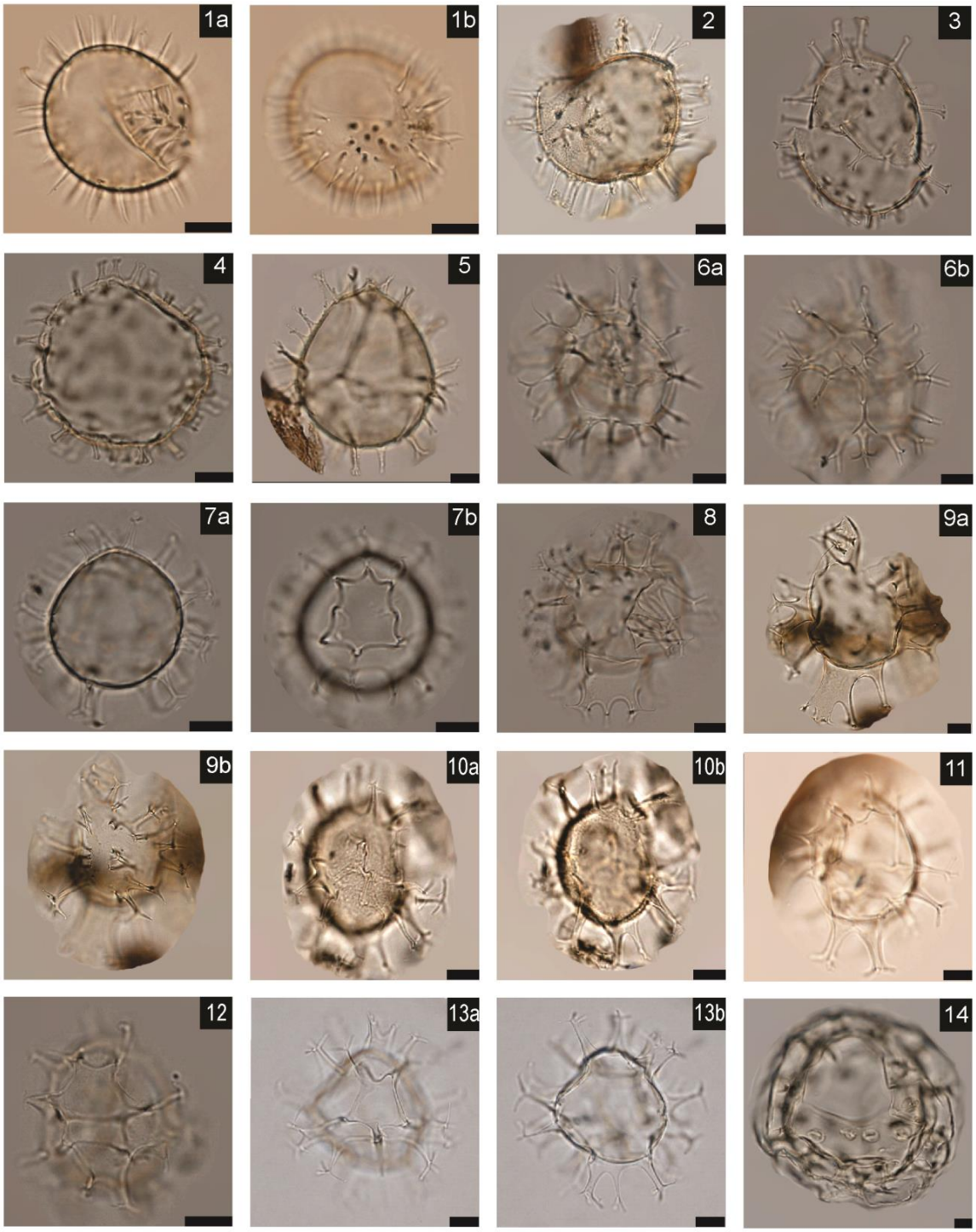

Plate 3-II. 1. *Operculodinium longispinigerum*, 2. *Operculodinium* sp., 3-4. *Polysphaeridium zoharyi*, 5. *Spiniferites bentorii*, 6-7. *Spiniferites hyperacanthus*, 8-9. *Spiniferites mirabilis*, 10. *Spiniferites pachydermus*, 11. *Spiniferites pacificus*, 12-13. *Spiniferites ramosus*, 14. *Tuberculodinium vancampoae*. The scale bars are 10 μm.

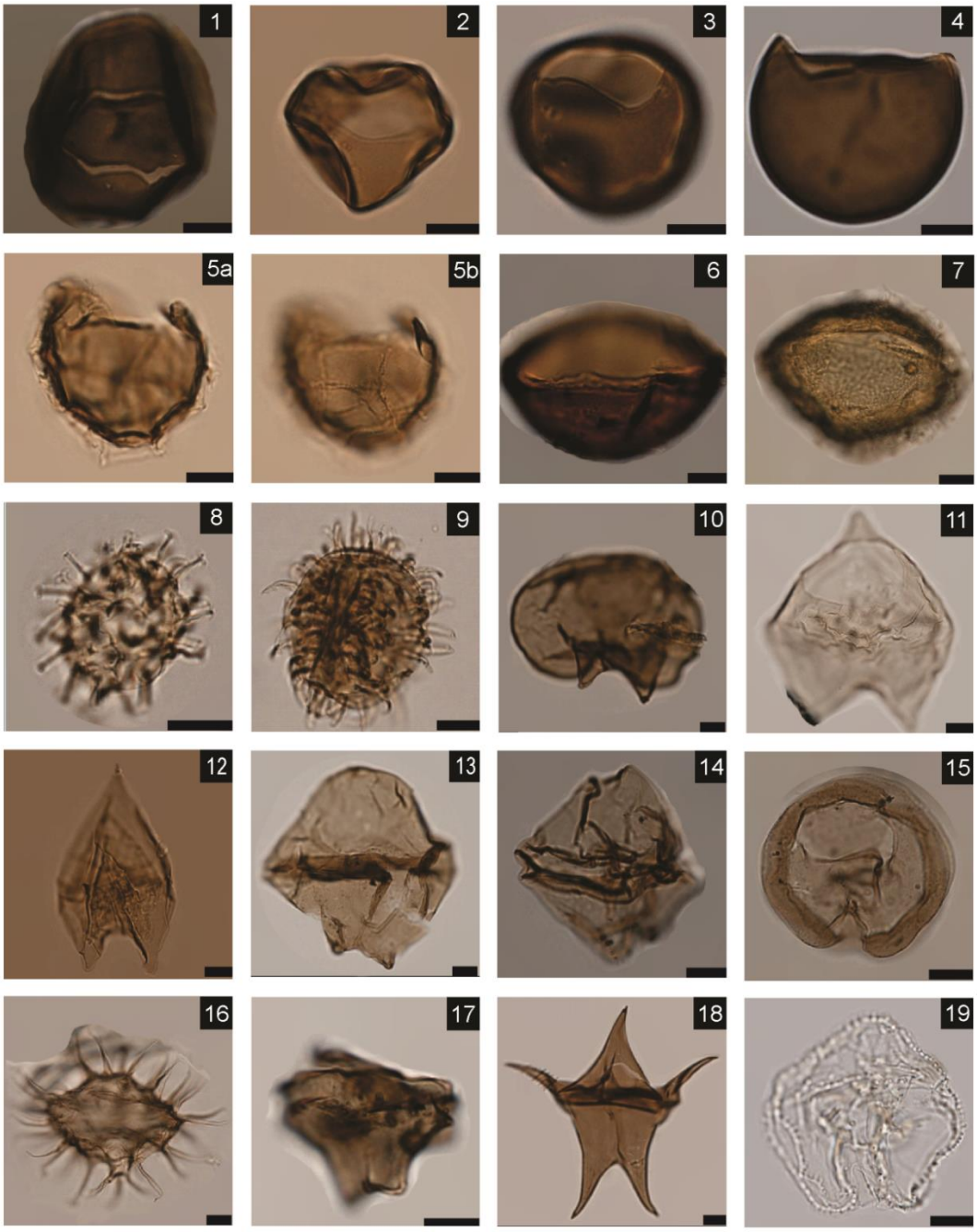

Plate 3-III. 1. *Brigantedinium cariacoense*, 2-3. *Brigantedinium* spp., 4. *Brigantedinium*-type A, 5. *Cryodinium* cf. *meridianum*, 6. *Dubridinium cavatum*, 7. *Dubridinium* sp., 8. *Echinidinium aculeatum*, 9. *Echinidinium* spp., 10. ? *Leipokatium invisitatum*, 11. Cyst of *Protoperidinium oblongum*, 12-14. Cysts of *Protoperidinium* spp., 15. *Selenopemphix nephroides*, 16. *Selenopemphix quanta*, 17. *Selenopemphix tholus*, 18. *Stelladinium reidii*, 19. *Trinovantedinium applanatum*. The scale bars are 10 µm.

3.3.3 Statistical analysis

The relative abundances of each dinoflagellate cyst taxon were calculated as percentages of the total counted cysts. The absolute abundances were expressed by concentrations. The concentrations of cysts (cysts g^{-1}) were calculated using the following formula: $C = \frac{L_{total} \cdot D_{counted}}{L_{counted} \cdot G}$, where C is the concentration of total or individual dinoflagellate cysts. L_{total} is the number of *Lycopodium clavatum* spores added to the sample. $L_{counted}$ and $D_{counted}$ are the numbers of counted *Lycopodium* grains and total cysts or individual dinoflagellate cysts in each sample, and G is the weight of the sample. Golden Software Surfer 10 was used to form the contour maps of relative and absolute abundances with the Kriging gridding method.

To compile SCS dataset, with includes data from Kawamura (2002; 2004) and of this study, cyst taxa should first be determined in agreement with each other. Table 3-3 shows that 56 cyst taxa were identified in this study and 46 taxa that were reported from Kawamura (2002; 2004). The most common dinoflagellate cyst taxa were consistent in both sets, e.g., autotrophic taxa of *Impagidinium aculeatum*, *Impagidinium paradoxum*, *Impagidinium patulum*, *Nematosphaeropsis labyrinthus*, *Operculodinium centrocarpum*, *Operculodinium longispinigerum*, *Polysphaeridium zoharyi*, *Spiniferites hyperacanthus*, *Spiniferites ramosus* and *Tuberculodinium vancampoae* and heterotrophic taxa of *Brigantedinium* spp., *Quinquecuspis concreta*, *Selenopemphix nephroides*, *Selenopemphix quanta*, *Stelladinium reidii* and *Trinovantedinium applanatum*. However, the consistency in identification of some morphotypes was impossible to ensure between the analysts (Zhen Li and Hiroshi Kawamura). For example, based on Kawamura (2002)

illustrations (Plates I-II of Kawamura, 2002), *Lingulodinium machaerophorum*, *Impagidinium strialatum*, and *Votadinium calvum* should be *Lingulodinium* sp., *Impagidinium sphaericum*, and cysts of *Protoperidinium oblongum* (Images 4-5 in Plate 3-I and Image 11 in Plate 3-III in this study). Different from *Lingulodinium machaerophorum*, the specimens of *Lingulodinium* sp. have narrower process bases compared to the middle part of the processes, and the tips of the processes are not rounded but sharpened (Image 9 in Plate 3-I) (McMinn, 1991). *Lingulodinium* sp. also differs from *Lingulodinium hemicystum* by wider middle parts of processes (Images 8-9 in Plate 3-I) (Li et al., 2017). *Operculodinium israelianum* and *Stelladinium stellatum* in Kawamura (2002) were re-identified as *Operculodinium* sp.-A and *Stelladinium reidii*, respectively, in Kawamura (2004). To avoid mistakes, we grouped these species and other uncertain species to their genus level with ".spp" to unify the cyst taxa of the two datasets (Table 3-3). After grouping, 31 taxa were attained in the SCS set that was used for cyst distribution and environmental factor analysis (Table 3-3).

We re-calculated the percentages of the taxa from Kawamura (2002; 2004) on the basis of the counting cyst sum excluding calcareous cysts and cysts of *Alexandrium* spp. Concentrations were re-calculated as cysts per gram of dry weight. Among 76 samples, most of the samples have very low cyst concentrations, and only 21 samples have counts more than 200 cysts. For percentage calculations, 38 samples were excluded since their counts were < 100 cysts (Figure 3-4). However, they were included in cyst concentration calculations (Figure 3-5).

Table 3-3. Lists of the dinoflagellate cyst taxa from this study and of Kawamura (2002; 2004), as well as the grouped taxa from both studies.

Cyst taxa from this study	Cyst taxa from Kawamura (2002; 2004)	Cyst taxa after compiled two datasets
Achomosphaera spp.	*Achomosphaera* spp.	*Achomosphaera* spp.
Cyst of *Alexandrium* spp.	*Alexandrium tamarensis* [Cyst of *Alexandrium* spp.]	Cyst of *Alexandrium* spp.
Bitectatodinium spongium	*Impagidinium aculeatum*	*Bitectatodinium spongium*
Dapsilidinium pastielsii	*Impagidinium paradoxum*	*Dapsilidinium pastielsii*
Impagidinium aculeatum	*Impagidinium patulum*	*Impagidinium aculeatum*
Impagidinium pallidum [*Impagidinium* spp.]	*Impagidinium sphaericum* [*Impagidinium* spp.]	*Impagidinium paradoxum*
Impagidinium paradoxum	*Impagidinium strialatum* [*Impagidinium* spp.]	*Impagidinium patulum*
Impagidinium patulum	*Impagidinium* spp. [*Impagidinium* spp.]	*Impagidinium* spp.
Impagidinium sphaericum [*Impagidinium* spp.]	*Lingulodinium machaerophorum* [*L. hemicystum*]	*Lingulodinium* spp.
Impagidinium cf. *sphaericum* [*Impagidinium* spp.]	*Lingulodinium machaerophorum*(short process) [*L. hemicystum*]	*Nematosphaeropsis labyrinthus*
Impagidinium strialatum [*Impagidinium* spp.]	*Nematosphaeropsis labyrinthus*	*Operculodinium centrocarpum*
Impagidinium spp. [*Impagidinium* spp.]	*Operculodinium centrocarpum*	*Operculodinium longispinigerum*
Lingulodinium hemicystum	*Operculodinium crassum* [*Operculodinium* spp.]	*Polysphaeridium zoharyi*
Lingulodinium spp. [*Lingulodinium* spp.]	*Operculodinium israelianum* [*Operculodinium* spp.]	*Spiniferites bentorii*
Nematosphaeropsis labyrinthus	*Operculodinium janduchenei* [*Operculodinium* spp.]	*Spiniferites hyperacanthus*
Operculodinium centrocarpum Sensu Wall and Dale 1966	*Operculodinium longispinigerum*	*Spiniferites miraiblis/membranaceus*
Operculodinium israelianum [*Operculodinium* spp.]	*Polysphaeridium zoharyi*	*Spiniferites ramosus*
Operculodinium cf. janduchenei [*Operculodinium* spp.]	*Spiniferites bentorii*	*Spiniferites* spp.
Operculodinium longispinigerum	*Spiniferites bulloideus* [*Spiniferites* spp.]	*Tuberculodinium vancampoae*
Operculodinium spp. [*Operculodinium* spp.]	*Spiniferites delicatus* [*Spiniferites* spp.]	*Brigantedinium* spp.
Cyst of *Pentapharsodinium dalei*	*Spiniferites hyperacanthus*	*Dubridinium* spp.
Polysphaeridium zoharyi	*Spiniferites mirablis*	*Echinidinium* spp.
Spiniferites bentorii	*Spiniferites membranaceus*	*Lejeunecysta sabrina*
Spiniferites bulloideus [*Spiniferites* spp.]	*Spiniferites ramosus*	Cyst of *Protoperidinium* spp.
Spiniferites delicates [*Spiniferites* spp.]	*Spiniferites* spp. [*Spiniferites* spp.]	*Polykrikos kofoidii*
Spiniferites hyperacanthus	*Tuberculodinium vancampoae*	*Quinquecuspis concreta*
Spiniferites cf. ludhamensis [*Spiniferites* spp.]	*Brigantedinium spp.* [*Brigantedinium spp.*]	*Selenopemphix nephroides*
Spiniferites membranaceus	*Diplopelta parva* [*Brigantedinium* spp.]	*Selenopemphix quanta*
Spiniferites mirabilis	*Lejeunecysta sabrina*	*Selenopemphix undulata*
Spiniferites pacificus	*Polykrikos kofoidii*	*Stelladinium reidii*
Spiniferites pachydermus [*Spiniferites* spp.]	Pre-encysted *Protoperidinium* [Cyst of *Protoperidinium* spp.]	*Trinovantedinium applanatum*
Spiniferites ramosus	*Quinquecuspis concreta*	
Spiniferites spp. [*Spiniferites* spp.]	*Selenopemphix nephroides*	
Tuberculodinium vancampoae	*Selenopemphix quanta*	
Brigantedinium cariacoense [*Brigantedinium* spp.]	*Stelladinium stellatum* [*Stelladinium reidii*]	
Brigantedinium irregulare [*Brigantedinium* spp.]	*Trinovantedinium applanatum*	
Brigantedinium simplex [*Brigantedinium* spp.]	*Votadinium calvum* [Cyst of *P. oblongum*]	
Brigantedinium spp. [*Brigantedinium* spp.]	*Votadinium spinosum* [Cyst of *Protoperidinium* spp.]	
Cryodinium cf. *meridianum*	Calcareous cysts	
Dubridinium caperatum [*Dubridinium* spp.]	*Cladopyxis* spp.	
Dubridinium cavatum [*Dubridinium* spp.]	*Cyclopsiella* spp.	
Echinidinium aculeatum [*Echinidinium* spp.]	*Cymatiosphaera*	
Echinidinium granulatum [*Echinidinium* spp.]	*Halodinium major*	
Echinidinium transparent [*Echinidinium* spp.]	*Pediastrum*	
Echinidinium spp. [*Echinidinium* spp.]	*Scrippsiella trochoidea*	
Cyst of *Pentaplacodinium saltonense*		
Cyst of *Protoperidinium oblongum*		
Cyst of *Protoperidinium* spp. [Cyst of *Protoperidinium* spp.]		
Lejeunecysta sabrina		
Leipokatium invisitatum		
Quinquecuspis concreta		
Selenopemphix nephroides		
Selenopemphix quanta		
Selenopemphix tholus		
Selenopemphix undulata		
Stelladinium reidii		
Trinovantedinium applanatum		

Note: "/" shows the species that have not been determined or have been grouped into other taxa in the compiled list.
[ ] shows the taxa that the species have been grouped into.

Detrended Correspondence Analysis (DCA) and Canonical Correspondence Analysis (CCA) were performed to quantify the relationship between the environmental

parameters and patterns of the dinoflagellate cyst distribution using CANOCO 4.5 for Windows software (ter Braak and Smilauer, 2002). Since the total counted number of cysts is less than 200 in most of the samples, the relative abundances calculated on the total counted number are not reliable for the samples that have rare cysts. Thus, the concentrations of individual dinoflagellate cysts are better options to correlate with environmental parameters through DCA and CCA.

DCA was first applied to test the linear or unimodal character of assemblage variability. The length of the first DCA gradient was 3.288 of the standard deviations for the cyst concentration dataset. The standard deviations were > 2, indicating that dinoflagellate cysts respond to environmental gradients in the unimodal character, justifying the need for the use of the CCA. Forward selection was applied to reduce the set of variables that could effectively explain the greatest amount of variance in the dinoflagellate cyst dataset. The relationship between the dinoflagellate cyst distribution and environmental parameters was assessed by species scores and their ordination patterns. Monte Carlo testing was used to determine the significance of each environmental variable. The level of significance of the variables indicates that the environmental variables are strongly related to the species data when $P < 0.005$.

3.4 Results

3.4.1 Dinoflagellate cyst assemblages from different geographic regions

Thirty-one cyst taxa were assembled from datasets of this study and Kawamura (2002, 2004) (Table 3-3). The cyst concentrations and assemblages vary from region to region (Figures 3-4 and 3-5). The region off Luzon has sparse dinoflagellate cysts: no

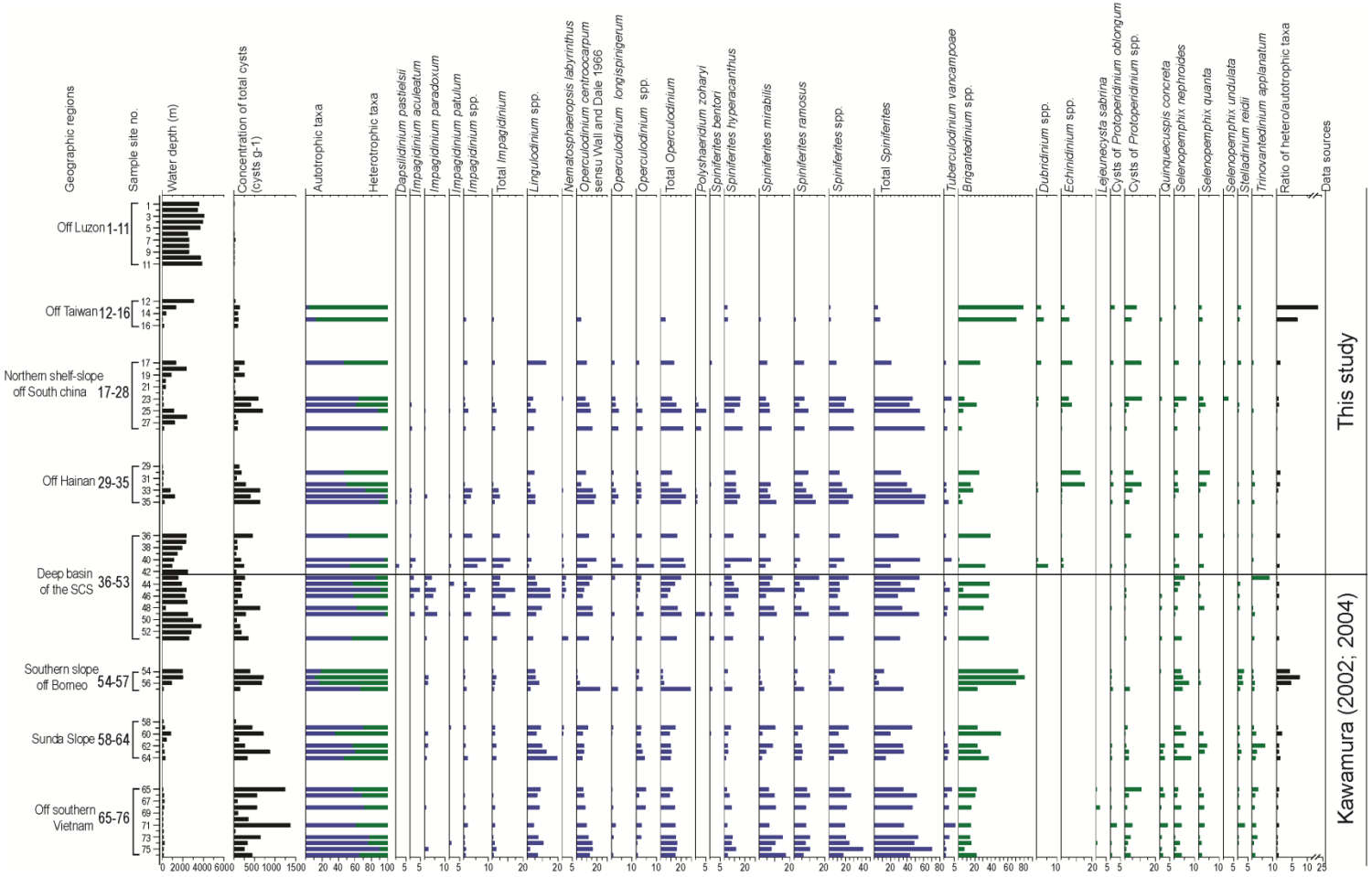

Figure 3-4. Total cyst concentrations (cysts g^{-1}) and concentrations of selected dinoflagellate cyst taxa (maximum>1.5%) from surface samples grouped by the regions. Heterotrophic taxa are shown in green and autotrophic taxa are in blue. The black line separates samples 1-42 (this study) from samples 43-76 (Kawamura, 2002; 2004). Samples with <100 counted cysts are not included in the percentage calculations.

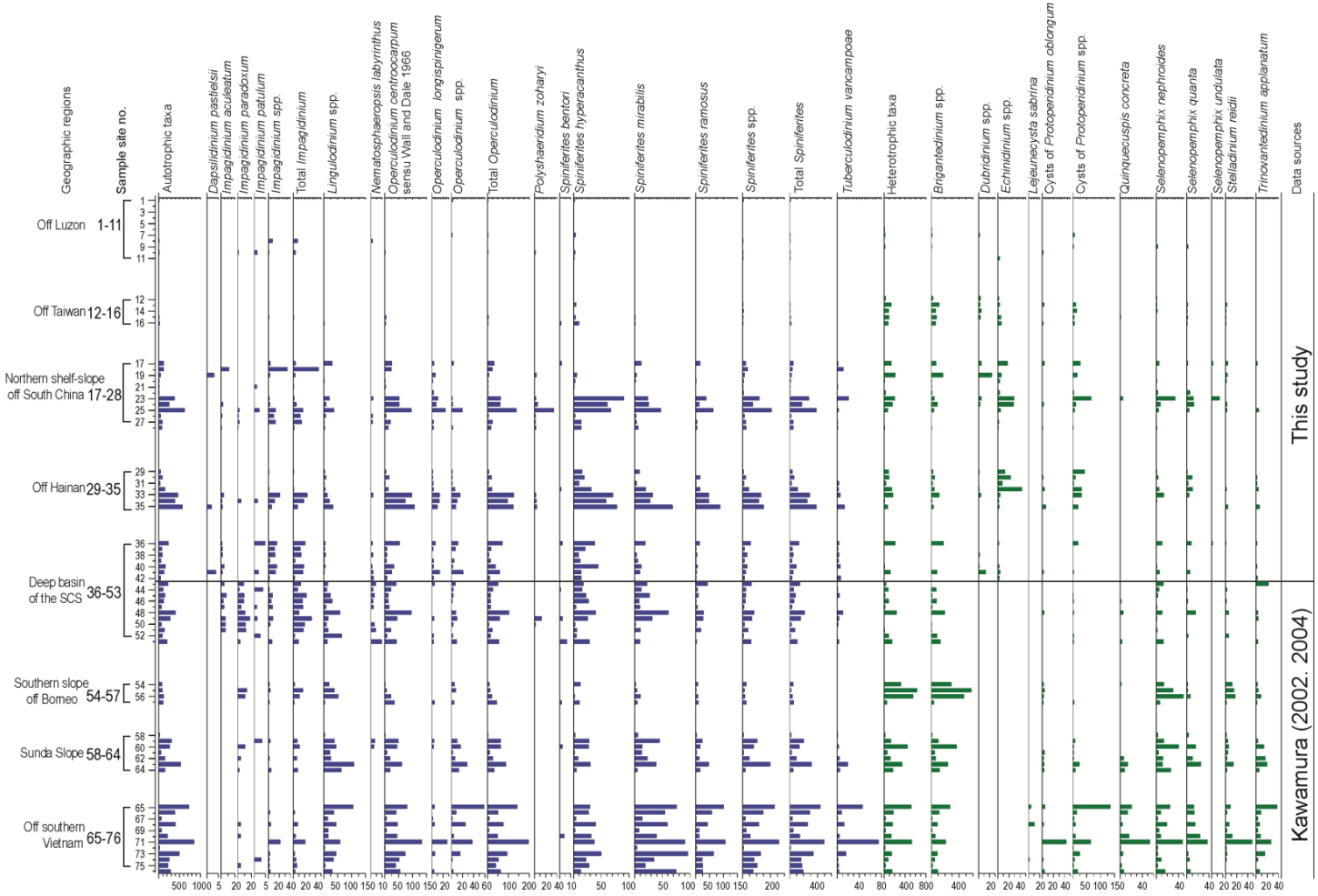

Figure 3-5. Concentrations (grains g^{-1}) of selected dinoflagellate cyst taxa in surface sediment samples that were grouped by the regions. Heterotrophic taxa are shown in green and autotrophic taxa are in blue. The black line separates samples 1-42 (this study) from samples 43-76 (Kawamura, 2002; 2004). Cyst concentrations in samples with < 100 counted cysts are also shown**.**

cysts were observed at sites 2-5, and only a few were found at sites 6-11 with total cyst concentrations from ~6 cysts g^{-1} to ~20 cysts g^{1} (Figure 3-4). Most of the cysts are autotrophic taxa except for site 7.

The region off Taiwan is characterized by the highest ratio of heterotrophic to autotrophic taxa, ranging from ~4 to 24 with an average of ~15 (Figure 3-4). Total cyst concentrations are very low in this region and vary from ~29 cysts g^{-1} to ~139 cysts g^{-1}. There are only two samples with cyst counts above 100 specimens. *Brigantedinium* spp. comprises ~72% of the assemblages and has the average concentration of ~66 cysts g^{-1} (Figure 3-5). *Impagidinium* cysts are observed sparsely.

The northern shelf-slope off South China has concentrations of total cysts ranging from ~14 cysts g^{-1} to 694 cysts g^{-1}, with an average of 215 cysts g^{-1}. The relative abundances of total *Spiniferites* increase westward from ~20% to ~61%, whereas the abundances of *Brigantedinium* spp. tend to decrease westward (Figure 3-4). Autotrophic taxa of *Operculodinium centrocarpum*, *Operculodinium longispinigerum*, *Polysphaeridium zoharyi*, *Spiniferites hyperacanthus*, *Spiniferites ramosus* and *Spiniferites* spp. have concentration trends similar to the total cyst concentrations (Figure 3-5). Total *Impagidinium* cysts have high relative abundances at site 26, whereas the highest concentration is observed at site 18 (Figure 3-4 and 3-5).

In the region off Hainan, concentrations of total dinoflagellate cysts and the relative abundance of total *Spiniferites* increase seaward. In contrast, relative abundances of *Brigantedinium* spp. and cysts of *Protoperidinium* spp. decrease from nearshore to offshore. *Echinidinium* spp. also decreases seaward from ~13% to 0, and the highest concentration is observed at site 33 (Figures 3-4 and 3-5).

In the deep basin of the SCS, concentrations of total cysts range from 52 to 630 cysts g^{-1}. The ratios of heterotrophic and autotrophic taxa are very low with an average of 0.38. Autotrophic taxa comprise ~79% of the assemblages, mostly consisting of *Operculodinium centrocarpum* (~12%), *Spiniferites hyperacanthus* (~12%), *Spiniferites* spp. (~10%), *Impagidinium* (~10%), and *Spiniferites mirabilis* (~5%), *Brigantedinium* spp. changes from 0% to 43% with an average of ~16% (Figure 3-4). The relative abundances of total *Impagidinium* have relatively constant values, and the same applies to *Nematosphaeropsis labyrinthus*. Concentrations of total *Spiniferites*, total *Operculodinium*, total *Impagidinium* and *Brigantedinium* spp. change from ~10 cysts g^{-1} to ~211 cysts g^{-1}, from ~6 cysts g^{-1} to ~103 cysts g^{-1}, from ~2 cysts g^{-1} to ~33 cysts g^{-1}, and from ~0 cysts g^{-1} to ~190 cysts g^{-1}, respectively (Figure 3-5).

The southern slope off Borneo has high ratios of heterotrophic to autotrophic taxa, averaging 4.18 and it has higher concentrations of total cysts (Figure 3-4). *Brigantedinium* spp. contributes ~60% to the assemblages, reaching the maximum of ~80%. Concentrations of *Brigantedinium* spp. and *Selenopemphix nephroides* here are the highest in the SCS (Figure 3-5).

The Sunda Shelf-Slope has similar relative abundances of total *Spiniferites* (~30%) and *Brigantedinium* spp. (~32%) (Figure 3-4). Concentrations of *Impagidinium* cysts were observed only at ~10 cysts g^{-1} and the relative abundances are from 0% to 2.4% (Figures 3-4 and 3-5). Different from the northern shelf-slope off South China, the Sunda Slope and the southern slope off Borneo have no *Dubridinium* spp., *Echinidinium* spp. and *Dapsilidinium pastielsii*.

The region off southern Vietnam, also the shallowest region, is characterized by the highest total cysts concentrations, ranging from ~30 cysts g^{-1} to 1371 cysts g^{-1} and with the average of 494 cysts g^{-1} (Figure 3-4). In this area, the ratio of heterotrophic to autotrophic taxa ranges from 0.10 to 0.71, averaging 0.45, and autotrophic taxa comprise 59% to 91% of the assemblages. *Spiniferites* cysts range from ~30% to ~70%, consisting mainly of *Spiniferites* spp. (~9%), *Spiniferites mirabilis* (~8%), *Spiniferites ramosus* (~8%) and *Spiniferites hyperacanthus* (~5%). *Operculodinium centrocarpum* and *Lingulodinium hemicystum* averages are ~9% and ~8%, respectively. *Brigantedinium* spp. is the dominant taxon among heterotrophic taxa and it ranges in the percentages from ~7% to ~22% with the average of ~16% (Figure 3-4). The concentrations of total *Spiniferites*, *Brigantedinium* spp., total *Operculodinium*, and *Lingulodinium hemicystum* vary from 12 cysts g^{-1} to 494 cysts g^{-1}, from 1 cysts g^{-1} to 197 cysts g^{-1}, from 38 cysts g^{-1} to 106 cysts g^{-1} and from 5 cysts g^{-1} to 268 cysts g^{-1}, respectively (Figure 3-5).

3.4.2 Distribution patterns of different dinoflagellate taxa

The maps of spatial distributions of total cyst concentrations, concentrations and percentages of individual dinoflagellate cyst taxa, and the ratio of heterotrophic to autotrophic taxa are shown in Figures 3-6 and 3-7. In general, the western SCS has higher cyst concentrations than the eastern region (Figure 3-6). Similar distributional patterns are observed for the concentrations of heterotrophic and autotrophic taxa (Figures 3-6 and 3-7). However, the highest values are highly variable. The region off southern Vietnam has the highest concentrations of total dinoflagellate cysts and autotrophic taxa, whereas the southern slope off Borneo has the highest concentrations of heterotrophic taxa (Figure

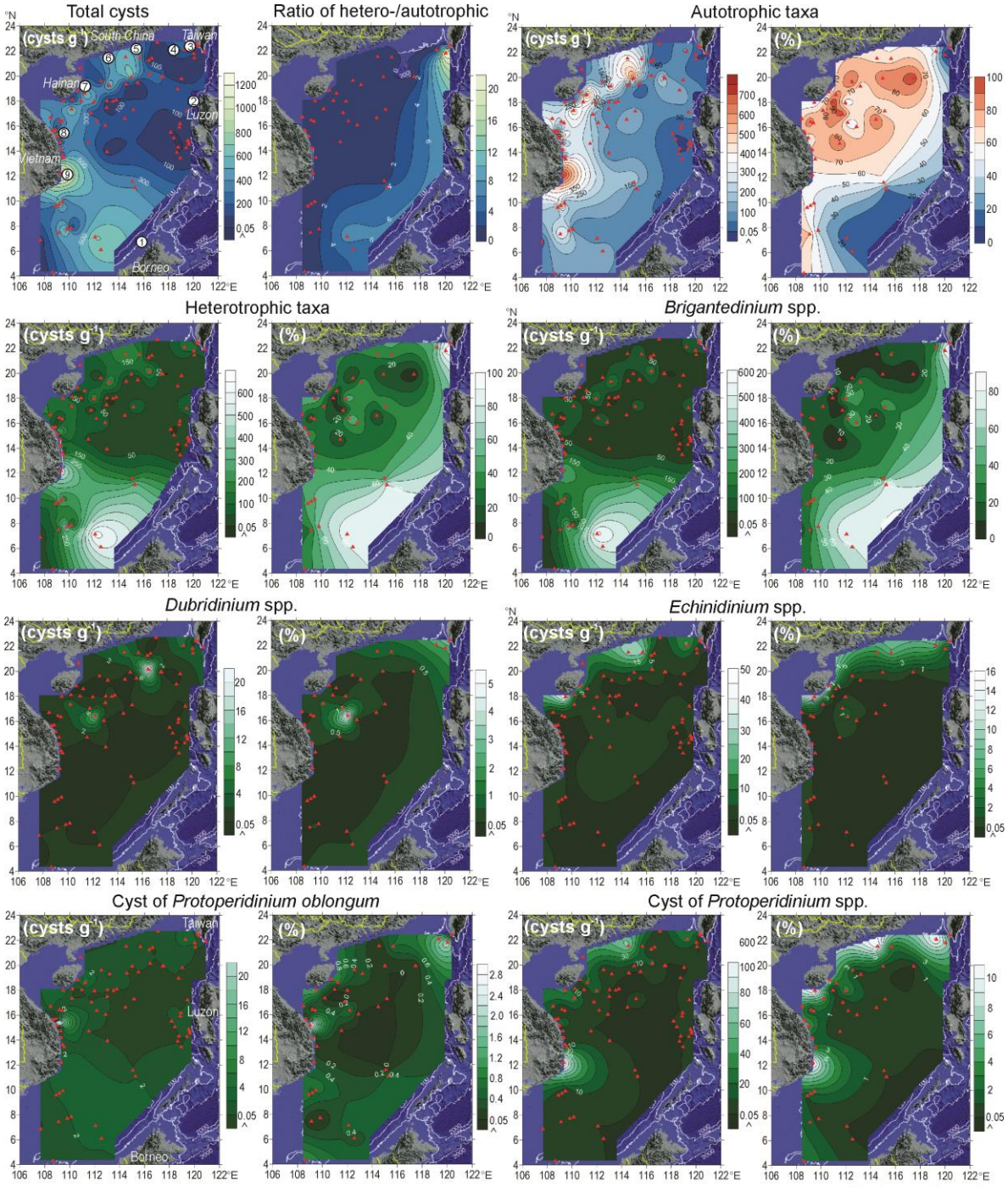

(To be continued)

Figure 3-6. Contour maps of total cyst concentrations (cysts g^{-1}), the ratios of hetero-/autotrophic taxa, concentrations and percentages of autotrophic cysts, heterotrophic taxa and selected heterotrophic taxa from the compiled datasets on this study and Kawamura (2002; 2004). Samples with < 100 counted cysts are excluded in the maps of percentages and the map of the ratio of hetero-/autotrophic taxa.

(To continue)

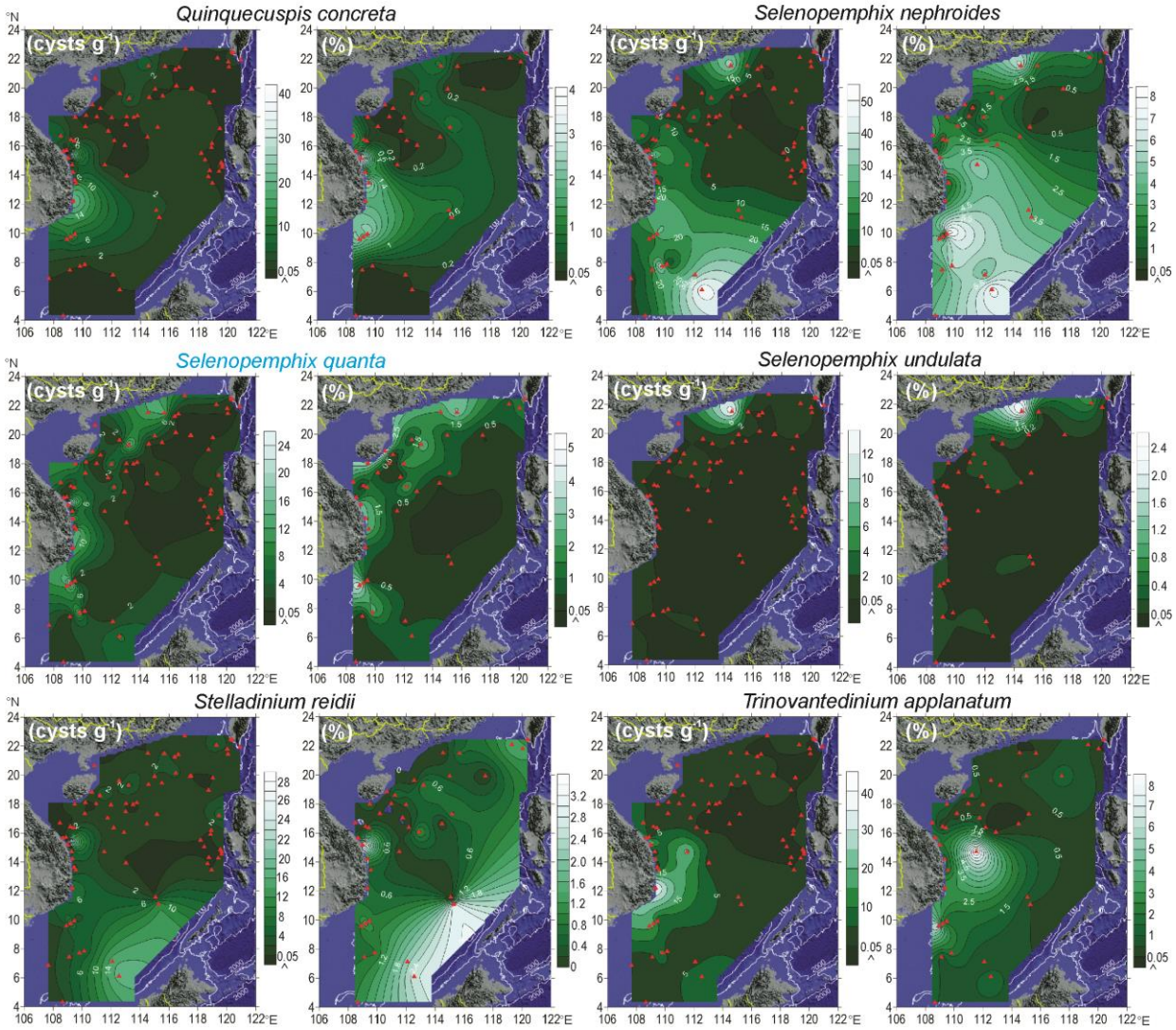

3-6). Total cyst concentrations and autotrophic taxa both have the lowest values in the deep regions off Luzon and Taiwan (Figure 3-6). The relative abundances of heterotrophic and autotrophic taxa have different distributional patterns. Relative abundances of heterotrophic taxa range from 0-10% in the northern deep basin to > 80% on the southern slope and in the region off Taiwan (Figure 3-6). Autotrophic taxa abundances have the lowest values on the southern slope and in the region off Taiwan and the highest on the slope of the northern SCS (Figure 3-6). The region off Taiwan has

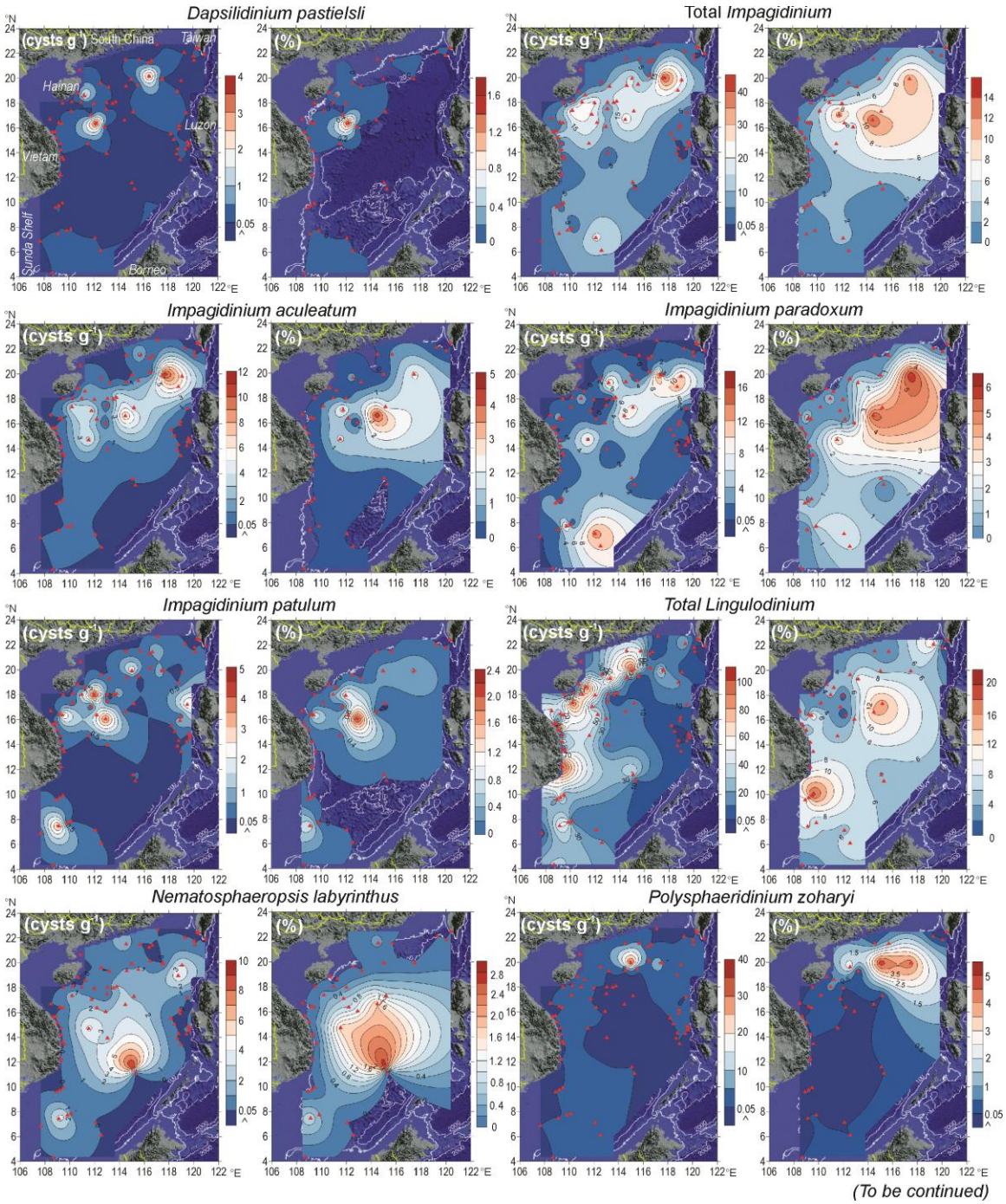

Figure 3-7. Contour maps of concentrations (cysts g^{-1}) and percentages of selected autotrophic taxa from the combiled dataset (this study and Kawamura (2002; 2004)). Samples with < 100 counted cysts are excluded in the maps of percentages.

(to continue)

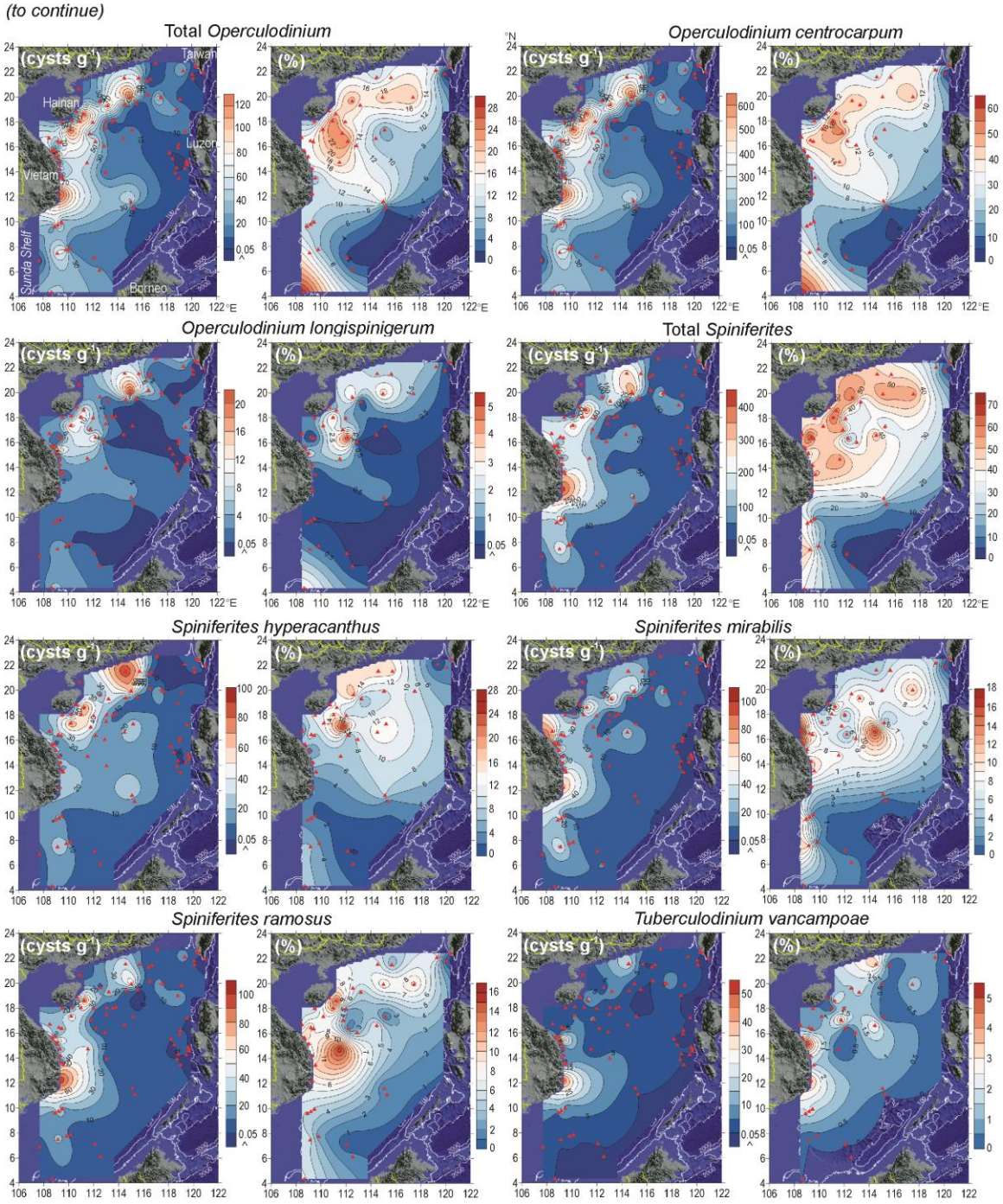

the highest ratios of heterotrophic to autotrophic taxa (~20), followed by the southern slope off Borneo (~4-6). The ratios are very low in the rest of the SCS (<2) (Figure 3-6).

Brigantedinium spp. has the highest abundances in the region off Borneo, and the relative abundances appear to be high near Taiwan (Figure 3-6). *Selenopemphix nephroides* and *Selenopemphix reidii* have distributional trends very similar to *Brigantedinium* spp., except for rather low percentages in the region off Taiwan. The highest concentrations of cysts of *Protoperidinium oblongum*, cysts of *Protoperidinium* spp., *Quinquecuspis concreta*, and *Trinovantedinium applanatum* are observed in an upwelling influenced coastal waters off southern Vietnam. In general, concentrations and relative abundances of these taxa have similar distributional trends. The highest values of their relative abundances are commonly in the region off Vietnam (Figures 3-6 and 3-7).

Echinidinium spp. and *Selenopemphix undulata* have the highest values of both concentrations and percentages on the northern shelf region off South China (Figure 3-6). *Echinidinium* spp. also shows high values in the region off Hainan (Figure 3-6). In general, *Dubridinium* spp. is found in low concentrations (0-24 cysts g^{-1}) and percentages (0-~5%) in the assemblages. The highest values are 24 cysts g^{-1} and ~5% in the deep basin of southern SCS (Figure 3-6).

Selenopemphix quanta and many autotrophic taxa including *Operculodinium centrocarpum, Spiniferites ramosus, Spiniferites mirabilis, Tuberculodinium vancampoae* and the percentages of total *Lingulodinium* have similar distributional patterns: the highest values on the northern slope off South China, Hainan, and southern Vietnam, and the lowest in the slope region off Borneo and/or Taiwan (Figures 3-6 and 3-7).

Operculodinium longispinigerum and *Spiniferites hyperacanthus* have their highest concentrations and percentages in the regions off Hainan and South China (Figure 3-7).

Spiniferites hyperacanthus displays the highest values closer to the coastal areas than *Operculodinium longispinigerum* (Figure 3-7).

High concentrations and percentages of total *Impagidinium*, *Impagidinium aculeatum*, *Impagidinium paradoxum*, *Impagidinium patulum*, *Nematosphaeropsis labyrinthus*, and *Polysphaeridium zoharyi* are all observed in the deep basin of the SCS (Figure 3-7). Most of them have the highest values in the slope-deep basin of the northern SCS. *Nematosphaeropsis labyrinthus* exhibits the highest concentrations (~10 cysts g^{-1}) and percentages (~3%) in the southern deep basin (Figure 3-7). Concentrations of *Impagidinium paradoxum* have high values in both northern and southern slope-basin regions (Figure 3-7).

Dapsilidinium pastielsii is observed in very low abundances with the concentrations from 0 to 4 cysts g^{-1} and percentages from 0 to ~2%. The highest values of both concentrations (4 cysts g^{-1}) and percentages (~2%) occur in the slope region off Hainan (Figure 3-7).

3.4.3 CCA analysis

CCA created an ordination in which the first two axes explain 23.3% of the variance in the species data and 66.7% of the variance in the fitted species data (Figure 3-8). Figure 3-8 shows that SST-Ja, WD, Chl-*a*-Ju and SSS-Ju are significantly correlated ($P<0.005$) with the CCA axes. The length of arrows on the ordination diagram in Figures 3-8a and 3-8b indicates the importance of the environmental variables that best explain the dinoflagellate cyst distribution. Therefore, SST-Ja is the most important environmental factor influencing the distribution of dinoflagellate cysts in the SCS shown

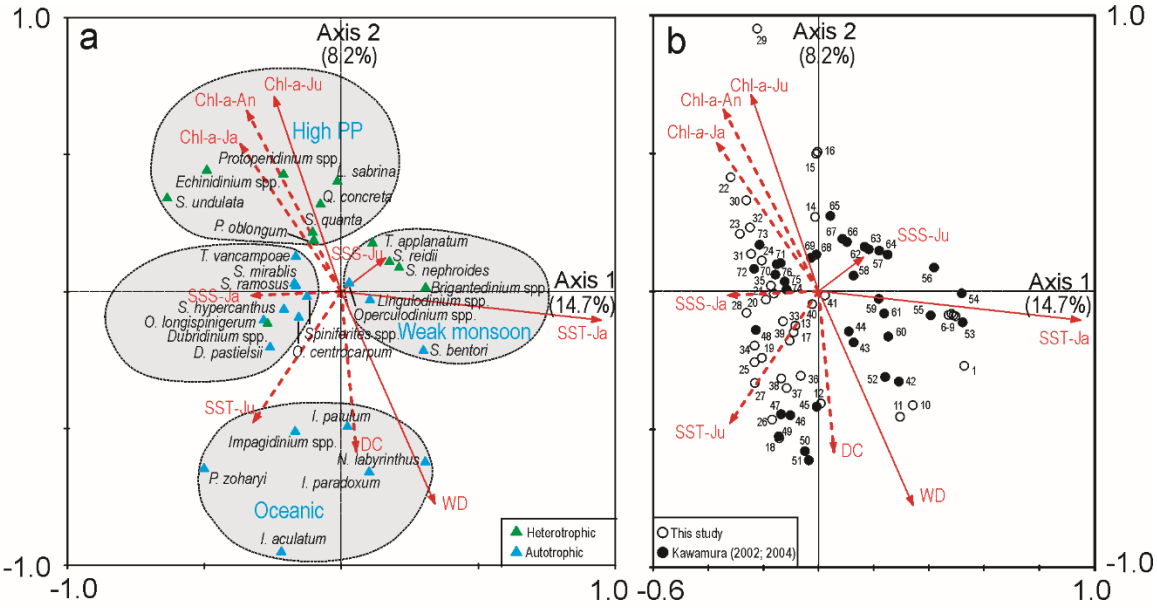

Marginal Effects

Variable	Lambda1
SST-Ja	0.14
WD	0.08
Chl-a-Ju	0.07
Chl-a-An	0.06
Chl-a-Ja	0.06
SST-Ju	0.05
DC	0.03
SSS-Ja	0.03
SSS-Ju	0.03

Conditional Effects

Variable	LambdaA	*P* value
SST-Ja	0.14	**0.002**
WD	0.06	**0.002**
Chl-a-Ju	0.06	**0.004**
SSS-Ju	0.03	**0.004**
Chl-a-Ja	0.01	0.184
DC	0.02	0.184
SST-Ju	0.01	0.364
SSS-Ja	0.01	0.428
Chl-a-An	0.00	0.984

Summary of CCA axes statistics

Axes	1	2	3	4	Total
Eigenvalues	0.147	0.082	0.068	0.021	0.983
P value	0.002				0.002
Species-environment correlations	0.760	0.793	0.763	0.686	
Cumulative % spp. data	14.90	23.30	30.20	32.40	
Cumulative % spp.-environment	42.70	66.70	86.60	92.80	

Figure 3-8. Canonical Correspondence Analysis (CCA) performed on dinoflagellate cyst concentrations (cysts g^{-1}) and environmental parameters. SST-Ja: mean sea-surface temperature in January; SST-Ju: mean sea-surface temperature in July; SSS-Ja: mean sea-surface salinity in January; SSS-Ju: mean sea-surface salinity in July; Chl-*a*-Ja: mean Chl-*a* concentration in January; Chl-*a*-Ju: mean Chl-*a* concentration in July; WD: water depth; DC: distance from the coastline. All data of SST, SSS and Chl-*a* are from 2002 to 2016. Ordination diagram showing species scores (8a) and sample scores (8b). Marginal effects, conditional effects and summary of RDA axes statistics are also shown. P-values <0.005 are statistically significant and highlighted in bold. Lambda (Λ) is the variation explained by each environmental variable, considered independently (marginal effect), or considered after all variables already incorporated in the model (conditional effect). Solid arrows represent forward-selected variables and dashed arrows represent non-significant environmental variables.

in Figure 3-8. The first axis of CCA is significantly correlated with SST-Ja and has a less important correlation with SSS-Ju. Figure 8a shows that the first CCA axis correlates positively with *Brigantedinium* spp., *Selenopemphix nephroides*, *Selenopemphix reidii*, *Trinovantedinium applanatum*, *Lingulodinium* spp., *Spiniferites bentorii* and *Operculodinium* spp., and negatively correlates with *Dapsilidinium pastielsii*, *Operculodinium longispinigerum*, *Operculodinium centrocarpum*, *Spiniferites* spp., *S Spiniferites hyperacanthus*, *Spiniferites mirabilis*, *Spiniferites ramosus*, *Tuberculodinium vancampoae* and *Dubridinium* spp.

The second CCA axis most likely represents Chl-*a*-Ju and the WD gradient (Figure 3-8). The species with the best fit for the positive second axis are heterotrophic taxa of cysts of *Protoperidinium* spp., *Echinidinium* spp., *Lejeunecysta sabrina*, *Tuberculodinium vancampoae*, *Votadinium* spp., *Quinquecuspis concreta*, *Selenopemphix quanta*, *Selenopemphix undulata* and cysts of *Protoperidinium oblongum*. The species in the negative direction of the second CCA axis are *Impagidinium* spp., *Impagidinium patulum*, *Impagidinium paradoxum*, *Impagidinium acculatum*, *Nematosphaeropsis labyrinthus*, and *Polysphaeridium zoharyi*. These are taxa commonly found in the open ocean environments.

Figure 3-8b shows the sample site scores plotted in the first and the second axes of the CCA and the correlation with the environmental parameters. The scores of the first and the second axes for each site are also plotted on the maps of SST-Ja, WD, Chl-*a* Ju and SST-Ju maps, the four significant factors (Figure 3-9). Sites with the highest positive scores of the first axis are in the slope-basin of the southern SCS and the region off Taiwan, where SST-Ja are high. The highest negative values are observed in the slope-

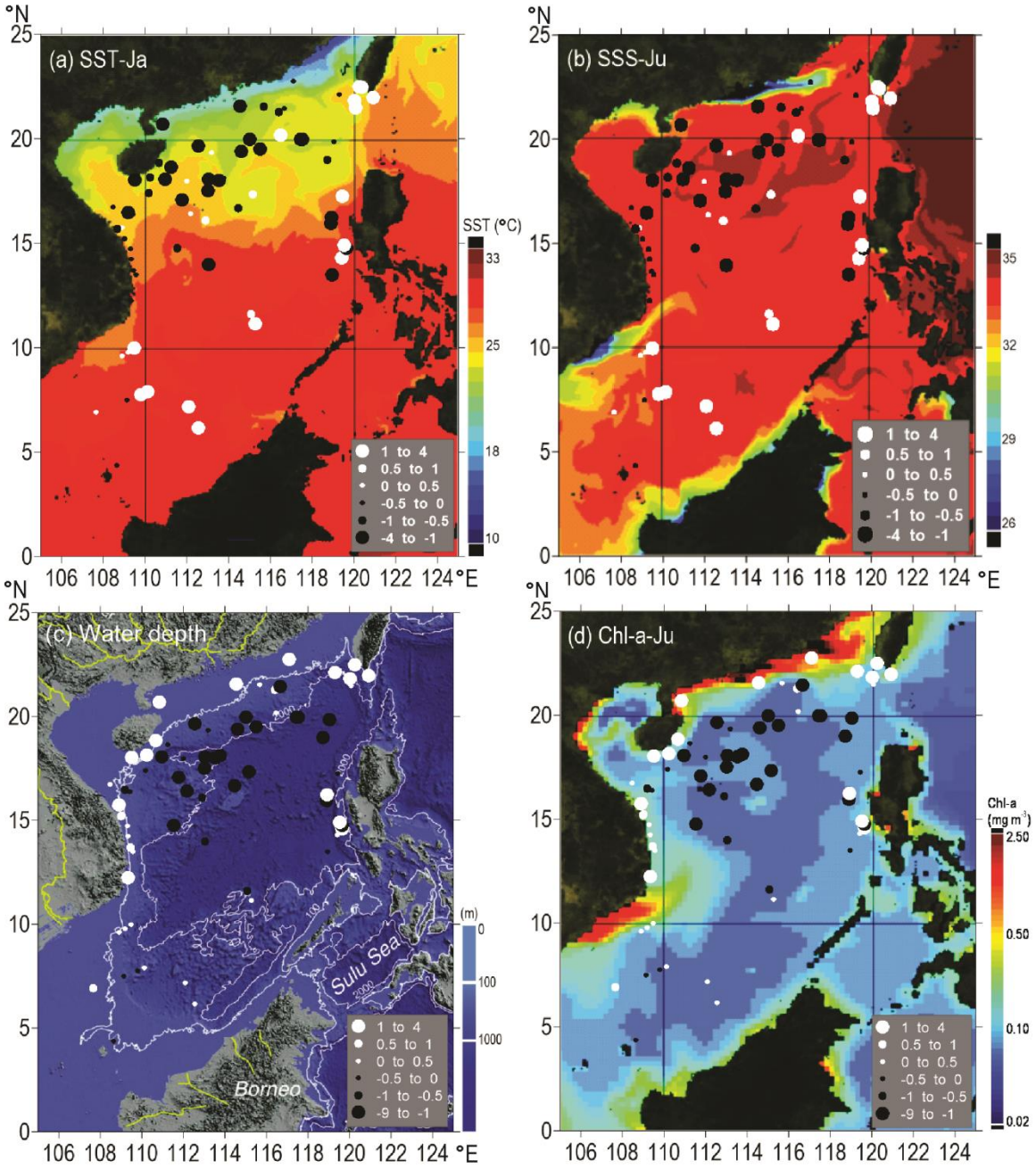

Figure 3-9. Maps showing the distribution of sample groups determined by the first and the second axes of CCA associated with (a) SST in January (SST-Ja), (b) SSS in July (SSS-Ju), (c) Water depth, and (d) Chl-*a* concentrations in July (Chl-*a*-Ju).

basin of the northern SCS (Figure 3-9a). Sites with the highest positive scores of the second axis are in the coast-shelf region, whereas the sites with the highest negative scores are found in the northern slope-basin of the SCS (Figure 3-9b).

3.5 Discussion

3.5.1 Concentrations of total cysts and heterotrophic taxa relevant to upwelling of the SCS

Our study of dinoflagellate cysts in surface sediments of the SCS reveals a wide range of cyst abundances and diverse assemblages. The regions off southern Vietnam, Borneo, Hainan and South China are characterized by high total concentrations (Figures 3-4 and 3-6). These regions are near active upwelling zones. However, other upwelling zones off western Taiwan and Luzon Islands show very low total cyst concentrations. Moreover, the concentrations are higher in the shelf-break zone than the sites of near coastal upwelling zones off South China and Hainan (Figure 3-6). A similar distributional pattern was also observed in the middle Atlantic Bight Shelf and the East China Sea where high primary productivity is induced by nutrients from deep waters due to intensified upwelling along the shelf-break (e.g., Lee et al., 1991; Wong et al., 2004; Benthuysen et al., 2014). Upwelling along shelf-break zone is usually triggered by a rapid change in the gradient of the bathymetry with higher pressure gradient (e.g., Hill and Johnson, 1974; Lill, 1979; Matano and Palma, 2008; Benthuysen et al., 2014). This interpretation seems to be not reasonable for the SCS because of lacking shelf-break upwelling in the northern SCS. In contrast, the SCS has a shallow mixed-layer with the depth of ~40 m in summer and of ~70 m in winter, much shallower than the water depth

of shelf-break (e.g., Wong et al., 2015). Southward to the adjacent open sea, the mixed layer depth becomes shallower at ~20 m in summer (Wong et al., 2007). Wong et al. (2015) interpreted that colder upper nutrient thermocline or nutricline waters below the shallower mixed-layer of the open SCS can extend freely on to the shelf of the northern SCS. This may increase nutrient landward from the shelf-break zone to the shelf. Internal waves may be the force to enhance the vertical mixing and transfer the cold and nutrient-rich waters to the surface mixed layer and to fuel primary productivity (e.g., Pan et al., 2012).

Heterotrophic dinoflagellates are mostly influenced by the distribution of their preferred prey (diatoms), whereas the distribution of autotrophic species more depends on the availability of light and dissolved nutrients (e.g., Dale, 1996; Pospelova et al., 2002). Many studies report that active upwelling or nutrient-rich regions are characterized by cyst assemblages dominated by the heterotrophic taxa (e.g., Dale, 1996; Zonneveld and Brummer, 2000; Zonneveld et al., 2001; Dale et al., 2002; Fujii and Matsuoka, 2006; Radi et al., 2007; Pospelova et al., 2008, 2010; Price and Pospelova, 2011; Bringué et al., 2013; Zonneveld et al., 2013). Thus, the proportion of heterotrophic taxa has been suggested as an indicator of nutrient availability associated with presence of upwelling zones or increasing shore proximity (e.g., Wall et al., 1977; Harland et al., 1983; Dale, 1996; Mudie and Rochon, 2001; Pospelova et al., 2004). Our study shows that the distribution of heterotrophic cyst concentrations is similar to the total cyst concentrations in general, but the highest values were found on the southern slope region off Borneo. The assemblages dominated by heterotrophic taxa and the highest percentages of heterotrophic taxa are both in the regions off Borneo and Taiwan, and are likely

associated with the upwelling in the SCS. The upwelling off Borneo forms and becomes stronger in winter and the upwelling off Taiwan usually intensifies to peak between December and March (e.g., Ndah et al., 2017). The winter upwelling off Borneo provides nutrients for phytoplankton blooms but it is not so strong as upwelling off Taiwan which exists during the entire year (e.g., Yan et al., 2015).

Some inconsistencies between the cyst concentrations and proportions of heterotrophic taxa might be also associated with plankton composition in response to nutrient levels, and that is reflected in the ratios of heterotrophs to autotrophs. Duarte et al. (2006) observed a Mediterranean coastal community and found a phenomenon in plankton that the ratio of heterotroph to autotroph biomass declined rapidly as heterotrophic biomass increased less than increases in the biomass of autotrophs after increasing nutrient inputs in an oligotrophic coastal community. A study on sediment traps of the SCS also showed that the ratios of heterotrophic to autotrophic dinoflagellate cysts declined when concentrations of total cysts increased in summer seasons because of the greater amplitude of increases in autotrophic taxa than in heterotrophic taxa (Li et al., 2018). In this study, the concentrations of autotrophic taxa in the western and the northern regions (>250 cysts g^{-1}) are much higher than those in the eastern and the southern regions (<100 cysts g^{-1}) (Figure 3-7), whereas the concentrations of heterotrophic taxa have the concentrations up to 250 cysts g^{-1} only in the regions off Borneo and southern Vietnam. In general, upwelling in the northern SCS is much more pronounced and stronger than in the southern SCS (e.g., Ndah et al., 2016). The upwelling off southern Vietnam, Hainan, and South China is developed and become stronger in summer, whereas the upwelling off Borneo, Luzon and southern Taiwan is

developed in winter. At the same time, much greater river inputs in summer also increase nutrients in the northern and the western SCS more than in the southern and the eastern SCS (e.g., Zhao, 1990; Yin et al., 2004; Kao and Milliman, 2008; Wang et al., 2009; Ogston et al., 2017). As a result, greater increase magnitudes of autotrophic taxa than heterotrophic taxa reflect greater nutrient inputs, but it causes much lower heterotrophic to autotrophic ratios in the northern and the western SCS (Figure 3-6).

3.5.2 Dinoflagellate cyst assemblages associated with SST and SSS

Brigantedinium spp., *Trinovantedinium applanatum*, *Selenopemphix reidii*, *Selenopemphix nephroides*, *Spiniferites bentorii*, and *Lingulodinium* spp. are positively related to the first axis of CCA (Figure 3-8). *Brigantedinium* spp. has the highest positive score, whereas *Operculodinium longispinigerum*, *Dapsilidinium pastielsii* and most *Spiniferites* are concentrated on the negative side of the second axis (Figure 3-8). SST-Ja is the most positive significant parameter of the first axis with another significant factor of SSS-Ju ($P<0.005$) (Figure 3-8). In winter, controlled by winter monsoon, SST is low due to the northeastern wind with cold air and the southwest currents with cold waters (e.g., Wang and Li, 2009). SST in winter is higher when the winter monsoon becomes weak. Conversely, in summer, influenced by summer monsoon, SSS is low due to the southwestern wind with warm and humid air, more freshwater inputs from rivers, and less influence from Kuroshio Current (e.g., Yuan et al., 2002; Wang and Li, 2009; Wu and Hsin, 2012). SSS in summer is higher when the summer monsoon becomes weak. Therefore, SST-Ja and in SSS-Ju in the SCS usually correspond to the weakened winter and summer monsoons, respectively. The weakened winter and summer monsoons also

generally reduced the upwelling intensity and vertical water exchange (e.g., Su and Pohlmann, 2009). This trend is reflected by the highest positive scores of the first axis of CCA at the sites in the southern slope-deep basin off Borneo and the south offshore of Taiwan whereas the highest negative scores at the sites in the northern slope-deep basin are observed with high salinity in July (Figures 3-9a and 3-9b).

In contrast, the negative relationship of the cyst assemblage consisting of *Spiniferites* spp., *Spiniferites hyperacanthus*, *Spiniferites mirabilis*, *Spiniferites ramosus*, *Tuberculodinium vancampoae, Operculodinium longispinigerum, Operculodinium centrocarpum, Dubridinium* spp. and *Dapsilidinium pastielsii* with SST-Ja and SSS-Ju is likely correlated with strong monsoons (Figure 3-8). The highest concentrations of the taxa are observed near the upwelling zones off southern Vietnam, Hainan, and south China or at the shelf-break areas influenced by internal waves (Figure 3-7).

Dapsilidinium pastielsii was reported as one of the living fossils in the Indo-Pacific warm pool (Mertens et al., 2014). It was widespread during the Miocene when the climate was much warmer than the present (e.g., Tong et al., 2009; Merterns et al., 2014). Li et al. (2017) reported *Dapsilidinium pastielsii* in the SCS in high abundances at ~7000–6000 cal yr BP when the air or water temperature was high and/or the Kuroshio Current intensified. In this study, for the first time, *Dapsilidinium pastielsii* was found in surface sediments from the SCS. *Dapsilidinium pastielsii* occurs only at the sites 19, 35 and 41 where water depth varies from ~160 m to ~1000 m. Based on fossil occurrences of *Dapsilidinium pastielsii* in the northwest and central Italy, Zevenboom et al. (1994) suggested that this species is neritic and thermophilic. Our observations indicate that *Dapsilidinium pastielssi* could live under much broader environmental conditions than it

was originally suggested. SSS-Ja is also high due to a strong Kuroshio Intrusion at the sites where we report *Dapsilidinium pastielsii* (Figure 3-3c). Thus, in addition to warmer SSTs, higher SSSs might be another important factor for *Dapsilidinium pastielsii* presence.

3.5.3 Oceanic dinoflagellate cyst assemblages

CCA results show that *Impagidinium*, *Nematosphaeropsis labyrinthus*, and *Polysphaeridium zoharyi* are associated with the negative values of the second CCA axis, and they are positively correlated with water depth and distances to the coastlines (Figure 3-8a). *Impagidinium aculeatum* has the highest negative score and cysts of *Protoperidinium* spp., together with *Echinidinium* spp. have the highest positive scores (Figure 3-8a). The samples with the highest negative scores are from the northern slope-basin of the SCS where salinity is higher due to the Kuroshio Current influence (Figures 3-9b and 3-9d). The concentrations and the percentages of total *Impagidinium*, consisting of *Impagidinium* spp., *Impagidinium aculeatum*, *Impagidinium paradoxum*, and *Impagidinium patulum*, as well as *Polysphaeridium zoharyi*, display the highest values in the slope-basin of the SCS (Figure 3-7). The highest values of concentrations and percentages of *Nematosphaeropsis labyrinthus* are in the southern deep basin (Figure 3-7), but the abundances, in general, are not very high (0-3%; 0-10 cysts g^{-1}).

After analyzing data of 2405 globally distributed surface sediment samples, Zonneveld et al. (2013) stated that *Impagidinium strialatum*, *Impagidinium patulum*, and *Impagidinium paradoxum* are restricted to a full-marine environment. These species are considered to indicate open oceanic, full-marine, low primary productivity settings with

well-ventilated bottom waters (e.g., Zonneveld et al., 2013). *Impagidinium aculeatum* is also a marine taxon (e.g., Dale, 1996; Rochon et al., 1999; de Vernal, 2001; Pospelova et al., 2008; Marret and Zonneveld; 2003; Zonneveld et al., 2013; Limoges et al., 2014). *Polysphaeridium zoharyi* is commonly observed in coastal fully marine subtropical to tropical regions that may have high productivity (Zonneveld et al., 2010). Its maximum (>40%) was observed in the Gulf of Mexico (Marret and Zonneveld, 2003) and off SW Mexico (Limoges et al., 2010). Our study shows that it occurs in very low abundances in the SCS with the highest concentrations (~35 cyst g-1) and percentages (~5%) (Figure 3-7). *Nematosphaeropsis labyrinthus* is considered a cosmopolitan species with a broad temperature tolerance (e.g., Zonneveld et al., 2013). However, it was also reported to be associated with oceanic and low productivity sites in the northeastern Pacific Ocean (e.g., Pospelova et al., 2004).

3.5.4 Dinoflagellate cyst assemblages associated with high chl-*a* concentration

Heterotrophic *Echinidinium* spp., *Selenopemphix undulata*, cysts of *Protoperidinium* spp., *Lejeunecysta sabrina*, *Quinquecuspis concreta*, *Selenopemphix quanta* and cysts of *Protoperidinium oblongum* are correlated with positive scores of the second CCA axis (Figure 3-8a). Cysts of *Protoperidinium* spp. have the highest positive score. Chl-*a*-Ju is indicated to be the most important parameter for the distributions of *Echinidinium* spp., cysts of *Protoperidinium* spp., *Lejeunecysta* s*abrina* and *Quinquecuspis concreta*. Figure 3-9d shows that the sites with high positive scores of the second CCA axis are in the coast-shelf regions where chl-*a* concentrations are high. The

sites with high negative scores were observed at the northern slope-deep basin where chl-*a* concentrations are low (Figure 3-9d).

The chl-*a* concentrations in the SCS are generally higher along the coast, rapidly decrease toward offshore, and become very low in the deep basin (Figure 3-9d). Influenced by the seasonal monsoons, there are clear chl-*a* differences between the eastern and the western coast of the SCS. The chl-*a* concentrations along the western coast enhance in summer and decline in winter, whereas this trend is reversed along the eastern coast (et al., Kuo et al., 2009). Chl-*a* concentrations generally represent the level of phytoplankton biomass and high concentrations are commonly associated with high primary productivity (e.g., Tang et al., 2004). In this study, the species that are positively correlated with chl-*a* concentrations belong to heterotrophic group, but they are not the dominant species in the cyst assemblages. Concentrations and percentages of these taxa are all much lower than those of *Brigantedinium* spp., the most dominant species among heterotrophic taxa in the SCS (Figure 3-7). Abundances of *Brigantedinium* spp. have been used as indicators of primary productivity (e.g., Zonneveld and Brummer, 2000; Marret and Zonneveld, 2003; Pospelova et al., 2008, 2015; Radi and de Vernal, 2008; Verleye and Louwye, 2010; Bringué et al., 2013; Price et al., 2013; de Vernal et al., 2013, Bringué et al., 2018). However, our results show that an assemblage dominated by cysts of *Protoperidinium* spp. rather than *Brigantedinium* spp. have a close positive relationship with chl-*a* concentrations (Figure 3-8).

3.6 Conclusions

Geographical distributions of dinoflagellate cysts were investigated in the SCS to determine environmental parameters driving cyst contributions and to identify taxa-indicators of modern environmental conditions. A total of ~ 56 cyst taxa were identified from 42 surface samples from the northern and the eastern SCS. Previously published data for 46 taxa from 34 surface sediment samples in the southern SCS were grouped into 31 taxa together with our new data. The most common heterotrophic taxa are *Brigantedinium* spp., *Echinidinium* spp., *Selenopemphix nephroides*, *Selenopemphix quanta*, *Selenopemphix reidii*, *Trinovantedinium applanatum*, and other cysts of *Protoperidinium* spp. Most abundant cysts of autotrophic dinoflagellates are the species belonging to *Impagidinium*, *Lingulodinium*, *Operculodinium*, *Spiniferites* and less abundant are *Nematosphaeropsis labyrinthus* and *Polysphaeridium zoharyi*, whereas *Dapsilidinium pastielsii* is rare.

In general, the western SCS has higher total cyst concentrations than the eastern region. The higher concentrations of total cysts occur centrally in the regions off southern Vietnam, Borneo (southern slope of SCS), Hainan and South China where active upwelling zones exist or internal waves occur along the shelf-break zones. The highest concentrations of total cysts and autotrophic cysts occur in the nearshore of southern Vietnam, and the lowest concentrations are in the deeper regions off Luzon and Taiwan. The highest abundances of heterotrophic taxa were observed on the southern slope off Borneo. The ratios of heterotrophic to autotrophic taxa have an opposite distributional trend to the total cyst concentrations, which might be induced by greater increases in autotrophic taxa than in heterotrophic taxa when nutrients increase.

Brigantedinium spp., *Selenopemphix nephroides*, and *Selenopemphix reidii* have similar distribution patterns with the highest abundances in the region off Borneo. The highest abundances of *Trinovantedinium applanatum*, cysts of *Protoperidinium oblongum*, cysts of *Protoperidinium* spp., and *Quinquecuspis concreta* were observed in the region off southern Vietnam. High abundances of total *Impagidinium*, *Impagidinium aculeatum*, *Impagidinium paradoxum*, *Impagidinium patulum*, *Nematosphaeropsis labyrinthus*, and *Polysphaeridium zoharyi* all were observed in the slope-deep basin, especially in the northern slope-basin influenced by the Kuroshio Current. Most of the other taxa have their highest abundances in the northern slope off South China, Hainan, and southern Vietnam, whereas the lowest values were observed in the regions off Borneo or Taiwan. *Dapsilidinium pastielsii* were observed at the sites in the north-western region of the SCS, with high SSS-Ja influenced by the Kuroshio Current in winter, negatively correlated with SST-Ja and SSS-Ju.

SST-Ja, WD, chl-*a*-Ju and SSS-Ju are the four most important factors in modern dinoflagellate cyst distributions in the SCS. *Brigantedinium* spp., *Selenopemphix nephroides*, *Selenopemphix reidii*, *T. applanatum*, and *Lingulodinium* spp. were positively correlated with the most important factor of SST-Ja and the factor of SSS-Ju. Distributions of these taxa reflect weak monsoons in both winter and summer. In contrast, autotrophic *Spiniferites* spp., *Spiniferites hyperacanthus*, *Spiniferites mirabilis*, *Spiniferites ramosus*, *Tuberculodinium vancampoae*, *Operculodinium longispinigerum*, *Operculodinium centrocarpum* and heterotrophic *Dubridinium* spp. might be linked to the stronger monsoons.

As expected, autotrophic *Impagidinium* spp., *Impagidinium patulum*, *Impagidinium paradoxum*, *Impagidinium aculeatum*, *Nematosphaeropsis labyrinthus* and *Polysphaeridium zoharyi* were found in the ocean environments, at the sites characterised by deep waters, away from the coastlines or nutrient sources. The highest abundances were documented in the northern SCS that is influenced by the Kuroshio Current.

Echinidinium spp., *Selenopemphix undulata*, cysts of *Protoperidinium* spp., cysts of *Protoperidinium oblongum*, *Lejeunecysta Sabrina*, *Quinquecuspis concreta*, and *Selenopemphix quanta* were positively correlated with chl-*a* concentrations and were associated with high primary productivity regions.

This is the first most comprehensive study of modern dinoflagellate cyst distributions and environmental impacts on the distributions in the SCS. It provides insights into different dinoflagellate cyst taxa correlated with specific environmental conditions, such as weakened monsoons, upwelling, open ocean environments, and primary productivity. This contributes important information for future paleoceanographic studies using dinoflagellate cysts. Our data also expand the existing global dinoflagellage database which is the basis for quantitative reconstruction of paleoceanographic conditions.

Acknowledgements

The Natural Sciences and Engineering Research Council of Canada (NSERC) CGS D3 fellowship (CGSD3-475098-2015) and Montalbano scholarship provided partial funding for this research to Z. Li. This work was also funded by NSERC through a Discovery grant (RGPIN/6388-2015) to V. Pospelova. She is the Hanse-

Wissenschaftskolleg (HWK) senior research fellow in marine and climate research at the Institute for Advanced Study (Germany).

Chapter 4

High-resolution palynological record of Holocene climatic and oceanographic changes in the northern South China Sea

Abstract

Palynological records of terrestrial palynomorphs and dinoflagellate cysts are investigated in a sediment core from the northern South China Sea (SCS) covering the last 12,500 years. Both terrestrial and marine palynomorph records show strong signals of the sea-level change during the studied interval. The highest herb pollen content was associated with extensive grasslands on the exposed shelf at the low sea-level stand during the Younger Dryas and early Holocene from ~12, 500 to 10,400 cal yr BP. The increase in fern spores and the decrease in concentrations of dinoflagellate cysts and terrestrial palynomorphs were observed during the sea-level rise interval from 12,500 to ~6,800 (or 6,000) cal yr BP. Then, the sea level became stabilized and consistently low dinoflagellate cyst abundances and high abundances of fern spores were recorded.

A high abundance of *Impagidinium* in the period ~12,000-10,400 cal yr BP possibly resulted from increased input of western Philippine Sea waters into the SCS and the branching of the Kuroshio Current. A short-term decrease of *Impagidinium* at ~11,700-11,000 cal yr BP corresponding to the MWP-1B event might be associated with input of the East China Sea waters through the Taiwan Strait.

The relationship between the sedimentation rates and the concentrations of terrestrial palynomorphs indicates water transport was dominant for pollen and spore dispersal before ~6,300 cal yr BP, whereas wind transport became more prominent

thereafter. The timing of this change corresponds to the highest sea-level stand at ~6,800-6,000 cal yr BP, when the present oceanographic setting was formed. The mid-Holocene Optimum can be seen by the highest abundance of subtropical-tropical broad-leaved arboreal pollen and by the highest abundances of warm water *Dapsilidinium pastielsii*. Three strengthened winter monsoon intervals at ~5,500 cal yr BP, 4,000 cal yr BP, and 2,500 cal yr BP are reflected by increases in *Pinus* pollen content after the present oceanographic condition formed.

4.1 Introduction

Studies of the South China Sea (SCS), located in the low-latitude Western Pacific Ocean and the East Monsoon climate region, play an important role in understanding climate change (e.g., Wang and Li, 2009). With well-preserved Holocene sedimentary strata and relatively high sedimentation rates, the northern SCS is considered one of the best areas for high-resolution paleoreconstructions of Holocene climatic and oceanographic changes. Significant efforts have been invested into reconstructions of the Holocene monsoon climate variability and hydrographic conditions, including the sea surface temperature (SST) and sea surface salinity (SSS), using a number of sediment cores from the northern SCS (e.g., Huang et al., 1997; Wang et al., 1999; Yu et al., 2005; He et al., 2008; Kong et al., 2014; Jiang et al., 2014; Dai and Weng, 2015). Most of these studies have shown similar general trends throughout the Holocene. However, the records of short-term monsoon climate or specific oceanographic events are not consistent or not always recorded by different proxies due to limited sampling resolution. These proxies include clay and grain-size records (Huang et al., 2011), alkenone-based SST (Huang et

al., 1997; Pelejero et al., 1999; Wang et al., 1999), diatoms (Huang et al., 2009; Jiang et al., 2014), and pollen (Zhang and Long, 2008; Li et al., 2010; Dai and Weng, 2015).

Kong et al. (2014) reported results of paleoenvironmental reconstructions that underscore differences in regional and local dynamics. These authors found a difference in two SST records over the past 8.0 kyr that were reconstructed by using a long-chain alkenone unsaturation index from offshore of the Pearl River submarine delta and the continental margin in the northern SCS. Their study suggests that the SST change was not synchronous in the two locations; rather, the SST gradient was developing in the northern SCS (Kong et al., 2014). Even when different proxies were used on the same sediment core, higher-resolution events of paleo-monsoon climate record or paleoceanographic parameters were at variance. For example, different SSSs were reconstructed by diatom (Jiang et al., 2014) and by $\delta^{18}O$ of foraminifera (Wang et al., 1999) from core 17940 from the north SCS.

For high resolution climatic and paleoceanographic reconstruction it is necessary to consider detailed factors impacting the records. On top of issues such as chronological resolution and different sensitivities of different proxies, biases induced by various laboratory techniques should not be ignored. For example, five weak Asian monsoon events reconstructed by Wang et al. (2005) are not corroborated by the results from Dykoski et al. (2005), although both studies used stalagmite $\delta^{18}O$ from Dongge Cave in mainland China.

In addition to the atmospheric temperature, precipitation, and river inputs, the currents from the western Pacific strongly influence the oceanographic conditions in the northern SCS, including the SST and SSS. Modern observations show that the open sea

area of the northern SCS remains relatively warm year-round because of the branch of the Kuroshio Current and the warm western Pacific waters from the Philippine Sea (Figure 4-1) (Xue et al., 2004; Yuan et al., 2006). As a result, the signal of the summer Monsoon in the northern SCS is not as strong as on land. Thus, proxies that reflect both terrestrial and marine information are ideally suited for reconstructions of past climatic and oceanographic conditions of the northern SCS. Terrestrial palynomorphs (including pollen, spores, and some freshwater algae) and marine dinoflagellate cysts are reliable proxies. Moreover, technically, terrestrial palynomorphs and dinoflagellate cysts can be extracted using the same laboratory technique and identified under a microscope simultaneously, which will greatly reduce method-related biases.

Pollen and spores in marine sediments come from terrestrial vegetation, are transported by winds or water (including currents and rivers), and are deposited in the sea together with other sedimentary particles. Far from the sources, the pollen in the deep sea of the SCS were perhaps less influenced by river inputs and probably were deposited through wind activity. Therefore, pollen preserved in sediment cores are commonly used to reconstruct past vegetation and climate, especially during glacial-interglacial cycles when the surrounding vegetation underwent major changes (e.g., Sun and Li, 1999; Sun et al., 2003; Zhang et al., 2011; Dai et al., 2015). However, during the Holocene, vegetation surrounding the SCS did not change as much as the vegetation during glacial-interglacial cycles. Sun and Li (1999) suggested that the vegetation during the last 10 kyr was close to that of the present, based on the similarity between pollen assemblages during the Holocene and in the surface sediment from the northern SCS. Therefore, to infer climatic changes during the Holocene, a more detailed understanding of pollen

transport and taphonomic conditions needs to be developed. For example, *Pinus* pollen, a most common genus in pollen assemblages from the region, is often interpreted as an indicator of cold climate because it is delivered primarily by winter monsoon to the SCS (e.g., Sun and Li, 1999), but in an open environment strongly influenced by water transport, an increase of *Pinus* pollen could be a signal of a strengthened hydrodynamic condition rather than a cooler climate (Heusser, 1988; Moss et al., 2005; Beaudouin et al., 2007). Thus, understanding the transport mechanism and taphonomy of *Pinus* pollen due to the sea-level rise is required to interpret environmental conditions.

Marine records of dinoflagellate cysts, which are directly associated with upper water masses, can also contribute to the reconstructions of past oceanographic and climatic conditions. Dinoflagellates are one of the major groups of modern marine plankton. Almost half of all dinoflagellate species are heterotrophic, whereas the other half are phototrophic; the latter are commonly referred as autotrophic (Dale, 2009). During their life cycle, many dinoflagellates produce resting cysts that are resistant to physical, chemical, and biological degradation because of organic walls (e.g., Dale, 1996). Distributions of modern dinoflagellate cysts in marine environments are controlled by sea-surface temperature (SST), salinity (SSS), primary productivity, sea-ice cover, and other oceanographic conditions (e.g., Harland, 1993; Dale, 1996; Rochon et al., 1999; de Vernal et al., 2001, 2005; Marret and Zonneveld, 2003; Pospelova et al., 2005, 2008; Zonneveld et al., 2013). Therefore, being preserved in sediments, organic-walled dinoflagellate cysts are commonly used as indicators of past environmental conditions (e.g., Dale, 1996; Zonneveld et al., 2008,; de Vernal et al., 2001, 2005; Mudie et al., 2002; Pospelova et al., 2015; Marret et al., 2009; Bringué et al., 2014). The ratio between

cysts produced by heterotrophic and autotrophic taxa is commonly considered an indicator of coastal proximity or primary productivity (e.g., Harland, 1983; Dale, 1996; Mudie and Rochon, 2001; Pospelova et al., 2008). Dinoflagellate cyst analysis has been carried out in the SCS by Zhao et al. (1992a, b), Mao and Harland (1993), Wu and Sun (2000), Kawamura (2004), Mao et al. (2007), and Wang et al. (2004, 2011). Wu and Sun (2000) investigated the distribution of the dinoflagellate cysts from the surface sediments in the SCS and reported spatial distributions of *Spiniferites* spp. as well as other common cyst taxa such as *Impagidinium*, *Operculodinium centrocarpum* sensu Wall and Dale 1966, *Polysphaeridium zoharyi*, *Lingulodinium machaerophorum* and cysts of *Protoperidinium*. Thus far, most of the work on dinoflagellate cysts in the SCS has focused on changes in dinoflagellate cyst assemblages for stratigraphy or ecological preference of individual taxa. No work has been performed on well-dated Holocene sediment cores to reconstruct past climatic or oceanographic conditions in the SCS based on dinoflagellate cysts.

In addition, most research cores used for Holocene research, except those from the Dongsha section of the SCS, have sedimentation rates too low to resolve centennial-scale paleoenvironmental events. Comparatively, the Zhujiang (Pearl River) section of the northern slope of the SCS has high sedimentation rates, with some sedimentary materials contributed by the Pearl River and by rivers in Southwest Taiwan. This section is only mildly influenced by turbidity currents as reflected by geochemical (Huang et al., 2016) and carbonate (Li et al., 2008) records. Thus, the Zhujiang section of the northern SCS provides an ideal location for high-resolution sedimentary studies of the Holocene

climate and oceanographic conditions. Reconstructions of climatic and oceanographic conditions in this section have not been carried out until now.

In this study, we use a sediment core from the Zhujiang Section of the northern SCS to conduct a high-resolution study of terrestrial palynomorphs with dinoflagellate cyst records over the past 12,500 years. Our objectives are: (1) to determine whether terrestrial (pollen and spores) and marine (dinoflagellate cysts) palynological assemblages record regional sea-level changes and the relevant hydrographic conditions in the SCS (e.g., the opening of the Taiwan Strait); (2) to interpret the signals of monsoon climate changes using pollen and dinoflagellate cysts after taking into account the potential impact of pollen and spore dispersal from sea-level variations; and (3) to determine short-term regional events by comparing our findings with reconstructions based on other paleo-proxies of climatic and oceanographic conditions.

4.2 Regional settings

4.2.1 Physiography

The South China Sea (SCS) is a marginal sea of the western Pacific. It is surrounded by the South China mainland, the Indochina Peninsula, and a chain of islands spanning from Luzon to Borneo (Figure 4-1). The SCS has a narrow shelf in the east, and the shelf widens to the west. On the northern shelf, submarine deltas were developed off the Pearl River, the Red River (Song Hong), and other small rivers. The northern continental slope is between the shelf-break zone and the deep basin, with a water depth of ~300-3700 m.

It is divided into the following five sections, based on directional, geomorphological, and

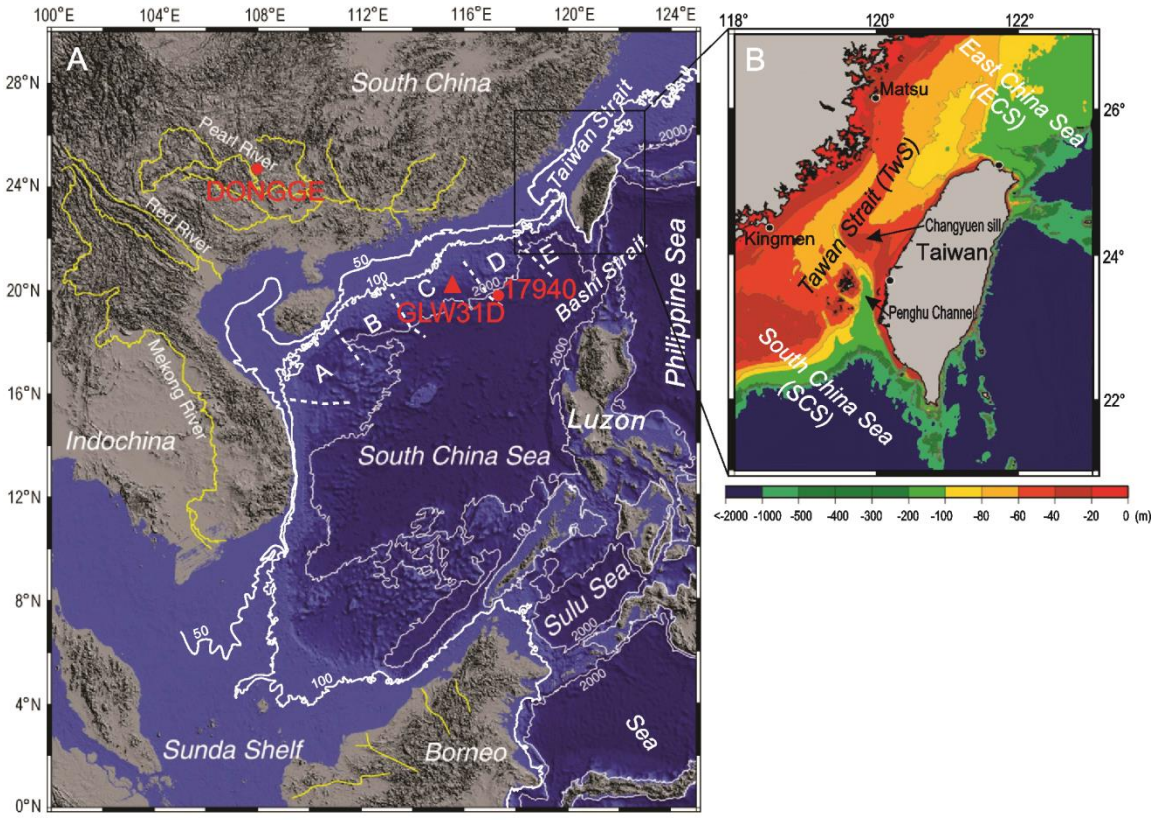

Figure 4-1. 1A.Map of the study area showing the location of GLW31D (this study) and 17940 (Jiang et al., 2014) sediment cores in the South China Sea (modified fromWang et al., 2008;Wang and Li, 2009). Five sections of the northern slope are marked: A. Yingqong, B. Shenhu, C. Zhujiang (Pearl River), D. Dongsha, and E. Taiwan Shoal sections (Wang et al., 2008). 1B. Bathymetric map of the Taiwan Strait (modified from Chen et al., 2016).

bathymetric characteristics: the Yingqong section, the Shenhu section, Zhujiang (Pearl River) section, the Dongsha section, and the Taiwan Shoal section (Figure 4-1) (Wang et al., 2008). The sedimentary accumulation rates in the Dongsha and Zhujiang sections are much higher than those in the other sections due to the high input of terrestrial material, but the sources of this material are different in these two sections. On the slope of the

Dongsha section, the sedimentary material is transported by bottom currents to form high-sedimentation-rate drifts (Ludmann et al., 2001; Shao et al., 2001), and ~40% of the terrestrial material comes from the Luzon region (Liu et al., 2008). In contrast, terrestrial material on the slope of Zhujiang Section is delivered by rivers from southwest Taiwan and by the Pearl River from the land of Southern China, having much less terrestrial material from the Luzon islands (Liu et al., 2008).

4.2.2 Modern climatic and oceanographic setting

The climate of the SCS region is characterized by the tropical East Asian Monsoon (EAM), with northeast wind in winter (October-April) and southwest wind in summer (mid-May-mid-September) (Figures 4-2A and 4-2B). The winter monsoon affects the SCS more strongly, and it lasts much longer than the summer monsoon (Wang and Li, 2009). The mean air temperature is ~15-25°C during the coldest month of January and is the warmest in July, at ~28°C. The mean annual rainfall is ~1,000-2,000 mm. The rainfall in the northern SCS is ~800 mm greater than evaporation during the humid season (April-October), whereas evaporation exceeds rainfall by ~600 mm during the dry season (November-March) (Yan, 1997).

The sea surface temperature (SST) ranges from 28.5°C to 29.5°C in summer. In winter, an intense western boundary current flows southward on the continental slope and transports cold water from the north, creating a distinct cold tongue (Figure 4-2C) (Liu et al., 2004b). The sea surface salinity (SSS) varies between 32.8 and 34.2 psu. In winter, the SSS is higher in the northern part of the SCS due to the Kuroshio Current's influence, and it declines southward because of increased precipitation. In summer, the SSS varies

to a lesser degree in the northern SCS than in the southern part of the sea (Wang and Li, 2009).

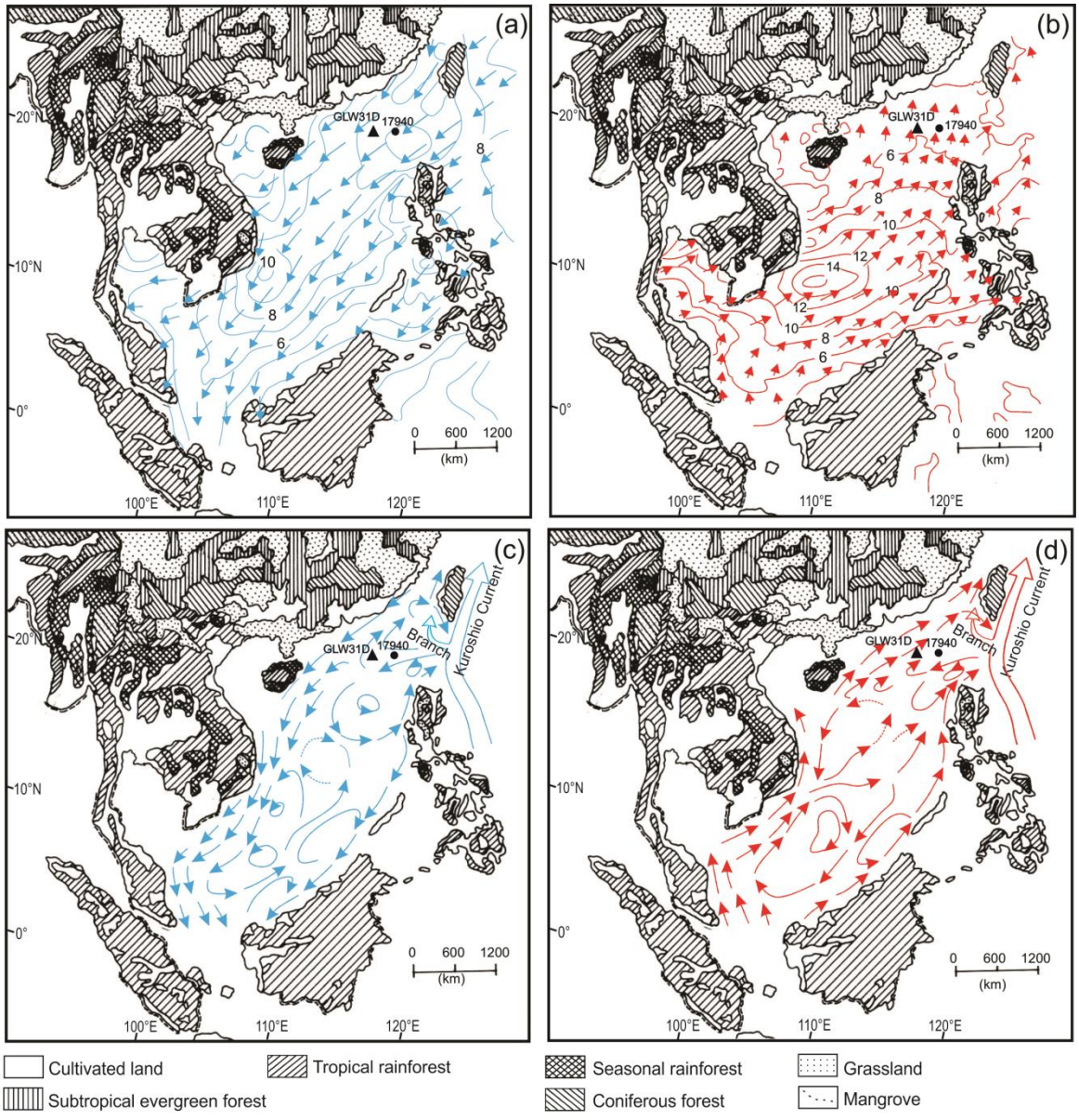

Figure 4-2. Maps showing major regional vegetation types as well as the surfacewinds and currents in the South China Sea (modified from Fang et al., 1998; Sun et al., 1999; Wang and Li, 2009). Surface winds over the SCS with wind velocity in (A) winter (December–February) and in (B) summer (June–August) (from Wang and Li, 2009); Surface circulation of the modern SCS in (C) winter and (D) summer (from Fang et al., 1998).

The surface water circulation in the SCS has seasonal trends. In winter, there is a basin-wide cyclonic gyre and the northeast coastal currents, whereas in summer, the basin-wide circulation splits into a weakened cyclonic gyre in the north and a strong anti-cyclonic gyre in the south with southwest coastal currents (Figures 4-2C and 4-2D) (Qu et al., 2002). Currently, the surface waters of the SCS exchange freely with waters from the neighbouring seas, while deeper water flows into the SCS primarily from the western Philippine Sea through the Bashi (or Luzon) Strait. In the SCS, the surface water is mixed with the deep water from the western Pacific and flows out at upper-intermediate depths (Qu et al., 2000). The water transport through the Bashi Strait influences the circulation and heat budget of the SCS. On the other hand, water from the Kuroshio Current, which forms in the east of the Philippines and flows northward along the coast of Luzon, branches into the SCS through the Bashi Strait (Yuan et al., 2002).

4.2.3 Modern surrounding vegetation

The regional vegetation surrounding the SCS is very diverse and includes the following: tropical rainforest, seasonal rainforest, tropical and subtropical grassland, subtropical evergreen forest, tropical and subtropical conifer forest, and mangrove along the coast (Figure 4-2) (Sun et al., 1999). The tropical rainforest is dominated by the families Fagaceae (*Castanopsis/Lithocarpus* and *Quercus*), Lauraceae (*Cinnamomum* spp., *Lindera* spp. and *Caryodaphnophis* spp.), Anacardiaceae (*Dracontomelum* spp.), Meliaceae (*Aphanamixis* spp., *Aglaia* spp. and *Chisocheton* spp.), Moraceae (*Artocarpus* spp. and *Ficus* spp.), Tiliaceae, Theaceae, Hamamelidaceae, and Magnoliaceae (Wu, 1980; Li et al., 2006b). Tropical vegetation elements gradually increase with decreasing

latitude, whereas the subtropical evergreen broadleaved forest gradually changes southward into the southern tropical monsoon forest and tropical moist rainforest in Southeast China. Most of the natural forests have been replaced by cropland due to intense agriculture developments, and the secondary successional plant *Pinus massoniana* now dominates hilly regions (Figure 4-2) (Li et al., 2006b; Dai and Weng, 2015).

4.3 Materials and Methods

4.3.1 Core collection, lithology, sub-sampling, and chronology

The 2.4 m gravity core GLW31D (20° 1'57.90"N, 115° 27'52.92"E, at 1,187 m water depth) was collected from the northern continental slope of the SCS in 2012 by the First Institute of Oceanography, State Oceanic Administration of China. The core was drained, split, described, photographed, and subsampled at the State Key Laboratory of Estuarine and Coastal Research, East China Normal University, China. The sediments mainly consist of dark grey clayey silts and silty clays, with both the median diameter and average grain size ranging from 6.8 to 7.5 (φ), as measured by a Laser Particle Analyzer (Malvern 2000). The occasional "sandy" grains were mainly foraminifera. A total of 118 samples of 2 cm each were subsampled continuously for pollen and spore (terrestrial palynomorph) analysis. Only 27 samples were selected for dinoflagellate cyst analysis.

The chronology of core GLW31D was established based on 12 accelerator mass spectrometry (AMS) ^{14}C measurements, performed by Beta Analytic Inc. on hand-picked planktonic foraminifera *Globigerinoides ruber* and *G. sacculifer* (Table 4-1). Age determinations were based on a Libby half-life of 5,568 years. The conventional

Table 4-1. AMS ^{14}C ages of core GLW31D.

Sample No.	Core depth (cm)	Material	Measured ^{14}C age (^{14}C yr BP)	$^{13}C/^{12}C$ (‰)	Conventional ^{14}C age (^{14}C yr BP)	Calibrated ^{14}C age (cal yr BP) *2σ range	**Median	Beta ID (Bate-)
GLW31D-5	4-6	*Globigerinoides ruber*, *G. sacculifer*	810 ± 30	0.9	1230 ± 30	779 - 650	710	386772
GLW31D-25	24-26	*Globigerinoides ruber*, *G. sacculifer*	2430 ± 30	0.7	2850 ± 30	2672 - 2386	2530	386773
GLW31D-45	44-46	*Globigerinoides ruber*, *G. sacculifer*	3490 ± 30	1	3920 ± 30	3918 - 3694	3810	386774
GLW31D-65	64-66	*Globigerinoides ruber*, *G. sacculifer*	4700 ± 30	1.3	5130 ± 30	5526 - 5309	5420	386775
GLW31D-85	84-86	*Globigerinoides ruber*, *G. sacculifer*	5510 ± 30	1.3	5940 ± 30	6379 - 6213	6300	386776
GLW31D-105	104-106	*Globigerinoides ruber*, *G. sacculifer*	6040 ± 30	0.4	6460 ± 30	6972 - 6767	6870	386777
GLW31D-123	122-124	*Globigerinoides ruber*, *G. sacculifer*	7440 ± 30	0.9	7860 ± 30	8341 - 8175	8260	386778
GLW31D-143	142-144	*Globigerinoides ruber*, *G. sacculifer*	2420 ± 30	-0.4	2820 ± 30	2615 - 2346	2480	390582
GLW31D-163	162-164	*Globigerinoides ruber*, *G. sacculifer*	8370 ± 30	1.2	8800 ± 30	9482 - 9313	9400	386780
GLW31D-183	182-184	*Globigerinoides ruber*, *G. sacculifer*	8770 ± 30	-0.1	9180 ± 30	10037 - 9687	9860	386781
GLW31D-203	202-204	*Globigerinoides ruber*, *G. sacculifer*	9810 ± 40	0.1	10220 ± 40	11246 - 11052	11150	386782
GLW31D-223	222-224	*Globigerinoides ruber*, *G. sacculifer*	9850 ± 40	1.2	10280 ± 40	11306 - 11107	11210	386783
GLW31D-235	234-236	*Globigerinoides ruber*, *G. sacculifer*	10730 ± 30	-0.1	11140 ± 30	12695 - 12538	12620	390583

[a] Relative area under the distributin curve.
[b] The median ages were rounded to the nearest multiple of 10 yr.

radiocarbon ages were calibrated using Calib 7.02 (http://calib.Qub.ac.uk/calib/calib.html) in which the data sets are from Hughen et al. (2004) and Reimer et al. (2009). The data were calculated with the Marine09 program and were corrected into calendar years (cal yr BP). The calibration curve is estimated at intervals of five yr for the range 0–10 cal kyr BP, 10 yr for 10–15 cal kyr BP (Hughen et al., 2004; Reimer et al., 2009). Therefore, technically, median ages rounded into the nearest multiple of 10 yr were used in the text since the errors of the measured data are less than 50 yr (30-40 yr) (Table 4-1). One sample at 142-144 cm depth was dated at 2,820±30 ^{14}C yr BP, which is much

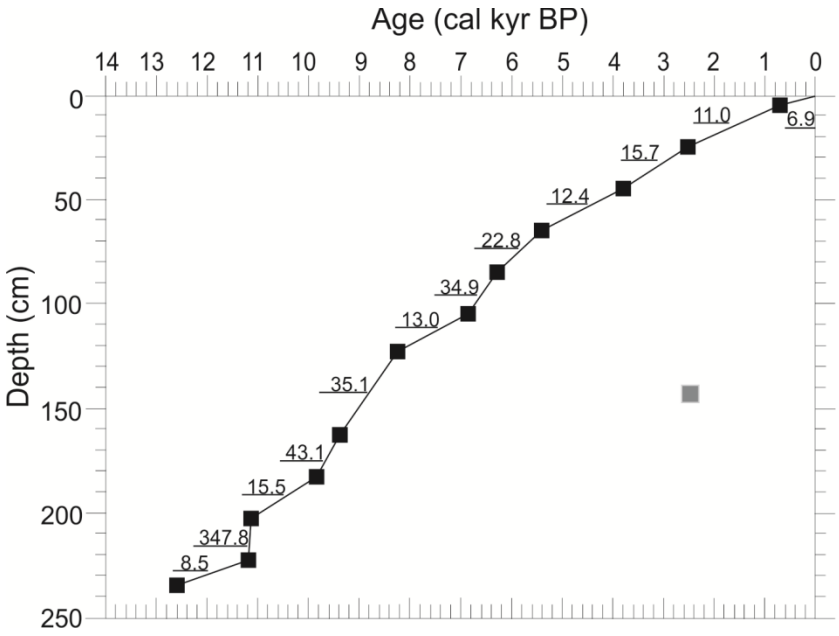

Figure 4-3. Age-depth relationship of core GLW31D shown by the calibrated dates plotted against sediment depth. Underlined numbers are the sedimentation rates (cm kyr^{-1}) calculated by linear interpolation between two adjacent ^{14}C ages. The 95% confidence intervals are too small to be shown on the plot.

younger than the overlying layers (Table 4-1 and Figure 4-3). Because it could have been contaminated by younger material in the laboratory due to human errors, this sample was excluded from further age calculations. The calibrated dates of the other eleven 11

samples are plotted against sediment depth and shown in Figure 4-3. All ages were calculated by linear interpolation between each adjacent pair of calibrated ages, and the sedimentation rates were estimated based on the age-depth linear relationship model (Figure 4-3). The accumulation rates range from ~7 cm kyr^{-1} to ~43 cm kyr^{-1}, with a much higher rate of ~347 cm kyr^{-1} in the lower part of the core (Figure 4-3). Each palynological sample is 2 cm, thus it represents ~50 to 290 yr on average, with the exception of ~6 yr at the ~200-225 cm depth.

4.3.2 Palynological sample preparation and identification

Pollen, spores, and dinoflagellate cysts were extracted using a standard palynological processing technique (Pospelova et al. 2005, 2010). All samples of known volume and dry weight were treated with 10% HCl to remove carbonates, 48% HF at room temperature to dissolve silicates, and by a second 10% HCl treatment to eliminate precipitated fluorosilicates (e.g., Price et al. 2016). To estimate the concentrations and fluxes of palynomorphs, one tablet of *Lycopodium clavatum* grains (batch no. 177745, University of Lund, Sweden) was added to each sample (Stockmarr, 1971; Mertens et al., 2009, 2012). The samples were sieved through a 120 μm Nitex nylon mesh and retained over a 10 μm mesh to remove fine and coarse particles. Before collecting the residue on the 10 μm Nylon mesh, the samples were gently sonicated for up to one minute. The residues were strew-mounted in glycerine jelly between a slide and a coverslip. To avoid any loss of delicate cysts through oxidation (e.g., Dale, 1976; Zonneveld et al., 1997, 2007; 2008), oxidizing reagents were not used (Marret, 1993; Hopkins and McCarthy,

2002; Mertens et al., 2009). All samples and slides were processed and stored at the Paleoenvironmental/Marine Palynology Laboratory, University of Victoria.

Palynological grains (e.g., pollen and spores, see Table 4-2 and Plates 4-I-4-IX), and dinoflagellate cysts, see Table 4-3 and Plates 4-X-4-XIV) were identified and counted using a Nikon Eclipse 80i optical microscope at 600× magnification or higher at 1,200× magnification. We use the term "terrestrial palynomorphs" to refer to pollen, spores, and some freshwater algae. Palynomorph concentrations, fluxes, and percentages were calculated separately on total terrestrial palynomorphs and on total dinoflagellate cysts. Total terrestrial palynomorphs (pollen and spores) and dinoflagellate cyst counts vary from 300 to 641 and from 301 to 388, respectively. An average of 350 grains of terrestrial palynomorphs and ~330 dinoflagellate cysts were counted per sample.

The identification of terrestrial palynomorphs was based on Huang (1972), Academia Sinica (1976, 1982), and Yamanoi (2003). Dinoflagellate cysts were identified according to Matsuoka and Bujak (1988), McMinn (1991), Rochon et al. (1999), Yu and Morozova (2013), Zonneveld and Pospelova (2015). Table 4-3 lists all dinoflagellate cyst taxa identified in core GLW31D, and it includes their autotrophic or heterotrophic affinity. We refer to dinoflagellate cysts produced by autotrophic and heterotrophic dinoflagellates as "autotrophic cysts" and "heterotrophic cysts", respectively. Folded brown cysts with obscured horns and/or granulated brown cysts were grouped as cysts of *Protoperidinium* spp. (Images 6-13 in Plate 4-XIV).

Table 4-2. List of all terrestrial palynomorphs (including pollen, spores, and some freshwater algae) identified in core GLW31D.

Conifer arboreal pollen	Broad-leaved arboreal pollen		Herb pollen		Mangrove pollen	Fern spores & Algae
Tropical	**Temperate**		**Mesophyte**	**Drought-torlerant**	**Mangrove**	**Monolete**
Dacrycarpus [Podacarpaceae]	*Alnus* [Betulaceae]	Loranthaceae	Aizoaceae	*Artemisia* [Compositae]	*Aegiceras corniculatuum*[Myrsinaceae]	*Anisocampium* [Athyriaceae]
Dacrydium [Podacarpaceae]	*Carpinus* [Betulaceae]	*Lonicera* [Caprifoliaceae]	Acanthaceae	*Aster*-type [Compositae]	*Avicennia* [Verbenaceae]	*Davallia* [Davalliaceae]
Podocarpus [Podacarpaceae]	*Celis* [Ulmaceae]	Magnoliaceae	Caryophyllaceae	Chenopodiaceae/Amaranthaceae	*Excoecaria* [Euphorbiaceae]	*Dictyodroma* [Athyriaceae]
Non-tropical	*Fagus* [Fagaceae]	*Mallotus* [Euphorbiaceae]	Celastraceae	*Ciraium*-type [Compositae]	*Rhizophora apiculata* [Rhizophoraceae]	*Diplazium zeylanicum* [Athyriaceae]
Cupressaceae	*Juglans* [Juglandaceae]	Meliaceae	*Celastrus* [Celastraceae]	Compositae	*Rhizophora mucronata* [Rhizophoraceae]	*Gymnogrammitis dareiformis*
Cedrus [Pinaceae]	*Quercus* [Fagaceae]	Menispermaceae	*Clerodendron* [Verbenaceae]	*Laggera*-type [Compositae]	*Rhizophora stylosa* [Rhizophoraceae]	[Gymnogrammitidaceae]
Cycas [Cycadaceae]	*Salix* [Salicaceae]	Moraceae	*Coelospermum* [Rubiaceae]	*Solidago*-type [Compositae]	*Sonneratia* [Sonneratiaceae]	*Leptochilus* [Polypodiaceae]
Picea [Pinaceae]	*Ulmus* [Ulmaceae]	*Myrica* [Myricaceae]	*Colquhounia* [Labiatae]	*Taraxacum*-type [Compositae]	**Back-mangrove**	*Monogramma* [Vittariaceae]
Pinus [Pinaceae]	**Tropical-subtropical**	Myristicaceae	Convolvulaceae	**Wetland**	*Brownlowia tersa* [Malvaceae]	Polypodiaceae
Taxodiaceae	*Ailanthus* [Rutaceae]	Myrtaceae	Crucifferae	*Acorus* [Acoraceae]	Combretaceae	*Phymatopsis* [Polypodiaceae]
Tsuga [Pinaceae]	*Alchornea* [Euphorbiaceae]	Oleaceae	Elatinaceae	Alismataceae	*Pandanus* [Pandanaceae]	*Polypodium* [Polypodiaceae]
	Aglaia [Meliaceae]	*Oroxylum* [Bignoniaceae]	Eriocaulaceae	Araceae		*Pyrrosia* [Polypodiaceae]
	Allophyllus [Sapindaceae]	Palmae	Fabaceae	*Balanophora spicata* [Balanophoraceae]		*Vittaria* [Vittariaceae]
	Altingia [Altingiaceae]	Passifloraceae	Gesneriaceae			**Trilete**
	Anacardiaceae	*Phyllanthus* [Euphorbiaceae]	*Gmelina* [Verbenaceae]	Cyperaceae		*Acrostichum* [Dennstaedtiaceae]
	Arenga [Palmae]	Piperaceae	Labiatae	Gentianaceae		*Archangiopteris* [Angiopteridaceae]
	Apocynaceae	*Polyalthia* [Annonaceae]	Lythraceae	Liliaceae		*Athyrium* [Dryopteridaceae]
	Araliaceae	Rosiaceae	Malpighiaceae	*Nymphoides* [Gentianaceae]		*Ceratopteris* [Pteridaceae]
	Arcangelisia [Menispermaceae]	*Rhodamnia* [Myrtaceae]	Malvaceae	*Polygonum* [Polygonaceae]		*Cibotium* [Dicksoniaceae]
	Berberidaceae	*Rhus* [Anacardiaceae]	*Peliosanthes* [Nepenthaceae]	Potamogetonaceae		*Cyathea* [Cyatheaceae]
	Bombax [Bombacaceae]	Rutaceae	*Plantago* [Plantaginaceae]	*Thalictrum* [Ranunculaceae]		*Dryopteris* [Dryopteridaceae]
	Camptotheca [Nyssaceae]	Samydaceae	*Plumbago* [Plumbaginaceae]	*Typha* [Typhaceae]		*Equisetum* [Equisetaceae]
	Carya [Juglandaceae]	Sapindaceae	Poaceae	*Utricularia* [Lentibulariaceae]		Gleicheniaceae
	Castanopsis [Fagaceae]	*Shorea* [Dipterocarpaceae]	Rubiaceae			Gymnogrammaceae
	Casuarina [Casuarinaceae]	*Spathodea* [Bignoniaceae]	*Rubia* [Rubiaceae]			Hemionitidaceae
	Chuniophoenix [Palmae]	Sterculiaceae	Saururaceae			*Hymenophyllum* [Hymenophyllaceae]
	Clausena [Rutaceae]	*Suriana* [Simaroubaceae]	Solanaceae			*Lygodium* [Schizaeaceae]
	Clerodendrum [Verbenaceae]	*Symplocos* [Symplocaceae]	Thymelaeaceae			*Lygodium microphyllum* [Schizaeaceae]
	Dipterocarpaceae	*Syzygium* [Myrtaceae]	*Triplostegia* [Dipsacaceae]			*Lycopodium* [Lycopodiaceae]
	Distylium [Hamamelidaceae]	*Tilia* [Tiliaceae]	Umbelliferae			Ophioglossaceae
	Elaeagnus [Elaeagnaceae]	*Toddalia* [Rutaceae]	Valeriavaceae			*Osmunda* [Osmundaceae]
	Elaeocarpus [Elaeocarpaceae]	*Zanthoxylum* [Rutaceae]	Verbenaceae			Parkeriaceae
	Eucalyptus [Myrtaceae]					*Pityrogramma* [Pteridaceae]
	Euphorbia [Euphorbiaceae]					*Plagiogyria* [Plagiogyriaceae]
	Evodia [Rutaceae]					*Pteridium* [Dennstaedtiaceae]
	Ficus [Moraceae]					*Pteris* [Pteridaceae]
	Garcinia [Clusiaceae]					*Salvinia* [Salviniaceae]
	Helicia [Proteaceae]					*Selaginella* [Selaginellaceae]
	Ilex [Aquifoliaceae]					**Freshwater algae**
	Lauraceae					*Concentricystes*
	Liquidambar [Altingiaceae]					*Zygnema*

Note: Some genera or species have been lumped into their respective family or genera in the table. The types are not strictly classified according to the geobotanical method; the grouping of broad-leaved arboreal pollen merely indicates that they can grow well in temperate and tropical-subtropical areas (Academia Sinica, 1982).

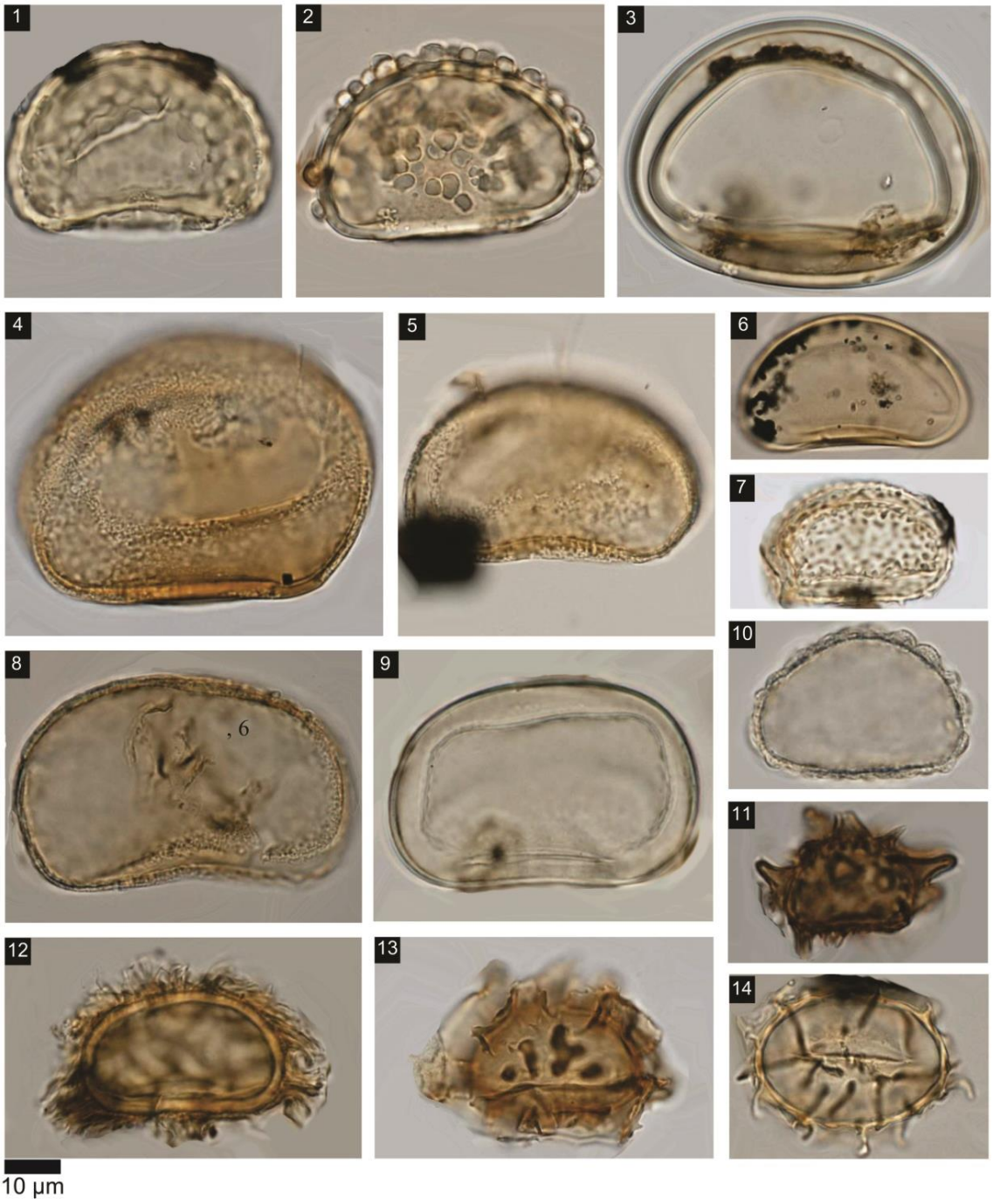

Plate 4-I. Monolete spores: 1. *Polypodium*, 2-5. *Pyrrosia*, 6. *Leptochilus*, 7. *Phymatopsis*, 8-9. *Vittaria*, 10. *Davallia*, 11. *Diplazium zeylanicum*, 12. *Gymnogrammitis dareiformis*, 13. *Dictyodroma*, 14. *Anisocampium.* The scale bar is 10 µm.

Plate 4-II. Trilete spores: 1-3. *Microlepia*, 4-5. *Cyathea*, 6-7. *Archangiopteris*, 8-10. *Lycopodium*, 11-16. *Selaginella*, 17. *Lygodium microphyllum*, 18-19. *Lygodium*, 20-21. *Pteris*, 22. *Cibotium*, 23. *Pityrogramma*, 24. Gymnogrammaceae. The scale bar is 10 µm.

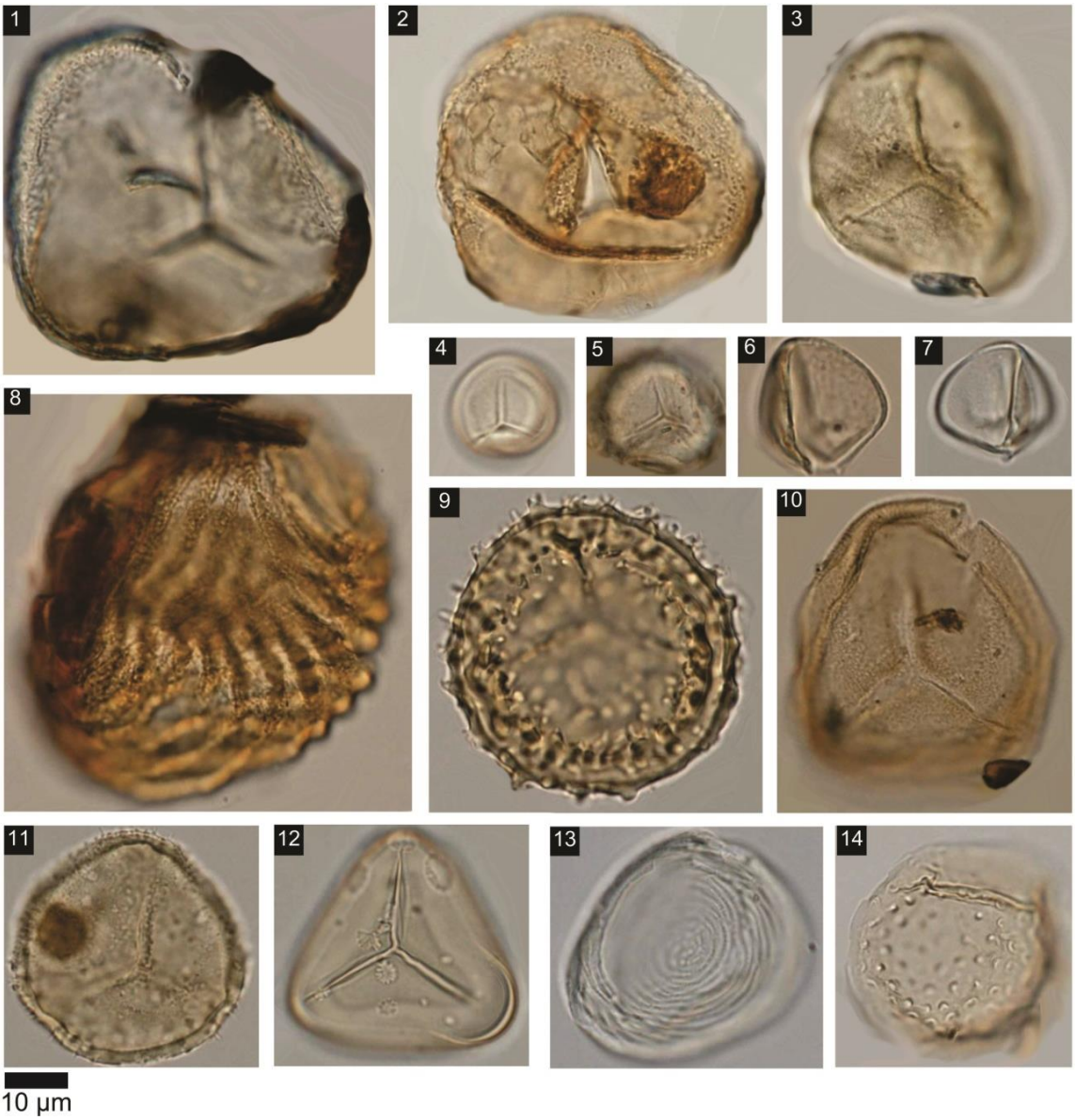

Plate 4-III. Trilete spores (1-12) and fresh water algae (13-14): 1-3. *Acrostichum,* 4-5. *Salvinia,* 6-7. *Monogramma*, 8. *Ceratopteris*, 9. *Osmunda,* 10-11. Hymenophyllaceae, 12. *Pteridium*, 13. *Concentricystes*, 14. *Zygnema*. The scale bar is 10 µm.

4.3.3 Statistical analysis

The relative abundances of each type were calculated as percentages of the total counted grains (terrestrial palynomorphs) or the total cysts (dinoflagellate cysts),

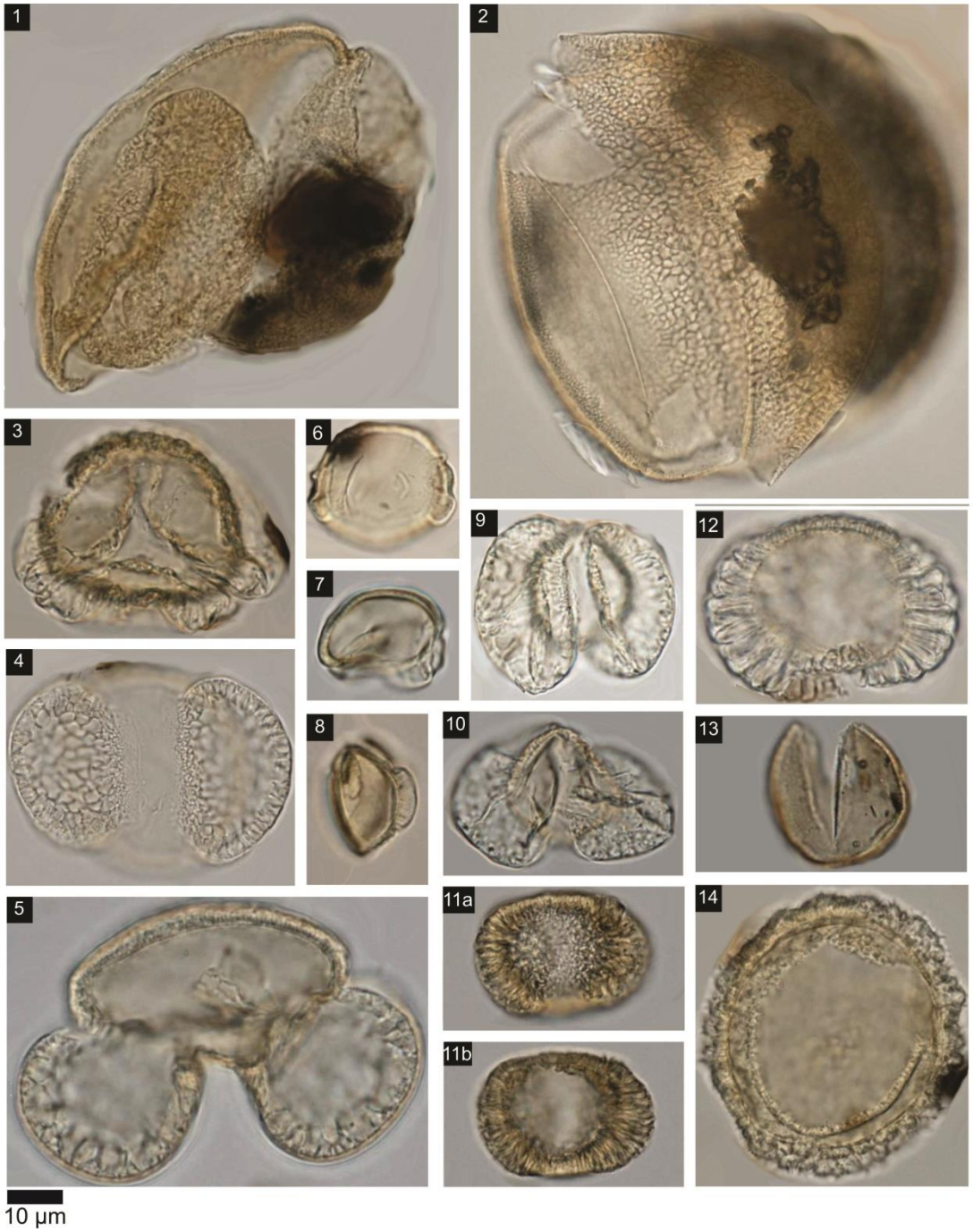

Plate 4-IV. Saccate pollen: 1-2. *Picea*, 3. *Dacrycarpus*, 4-5. *Pinus*, 6-8. *Pinus*? - small type, 9-10. *Podocarpus*, 11. *Dacrydium*? - small type, 12. *Dacrydium*, 13. Cupressaceae, 14. *Tsuga*. Scale bar is 10 µm.

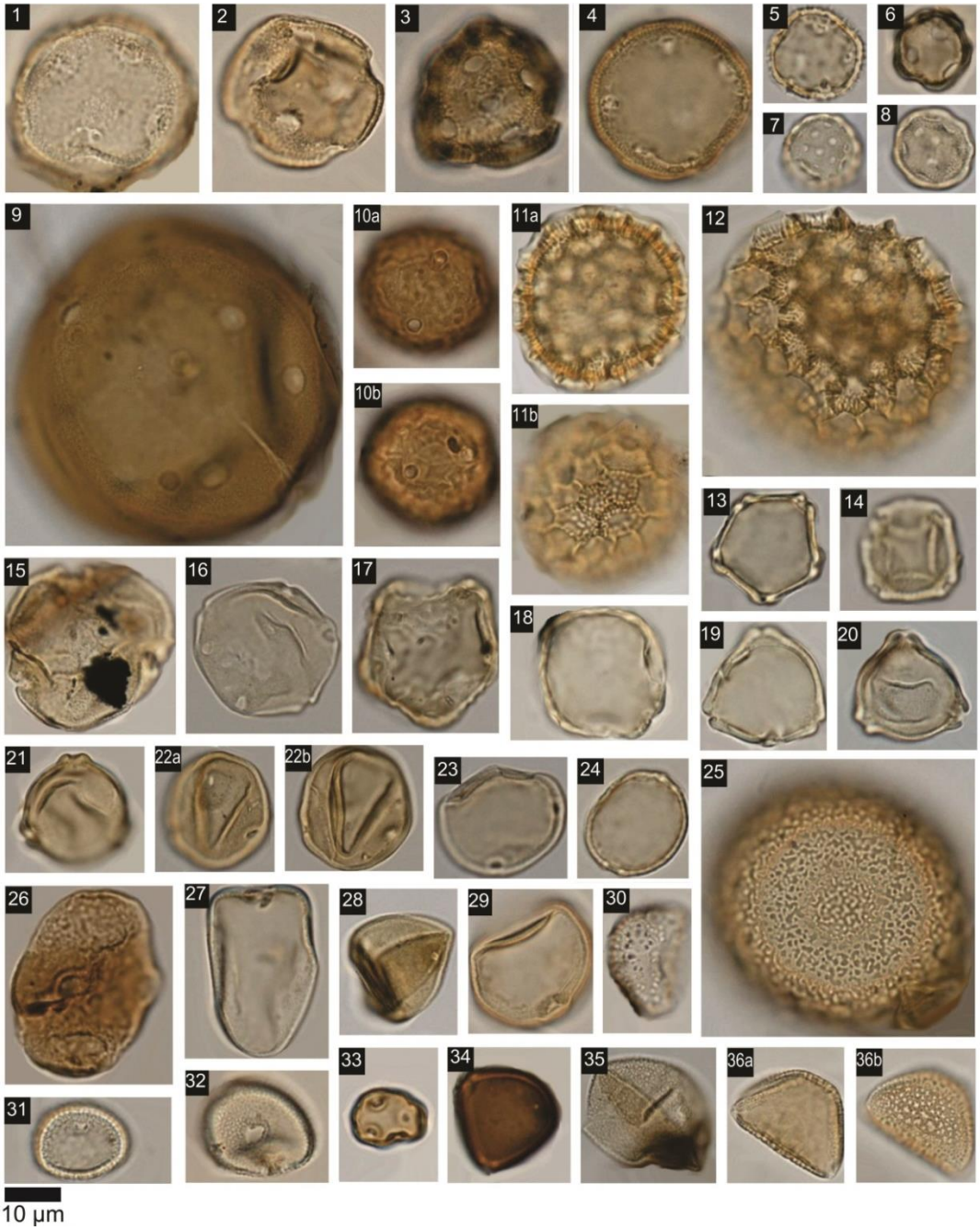

Plate 4-V. Porate pollen: 1-2. *Altingia*, 3. Caryophyllaceae, 4. *Plantago*, 5. Alismataceae, 6. *Balanophora spicata*, 7. Chenopodiaceae/Amaranthaceae, 8. *Thalictrum*, 9-10. Malpighiaceae, 11-12. *Polygonum*, 13-14. *Alnus*, 15. *Tilia*, 16. *Juglans*, 17-18. *Ulmus*, 19-20. *Myrica*, 21. *Casuarina*, 22. *Carya*, 23. Moraceae, 24. *Ficus*, 25. *Polyalthia*, 26. *Sonneratia*, 27. Cyperaceae, 28-29. Poaceae, 30. *Pandanus*, 31-32. *Typha*, 33-34. Apocynaceae, 35. Potamogetonaceae, 36. Myristicaceae. The scale bar is 10 µm.

Plate 4-VI. Colpate pollen: 1. *Utricularia*, 2. Elatinaceae, 3. *Oroxylum*, 4-5. *Clerodendron*, 6-9. *Distylium*, 10. Aizoaceae, 11. *Colquhounia*-type, 12-13. Berberidaceae, 14-16. *Rubia*, 17. Loranthaceae, 18. Ranunculaceae, 19. *Shorea*, 20-22. *Quercus*, 23-24. Oleaceae, 25-26. Crucifferae, 27-28. *Arcangelisia* type, 29. *Cycas*, 30. Piperaceae, 31-32. Liliaceae, 33. *Arenga*, 34. *Chuniophoenix*, 35. Araceae. The scale bar is 10 µm.

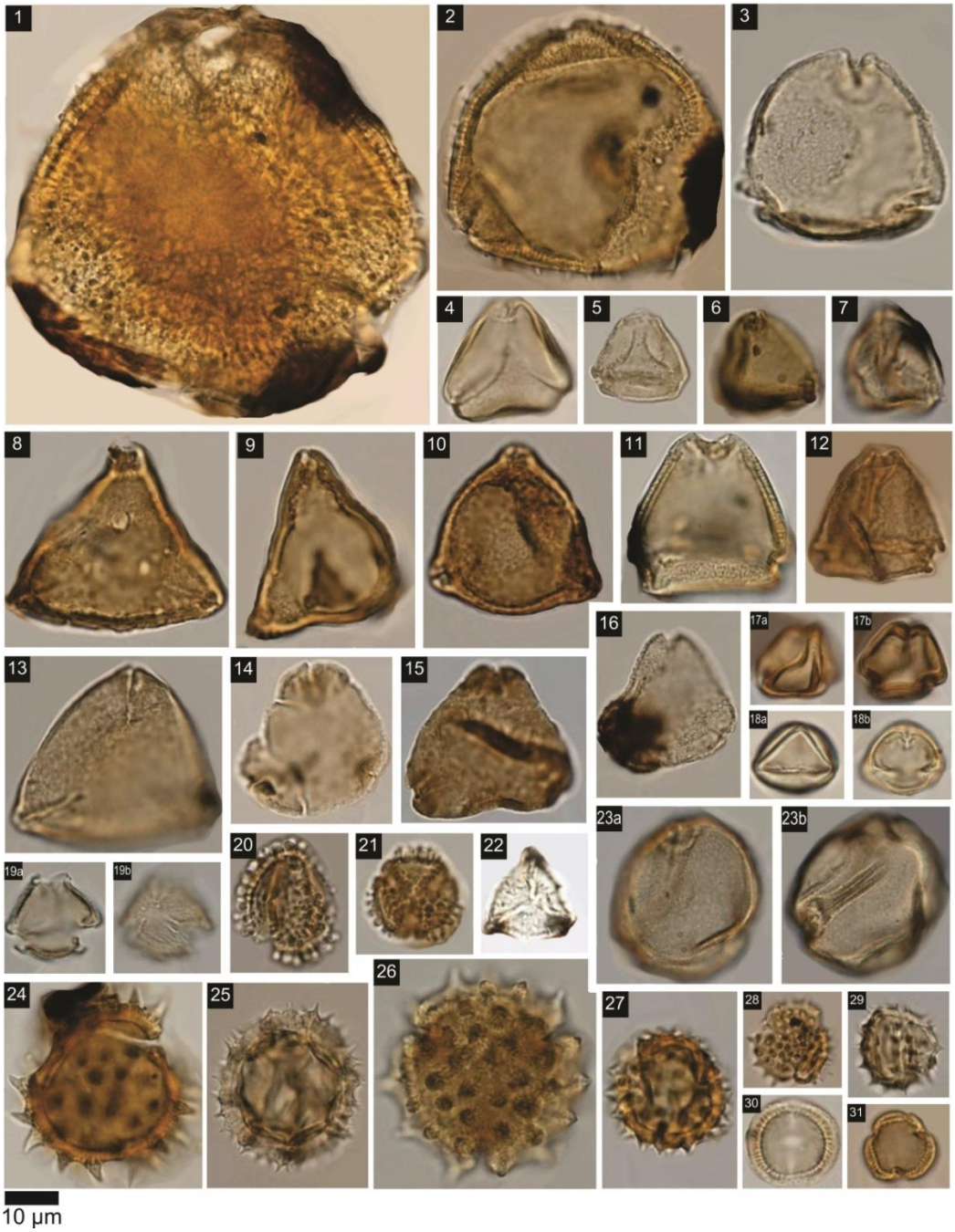

Plate 4-VII. Tricolporate and angular-amb triporate pollen (8-9): 1. *Triplostegia*, 2. *Lonicera*, 3. *Brownlowia tersa*, 4. *Eucalyptus*, 5. *Syzygium*, 6-7. *Rhodamnia*, 8-9. *Helicia*, 10. *Elaeagnus*, 11. *Camptotheca* type, 12. Sapindaceae, 13. *Suriana*, 14-16. *Allophyllus*, 17. Myrsinaceae, 18. *Elaeocarpus*, 19. *Ailanthus*, 20. Lythraceae, 21-22. *Ilex*, 23. *Fagus*-type, 24. *Laggera*-type, 25. *Taraxacum*-type, 26. *Ciraium*-type, 27. *Solidago*-type, 29-28. *Aster*-type, 30-31. *Artemisia*. Scale bar is 10 µm.

Plate 4-VIII. Tricolporate and multi-porate pollen: 1-4. *Evodia*, 5. *Toddalia*, 6-12. Rutaceae, 13-17. Celastraceae, 18-21. Anacardiaceae, 22. *Rhus*, 23-24. Euphorbiaceae, 25-27. *Euphorbia*, 28-29. *Fagus*, 30-33. *Phyllanthus*. The scale bar is 10 µm.

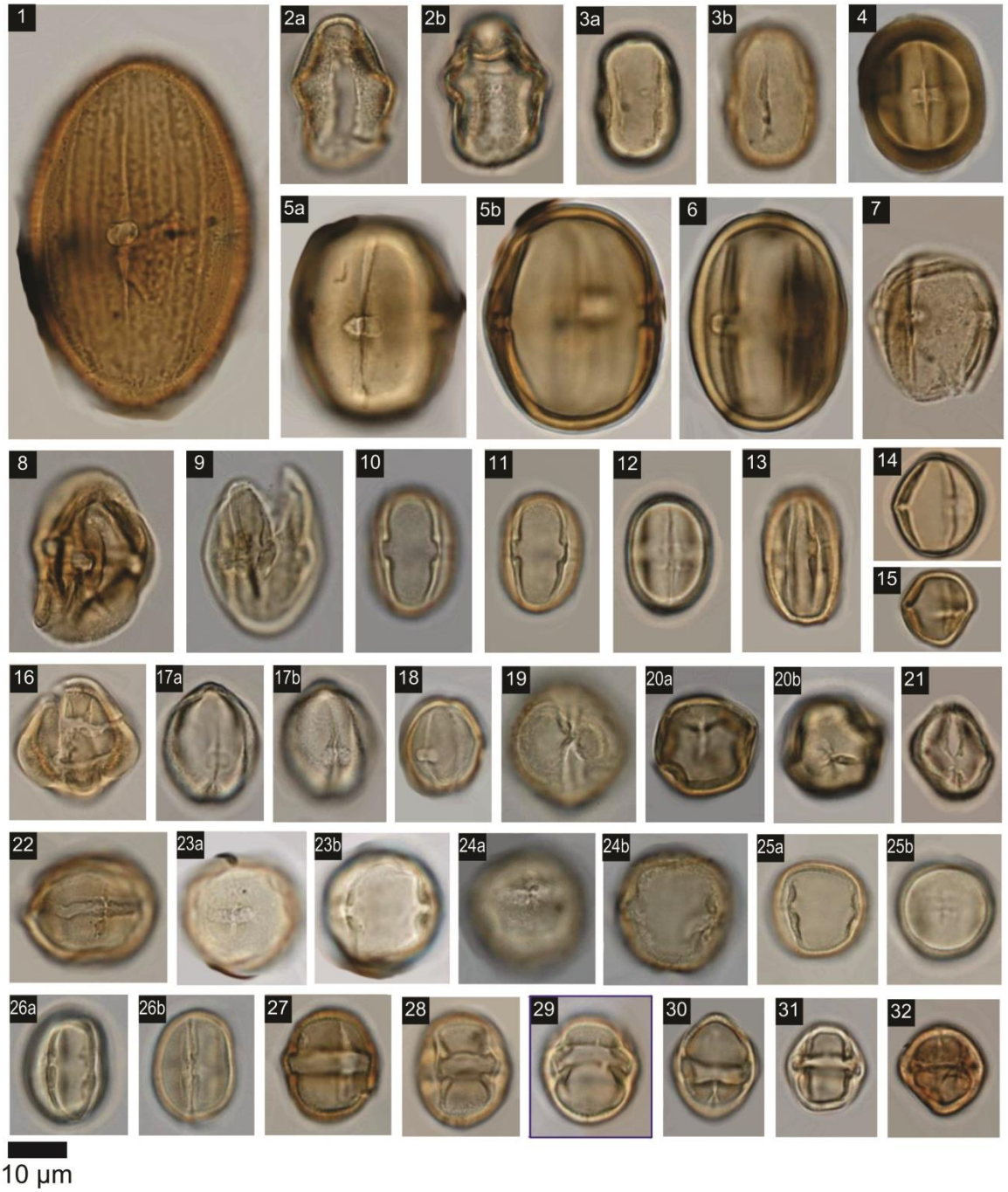

Plate 4-IX. Tricolporate pollen: 1. *Strobilanthes*, 2. *Duabanga*, 3-4. Undetermined, 5-6. Sapotaceae, 7-9. Leguminosae, 10-13. *Castanopsis*/*Lithocarpus*, 14-15. *Solanum*, 16-17. *Lumnitzera*, 18. *Terminalia*, 19. Caesalpiniaceae, 20. *Casearia*-type? 21. Saurauiaceae, 22. *Mallotus*, 23-24. *Homonoia*, 25. *Macaranga*, 26. *Aegiceras corniculatum*, 27-29. *Rhizophora apiculata*, 30. *Rhizophora mucronata*, 31-32. *Rhizophora stylosa*. The scale bar is 10 µm.

including unidentified palynomorphs, into the total sums. Both dry weight (grains g^{-1} or cysts g^{-1}) and volume concentrations (grains cm^{-3} or cysts cm^{-3}) were calculated using the formula: C_m (or C_v) = (L_{total}*$P_{counted}$)/($L_{counted}$*G (or V)), where C_m and C_v are the dry weight and volume concentrations, respectively. L_{total} is the number of *Lycopodium* spores added to the sample. $L_{counted}$ and $P_{counted}$ are the numbers of counted *Lycopodium* grains and palynological grains or dinoflagellate cysts in each sample. G is the dry weight and V the volume of each sample.

Flux is the number of palynological grains or dinoflagellate cysts accumulated per area (e.g., one square centimetre) per time period (e.g., one year) (Bradley, 2015). In this study, the fluxes (grains cm^{-2} y^{-1} or cysts cm^{-2} y^{-1}) of terrestrial palynomorphs and dinoflagellate cysts were calculated according to their volume concentrations and sedimentary accumulation rates using the following formula: $F = C_v * S_{rate}$, where C_v is the volume concentration of the palynomorphs, and S_{rate} is the sediment accumulation rate of each sample (Figure 4-3).

All palynological diagrams were created with Tilia 1.5.12 software (Grimm, 1991, 1992). Only selected taxa of pollen, spores, and dinoflagellate cysts are shown in Figures 4-4 and 4-5. Terrestrial palynomorph and dinoflagellate cyst zones were determined by conducting a stratigraphically constrained cluster analysis using constrained cluster analysis (CONISS). Square root transformations and Edwards and Cavalli-Sforza's chord distances were chosen to be dissimilarity coefficients (Grimm, 1992).

4.4 Results

4.4.1 Terrestrial palynomorphs

Terrestrial palynomorphs (TP) of ~186 taxa were identified in 118 samples of the core (Table 4-2, Plates 4-I-4-IX). Most of them were observed in small numbers because all pollen and spore assemblages were overwhelmingly dominated by *Pinus* pollen with a large contribution of fern spores of Polypodiaceae and Gleicheniaceae (Figure 4-4). According to the suitable environments of pollen and spore-producing plants, we grouped them as tropical conifer arboreal pollen (AP), non-tropical conifer AP, temperate broad-leaved AP, tropical-subtropical broad-leaved AP, mangrove, back-mangrove, mesophyte herb, drought-tolerant herb, wetland herb, monolete fern spore, trilete fern spore, or freshwater algae (see Table 4-2).

The total TP concentrations range from ~630 grains cm^{-3} to ~4,200 grains cm^{-3} or ~1,000 to 7,700 grains g^{-1} (Figure 4-4). *Pinus* pollen are dominant throughout the core, ranging from ~30 to 75%. Among the fern spores, Polypodiaceae and Gleicheniaceae are most common and contribute from ~10 to 50 % to TP assemblages. Other common genera are *Cyathea*, *Pteris*, and *Pteridium* in fern spores; *Castanopsis* and *Quercus* in AP; and Poaceae, Rubiaceae, and Cyperaceae in herb pollen. Mangrove types appear only occasionally. Five terrestrial palynomorph zones (PI-PV) and two subzones were determined by CONISS based on the percentage of all terrestrial palynomorph taxa (Figure 4-4).

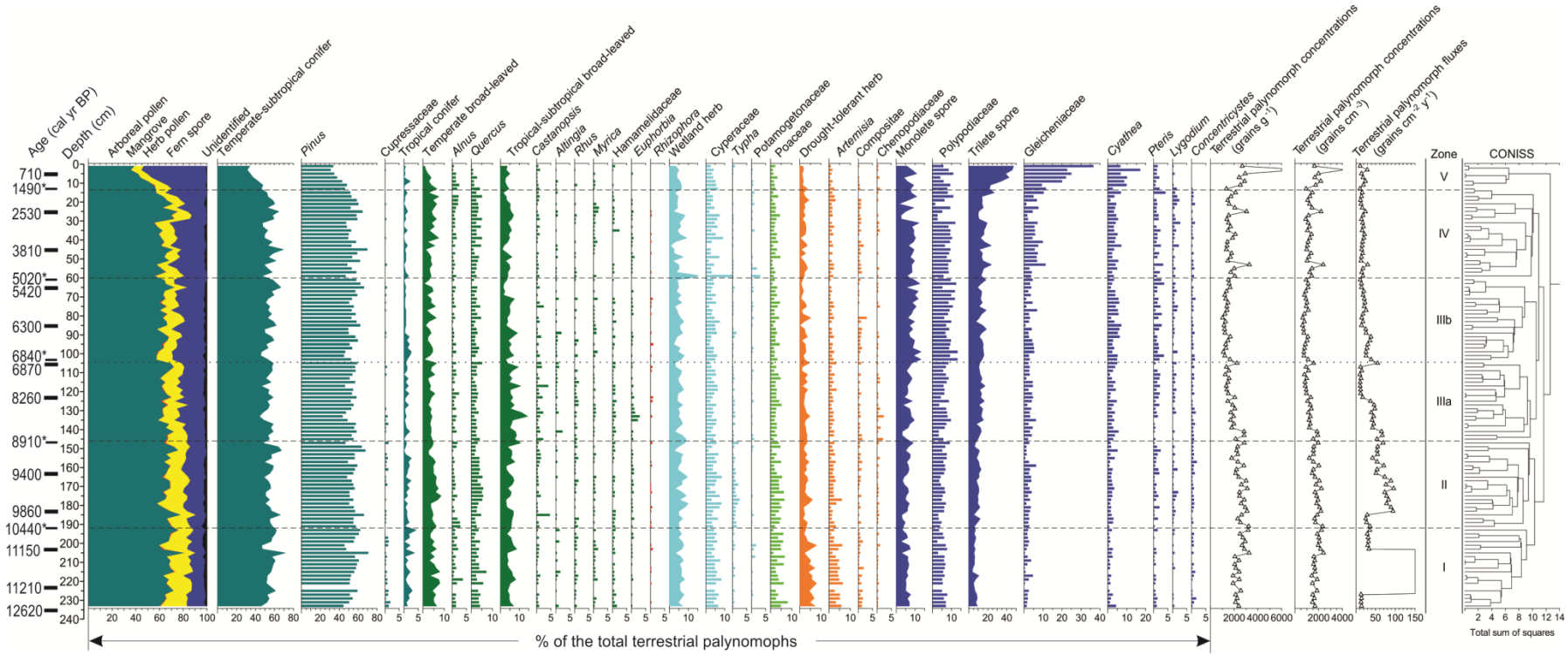

Figure 4-4. Terrestrial palynomorph assemblage composition (percentage %), total concentrations (grains g^{-1} and grains cm^{-3}), and fluxes (grains cm^{-2} y^{-1}) from core GLW31D. Only major pollen and spore types (exceeding 2%) are shown. The dashed lines across the figure distinguish palynological zones and subzones (PI to PV). Zonation is determined from constrained cluster analysis (CONISS) based on pollen and spore percentages, and the dendrogram is shown on the right.

.

4.4.1.1 Terrestrial palynomorph zone PI（from 233 to 192 cm; ~12,380 to ~10,440 cal yr BP）

Zone PI is characterized by the highest abundance of herb pollen (~17%) in the entire core, with the main contribution from Poaceae, *Artemisia*, and Cyperaceae. Both Poaceae (up to 8%) and especially *Artemisia* (up to 6 %) have their maximum percentages in this zone (Figure 4-4), whereas fern spores show the lowest abundances here. The trend of total TP fluxes notably contrasts with the trend of the concentrations (Figure 4-4). In general, the TP assemblages in this zone are dominated by AP, mostly contributed by *Pinus* pollen. Pollen of tropical conifers are found only in trace amounts (Figure 4-4). *Quercus* pollen is a dominant component of the broad-leaved AP group.

4.4.1.2 Terrestrial palynomorph zone PII (from 192 to 145 cm; ~10,440 to ~8,910 cal yr BP)

Zone PII is marked by the highest abundance of *Quercus* (up to ~6%) pollen and an increase in trilete spores up to the average of ~10%, compared to an average of ~7% in zone PI (Figure 4-4). Pollen of drought-tolerant herbs decreases notably during this interval, whereas *Typha* pollen increases and contributes ~2% (only ~0.3% in zone PI) to the assemblages in this zone (Figure 4-4). The trends in the fluxes and concentrations are similar (Figure 4-4). Pollen and spore concentrations range from 1,194 grains cm^{-3} to 2,328 grains cm^{-3}.

4.4.1.3 Terrestrial palynomorph zone PIII (from 145 to 60 cm; ~8,910 to 5,020 cal yr BP)

Zone PIII is characterized by a decline in *Quercus* to ~ 2% and an increase in trilete spores, with an average of ~13% (Figure 4-4). Tropical-subtropical broad-leaved AP increases up to the highest abundances (averaging ~7%) in subzone PIIIa (from 8,910 to 6,840 cal yr BP), followed by a slight decline (averaging ~5%) in subzone PIIIb (from 6,840 to 5,020 cal yr BP). Spores of Polypodiaceae and *Cyathea* continuously increase in subzone PIIIb up to an average of ~9% and ~4%, respectively. Thus, they have doubled or tripled in their abundances in zone PIII compared to zone PII (Figure 4-4). The percentages of fern spores continuously increase, whereas herb pollen decline in both the drought-tolerant and wetland groups. The total pollen and spore concentrations are noticeably lower during this interval (averaging ~1,240 grains cm^{-3} in subzone PIIIa and ~890 grains cm^{-3} in subzone PIIIb) compared to other palynological zones (Figure 4-4).

4.4.1.4 Terrestrial palynomorph zone PIV (from 60 to 13 cm; ~5,020 to 1,490 cal yr BP)

The PIV interval is characterized by an increase in Gleicheniaceae spores (to an average of ~5%), which become dominant in the trilete spore group, prevailing over *Cyathea* spores. The *Pinus* pollen abundance declines slightly, with two peaks at ~ 30 cm and ~50 cm. Pollen of *Quercus, Alnus*, and Cyperaceae increase in abundance. Tropical-subtropical broadleaved AP of *Altingia*, *Myrica*, *Rhus*, and *Euphorbia* appear less frequently in this zone than in PIII.

4.4.1.5 Terrestrial palynomorph zone PV (from 13 to 0 cm; after ~1,490 cal yr BP)

Zone PV is characterized by a notable decrease in AP and an increase in fern spores (Figure 4-4). The percentages of Pinus pollen are the lowest in the core, averaging ~39%.

Fern spores of Cyathea and Gleicheniaceae increase in this zone, with the latter reaching up to 40% in the top samples. The total pollen and spore concentrations and fluxes vary greatly during this interval and increase up to 4,200 grains cm^{-3} and 30 grains cm^{-2} yr^{-1}, respectively.

4.4.2 Dinoflagellate cysts

Well-preserved dinoflagellate cysts of 67 taxa were recorded from 27 samples in core GLW31D (Table 4-3). On average, dinoflagellates of autotrophic and heterotrophic affinity contribute equally to the cyst assemblages (51 and 49%, respectively) (Figure 4-5). The ratio between autotrophic and heterotrophic taxa in the core ranges from 0.5 to 2.7, with an average of 1.1 (Figure 4-5). The ratio of autotrophic to heterotrophic taxa shows a slight upward increase for up to ~60 cm, and then it decreases to the minimum at the top of the core. The most common dinoflagellate cyst taxa found consistently throughout are autotrophic *Spiniferites*, *Operculodinium centrocarpum* sensu Wall and Dale 1966, *Lingulodinium hemicystum*, *Impagidinium*, *Polysphaeridium zoharyi*, and heterotrophic *Brigantedinium*, cysts of *Protoperidinium* spp., *Echinidinium*, *Dubridinium cavatum* (Figure 4-5). *Lingulodinium hemicystum* cysts in the SCS were previously identified as *L*. machaerophorum (e.g., Mao and Harland, 1993; Qi et al., 1996; Wu and Sun, 2000; Kawamura, 2004). However, *L*. *hemicystum* differs from *L*. *machaerophorum* by having an epicystal archeopyle and a lack of striation on the process base and/or hairs on the distal ends of the processes (McMinn, 1991). *Lingulodinium* cysts with long and broad processes as well as small size were counted as *Lingulodinium* sp. (Plate 4.10, Figure 14). A more detailed genetic study should be carried out to separate these two cyst

Table 4-3. List of all dinoflagellate cyst taxa identified in core GLW31D.

Autotrophic	Heterotrophic
Achomosphaera spp.	*Brigantedinium cariacoense*
Bitectatodinium spongium	*Brigantedinium irregulare*
Bitectatodinium tepikiense	*Brigantedinium simplex*
Cryodinium meridianum	*Brigantedinium* spp.
Impagidinium aculeatum	*Dubridinium caperatum*
Impagidinium pallidum	*Dubridinium cavatum*
Impagidinium paradoxum	*Echinidinium aculeatum*
Impagidinium patulum	*Echinidinium granulatum*
Impagidinium sphaericum sensu Rochon et al. 1999	*Echinidinium transparantum*
Impagidinium strialatum	*Echinidinium* spp.
Impagidinium sp. (<20 µm)	*Lejeunecysta oliva*
Impagidinium spp.	cf. *Lejeunecysta sabrina*
Lingulodinium hemicystum	*Lejeunecysta* spp.
Melitasphaeridium choanophorum	Cyst of Protoperidinium americanum
Nematosphaeropsis labyrinthus	Cyst of *Protoperidinium oblongum*
Operculodinium centrocarpum sensu Wall and Dale 1966	Cyst of *Protoperidinium* - type A
Operculodinium israelianum	Cysts of *Protoperidinium* spp.
Operculodinium cf. *janduchenei*	*Quinquecuspis concreta*
Operculodinium longispinigerum	*Selenopemphix alticincta*
Operculodinium spp.	*Selenopemphix nephroides*
Cyst of *Pentapharsodinium dalei*	*Selenopemphix quanta*
Polysphaeridium zoharyi	*Selenopemphix* spp.
Spiniferites belerius	*Stelladinium reidii*
Spiniferites bentorii	*Trinovantedinium applanatum*
Spiniferites bulloideus	
Spiniferites delicates	
Spiniferites hyperacanthus	
Spiniferites cf. *ludhamensis*	
Spiniferites mirabilis	
Spiniferites pacificus	
Spiniferites pachydermus	
Spiniferites ramosus	
Spiniferites - types A, B, D	
Spiniferites spp.	
Tectatodinium pellitum	
Tuberculodinium vancampoae	

species of *Lingulodinium* or to confirm a larger-than-described morphological variation within one species. The total concentrations of dinoflagellate cysts range from 580 cysts cm^{-3} to 2,210 cysts cm^{-3} or 830 to 3,170 cysts g^{-1} (averaging ~950 cysts cm^{-3} and ~1,370 cysts g^{-1}, respectively) (Figure 4-5). Concentrations of individual cysts have general trends similar to that of the total concentrations (Figure 4-6). The cyst fluxes vary from ~6 to 770 cysts cm^{-2} yr^{-1}, with the highest values in the bottom section of the core (Figure 4-5). The cyst concentrations and fluxes have similar trends throughout the core. The CONISS results together with visual inspection of the total dinoflagellate cyst

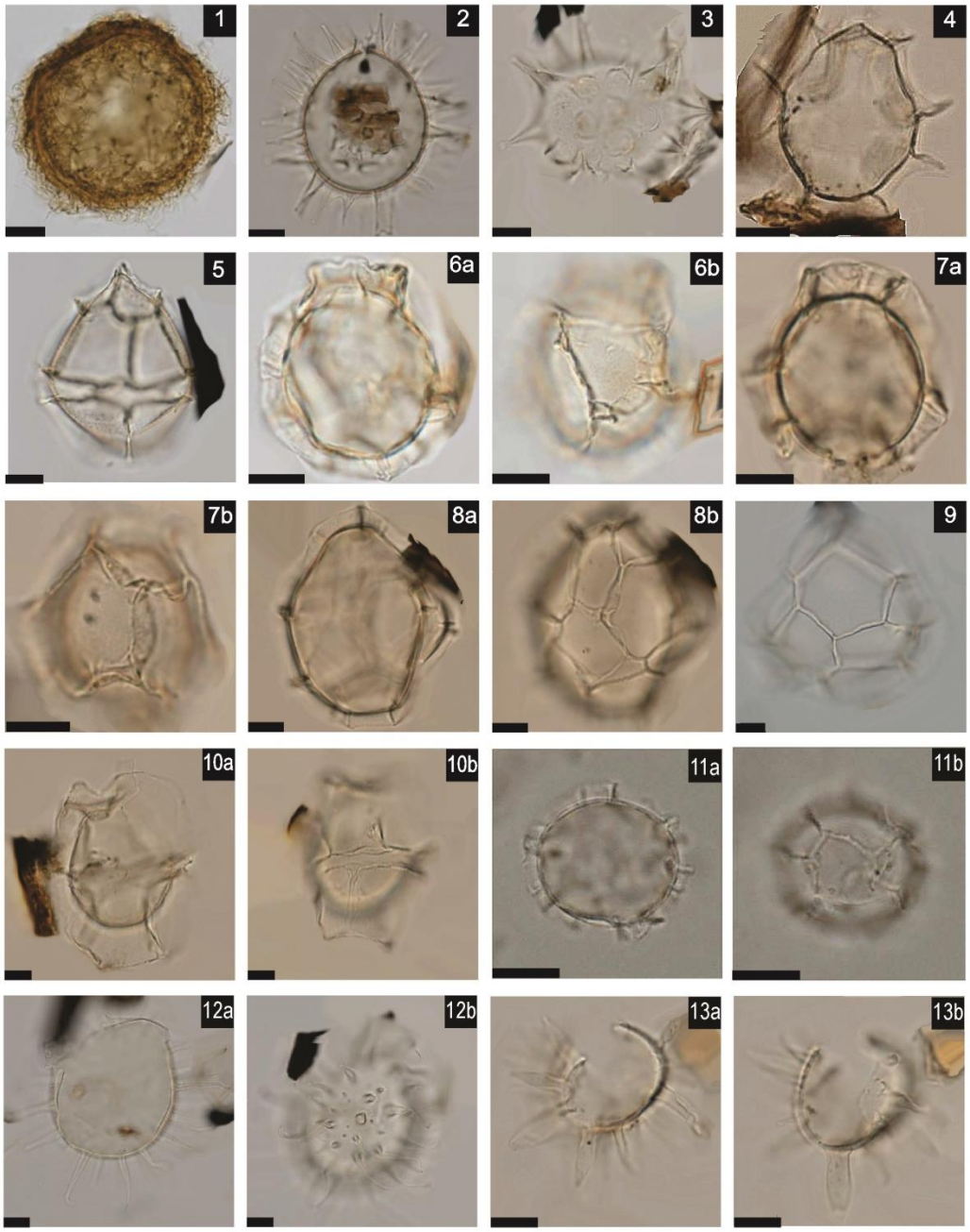

Plate 4-X. Dinoflagellate cysts: 1. *Bitectatodinium spongium*, 2–3. *Dapsilidinium pastielsii*, 4. *Impagidinium aculeatum*, 5. *Impagidinium sphaericum* sensu Rochon et al., 1999, 6–7. *Impagidinium strialatum*, 8–9. *Impagidinium patulum*, 10. cf. *Pentadinium netangei*, 11. Impagidinium sp., 12. *Lingulodinium hemicystum*, 13. *Lingulodinium* sp. The scale bars are 10 μm.

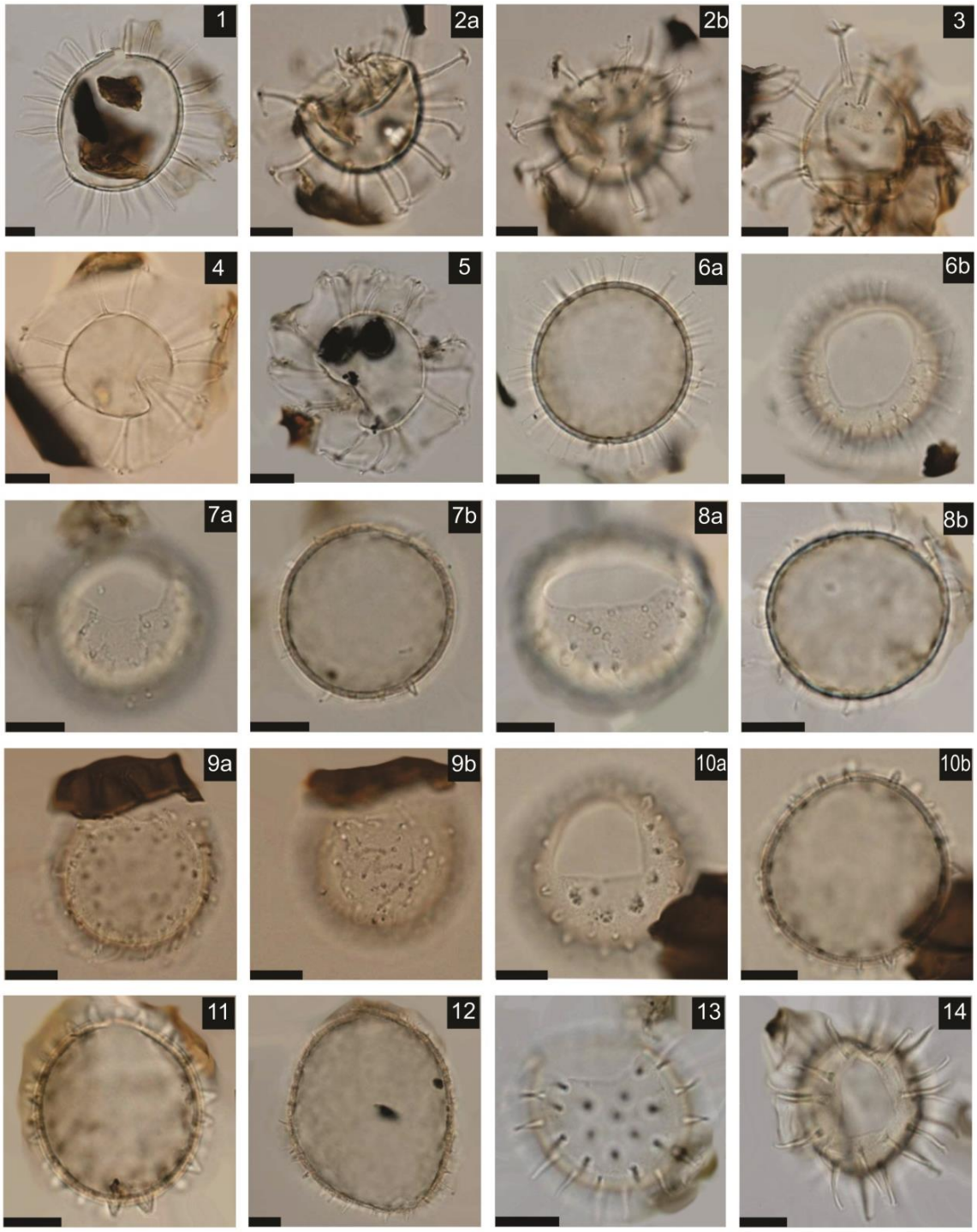

Plate 4-XI. Dinoflagellate cysts: 1. *Lingulodinium hemicystum*, 2-3. *Melitasphaeridium choanophorum*, 4-5. *Nematosphaeropsis labyrinthus*, 6-10. *Operculodinium centrocarpum* sensu Wall and Dale 1966, 11. *Operculodinium* cf. *janduchenei*, 12. *Operculodinium israelianum*, 13-14. *Operculodinium longispinigerum*. The scale bars are 10 μm.

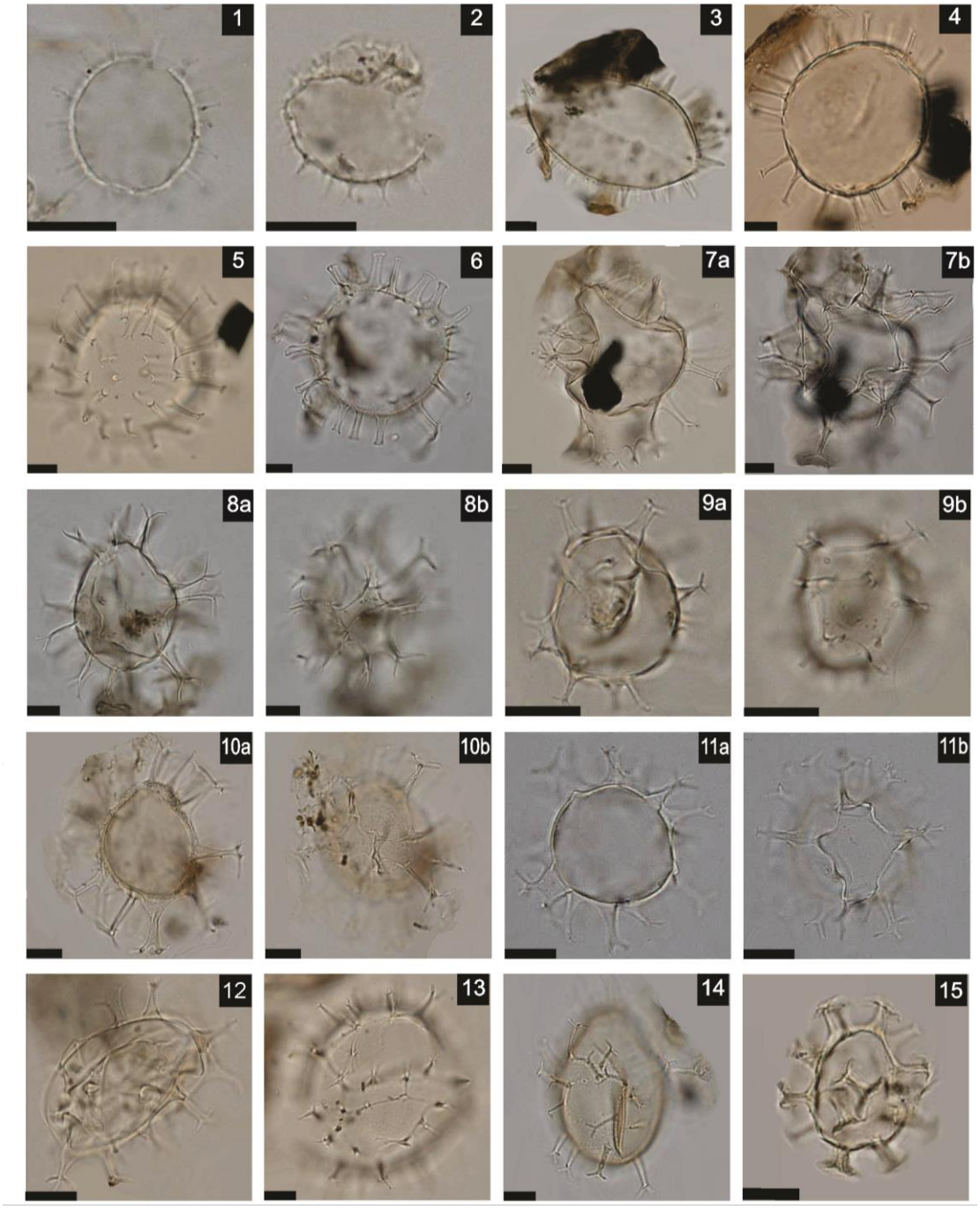

Plate 4-XII. Dinoflagellate cysts: 1–2. Cysts of *Pentapharsodinium dalei*, 3. *Lingulodinium* sp., 4–5. *Polysphaeridium zoharyi*, 6. *Polysphaeridium* sp., 7. *Spiniferites mirabilis*, 8. *Spiniferites ramosus* -type A, 9. *Spiniferites ramosus* - type B, 10. *Spiniferites* cf. *ludhamensis*, 11. *Spiniferites* - type D, 12. *Spiniferites* spp., 13. *Spiniferites hyperacanthus*, 14. *Spiniferites* cf. *multisphaerus*, 15. *Achomosphaera* spp. The scale bars are 10 μm.

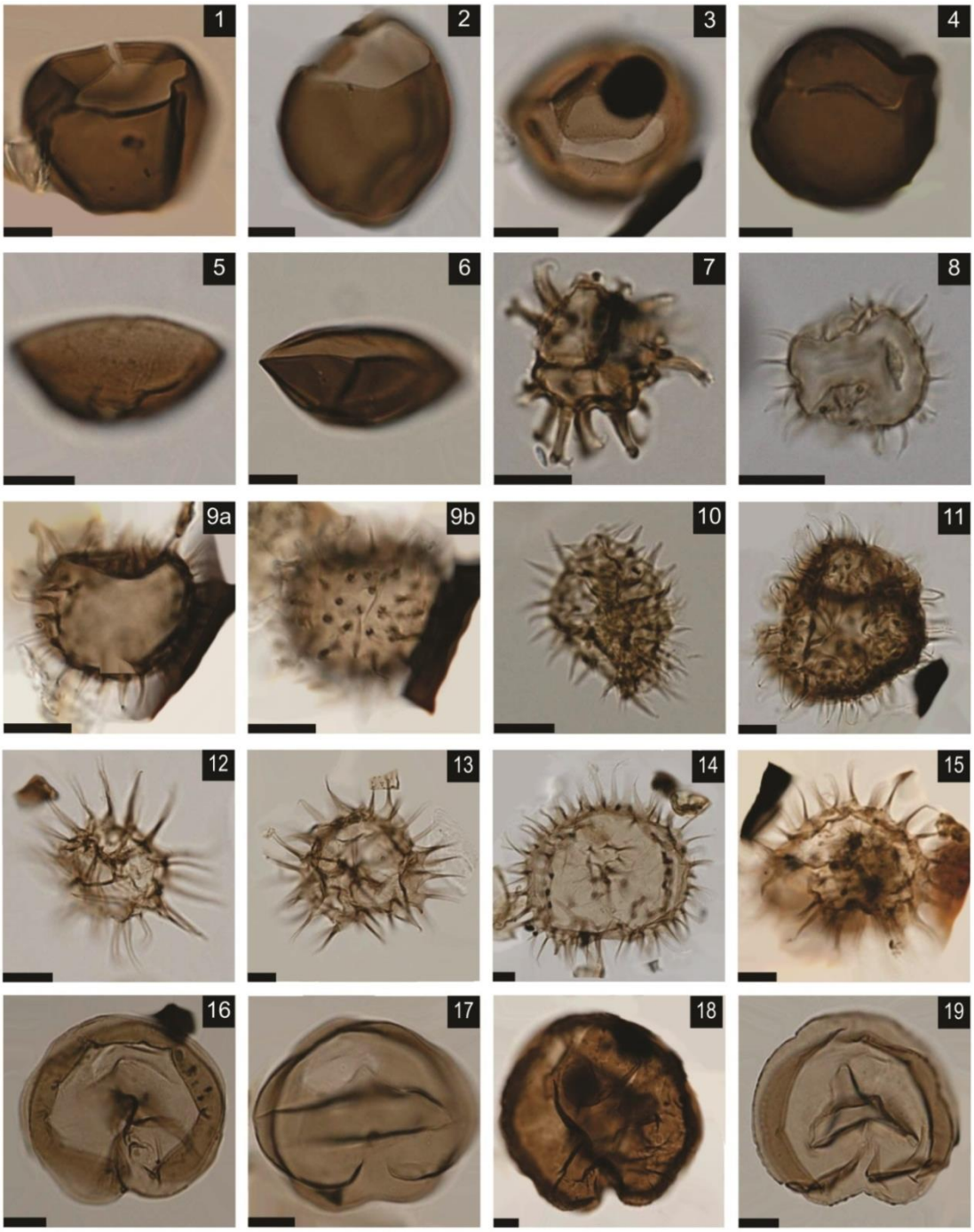

Plate 4-XIII. Dinoflagellate cysts: 1. *Brigantedinium simplex*, 2. *Brigantedinium* sp., 3. *Brigantedinium cariacoense*, 4. *Brigantedinium irregulare*, 5-6. *Dubridinium cavatum*, 7. *Echinidinium aculeatum*, 8. *Echinidinium granulatum*, 9-11. *Echinidinium* spp., 12-13. *Selenopemphix* cf. *quanta*, 14-15. *Selenopemphix quanta*. 16-17. *Selenopemphix nephroides*, 18-19. *Selenopemphix undulata*. The scale bars are 10 μm.

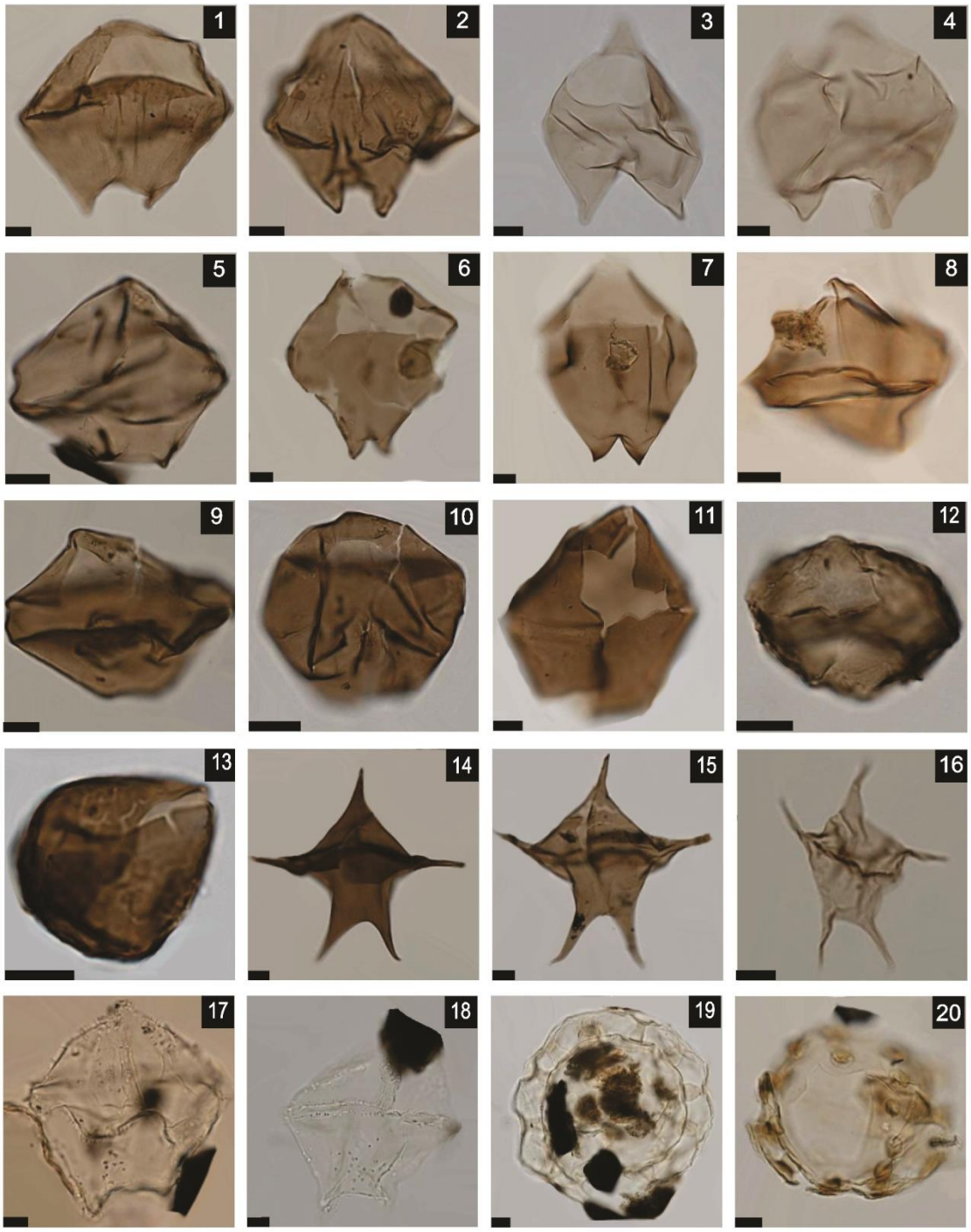

Plate 4-XIV. Dinoflagellate cysts: 1–2. *Quinquecuspis concreta*, 3–4. cysts of *Protoperidinium oblongum*, 5. cf. *Lejeunecysta sabrina*, 6–7. Cysts of *Protoperidnium latissimum*, 8–13. Cysts of *Protoperidinium* spp., 14–16. *Stelladinium reidii*, 17–18. *Trinovantedinium applanatum*, 19–20. *Tuberculodinium vancampoae*. The scale bars are 10 μm.

assemblages in core GLW31D led to the identification of three cyst zones (DI–DIII) (Figures 4-5 and 4-6):

4.4.2.1 Dinoflagellate cyst zone DI (from 233 to ~192 cm; before ~10,440 cal yr BP)

Zone DI is characterized by the highest abundance of heterotrophic taxa (averaging ~56%), which is mainly contributed by the species *Brigantedinium* (~40%) and other cysts of *Protoperidinium* spp. (~7%). The relative abundances of total *Spiniferites* (~16%) are the lowest in the core, whereas the total *Impagidinium* have the highest percentages (~8%) and concentrations (averaging ~150 cysts g^{-1}). *Operculodinium centrocarpum* sensu Wall and Dale 1966 contributes ~13% to the cyst assemblages (Figure 4-5) and has average concentrations of ~280 cysts g^{-1} (Figure 4-6). This zone has the highest total cyst concentrations and fluxes (Figure 4-5).

4.4.2.2 Dinoflagellate cyst zone DII (from ~192 to ~105 (or 91) cm; ~10,440 to 6,870 (~6,470) cal yr BP)

This interval is marked by a decrease in total *Brigantedinium* (~30%), *Impagidinium* (~4%) and *Operculodinium* (~12%), along with an abrupt increase in total *Spiniferites* (~27%) and cysts of *Protoperidinium* spp. (~11%) (Figure 4-5). Total and individual dinoflagellate cyst concentrations and fluxes are noticeably lower in this zone (Figures 4-5 and 4-6). The total cyst concentrations decreased to the range of ~680-1,660 cysts cm^{-3}, and the total cyst fluxes declined to an average of ~26 cysts cm^{-2} yr^{-1}, which is one order of magnitude lower than in zone DI (Figure 4-5). The boundary between the DII and DIII zones is somewhere between 105 and 91 cm (or ~6,870 and ~6,470 cal yr BP). However,

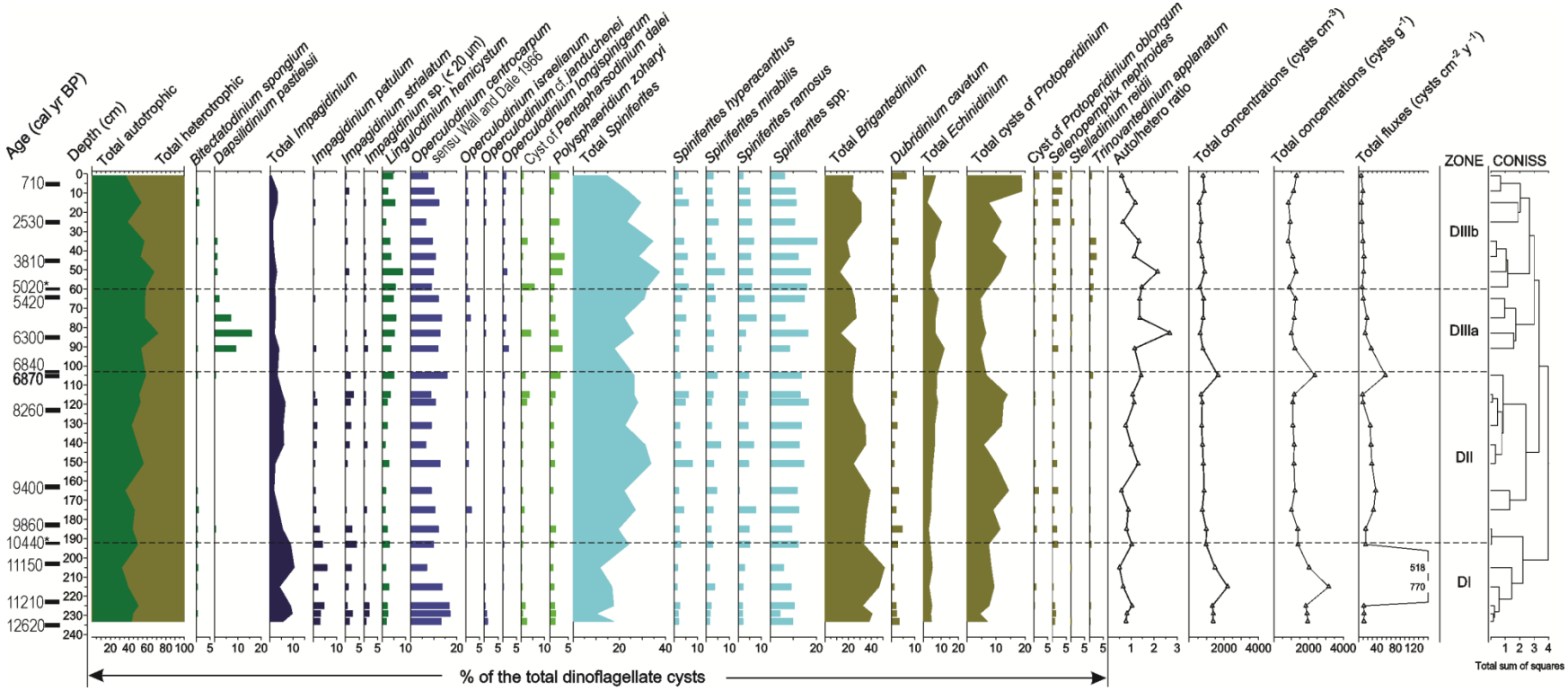

Figure 4-5. Percentages (%) of selected dinoflagellate cyst taxa from core GLW31D. Cysts produced by heterotrophic taxa are shown in brown and those produced by autotrophic taxa in other colours. The dashed lines across the figure distinguish dinoflagellate cyst zones (DI to DIII). Zonation is determined from constrained cluster analysis (CONISS) based on dinoflagellate cyst percentages, and the dendrogram is shown on the right.

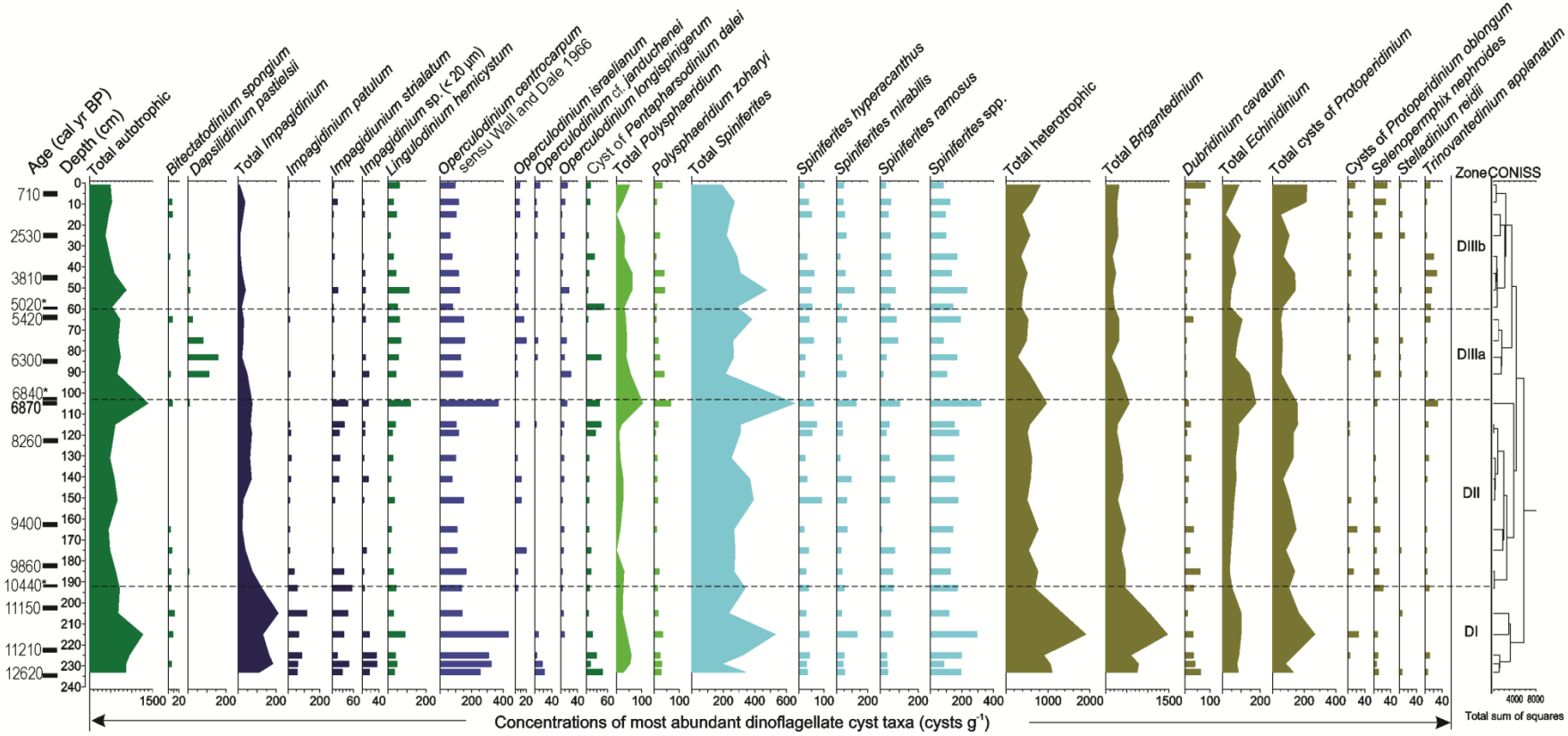

Figure 4-6. Concentrations (cysts g^{-1}) of selected dinoflagellate cyst taxa from core GLW31D. Cysts produced by heterotrophic taxa are shown in brown, and others in various colours are produced by autotrophic taxa. The dashed lines across the figure distinguish dinoflagellate cyst zones (DI to DIII). Zonation is determined from constrained cluster analysis (CONISS) based on concentrations of individual dinoflagellate cysts and the dendrogram is shown on the right.

due to a low sampling resolution for dinoflagellate cysts in this part of the core, we are unable to provide the exact time for this major transition.

4.4.2.3 Dinoflagellate cyst zone DIII (from ~104 (or 91) to 0 cm; after ~6,870 (~6,470) cal yr BP)

This zone is characterized by consistently low values of the total cyst concentrations and fluxes (averaging ~740 cysts cm^{-3} or ~1,080 cysts g^{-1}, and ~12 cysts cm^{-2} yr^{-1}, respectively) after a peak at the boundary with zone DII (Figure 4-5). The concentrations of *Brigantedinium* and most other heterotrophic taxa decreased to the lowest in the core (Figure 4-6). Both *Lingulodinium hemicystum* and *Polysphaeridium zoharyi* increase in their abundances (Figure 4-5). Two subzones were determined:

Subzone DIIIa (from ~104 (or 91) cm to 60 cm) is marked by a sharp increase in *Dapsilidinium pastielsii* (averaging ~9% and ~94 cysts g^{-1}) and a moderate increase in cysts of autotrophic taxa (averaging ~61%; ratio of autotrophic to heterotrophic taxa at ~1.7), primarily due to *Operculodinium centrocarpum* sensu Wall and Dale 1966, *Lingulodinium hemicystum*, and *Polysphaeridium zoharyi* (Figure 4-5). Contributions of *Impagidinium* (< 3%) to the cyst assemblages are almost twice as low in this zone compared to DI and DII. A decline in total *Brigantedinium* and *Spiniferites*, as well as in cysts of *Protoperidinium* spp., was observed during this interval (Figure 4-5).

Subzone DIIIb (from 60 to 0 cm) is characterized by a decrease to 52% of autotrophic taxa, primarily due to a decline in *Operculodinium centrocarpum* sensu Wall and Dale 1966 (averaging ~12%) and total *Impagidinium* (averaging ~2%), with the latter reaching ~0.5% in the surface sample. *Dapsilidinium pastielsii* was found only in small numbers in the lower part of this subzone, and it is absent above ~30 cm. Total

Spiniferites showed an upward declining trend from ~37 to 15%, as reflected in the autotrophic to heterotrophic ratio (Figure 4-5). A similar trend can also be seen in the total *Spiniferites* concentrations (Figure 4-6). The abundance of the heterotrophic taxa increases, primarily due to an increase in cysts of *Protoperidinium* spp. (~12%) and *Dubridinium cavatum* (~2.5%), with some contribution of *Selenopemphix nephroides* (~1.5%) and *Trinovantedinium applanatum* (~1%).

4.5 Discussion

4.5.1 Major TP proxies of environmental and climatic change in the SCS region

Pollen and spores in marine sediments originally come from the surrounding terrestrial vegetation. They are commonly transported by winds or water (including ocean currents and/or rivers) and then deposited along with other sedimentary particles. Therefore, it is crucial to understand the mechanisms of terrestrial palynomorph dispersal in order to interpret marine palynological data correctly. At the beginning of the Holocene, the global sea-level stood lower than it is today, so that a large part of the SCS continental shelf was exposed and covered by extensive grasslands. Thus, a high content of herb pollen in TP assemblages from the SCS and high TP concentrations are commonly used as key indicators of this landscape associated with short-distance TP transport and close proximity to shorelines (e.g., Sun and Li, 1999; Li et al., 2010; Dai et al., 2014).

Both wind and water play important roles in TP dispersal and deposition in marine environments. High sedimentation rates have a dilution effect on pollen and spore concentrations if their dispersal is primarily controlled by wind (e.g., Xu et al., 2005;

Beaudouin et al., 2007). This means that TP concentrations are negatively correlated with sedimentation rates at the site. Our results show that over the past 10,500 yr, the relationship between TP concentrations and sedimentation rates is mostly positive prior to ~6,300 cal yr BP (Figure 4-7A), and it becomes negative in the younger section of the core (Figure 4-7B). The correlation coefficient (R^2) is 0.463 before 6,300 cal yr BP, and even higher up to 0.989 when one outlier data point at 8,260 cal yr BP is excluded. This indicates that pollen and spore transport and deposition prior to ~6,300 cal yr BP were primarily controlled by hydrodynamic action (e.g., rivers or currents). Therefore, the TP record dominated by *Pinus* pollen before ~6,300 cal yr BP reflects hydrographic conditions rather than strong winter monsoon climate.

Pinus pollen and fern spores have been widely used as indicators of hydrodynamic conditions because they were supposed to be more easily dispersed by flotation in water than other TP types (e.g., Florin, 1963; Heusser, 1988; Sun et al., 1999; Duplessy et al., 2001; Li et al., 2008, 2010; Dai et al., 2014). However, an experimental work by Zheng et al. (2011) revealed that *Pinus* pollen sank faster than herb pollen or spores, and suggested that hydrodynamic sorting is not prominent for the long-distance transport of *Pinus* pollen and that wind plays a critical role in *Pinus* pollen transportation. Unfortunately, this experiment was designed to observe the settling rate in a still water environment, not a strong hydrodynamic regime similar to river or marine environments (Zheng et al., 2011). Water sorting effects or current influences on various suspended particles have not been investigated. Dai et al. (2014) did not find a close relationship between the wind direction and concentration or percentage gradient of *Pinus* from surface sediments in the Pearl River Delta and the northern SCS. According to Dai et al.

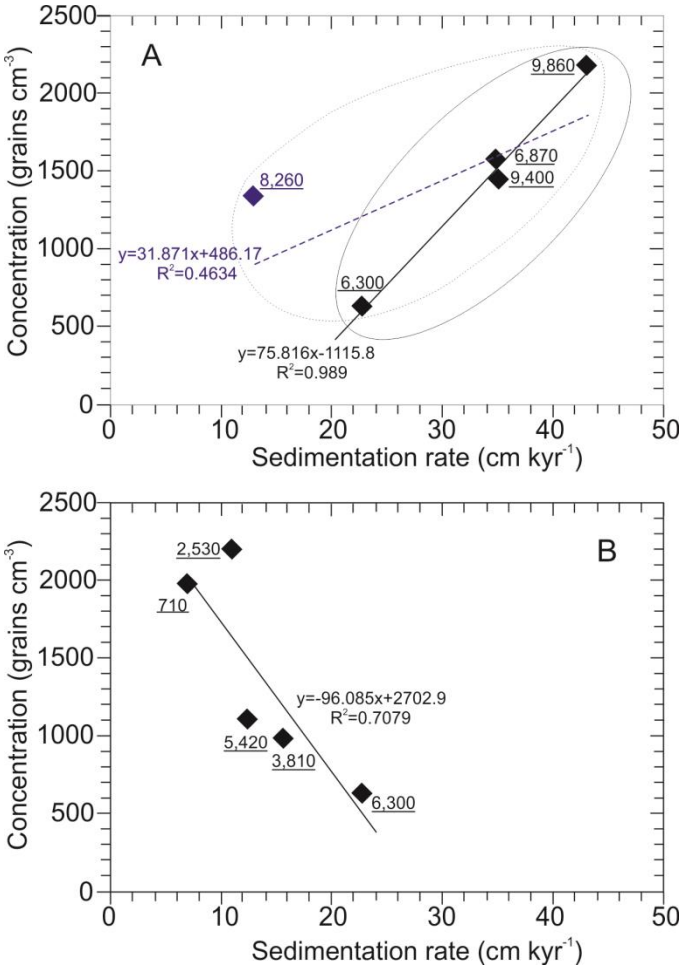

Figure 4-7. Relationship between terrestrial palynomorph concentrations and sedimentation rates. A. A positive relationship prior to ~6300 cal yr BP. The dashed line shows the case including one point outlier at ~8260 cal yr BP. B. A negative relationship after ~6300 cal yr BP. Underlined numbers are the calibrated ages.

(2014), this demonstrates the primary influence of ocean currents or river plumes for *Pinus* pollen transport over air flow. This complicates the use of *Pinus* pollen as an indicator of monsoon climate in a notable sea-level rise stage, because we do not know which one, wind or water, dominated in *Pinus* pollen dispersal. Tropical-subtropical broad-leaved AP, closely associated with the tropical and subtropical rainforest (Dai et

al., 2014), can thus be used as direct indicators of climate change, despite their low abundances before ~6,300 cal yr BP.

The negative relationship (Figure 4-7B) between TP concentrations and sedimentation rates after ~6,300 cal yr BP indicates that wind transport prevailed over water transport for pollen dispersal. This roughly coincides with the onset of modern oceanographic conditions in the SCS. Studies of pollen distributions in surface sediment samples from the northern SCS have shown that *Pinus* pollen are mostly transported by the northeastern winter monsoon from the southern mainland of China and Taiwan (e.g., Sun et al., 1999; Zhang et al., 2002; Dai et al., 2014). Therefore, *Pinus* pollen can be used as an indicator of the winter monsoon strength after ~6,300 cal yr BP.

4.5.2 Sea-level change as reflected in the terrestrial palynomorph and dinoflagellate cyst records

4.5.2.1 During ~12,500-~10,400 cal yr BP

Post-glacial relative sea-level fluctuations in the SCS region had a prominent impact on the hydrographic and environmental conditions of this marginal sea. Sea-level curves based on a number of sea-level indicators (e.g., mangrove peat, corals, oyster beds, tubeworms, and beach rock exposures or other intertidal deposits) have been proposed for the SCS region over the last two decades (Figure 4-8) (e.g., Zong, 2000; Hanebuth et al., 2000; 2011; Liu et al., 2004; Tanabe et al., 2006). These data provide essential information about the timing of major hydrographic changes.

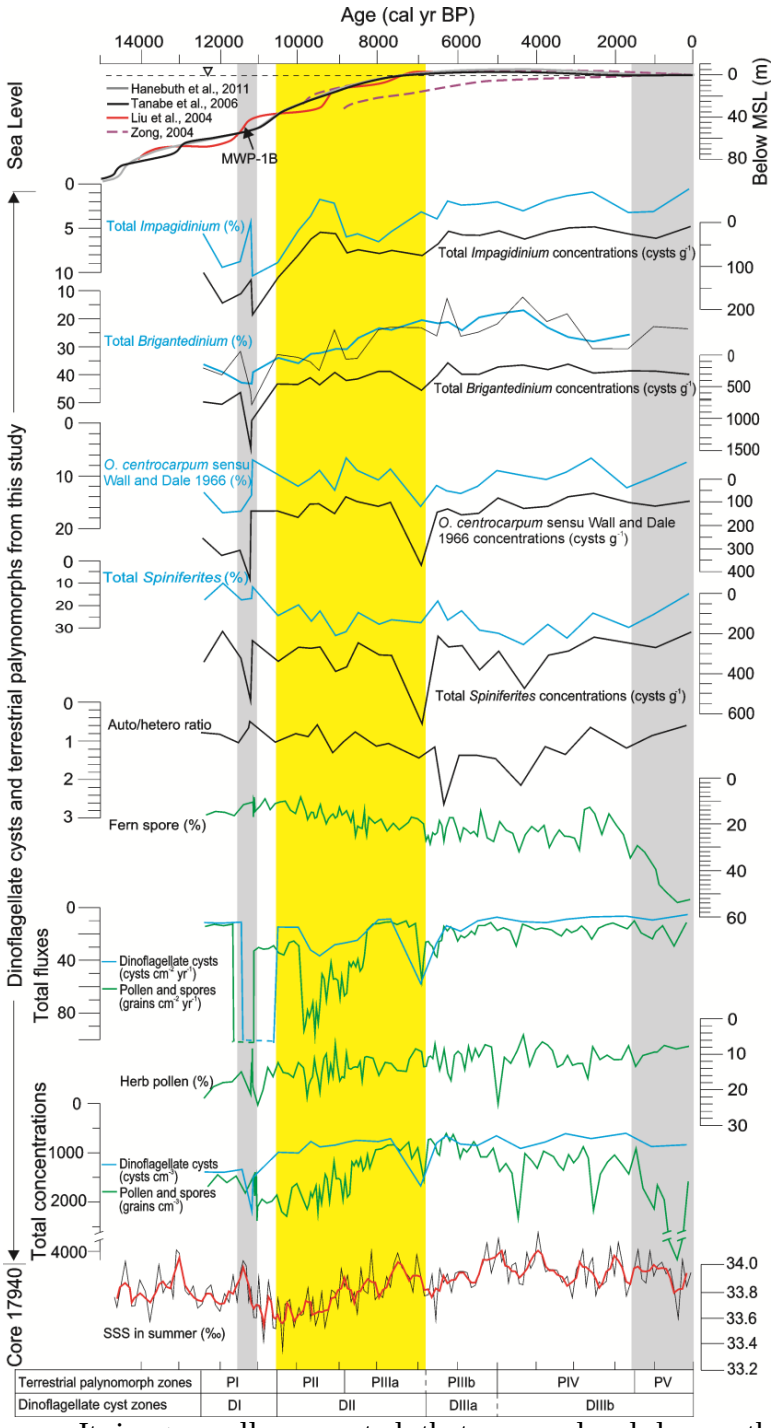

Figure 4-8. Selected dinoflagellate cyst, terrestrial palynomorph data, and palynological zones from this study are shown along with the regional sea-level change during the Holocene (Liu et al., 2004a, 2004b; Zong, 2004; Tanabe et al., 2006; Hanebuth et al., 2011). The SSS curve is from Jiang et al. (2014) and is based on diatom records from core 17940. The grey band at ~11,700–11,000 cal yr BP marks a short-term MWP-1B event associated with the rapid sea-level rise (Hanebuth et al., 2000; Liu et al., 2004a, 2004b) and the opening of the Taiwan Strait. The yellow band indicates the period of the Holocene sea-level rise and the landward shoreline migration. The grey band at ~1500 cal yr BP corresponds to intensified human activities in the watersheds.

It is generally accepted that a sea level lower than ~-60-50 m (prior to the Holocene) caused the Taiwan Strait to expose the "Dongshan Land Bridge" (Cai, 1997), so that the coastal water of the East China Sea (ESC) could not flow into the SCS through the Taiwan Strait as in the modern setting. The Bashi (Luzon) Strait is the major channel

allowing water exchange between the SCS and the western Pacific through the Philippine Sea (e.g., Ning et al., 2004; Cheng et al., 2005). The Kuroshio Current flow into the SCS is restricted by the Changyuen sill (Figure 4-1B), and one of its branches intrudes into the SCS and flows southwestward along the shelf break (Figure 4-2) (e.g., Shaw, 1996; Ning et al., 2004; Caruso et al., 2006). Thus, prior to the opening of the Taiwan Strait, less-nutrient and more-saline waters from the western Philippine Sea flowed into the SCS only through the Bashi Strait, without the influence from the ESC water through the Taiwan Strait. It could be speculated that if the Bashi Strait was narrower during the low sea-level stand, then the force of flow from the western Philippine Sea into the northern part of the SCS could be stronger due to jet action. During the Younger Dryas and the beginning of the Holocene, the continuous sea-level rise reached ~-60-50 m (e.g., Tanebe et al., 2006; Hanebuth et al., 2011). This resulted in the opening of the Taiwan Strait, the widening of the Bashi Strait, and the branching of the Kuroshio Current into the SCS. The warm Kuroshio water had relatively low nutrient concentrations and flowed westward along the northern shelf margin of the SCS (Shaw, 1991; Ning et al., 2004). The opening of the Taiwan Strait at ~12,000-11,000 cal yr BP allowed the input of the ECS waters to the SCS (e.g., Liu et al., 2013). These major oceanographic events would have impacted the local SST (e.g., Wang et al., 1999; Oppo and Sun, 2005), SSS (e.g., Jiang et al., 2006), marine primary productivity (e.g., Higginson et al., 2003), and input of terrestrial material to the shelf break. Our results reveal that TP and dinoflagellate cysts have responded to such changes in the northern SCS over the Younger Dryas and the Holocene.

In general, the TP and dinoflagellate cyst records from core GLW31D are in broad agreement with the sea-level change and known paleoenvironmental conditions in this region. During the Last Glacial Maximum (LGM), the sea-level was at ~130 m below the present sea-level stand, and the (paleo)shoreline was near the outer shelf in the northern SCS (Chen, 1997). Extensive grasslands were developed on the exposed shelf (e.g., Li et al., 2010; Zhang et al., 2011). After the LGM, the sea level continuously rose, reaching ~-60-50 m at ~12,000-11,000 cal yr BP (e.g., Tanebe et al., 2006; Hanebuth et al., 2000, 2011). The onset of the Holocene is recorded by a rapid rise in air temperatures, as recorded in Dongge Cave stalagmites by $\delta^{18}O$ (Figure 4-9) (Dykoski et al., 2005), and a rise in winter SSTs, shown by the diatom record from core 17940 (Jiang et al., 2014) (Figure 4-9). Our TP data from core GLW31D show that herb pollen and the drought-tolerant group (see zone PI, Figure 4-4) exhibit the highest values during ~12,500-10,400cal yr BP (Figures 4-4 and 4-8). This zone reflects grassland environments on the exposed shelf (e.g., Li et al., 2006b, 2010; Zheng et al., 2013) and the close proximity of the site of core GLW31D to the shore, as herb pollen are usually transported only within a short distance (Sun et al., 1999; Li et al., 2010; Zhang et al., 2011; Dai et al., 2015).

The close proximity of the shoreline to the core site is indirectly supported by the high abundances of heterotrophic dinoflagellate cysts during this interval (zone DI) as well as by the highest total cyst concentrations and fluxes (Figure 4-5). These parameters are known to be greater in coastal areas of elevated primary productivity (e.g., Zonneveld and Brummer, 2000; Marret and Zonneveld, 2003; Radi and de Vernal, 2004; Radi et al., 2007; Pospelova et al., 2008; Zonneveld et al., 2013; Heikkilä et al, 2014). High abundances of *Brigantedinium* and other cysts of *Protoperidinium* spp., as well as lower

values of the autotrophic/heterotrophic cyst ratio, are typical for near-shore environments with elevated nutrient supply (e.g., Harland, 1983; Dale, 1996; Mudie and Harland, 1996). Interestingly, this DI zone also has the highest abundances of *Impagidinium* species (Figures 4-5 and 4-8), which usually dominate cyst assemblages in open ocean oligotrophic environments (e.g., Harland, 1983; Zonneveld et al., 2013; Zonneveld and Pospelova, 2015). Such contrasting dinoflagellate cyst assemblages were previously reported from the SCS in the cyst-based Quaternary paleoenvironmental study by Mao and Harland (1993). The authors concluded that sea-level fluctuations in the SCS were indeed reflected by the presence of oceanic *Impagidinium* species and cysts of *Protoperidinium* species. The latter were "reacting to the increased nutrient supply" due to the "sea-level drops rejuvenating the regional river systems" (Mao and Harland, 1993). *Impagidinium* species were also found in higher abundances in surface samples of the SCS near the Shenhu and Taiwan Shoal Sections, where the influence of the Philippine Sea waters is the greatest (Wu and Sun, 2000). Thus, our data support the suggestion that there has been an intensification of the water flow through the Bashi Strait from the western Philippine Sea into the northern part of the SCS at ~12,000 to ~10,400 cal yr BP (e.g., Huang et al., 1997; Wang et al., 1999, 2000; Jian et al., 2001).

A short-term event (sample UVic 14-174) can be seen in our records at ~11,700-11,000 cal yr BP (Figures 4-5 and 4-7), as reflected in a sharp increase in total cyst concentrations and fluxes. This event is also characterized by a decline of *Impagidinium*, as well as by the increase of opportunistic *Operculodinium centrocarpum* sensu Wall and Dale 1966, total *Spiniferites*, and *Brigantedinium* (Figure 4-8). A dramatic increase in the sedimentation rate (Figure 4-3) and the highest flux of TP also happened at the same

time. This abrupt change can also be seen as a peak of the summer SSS reconstructed by diatoms in sediment core 17940 (Figure 4-8) by Jiang et al. (2014). This abrupt event could be associated with a change in the local environment due to the Taiwan Strait opening, which coincided with the second melt-water pulse (MWP-1B) in the post glaciation (Figure 4-8) (Hanebuth et al., 2000; Liu et al., 2004). Prior to this event, the Taiwan Strait was exposed as a "land-bridge" connecting mainland China and the Taiwan Island. There was no water exchange between the SCS and the ECS. At ~11,700-11,000 cal yr BP, the sea level had risen to an elevation of approximately -50 m (Figure 4-8) (e.g., Tanebe et al., 2006; Hanebuth et al., 2011), and the shorelines had migrated to near the current 50 m isobaths. Liu and Chen (1995) and Chen (1997) reported this paleo-shoreline at ~50 m isobaths in the northern shelf of the SCS and provided extensive evidence of a coastal environment along 50 m isobaths from seismic profiles (e.g., disappearance of paleo-channel below -50 m depth, paleo-deltas), geomorphological units (e.g., lagoons, sand bars, beach scarps), sediments (e.g., beach rocks), sedimentary structures (e.g., scour and fill structure), fossils (e.g., brackish molluscs and shell layers), and mineral records (e.g., abundant heavy mineral zones). The Taiwan Strait was open to the East China Sea at this period, and waters from the SCS and the ECS began to exchange freely. The pulse of colder and lower SSS water from the ECS through the strait and the limited input of waters from the western Philippine Sea most likely resulted in a rapid decrease of *Impagidinium* during this short-term event. On the other hand, since that time, the main sources of terrestrial sediments had changed from the Pearl River to the rivers from Southwest Taiwan (e.g., Huang et al., 2011). It has been suggested that following the short pulse event of the ECS water input to the SCS, the

Kuroshio Current branched into the Taiwan Strait (e.g., Wang and Chern, 1988; Jan et al., 2002) and weakened the influence of the ECS on the SCS. This could explain the return of the *Impagidinium* abundance to the previously high levels for the rest of the DI zone.

4.5.2.2 During ~10,400-~6,800 (or 6,000) cal yr BP

The continuous and rapid sea-level rise in the western Pacific margin region during the early Holocene reached the maximum at ~6,800-6,000 cal yr BP (Figure 8) (e.g., Zong, 2004; Tanebe et al., 2006; Hanebuth et al., 2011). Thus, the coastal shorelines migrated to their present-day locations. In our records, the TP concentrations and herb pollen content show a declining trend from the highest values in the early Holocene to the lowest values at ~6,000 cal yr BP (Figure 4-4). This trend can be explained by the fact that the TP transport paths became longer as the shorelines migrated landwards (Figure 4-8). Correspondingly, the fern spore proportions were enriched by the water sorting effects, resulting in the increase of fern spores in the TP assemblages (e.g., Florin, 1963; Heusser, 1988; Duplessy et al., 2001; Li et al., 2008). Dai et al. (2014) found that *Pinus*, Poaceae, Cyperaceae, and fern spores are most abundant in the river mouth and decrease with increasing distance from land, suggesting that they are mainly derived from the Pearl River drainage basin and strongly dispersed by river plume and ocean currents. Moreover, in contrast to dilution effects due to high sedimentation rates when pollen dispersal depends primarily on wind (e.g., Xu et al., 2005; Beaudouin et al., 2007), palynological concentrations were positively correlated with sedimentation rates (Figure 4-7A). The covariance of TP concentrations and sedimentation rates indicates that water prevails over wind in pollen and spore dispersal (Li et al., 2010).

The landward migrated shorelines and the deepening of the SCS caused a reduction in nutrient supply to the core site, thus ultimately affecting marine primary productivity and causing the decrease of total dinoflagellate cyst concentrations and fluxes (e.g., Pospelova et al., 2006, 2008, 2015; Bringué et al., 2013). The decrease in the ratio of autotrophic to heterotrophic taxa and the decrease in *Brigantedinium* and *Operculodinium centrocarpum* sensu Wall and Dale 1966 in the DIII zone are indicative of a decreasing marine primary productivity (e.g., Dale, 1996; Radi and de Vernal, 2004; Zonneveld et al., 2013). Conversely, the increase of total *Echinidinium* and *Spiniferites* can be associated with a lowering of nutrient supply and warming of the surface waters in the Pacific (e.g., Pospelova et al., 2008, 2015; Bringué et al., 2013, 2014). A previous study of spatial distributions of dinoflagellate cysts in surface sediments from the SCS also reported that modern dinoflagellate cyst concentrations and abundances of *Operculodinium centrocarpum* sensu Wall and Dale 1966 generally decline in the direction from the coast to the deeper parts of the sea (Wu and Sun, 2000). Thus, the early and middle Holocene sea-level rise in the SCS is reflected in the TP (PII and PIIIa) and dinoflagellate cyst (DII) records from core GLW31D.

4.5.2.3 After ~6,800 (or 6,000) cal yr BP

After ~6,800 (or 6,000) cal yr BP, the dinoflagellate cyst and TP records generally show stable hydrographic conditions (Figure 4-8). This time interval corresponds to the highest sea-level stand in the SCS during the Holocene (e.g., Liu et al., 2004a; Tanabe et al., 2006). Minor changes in total dinoflagellate cyst concentrations and major changes in the cyst assemblage composition (zone DIII) after ~6,800 cal yr BP were most likely

caused by climatic changes. The presence of *Dapsilidinium pastielsii* and high relative abundances of *P. zoharyi* and *Lingulodinium* can only be observed in the moderately productive coastal regions that are characterised by high SSTs and SSSs in the upper water column (e.g., Holl et al., 2000; Zonneveld et al., 2013; Zonneveld and Pospelova, 2015; Wu and Sun, 2000). A rapid increase in fern spores, especially after ~1,500 cal yr BP, provides evidence of the intense deforestation as a result of human interference (e.g., Sun and Li, 1999; Li et al., 2006a, 2009).

4.5.3 Climate change

4.5.3.1 During ~12,500-~10,400 cal yr BP

A number of paleoclimate reconstructions have revealed that the records of monsoonal climate from the marine environment were strongly influenced by a significant sea-level rise during the last deglaciation and the Holocene (e.g., Steinke et al., 2006; Zhao et al., 2006; Griffiths et al., 2009). Our data have shown that major trends in the sea-level change had a strong influence on TP and dinoflagellate cyst records in the northern SCS. Taking into account the impacts of the sea-level change on TP dispersal and sources, several monsoon climatic events can be observed in the core GLW31D record. These events can be matched to the corresponding events from terrestrial (e.g., Dongge Cave, Dykoski et al., 2005) and marine (core 17940, Jiang et al., 2014) records from the region (Figure 4-9).

Extensive grasslands on the exposed shelf of the SCS during the Younger Dryas and the beginning of the Holocene were previously reported in many sediment cores from the region by the high content of herb pollen (e.g., Sun and Li, 1999; Li et al., 2010; Zheng et

al., 2011, 2013; Dai and Weng, 2015; Dai et al., 2015). Traditionally, this was interpreted as a signal of dry conditions (e.g., Sun and Li, 1999; Li et al., 2010; Zheng et al., 2011, 2013). However, because *Artemisia*-dominated herb pollen could be transported by multiple pathways (e.g., rivers, currents, and wind) and from various sources, it is not justifiable to consider an increase in *Artemisia*-dominated herb pollen only as a dry climate indicator (e.g., Dai and Weng, 2015; Dai et al., 2015). Our data demonstrate that pollen transport by rivers or currents prevailed over the wind prior to ~6,300 cal yr BP (Figure 4-7). Cyperaceae pollen are generally predominant in herb pollen assemblages, although the highest content of *Artemisia* appeared at the bottom of the core (Figure 4-4). Thus, it can be interpreted as the presence of humid conditions during that time. These interpretations are supported by stable oxygen isotope data from Dongge Cave and indicate Asian summer monsoon intensification (Dykoski et al., 2005; Wang et al., 2005).

4.5.3.2 During ~10,400-~6,800 (or 6,000) cal yr BP

Wetter and warmer conditions were established after ~10,400 cal yr BP, as indicated by the decline in *Artemisia* and the increases in wetland herb and broad-leaved *Quercus* pollen. The highest subtropical and tropical TP content occurred at ~9,000-6,000 cal yr BP, which is consistent with high winter SSTs in the Dongsha Section of the northern slope of SCS (core 17940) and stable oxygen isotope records from the speleothems in Dongge Cave (Figure 4-9). This warm and wet climate corresponds to the mid-Holocene Optimum, and it is recorded by many proxies in the Asian monsoon region (e.g., Yi et al., 2003; Li et al., 2006a; Nahm et al., 2013). The record of highly diverse TP assemblages in zone PIII should be associated with the warmer and wetter

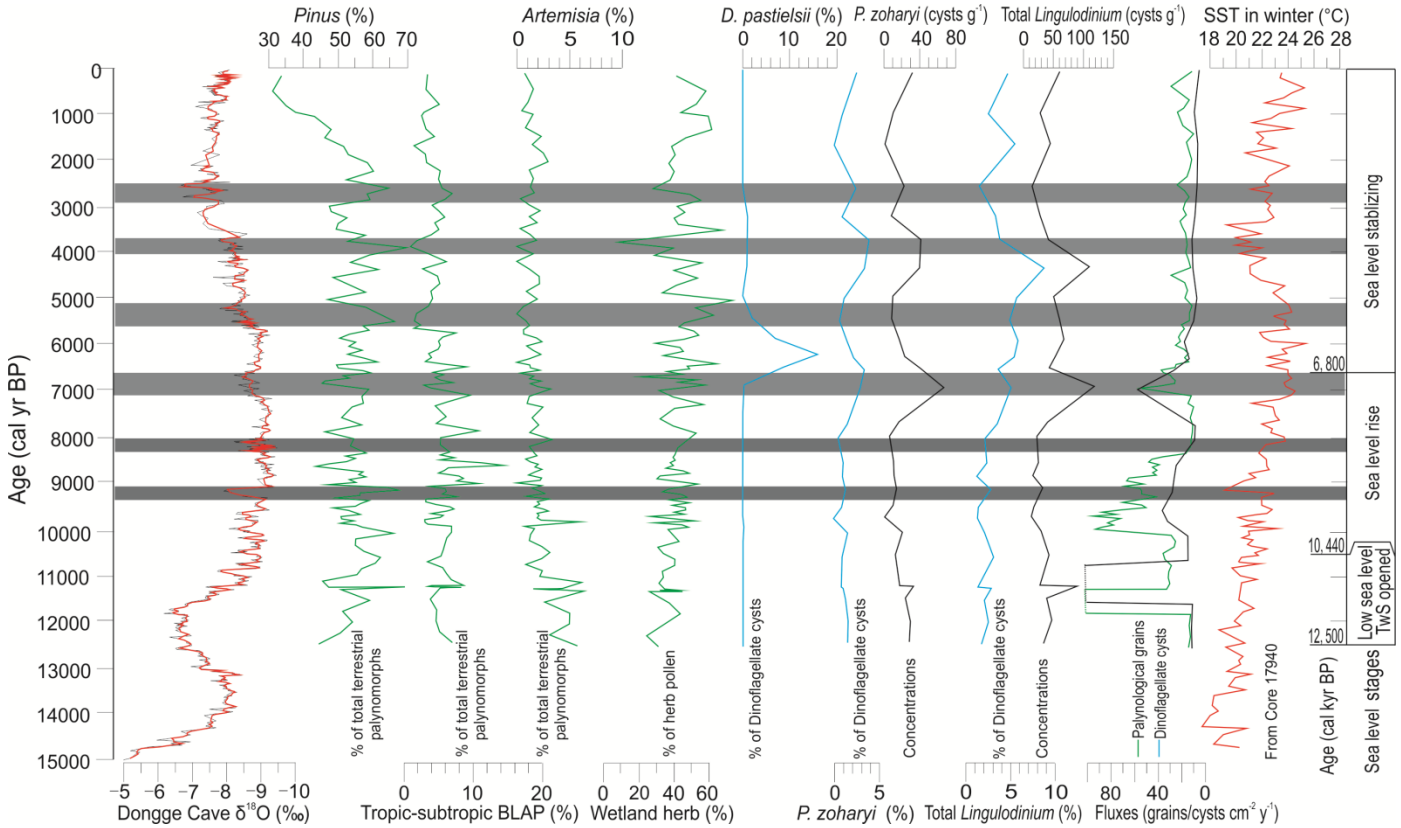

Figure 4-9. Pollen and dinoflagellate cyst data from core GLW31D are plotted along with the previously published δ18O record fromthe Dongge Cave (Dykoski et al., 2005;Wang et al., 2005) and reconstructedwinter SSTs fromcore 17940 (Jiang et al., 2014). The right side shows the stages of the Holocene sea level change from Liu et al. (2004a, 2004b), Zong (2004), Tanabe et al. (2006), and Hanebuth et al. (2011). Grey bands mark three intervals with low subtropical and tropical broad-leaved AP contents prior to ~6800–6000 cal yr BP and three intervals with high Pinus abundance thereafter, corresponding to six cooling air temperature events as reflected by $\delta^{18}O$ cave records.

conditions, when terrestrial vegetation in the surrounding area of the SCS was flourishing.

The abrupt increase of *Dapsilidinium pastielsii* in dinoflagellate cyst zone DIIIa reflects stable high SSTs that are well matched with the SST record from core 17940 (Figure 4-9). *Dapsilidinium pastielsii* is a "living fossil" thought to have gone extinct in the early Pleistocene, but this species was recently discovered in the Indo-Pacific warm pool (Mertens et al., 2014). *Dapsilidinium pastielsii* was widespread during the Miocene, when the latitudinal temperature gradient declined in the world's oceans (e.g., Tong et al., 2009), and it is known that the Middle Miocene Climatic Optimum had been even warmer than present conditions (e.g., Flower and Kennett, 1993; Shi et al., 2014). Therefore, abundant *Dapsilidinium pastielsii* should be associated only with high SST environments (Mertens et al., 2014). Thus, based on the ecological preferences of *Dapsilidinium pastielsii*, DIIIa corresponds to the warmest SSTs in our record. Such SST increase could be caused by the rise in local air and water temperature or the intensification of the Kuroshio Current at ~7,000-6,000 cal yr BP (Liu et al., 2013).

However, some timing offset of the mid-Holocene Optimum can be seen when stalagmite, pollen, and dinoflagellate cyst records are compared (Figure 4-9). Oxygen isotopes of stalagmites from Dongge Cave (Dykoski et al., 2005; Wang et al., 2005) indicate that the mid-Holocene Optimum started at the early Holocene and lasted until approximately ~7,200 cal yr BP in South China. Pollen records from northern China showed that the Optimum started and ended much later, at ~8,000 cal yr BP and ~4,000 cal yr BP, respectively (Liu et al., 2015). The pollen records in our study show the Holocene Optimum at ~9,000 to ~6,000 cal yr BP, which is earlier than that recorded in

northern China or the northern EAM region but later than the period indicated by stalagmites. The impact of various geographic and hydrodynamic conditions on (paleo)records should not be ignored. For example, an intensified summer monsoon could also increase river discharge and, in turn, induce a high input of TP. The freshwater alga of *Concentricystes* and *Zygnema* can be associated with such fluvial inputs (Figure 4-4).

Dykoski et al. (2005) and Wang et al. (2005) measured oxygen isotopes of speleothems from Dongge Cave, southern China, and provided a continuous history of the Asian monsoon over the past 9,000 yr. During the weak summer monsoon periods, as recorded in Dongge Cave, *Pinus* pollen did not show signs of cooling, although subtropical-tropical broad-leaved pollen appears to be associated with these events.

4.5.3.3 After ~6,800 (or 6, 000) cal yr BP

After ~6,800 (or 6,000) cal yr BP, the sea level reached the highest level, that is, similar to or slightly higher than at present (Figure 4-8) (Zong, 2004; Tanabe et al., 2006), and the modern hydrographic frame was formed only afterwards. Wind became the main pathway for pollen transport to the site (Figure 4-7). Increases in the abundance of *Pinus* pollen, which were brought from the China mainland and Taiwan by the northeast winter monsoon (e.g., Sun et al., 1999; Luo et al., 2013) reflect three intervals of intensified winter monsoon. These intervals are in approximate agreement with the records from the Dongge Cave and correspond to ~5,500 cal yr BP, 4,000 cal yr BP and 2,500 cal yr BP (Figure 4-9).

More-detailed information on the Asian monsoon climate could be provided by dinoflagellate cysts if we refine their seasonal environmental preferences in the SCS. This requires a detailed and long-term study of dinoflagellate cysts in sediment traps in the sea.

4.6 Conclusions

High-resolution reconstructions of the Asian monsoon climate and oceanographic conditions during the Holocene have previously been carried out in the northern SCS (e.g., Huang et al., 1997; Wang et al., 1999; Yu et al., 2005; He et al., 2008; Kong et al., 2014; Jiang et al., 2014; Dai and Weng, 2015). However, the interpretations and/or timing of reconstructed events as recorded by various proxies are inconsistent. This could be due to the biases resulted from differences in methods, site locations, or the limitations of individual proxies. In this study, for the first time, terrestrial (pollen, spore, and some freshwater alga) and marine (dinoflagellate cysts) palynological records in the same sediment core (GLW31D) from the northern SCS were investigated. Terrestrial and marine palynomorph extraction and identification in the same laboratory and on the same core greatly reduced possible methodological biases.

Well-preserved TP and dinoflagellate cysts were recovered with concentrations at thousands of grains or cysts per cubic centimetre. Two major boundaries, at ~10,400 cal yr BP and ~6,800 (or 6,000) cal yr BP, were recorded by assemblages of TP and dinoflagellate cysts. These boundaries appear to be associated with the timing of the major sea-level rise and known hydrographic reorganizations of the SCS during the Holocene. The highest herb pollen abundance at the low sea-level stand during the onset

of the Holocene reflects the close proximity of grasslands on the exposed shelf of the northern SCS. During the interval of regional relative sea-level rise prior to ~6,800 (or 6,000) cal yr BP, the fern spore content had increased due to hydrodynamic sorting, whereas the concentrations and fluxes of dinoflagellate cysts had decreased. The latter effect can be explained by the decrease of marine primary productivity due to migration of the coastline inland, thus moving the sources of nutrient input away from the core site. Steadily low total dinoflagellate cyst concentrations and the highest fern spore percentage were observed after the sea-level stabilization from ~6,800 (or 6,000) cal yr BP to the present.

High abundances of *Impagidinium*, the genus associated with nutrient-depleted oceanic waters, appeared at the transition period of ~12,000-10,400 cal yr BP. This was interpreted as the result of the increased input of western Philippine Sea waters into the SCS and the branching of the Kuroshio Current. A short-term decrease of *Impagidinium* at ~11,700-11,000 cal yr BP corresponds to the MWP-1B event, or an abrupt interval of sea-level rise might be associated with the Taiwan Strait opening and the beginning of water exchange between the SCS and the ECS. According to the sea-level data in this region, the sea rose to the highest level at ~6,800-6,000 cal yr BP (e.g., Liu et al., 2004a, Tanabe et al., 2006; Henabuth et al., 2010), when it was close to or slightly higher than the present level, and the modern oceanographic frame was formed. Consistent with this pattern, our data show the positive relationship between the sedimentation rates and the TP concentrations prior to ~6,300 cal yr BP, whereas a negative relationship was observed thereafter. This indicates that the water-dominated mechanism for the transport of TP grains was replaced by the wind-dominated mechanism after ~6,300 cal yr BP,

when the sea level became relatively stable. Considering the changes of hydrographic and TP taphonomic conditions due to the sea-level rise, the mid-Holocene Optimum was reflected by the highest abundances of subtropical-tropical broad-leaved AP in TP assemblages and by the increase of warm *Dapsilidinium pastielsii*. The strengthened summer monsoon in the mid-Holocene that induced an intensified river input and increased SSTs is recorded by the increase of *Polysphaeridium zoharyi* and *Lingulodinium*. Three strengthened winter monsoon intervals at ~5,500 cal yr BP, 4,000 cal yr BP, and 2,500 cal yr BP are marked by increases in *Pinus* pollen that was transported by the northeast winter monsoons, similarly to the present transport mechanism which wind rather than water is the dominant transport way under the present oceanographic frame. The intensified human activity through deforestration for cultivated fields in the watershed is reflected by the rapid increase in fern spores after ~1,500 cal yr BP.

Acknowledgements

The Natural Sciences and Engineering Research Council of Canada (NSERC) CGS D3 fellowship, Montalbano scholarship, and the National Science and Technology Major Projects of China grant (2011ZX05056-001-02) provided partial funding for this research to Z. Li. This work was also funded by NSERC through a Discovery grant (312305) to V. Pospelova. She is the Hanse-Wissenschaftskolleg (HWK) senior research fellow in marine and climate research at the Institute for Advanced Study (Germany). L. Liu was partially supported by the National Key Project (GASI-GEOGE-05) from the State Oceanography Administration of China in this work.

Chapter 5

Conclusions

For the first time, detailed analysis of terrestrial (pollen and spores) and marine (dinoflagellate cysts) palynological records in samples from sediment traps, surface sediments and one sediment core in the SCS were conducted for reconstructing Holocene East Asian Monsoon climate and oceanographic history of the northern South China Sea. A total of 67 dinoflagellate cyst taxa and a total of 186 pollen and spore taxa were identified. The study on sediment trap revealed the seasonal dynamics of pollen, spores and dinoflagellate cysts and identified specific indicators (e.g., *Pinus* pollen, *Ulmus* pollen, and fern spores) for EAM and environmental parameters. The dinoflagellate cyst records in the surface sediment of the entire SCS showed distributional patterns of dinoflagellate cysts in different geographic regions and the role of environmental factors in the dinoflagellate cyst assemblages and concentrations. Terrestrial and marine palynomorphs in one sediment core from the northern SCS reflected Holocene EAM and oceanographic events on centennial time scales controlled with high-resolution ^{14}C AMS ages.

In this study, twenty four samples from sediment traps deployed in the southwest Taiwan waters of the SCS in winter monsoon (March-April) and summer monsoon (July-August) seasons were used for seasonal dynamics influencing palynomorph distributions and reliable indicators of monsoons. Associated with transport by the northwest wind in March–April when pollen are produced by the vegetation in the South China and Taiwan Island, *Pinus* and *Ulmus* pollen were identified as good indicators of winter monsoon.

Controlled by fluvial transport, fern spores could be indicators of summer monsoon since they were enriched by intensified river inputs in summers shown by RDA results. High relative abundances and fluxes of Poaceae pollen are not indicators of summer monsoons but related to cultural activities. The increased fluxes of almost all dinoflagellate cyst taxa during July–August were related to the decreased sea-surface salinity (SSS) due to the greater river water inputs and nutrients. Dinoflagellate cyst assemblages were dominated by cysts produced by heterotrophic taxa, especially *Brigantedinium* spp. at 68–91%. Proportionally higher increases of autotrophic taxa resulted in lower heterotrophic to autotrophic ratios in July–August, perhaps associated with more light availability.

Forty two surface sediment samples from the northern and the eastern SCS were investigated for dinoflagellate cyst distributions. Combined with previously published data of Kawamura (2002; 2004) from the southern and the western SCS, the distribution patterns of 31 dinoflagellate cyst taxa and their relationship with environmental parameters were described. Four high total cyst concentration regions occur off the southern Vietnam, Borneo, Hainan, and South China. The highest concentrations occur off southern Vietnam. The lowest cyst concentrations are off Luzon. The distribution patterns link to stronger summer coast upwelling in the western and northern regions than winter coast upwelling in the eastern and southern regions.

Based on CCA results performed on dinoflagellate cyst dataset and environmental parameters, we found that sea-surface temperature in January is the most important factor related to dinoflagellate cyst distributions, followed by water depth, chl-*a* concentrations and SSS in July. Four dinoflagellate cyst groups were identified that reflect measured environmental parameters. *Brigantedinium* spp., *Selenopemphix nephroides*, and

Selenopemphix reidii were likely associated with weak monsoons since these taxa were positively correlated with SST in January and SSS in July. *Impagidinium* spp., *Nematosphaeropsis labyrinthus*, and *Polysphaeridium zoharyi* are positively correlated with water depth and distance to the coastline, and can form a group of indicators of a more oceanic environment rather than near shore settings. Cysts of *Protoperidinium* spp., cyst of *P. oblongum*, *Selenopemphix quanta*, *Selenopemphix undulata*, *Q. concreta* and *Echinidinium* spp. are positively correlated with chl-*a* concentrations and PP.

High resolution terrestrial and marine palynological records from one sediment core in the northern SCS reflected the EAM climatic and oceanographic events since 12,500 cal yr BP. First our study provided insight on the onset of Taiwan Strait opening shown by the abundances of *Impagidinium* spp.: it likely starting at ~11.7–11.0 cal kyr BP, when a relative sea level rose rapidly due to the MWP-1B event and water from the East China Sea input through the Taiwan Strait.

The proxies used for paleoclimate reconstructions are usually also influenced by environmental changes in the past. It is necessary to understand their depositional conditions relevant to environments such as sea-level change, coastline migrations, or possible pathways to the depositing sites. We found that the palynological record was related to environmental changes such as sea-level rise rather than EAM variation before the modern oceanographic frame arose at ~~6.8–6.0 cal kyr BP. Three relative sea-level stages are well reflected by both marine dinoflagellate cysts and terrestrial pollen & spores with major boundaries at ~10.4 cal kyr BP and ~6.8 (or 6.0) cal kyr BP. The relative sea level was stabilized at ~6.8–6.0 cal kyr BP during which total pollen and spores kept consistant low values.

Pollen and spores came from terrestrial sources. Wind and water both play important roles in their transportation. Therefore, only after the oceanographic conditions were stable, the changes of monsoon indicators selected under the modern oceanographic conditions can be ascribed to climate factors. In this study, after the modern oceanographic frame forms at ~6.8 cal kyr BP, high abundances of *Pinus* pollen reveal three strengthened winter monsoon intervals at ~5.5, ~4.0, and ~2.5 cal kyr BP.

This study contributes to the research field of Quaternary climate and environment history by refining palynological indicators of winter and summer monsoons, assessing palynological assemblages for the EAM and (paleo)oceanographic conditions, and high-resolution of Holocene EAM and environmental changes in the SCS. This is the first study of palynomorphs including terrestrial and marine taxa from sediment traps, surface sediments to sediment cores in systematics in the SCS. This study provides insights on the individual palynomorph taxa relevant to the specific environmental parameters, and Holocene EAM climate and oceanographic events at high-resolution. The reconstructed short-term strengthened winter monsoon events and the warmest optimum contribute to a comparison of the past EAM records between land and sea for the study of their driving mechanisms. The data also help to expand the database of global dinoflagellate cysts for quantitative reconstructions of EAM and oceanographic conditions in the past. For quantitative reconstructions of past EAM and oceanographic environments, the more detailed we understand the EAM influences on individual taxa of pollen, spores and dinoflagellate cysts as well as their assemblages, the more accurate the reconstructions could be. Thus, studies of annual and/or multiannual time series of pollen, spores and dinoflagellate cysts from modern sediment traps at multiple sites in the SCS and

complementary analysis on a series of surface sediments from coast to the deep basin off Borneo would be a priority for future research.

Bibliography

Academia Sinica: Institute of Botany and South China Institute of Botany, 1982. Angiosperm pollen flora of tropic and subtropic China. Science Press, Beijing.

Academia Sinica: Institute of Botany, 1976. Sporae Pteridophytorum sinicorum. Science Press, Beijing.

An, Z., 2000. The history and variability of the East Asian paleomonsoon climate. Quaternary Science Review 19, 171–187.

Aydin, H., Matsuoka, K., Minareci, E., 2011. Distribution of dinoflagellate cysts in recent sediments from Izmir Bay (Aegean Sea, Eastern Mediterranean). Marine Micropaleontology 80, 44–52.

Bai, Y., Huang, T.H., He, X., Wang, S.-L., Hsin, Y.-C., Wu, C.-R., Zhai, W., Lui, H.-K., Arthur Chen, C.-T., 2015. Intrusion of the Pearl River plume into the main channel of the Taiwan Strait in summer. Journal of Sea Research 95, 1–15.

Bakun, A., Agostini, V.N., 2001. Seasonal patterns of wind induced upwelling/downwelling in the Mediterranean Sea. Scientia Marina 65(3), 243–257.

Bard, E., Hamelin, B., Arnold, M., Montaggioni, L., Cabioch, G., Faure, G., Rougerie, F., 1996. Deglacial sea-level record from Tahiti corals and the timing of global meltwater discharge. Nature 382, 241-244.

Bard, E., Hamelin, B., Delanghe-Sabatier, D., 2010. Deglacial meltwater pulse 1B and Younger Dryas sea levels revisited with boreholes at Tahiti. Science 327, 1235-1237.

Beaudouin, C., Suc, J.P., Escarguel, G., Arnaud, M., Charmasson, S., 2007. The significance of pollen signal in present-day marine terrigenous sediments: the example of the Gulf of Lions (western Mediterranean Sea). Geobios 40, 159–172.

Benthuysen, J., Thomas, L.N., Lentz, S.J., 2014. Rapid generation of upwelling at a shelf break caused by buoyancy shut down. Journal of Physical Oceanography 45, 294–312.

Birks, H.J.B., Line, J.M., 1992. The use of rarefaction analysis for estimating palynological richness from Quaternary pollen-analytical data. The Holocene 2, 1–10.

Bond, G., Showers, W., Cheseby, M., Lotti, R., Almasi, P., deMenocal, P., Priore, P., Cullen, H., Hajdas, I., Bonani, G., 1997. A pervasive millennial-scale cycle in North Atlantic Holocene and glacial climate. Science 278, 1257–1266.

Bonnet, S., de Vernal, A., Gersonde, R., Lembke-Jene, L., 2012. Modern distribution of dinocysts from the North Pacific Ocean (37 – 64°N, 144°E –148°W) in relation to hydrographic conditions, sea-ice and productivity. Marine Micropaleontology 84–85, 87–113.

Bouimetarhan, I., Marret, F., Dupont, L., Zonneveld, K., 2009. Dinoflagellate cyst distribution in marine surface sediments off West Africa (17 – 6°N) in relation to sea surface conditions, freshwater input and seasonal coastal upwelling. Marine Micropaleontology 71, 113–130.

Bouimetarhan, I., Prange, M., Schefuß, E., Dupont, L., Lippold, J., Mulitza, S., Zonneveld, K., 2012. Sahel megadrought during Heinrich Stadial 1: evidence for a three-phase evolution of the low- and mid-level West African wind system. Quaternary Science Review 58, 66–76.

Bradley, R.S., 1999. Paleoclimatology: Reconstructing Climates of the Quaternary. Academic Press, San Diego. pp. 11-15.

Bradley, R.S., 2015. Paleoclimatology: Reconstructing Climates of the Quaternary (3rd Edition). Elsevier Inc. Publish, p. 413.

Bringué, M., Pospelova, V., Pak, D., 2013. Seasonal production of organic-walled dinoflagellate cysts in an upwelling system: A sediment trap study from the Santa Barbara Basin, California. Marine Micropaleontology 100, 34–51.

Bringué, M., Pospelova, V. and Field, D.B., 2014. High resolution sedimentary record of dinoflagellate cysts reflects decadal variability and 20th century warming in the Santa Barbara Basin. Quaternary Science Reviews 105, 86–101.

Bringué, M., Pospelova, V., Calvert, S.E., Enkin, R.J., Lacourse, T., Ivanochko, T., 2016. High resolution dinoflagellate cyst record of environmental change in Effingham Inlet (British Columbia, Canada) over the last millennium. Palaeogeography, Palaeoclimatology, Palaeoecology 441, 787–810.

Bringué, M., Thunell, B.C., Pospelova, V., Pinckney, J.L., Romero, O.E., Tappa, E.J., 2018. Physico-chemical and biological factors influencing dinoflagellate cyst production in the Cariaco Basin. Biogeosciences, 15, 2325–2348.

Cai, B., 1997. “Dongshan Land Bridge” and the earliest human in Taiwan. J. Zhangzhou Teachers College 3, 31–36 (in Chinese).

Candel, M.S., Radi, T., de Vernal, A., Bujalesky, G., 2012. Distribution of dinoflagellate cysts and other aquatic palynomorphs in surface sediments from the Beagle Channel, Southern Argentina. Marine Micropaleontology 96–9, 1–12.

Caruso, M.J., Gawarkiewicz, G.G., Beardsley, R.C., 2006. Interannual Variability of the Kuroshio Intrusion in the South China Sea. Journal of Oceanography 62, 559–575.

Chen, D., Fang, K.Y., Li, Y.J., Dong, Z.P., Zhang, Y., Zhou, F.F., 2016. Response of Pinus taiwanensis growth to climate changes at its southern limit of Daiyun Mountain, mainland China Fujian Province. Science China Earth Science 59, 328–336.

Chen, H.-W., Liu, C.-T.,Matsuno, T., Ichikawa, K., Fukudome, K., Yang, Y., Doong, D.-J., Tsai, W.-L., 2016. Temporal variations of volume transport through the Taiwan Strait, as identified by three-year measurements. Continental Shelf Research 114, 41–53.

Chen, J., 1997. Submarine paleo-shorelines in the northern South China Sea. Marine Geology 1, 19–30 (in Chinese with English abstract).

Chen, L., 1992. Features of the East Asian monsoon. In: Murakami, M., Ding, Y. (Eds.), Studies of Asian Monsoon in Japan and China. Meteorology Research Institute, Ibaraki, Japan, pp. 220–235.

Chen, Y.-L.L., Chen, H.Y., 2006. Seasonal dynamics of primary and new production in the northern South China Sea: The significance of river discharge and nutrient advection. Deep-Sea Research I 53, 971–986.

Cheng, X., Huang, B., Jian, Z., Zhao, Q., Tian, J., Li, J., 2005. Foraminiferal isotopic evidence for monsoonal activity in the South China Sea: a present-LGM comparison. Marine Micropaleontology 54, 125–139.

Committee on Ecological impacts of Climate Change. 2008. Ecological Impacts of Climate Change. Press: The National Academies Press, Washington, D.C. pp.11-15.

Cronin, T.M., 2012. Rapid sea-level rise. Quaternary Science Reviews 56, 11-30.

Crouch, E.M., Mildenhall, D.C., Neil, H.L., 2010. Distribution of organic-walled marine and terrestrial palynomorphs in surface sediments, offshore eastern New Zealand. Marine Geology 270, 235–256.

Crowley, G.M., Grindrod, J., Kershqw, A.P., 1994. Modern pollen deposition in the tropical lowlands of northeast Queensland, Australia. Review of Palaeobotany and Palynology 83, 299–327.

Dai, L., Weng, C., 2015. Marine palynological record for tropical climate variations since the late last glacial maximum in the northern South China Sea. Deep-Sea Research II 122, 153–162.

Dai, L., Weng, C., Lu, J., Mao, L., 2014. Pollen quantitative distribution in marine and fluvial surface sediments from the northern South China Sea: New insights into pollen transportation and deposition mechanisms. Quaternary International 325, 136–149.

Dai, L., Weng, C., Mao, L., 2015. Patterns of vegetation and climate change in the northern South China Sea during the last glaciation inferred from marine palynological records. Palaeogeography, Palaeoclimatology, Palaeoecology 440, 249–258.

Dale, B., 1976. Cyst formation, sedimentation, and preservation: factors affecting dinoflagellate assemblages in recent sediments from Trondheims fjord, Norway. Review Palaeobotany and Palynology 22, 39–60.

Dale, B., 1992. Dinoflagellate contributions to the open ocean sediment flux. In: Honjo, S. (Ed.), Dinoflagellate contributions to the deep sea. Ocean Biocoenosis Vol. 5. Woods Hole Oceanographic Institution, Woods Hole, pp. 1–32.

Dale, B., 1996. Dinoflagellate cyst ecology: modeling and geological applications. In: Jansonius, J., McGregor, D.C. (Eds.), Palynology: principles and applications. AASP Foundation, pp. 1249–1275.

Dale, B., 2001. Marine dinoflagellate cysts as indicators of eutrophication and industrial pollution: a discussion. Science of the Total Environment 264, 235–240.

Dale, B., 2009. Eutrophication signals in the sedimentary record of dinoflagellate cysts in coastal waters. Journal of Sea Research 61, 103–113.

Dale, B., Thorsen, T.A., Fjellsa, A., 1999. Dinoflagellate cysts as indicators of cultural eutrophication in the Oslofjord, Norway. Estuarine, Coastal and Shelf Science 48, 371–382.

Dale, B., Dale, A.L., Jansen, J.H.F., 2002. Dinoflagellate cysts as environmental indicators in surface sediments from the Congo deep-sea fan and adjacent regions. Palaeogeography, Palaeoclimatology, Palaeoecology 185, 309–338.

D'Costa, P.M., Anil, A.C., Patil, J.S., Hegde, S., Chourasia, M., 2008. Dinoflagellates in a mesotrophic, tropical environment influenced by monsoon. Estuarine, Coastal and Shelf Science 77, 77–90.

Delwiche, C., 2007. CHAPTER 10 - The Origin and Evolution of Dinoflagellates. In: Falkowski, P.G., Knoll, A.H., (Eds.), Evolution of Primary Producers in the Sea. pp.191–205. https://doi.org/10.1016/B978-0-12-370518-1.X5000-0.

de Menocal, P.B., Ortiz, J., Guilderson, T. and Sarnthein, M., 2000. Coherent high- and Low-latitude climate variability during the Holocene warm period. Science 288, 2198-2202.

de Vernal, A., Rochon, A., Turon, J.L., Matthiessen, J., 1997. Organic-walled dinoflagellate cysts: Palynological tracers of sea-surface conditions in middle to high latitude marine environments. Geobios 30, 905-920.

de Vernal, A., Henry, M., Matthiessen, J., Mudie, P.J., Rochon, A., Boessenkool, K.P., Eynaud, F., Grosfjeld, K., Guiot, J., Hamel, D., Harland, R., Head, M.J., Kunz-Pirrung, M., Levac, E., Loucheur, V., Peyron, O., Pospelova, V., Radi, T., Turon, J.L., Voronina, E., 2001. Dinoflagellate cyst assemblages as tracers of sea-surface conditions in the northern North Atlantic, Arcticandsub-Arcticseas: the new 'n=677' data base and its application for quantitative palaeoceanographic reconstruction. Journal of Quaternary Science 16, 681–698.

de Vernal, A., Eynaud, F., Henry, M., Hillaire-Marcel, C., Londeix, L., Mangin, S., Matthiessen, J., Marret, F., Radi, T., Rochon, A., Solignac, S., Turon, J.L., 2005. Reconstruction of sea-surface conditions at middle to high latitudes of the Northern Hemisphere during the Last Glacial Maximum (LGM) based on dinoflagellate cyst assemblages. Quaternary Science Reviews 24, 897–924.

Devillers, R., de Vernal, A., 2000. Distribution of dinoflagellate cysts in surface sediments of the northern North Atlantic in relation to nutrient content and productivity in surface waters. Marine Geology 166, 103–124.

D'Silva, M.S., Anil, A.C., Borole, D.V., Nath, B.N., Singhal, R.K., 2012. Tracking the history of dinoflagellate cyst assemblages in sediments from the west coast of India. Journal of Sea Research 73, 86–100.

D'Silva, M.S., Anil, A.C., Sawant, S.S., 2013. Dinoflagellate cyst assemblages in recent sediments of Visakhapatnam harbour, east coast of India: Influence of environmental characteristics. Marine Pollution Bulletin 66, 59–72.

Duarte, C.M., Agustí, S., Gasol, J.M., Vaqué, D., Vazquez-Dominguez, E., 2006. Effect of nutrient supply on the biomass structure of planktonic communities: an experimental test on a Mediterranean coastal community. Marine Ecology Progress Series 206, 87–95.

Duplessy, J.C., Ivanova, E., Murdmaa, I., Peterne, M., Labeyrie, L., 2001. Holocene paleoceanography of the Northern Barents Sea and variations of the northward heat transport by Atlantic Ocean. Boreas 30, 2–16.

Dykoski, C.A., Edwards, R.L., Cheng, H., Yuan, D., Cai, Y., Zhang, M., Lin, Y., Qing, J., An, Z., Revenaugh, J., 2005. A high-resolution, absolute-dated Holocene and

deglacial Asian monsoon record from Dongge cave, China. Earth Planetary Science Letter 233, 71–86.

Edwards, L.E., Mudie, P.J., de Vernal, A., 1991. Pliocene paleoclimatic reconstructions using dinoflagellate cysts: comparison of methods. Quaternary Science Reviews 10, 259–274.

Ellegaard, M., Clarke, A.L., Reuss, N., Drew, S., Weckström, K., Juggins, S., Anderson, N.J., Conley, D.J., 2006. Multi-proxy evidence of long-term changes in ecosystem structure in a Danish marine estuary, linked to increased nutrient loading. Estuarine Coastal Shelf Science 68, 567 – 578.

Ellegaard, M., Dale, B., Mertens, K.N., Pospelova, V., Ribeiro, S., 2017. Chapter 12 Dinoflagellate cysts as proxies for Holocene environmental change in estuaries: Diversity, abundance and morphology. In: Weckström, K., Saunders, K.M., Gell, P.A., Skilbeck, C.G. (Eds.), Applications of paleoenvironmental techniques in estuarine studies, Developments in paleoenvironmental pesearch 20. Springer, Dordrecht, pp. 295–312.

Eshet, Y., Almogi-Labin, A., Bein, A., 1994. Dinoflagellate cysts, paleoproductivity and upwelling systems: A Late Cretaceous example from Israel. Marine Micropaleontology 23, 231–240.

Esper, O., Zonneveld, K., 2002. Distribution of organic-walled dinoflagellate cysts in surface sediments of the Southern Ocean (eastern Atlantic sector) between the subtropical front and the Weddell Gyre. Marine Micropaleontology 46, 177–208.

Fairbanks, R.G., 1989. A 17,000 year glacio-eustatic sea level record: influence of glacial melting rates on the Younger Dryas event and deep ocean circulation. Nature 342, 637-642.

Fang, G.H., Fang,W.D., Fang, Y., Wang, K., 1998. A survey of studies on the South China Sea upper ocean circulation. Acta Oceanography. Taiwanica 37, 1–16.

Fang, G., H. Chen, Z. Wei, Y. Wang, X. Wang, and C. Li, 2006: Trends and interannual variability of the South China Sea surface winds, surface height, and surface temperature in the recent decade. Journal of Geophysical Research 111, C11S16.

Fang, G.H.,Wang, G., Fang, Y., Fang,W.D., 2012. A review on the South China Sea western boundary current. Acta Oceanolocia Sinca 31 (5), 1–10.

Florin, R., 1963. The distribution of conifer and taxad genera in time and space. Acta Horti Bergiani 20, 121–312.

Flower, B.P., Kennett, J.P., 1993. Middle Miocene ocean/climate transition: high-resolution oxygen and carbon isotopic records from DSDP Site 588A, southwest Pacific. Paleoceanography 8, 811–843.

Fu, G. (Ed.), 2012. Flora Republicae Popularis Sinicae (FRPS) (online: www.eflora.cn), Qingdao Press: Qingdao.

Fujii, R., Matsuoka, K., 2006. Seasonal change of dinoflagellates cyst flux collected in a sediment trap in Omura Bay. West Japan. Journal of Plankton Research 28, 131–147.

Gan, J., Cheung, A., Guo, X., Li, L., 2009. Intensified upwelling over a widened shelf in the northeastern South China Sea. Journal of Geophysical Research 114, C09019.

García-Moreiras, I., Pospelova, V., García-Gil, S., Sobrino, C.M., 2018. Climatic and anthropogenic impacts on the Ría de Vigo (NW Iberia) over the last two centuries: A high-resolution dinoflagellate cyst sedimentary record. Palaeogeography, Palaeoclimatology, Palaeoecology 504, 201–218.

Godhe, A., McQuoid, M.R., 2003. Influence of benthic and pelagic environmental factors on the distribution of dinoflagellate cysts in surface sediments along the Swedish west coast. Aquatic Microbial Ecology 32, 185-201.

Godhe, A., Norén, F., Kuylenstierna, M., Ekberg, C., Karlson, B., 2001. Relationship between planktonic dinoflagellate abundance, cysts recovered in sediment traps and environmental factors in the Gullmar Fjord, Sweden. Jounal of Plankton Research 23, 929–938.

Griffiths, M.L., Drysdale, R.N., Gagan, M.K., Zhao, J., Ayliffe, K.L., Hellstrom, J.C., Hantoro, W.S., Frisia, S., Feng, Y., Cartwright, I., Pierre, E.S., Fischer, M.J., Suwargadi, B.W., 2009. Increasing Australian–Indonesian monsoon rainfall linked to early Holocene sea-level rise. Nature Geoscience 2, 636–639.

Grimm, E.C., 1991. Tilia-Graph Program. Illinois State Museum, Springfield, IL.

Grimm, E.C., 1992. Tilia Program. Illinois State Museum, Springfield, IL.

Griraaudeau, J., Cremer, M., Manthe, S., Labeyrie, L., Bond, G., 2000. Coccolith evidence for instabilities in surface circulation south of Iceland during Holocene times. Earth and Planetary Science Letters 179, 257-268.

Gurdebeke, P.R., Pospelova, V., Mertens, K.N., Dallimore, A., Chana, J., Louwye, S., 2018. Diversity and distribution of dinoflagellate cysts in surface sediments from fjords of western Vancouver Island (British Columbia, Canada). Marine Micropaleontology 143, 12–29.

Hammer, Q., Harper, D.A.T., Ryan, P.D., 2001. PAST: paleontological statistics software package for education and data analysis. Palaenotologia Electronica 4 (1), 9.

Hanebuth, T., Stattegger, K., Grootes, P.M., 2000. Rapid flooding of the Sunda shelf: a lateglacial sea level record. Science 288, 1033–1035.

Hanebuth, T., Voris, H.K., Yokoyama, Y., Saito, Y., Okuno, J., 2011. Formation and fate of sedimentary depocentres on Southeast Asia's Sunda Shelf over the past sea level cycle and biogeographic implications. Earth Science Review 104, 92–110.

Harland, R., 1973. Dinoflagellate cysts and acritarchs from the Bearpaw Formation (Upper Campanian) of southern Alberta, Canada. Palaeontology 16, 665–706.

Harland, R., 1983. Distribution maps of recent dinoflagellate cysts in bottom sediments from the North Atlantic Ocean and adjacent seas. Palaeontology 26, 321–387.

Harland, R., Pudsey, C.J., 1999. Dinoflagellate cysts from sediment traps deployed in the Bellingshausen, Weddell and Scotia seas. Antarctica. Marine Micropaleontology 37, 77–99.

Harland, R., Asteman, I.P., Nordberg, K., 2013. A two-millennium dinoflagellate cyst record from Gullmar Fjord, a Swedish Skagerrak sill fjord. Palaeogeography, Palaeoclimatology, Palaeoecology 392, 247–260.

He, J., Zhao, M., Li, L., Wang, H., Wang, P., 2008. Biomarker Evidence of Relatively Stable Community Structure in the Northern South China Sea during the Last Glacial and Holocene. Terrestrial, Atmospheric and Oceanic Sciences, 377–387.

Head, M.J., 1996. Chapter 30.Modern dinoflagellate cysts and their biological affinities. In: Jansonius, J., McGregor, D.C. (Eds.), Palynology: principles and applications. American Association of Stratigraphic Palynologists, Dallas, USA, pp. 1197–1248.

Head, M.J., Harland, R., Matthiessen, J., 2001. Cold marine indicators of the late Quaternary: the new dinoflagellate cyst genus Islandinium and related morphotypes. Journal of Quaternary Science 16(7), 621–636.

Heikkilä, M., Pospelova, V., Hochheim, K. P., Kuzyk, Z. Z. A., Stern, G. A., Barber, D. G., Macdonald, R. W., 2014. Surface sediment dinoflagellate cysts from the Hudson Bay system and their relation to freshwater and nutrient cycling. Marine Micropaleontology 106, 79–109.

Heikkilä, M., Pospelova, V., Forest, A., Stern, G.A., MacDonald, R.W., 2016. Dinoflagellate cyst production over an annual cycle in seasonally ice-covered Hudson Bay. Marine Micropaleontology 125, 1–24.

Hessler, I., Young, M., Holzwarth, U., Mohtadi, M., Lückge, A., Behling, H., 2013. Imprint of eastern Indian Ocean surface oceanography on modern organic-walled dinoflagellate cyst assemblages. Marine Micropaleontology 101, 89–105.

Heusser, L.E., 1988. Pollen distribution in marine sediments on the continental margin off northern California. Marine Geology 80, 131–147.

Higginson, M.J., Maxwell, J.R., Altabet, M.A., 2003. Nitrogen isotope and chlorin paleoproductivity records from the northern South China Sea: remote vs. local forcing of millennial-and orbital-scale variability. Marine Geology 201, 223–250.

Hill, R.B., Johnson, J.A., 1974. A theory of upwelling over the shelf break. Journal of Physical Oceanography 4, 19–26.

Holl, C., Zonneveld, K. A. F., Willems, H., 2000. Organic-walled dinoflagellate cyst assemblages in the tropical Atlantic Ocean and oceanographical changes over the last 140 ka. Palaeogeography, Palaeoclimatology, Palaeoecology 160, 69–90.

Holzwarth, U., Esper, O., Zonneveld, K., 2007. Distribution of organic-walled dinoflagellate cysts in shelf surface sediments of the Benguela upwelling system in relationship to environmental conditions. Marine Micropaleontology 64, 91-119.

Hong, H., Chai, F., Zhang, C., Huang, B., Jiang, Y., Hu, J., 2011. An overview of physical and biogeochemical processes and ecosystem dynamics in the Taiwan Strait. Continental Shelf Research 31, S3–S12.

Hopkins, J.A., McCarthy, F.M.G., 2002. Post-depositional palynomorph degradation in Quaternary shelf sediments: a laboratory experiment studying the effects of progressive oxidation. Palynology 26, 167–184.

Hsiung, K.-H., Saito, Y., 2017. Sediment trapping in deltas of small mountainous rivers of southwestern Taiwan and its influence on East China Sea sedimentation. Quaternary International 455, 30–44.

Hu, J., Wang, X.H., 2016. Progress on upwelling studies in the China seas. Review of Geophysics 653–673.

Huang, C., Liew, P.M., et al. 1997. Deep sea and lake records of the Southeast Asian paleo-monsoons for the last 25 thousand years. Earth Planet Science Letter 146, 59–72.

Huang, C., Wu, S., Zhao, M., Chen, M.-T., Wang, C., Tu, X., Yuan, P., 1997. Surface ocean and monsoon climate variability in the South China Sea since the last glaciation. Marine Micropaleontology 32, 71–94.

Huang, C.-Y., Liew, P.-M., Zhao, M., Chang, T.-C., Kuo, C.-M., Chen, M.-T., Wang, C.-H., Zheng, L.F., 1997. Deep sea and lake records of the Southeast Asian paleo-monsoons for the last 25 thousand years. Earth Planet Science Letter 146, 59–72.

Huang, J., Li, A., Wan, S., 2011. Sensitive grain-size records of Holocene East Asian summer monsoon in sediments of northern South China Sea slope. Quaternary Research 75, 734–744.

Huang, J., Wan, S., Xiong, Z., Zhao, D., Liu, X., Li, A., Li, T., 2016. Geochemical records of Taiwan-sourced sediments in the South China Sea linked to Holocene climate changes. Palaeogeography, Palaeoclimatology, Palaeoecology 441, 871–881.

Huang, R., Chen, D., Liu, Y., 2012. Characteristics and causes of the occurrence of flooding disaster and persistent heavy rainfall in the Yangtze River valley of China. Journal of Chendu University of Information Technology 27, 1–18 (Chinese with English abstract).

Huang, T.C., 1972. Pollen Flora of Taiwan. National Taiwan University. Botany Department Press, Taipei, p. 297.

Huang, T.H., Chen, C.T.-A., Zhang,W.-Z., Zhuang, X.-F., 2015. Varying intensity of Kuroshio intrusion into Southeast Taiwan Strait during ENSO events. Continental Shelf Research 103, 79–87.

Huang, Y., Jiang, H., Sarnthein, M., Knudsen, K.L., Li, D. 2009. Diatom response to changes in palaeoenvironments of the northern South China Sea during the last 15000 years. Marine Micropaleontology 72, 99–109.

Hughen K.A, Baillie, M.G.L, Bard, E., Beck, J.W., Bertrand, C.J.H., Blackwell, P.G., Buck, C.E., Burr, G.S., Cutler, K.B., Damon, P.E., Edwards, R.L., Fairbanks, R.G., Friedrich, M., Guilderson, T.P., Kromer, B., McCormac, G., Manning, S., Ramsey, C.B., Reimer, P.J., Reimer, R.W., Remmele, S.,Southon, J.R., Stuiver, M., Talamo, S., Taylor, F.W., van der Plicht, J., Weyhenmeyer, C.E., 2004. Marine04 marine radiocarbon age calibration, 0–26 cal kyr BP. Radiocarbon 46(3), 1059–1086.

Nahm, W.-H., Kim, J.K., Kim, J.-Y., Yi, S., Lim, J., Kim, J.C., 2013. The Holocene climatic optimum in Korea: evidence from wetland records. Palaeogeography, Palaeoclimatology, Palaeoecology 376, 163–171.

Jacobson, D.M., Anderson, D.M., 1996. Widespread phagocytosis of ciliates and other protists by marine mixotrophic and heterotrophic thecate dinoflagellates. Journal of Phycology 32, 279–285.

Jan, S., Wang, J., Chern, C.-S., Chao, S., 2002. Seasonal variation of the circulation in the Taiwan Strait. Journal of Marine System 35, 249–268.

Jian, Z., Huang, B., Lin, H., Kuhnt, W., 2001. Late Quaternary upwelling intensity and East Asian monsoon forcing in the South China Sea. Quaternary Research 55, 363–370.

Jiang, H., Knudsen, M. F., Seidenkrantz, M.-S., Zhao, M., Sha, L., Ran, L., 2014. Diatom-based reconstruction of summer sea-surface salinity in the South China Sea over the last 15 000 years. Boreas 43, 208–219.

Jiang, H., Björck, S., Ran, L., Huang, Y., Li, J., 2006. Impact of the Kuroshio Current on the South China Sea based on a 115 000 year diatom record. Journal of Quaternary Science 21, 377–385.

Jiang, J., Qian, Y., 2000. The general character of precipitation over the South China Sea. Acta Meteorologica Sinica 58 (1), 60-69 (in Chinese with English abstract).

Jiang, T., Zhang, R. Blender, R., Fraedrich, K., 2005. Yangtze Delta floods and droughts of the last millennium: abrupt changes and long term memory. Theoretical and Applied climatology 82, 131–141.

Jing, Z., Qi, Y., Hua, Z., Zhang, H., 2009. Numerical study on the summer upwelling system in the northern continental shelf of the South China Sea. Continental Shelf Research 29, 467–478.

Kao, S.J., Milliman, J.D., 2008.Water and sediment discharge from small mountainous rivers, Taiwan: the roles of lithology, episodic events, and human activities. Journal of Geology 116, 431–448.

Kawamura, H., 2002. Marine palynological records in the southern South China Sea over the last 44 kyr. PhD thesis, Christian-Albrechts-Universität zu Kiel, 145 pp.

Kawamura, H., 2004. Dinoflagellate cyst distribution along a shelf to slope transect of an oligotrophic tropical sea (Sunda Shelf, South China Sea). Phycological Research 52, 355–375.

Kim, S.Y., Lim, D.I., Cho, H.J., 2012. Dinoflagellate cyst assemblages from the northern shelf sediments of the East China Sea: An indicator of marine productivity. Marine Micropaleontology 96–97, 75–83.

Kokinos, J.P., Anderson, D.M., 1995. Morphological development of resting cysts in cultures of the marine dinoflagellate *Lingulodinium polyedrum* (= L. machaerophorum). Palynology 19, 143–166.

Kong, D., Zong, Y., Jia, G., Wei, G., Chen, M.-T., Liu, Z., 2014. The development of late Holocene coastal cooling in the northern South China Sea. Quaternary International 349, 300–307.

Kumar, A., Patterson, R.T., 2002. Dinoflagellate cyst assemblages from Effingham Inlet, Vancouver Island, British Columbia, Canada. Palaeogeography, Palaeoclimatology, Palaeoecology 180, 187–206.

Kuo, C.-C., Gan, T.Y., Yu, P.-S., 2010. Seasonal streamflow prediction by a combined climate-hydrologic system for river basins of Taiwan. Jounal of Hydrology 387, 292–303.

Kuo, N.-J., Hoi, C.-R., Lo, Y.-T., Huang, S.-J., Chang, L., 2009. Analysis of chlorophyll-*a* concentration around the South China Sea from ocean color images. In: Oceans 2009–Europe, pp 1–4.

Kutzbach, J.E., 1974. Fluctuations of climate-monitoring and modelling. World Meteorological Organization Bulletin 23, 155-163.

Lambeck, K., 1993. Glacial rebound and sea-level change: an example of a relationship between mantle and surface processes. In: R. Wortel, U. Hansen and R. Sabadini (Editors), Relationships between Mantle Processes and Geological Processes at or near the Earth's Surface. Tectonophysics 223, 15-37.

Lee, T., Yoder, J., Atkinson, L., 1991. Gulf Stream frontal eddy influence on productivity of the south east US continental shelf. Journal of Geophysical Research 96, 22191–22205.

Lentin, J.K., Williams, G.L., 1993. Fossil Dinoflagellates: Index to Genera and Species. Dallas, TX: AASP Contribution Series.

Lewis, J., Dodge, J.D., Powell, A.J., 1990. Quaternary dinoflagellate cysts from the upwelling system offshore Peru, hole 686B, ODP Leg 112. Proceedings of the Ocean Drilling Program, Scientific Results 112, 323–328.

Li, C.-F., Chytry, M., Zeleny, D., Chen, M.-Y., Chen, T.-Y., Chiou, C.-R., Hsia, Y.-J., Liu, H.-Y., Yang, S.-Z., Yeh, C.-L., Wang, J.-C., Yu, C.-F., Lai, Y.-J., Chao, W.-C., Hsieh, C.-F., 2013. Classification of Taiwan forest vegetation. Applied Vegetation Science 16, 698–719.

Li, J.P., Zeng, Q.C. 2002. A unified monsoon index. Geophysical Research Letters 29, 1151–1154.

Li, X., Liu, J., Chen, F., Zhang, X., 2008. Carbonate cycles since the late Pleistocene in the northern South China Sea. Quaternary Sciences 28, 431–436 (in Chinese with English abstract).

Li, X., Zhou, W., An, Z., John, D., 2003. The vegetation and monsoon variations at the desert-boess transition belt at Midiwan in northern China for the last 13 ka. The Holocene 13, 779–784.

Li, Z., Saito, Y., Matsumoto, E., Wang, Y., Tanabe, S., Vue, Q., 2006a, Climate change and human impact on the Song Hong (Red River) Delta, Vietnam, during the Holocene. Quaternary International 144, 4–28.

Li, Z., Satio, Y., Matsumoto, E., Wang, Y., Haruyama, S., Hori, K., Doanh, L., 2006b. Palynological record of climate change during the last deglaciation from the Song Hong (Red River) delta, Vietnam. Palaeogeography, Palaeoclimatology, Palaeoecology 235, 406–430.

Li, Z., Zhang, Z., Li, J., Li, Z., Liu, L., Fan, H., Li, G., 2008. Pollen distribution in surface sediments of a mangrove system, Yingluo Bay, Guangxi, China. Review of Palaeobotany and Palynology 152, 21–31.

Li, Z., Saito, Y., Dang, P.X., Matsumoto, E., Vu, Q.L., 2009. Warfare rather than agriculture as a critical influence on fires in the late Holocene, inferred from northern Vietnam. Proceedings of the National Academy of Sciences of the United States of America (PNAS) 106 (28), 11472–11477.

Li, Z., Zhang, Y., Li, Y., Zhao, J., 2010. Palynological records of Holocene monsoon change from the Gulf of Tonkin (Beibuwan), northwestern of South China Sea. Quaternary Research 74, 8–14.

Li, Z., Saito, Y.,Mao, L., Tamura, T., Li, Z., Song, B., Zhang, Y., Lu, A., Sieng, S., Li, J., 2012. Mid-Holocenemangrove succession and its response to sea-level change in the upper Mekong River Delta, Cambodia. Quaternary Research 78, 386–399.

Li, Z., Pospelova, V., Liu, L., Zhou, R., Song, B., 2017. High-resolution palynological record of Holocene climatic and oceanographic changes in the northern South China Sea. Palaeogeography, Palaeoclimatology, Palaeoecology 483, 94–124.

Li, Z., Pospelova, V., Lin, H.-L., Liu, L., Song, B., 2018. Seasonal dinoflagellate cyst production and terrestrial palynomorth deposition in the monsoon influenced South China Sea: A sediment trap study from the Southwest Taiwan waters. Review of Palaeobotany and Palynology 257, 117-139.

Liang, W.-D., Yang, Y., Tang, T.Y., Yung, T., Chuang, W.-S., 2008. Kuroshio in the Luzon Strait. Journal of Geophysical Research 113, 1–19.

Liew, P., Lee, C., Kuo, C., 2006. Holocene thermal optimal and climate variability of EAM inferred from forest reconstruction of a subalpine pollen sequence, Taiwan. Earth and Planetary Science Letters 250, 596–605.

Lill, C.C., 1979. Upwelling over the Shelf Break. Journal Physical Oceanography 9, 1044–1047.

Limoges, A., Kielt, J. F., Radi, T., Ruiz-Fernandez, A. C., de Vernal, A., 2010. Dinoflagellate cyst distribution in surface sediments along the south-western Mexican coast (14.76°N to 24.75°N). Marine Micropaleontology 76, 104–123.

Limoges, A., de Vernal, A., Nieuwenhove, N.V., 2014. Long-term hydrological changes in the northeastern Gulf of Mexico (ODP-625B) during the Holocene and late Pleistocene inferred from organic-walled dinoflagellate cysts. Palaeogeography, Palaeoclimatology, Palaeoecology 414, 178–191.

Lin, H.L., 2014. The seasonal succession of modern planktonic foraminifera: Sediment traps observations from southwest Taiwan waters. Continental Shelf Research 84, 13-22.

Lin, H.L., Sheu, D.D.D., Yang, Y., Chou, W.C., Huang, G.W., 2011. Stable isotopes in modern planktonic foraminifera: sediment trap and plankton tow results from the South China Sea. Marine Micropaleontology 79, 15-23.

Lin, P., 1990. Vegetation in Fujian. Science-Technics of Fujiang Press, Fuzhou.

Lirdwitayaprasit, T. 1998a. Distribution of dinoflagellate cysts in the surface sediment of South China Sea: Area 2. Off Sabah, Sarawak and Brunei Darussalam. Second Technical Seminar on Marine Fishery Resources Survey in the South China Sea, Area II: West coast of Sabah, Sarawak and Brunei Darussalam. Kuala Lumpur, pp. 310–22.

Lirdwitayaprasit, T. 1998b. Distribution of dinoflagellate cysts in the surface sediment of the South China Sea, Area I: Gulf of Thailand and East Coast of Malasia Peninsula. First Technical Seminar on Marine Fishery Resources Survey in the South China Sea, Area I: Gulf of Thailand and East Coast of Peninsula Malaysia. Kuala Lumpur, pp. 311–26.

Liu, J., Chen, M., Chen, Z., Yan, W., 2010. Clay mineral distribution in surface sediments of the South China Sea and its significance for sediment sources and transport. Journal of Oceanology and Limnology 28, 407–415.

Liu, J., Li, T., Xiang, R., Chen, M., Yan, W., Chen, Z., Liu, F., 2013. Influence of the Kuroshio Current intrusion on Holocene environmental transformation in the South China Sea. The Holocene 23, 850–859.

Liu, J., Yan, W., Chen, Z., Chen, H., Lu, J., 2014. Comment on “Holocene evolution in weathering and erosion patterns in the Pearl River delta” by Hu et al. Geochemistry, Geophysics, Geosystems 15, 2727–2731.

Liu, J., Chen, J., Zhang, X., Li, Y., Rao, Z., Chen, F. 2015. Holocene East Asian summer monsoon records in northern China and their inconsistency with Chinese stalagmite $\delta^{18}O$ records. Earth-Science Reviews 148, 194–208.

Liu, J, Xiang, R., Kao, S.-J., Fu, S., Zhou, L., 2016. Sedimentary responses to sea-level rise and Kuroshio Current intrusion since the Last Glacial Maximum: Grain size and clay mineral evidence from the northern South China Sea slope. Palaeogeography, Palaeoclimatology, Palaeoecology 450, 111–121.

Liu, J.P., Liu, C.S., Xu, K.H., Milliman, J.D., Chiu, J.K., Kao, S.J., Lin, S.W., 2008. Flux and fate of small mountainous rivers derived sediments into the Taiwan Strait. Marine Geology 256, 65–76.

Liu, J.P., Milliman, J.D., Gao, S., Cheng, P., 2004a. Holocene development of the Yellow River's subaqueous delta, Norther Yellow Sea. Marine Geology 209, 45-67.

Liu, Q., Jiang, X., Xie, S.-P., Liu, W., 2004b. A gap in the Indo-Pacific warm pool over the South China Sea in boreal winter: Seasonal development and interannual variability. Journal of Geophysical Research 109, C07012.

Liu, Y., Chen, J., 1995. Sea level change and the records of paleo-shoreline since the late Pleistocene. Studia Marina Sinica 11, 2–6 (in Chinese).

Liu, Z., Tuo, S., Colin, C., Liu, J.T., Huang, C.-Y., Selvaraj, K., Chen, C.-T.A., Zhao, Y., Siringan, F.P., Boulay, S., Chen, Z. 2008. Detrital fine-grained sediment contribution from Taiwan to the northern South China Sea and its relation to regional ocean circulation. Marine Geology 255, 149–155.

Londeix, L., Herreyre, Y., Turon, J.L., Fletcher, W., 2009. Last Glacial to Holocene hydrology of the Marmara Sea inferred from a dinoflagellate cyst record. Review of Palaeobotany and Palynology 158, 52–71.

Long, H., Lai, Z., Wang, N., Li, Y., 2010. Holocene climate variations from Zhuyeze terminal lake records in EAM margin in arid northern China. Quaternary Research 74, 46–56.

Ludmann, T., Wong, H.K., Wang, P., 2001. Plio-Quaternary sedimentation processes and neotectonics of the northern continental margin of the South China Sea. Marine Geology 172, 331–358.

Luo, C., Chen, M., Xiang, R., Liu, J., Zhang, L., Lu, J., Yang, M., 2013. Characteristics of modern pollen distribution in surface sediment samples for the northern South China Sea from three transects. Quaternary International 286, 148–158.

Luo, C., Chen, M., Xiang, R., Liu, J., Zhang, L., Lu, J., Yang, M., 2014. Modern pollen distribution in marine sediments from the northern part of the South China Sea. Marine Micropaleontology 108, 41-56.

Luo, C., Jiang, C., Yang, M., Chen, M., Xiang, R., Zhang, L., Liu, J., Pan, A., 2016a. Transportation models of pollen in surface waters in the South China Sea and their environmental significance. Review of Palaeobotany and Palynology 225, 95-105.

Luo, C., Lin, G., Chen, M., Xiang, R., Zhang, L., Liu, J., Pan, A., Yang, S., Yang, M., 2016b. Characteristics of pollen in surface sediments from the southern South China Sea and its paleoclimatic significance. Palaeogeography, Palaeoclimatology, Palaeoecology 461, 12-28.

Mao, L., David, J.B., Fujiki, T., Li, Z., Dai, L., Weng, C., 2012. Key to mangrove pollen and spores of southern China: An aid to palynological interpretation of Quaternary deposits in the South China Sea. Review of Palaeobotany and Palynology 176–177: 41–67.

Mao, S., Hariand, R., 1993. Quaternary organic-walled dinoflagellate cysts from the South China Sea and their paleoclimatic significance. Palynology 17, 47–65.

Mao, S., Li, J., Qin, X., Wu, G., Harland, R., 2007. Dinoflagellate cysts and environmental evolution of the Oligocene to lower Miocene at site 1148, ODP Leg 184, South China Sea. Palynology 31, 37–52.

Marret, F., 1993. Les effets de l'acétolyse sur les assemblages des kystes de dinoflagellés. Palynosciences 2, 267–272.

Marret, F., de Vernal, A., 1997. Dinoflagellate cyst distribution in surface sediments of the southern Indian Ocean. Marine Micropaleontology 29, 367–392.

Marret, F., Zonneveld, K.A.F., 2003. Atlas of organic-walled dinoflagellate cyst distribution. Review of Palaeobotany and Palynology 125, 1–200.

Marret, F., Kim, S.Y., Scourse, J., 2013. A 30,000 yr record of land-ocean interaction in theeastern Gulf of Guinea. Quaternary Research 80, 1–8.

Matano, R.P., Palma, E.D., 2008. On the upwelling of downwelling currents. Journal of Physical Oceanography 38, 2482–2500.

Matsuoka, K., 1988. Cyst-theca relationships in the diplopsalid group (Peridiniales, Dinophyceae). Review Palaeobotany and Palynology 56, 95–122.

Matsuoka, K., 2001. Further evidence for amarine dinoflagellate cyst as an indicator of eutrophication in Yokohama Port, Tokyo Bay, Japan. Comments on a discussion by B. Dale. Science of the Total Environment 264, 221–233.

Matsuoka, K., Bujak, J.P., 1988. Cenozoic dinoflagellate cysts from the Navarin Basin, Norton Sound and St. George Basin, Bering Sea, Bull. Faculty of Liberal Arts. Nagasaki University (Natural Science) 29 (1), 1–147.

Matsuoka, K., Kawami, H., Nagai, S., Iwataki, M., Takayama, H., 2009. Re-examination of cyst–motile relationships of *Polykrikos kofoidii* Chatton and *Polykrikos schwartzii* Bütschli (Gymnodiniales, Dinophyceae). Review of Palaeobotany and Palynology 154, 79–90.

McMinn, A., 1991. Recent Dinoflagellate Cysts from Estuaries on the Central Coast of New South Wales, Australia. Micropaleontology 37, 269–287.

Mertens, K.N., Riberio, S., Bouimetarhan, I., Caner, H., Nebout, N.C., Dale, B., de Vernal, A., Ellegaard, M., Filipova, M., Godhe, A., Goubert, E., Gorsfjeld, K., Holzwarth, U., Kotthoff, U., Leroy, S.A.G., Londeix, L., Marret, F., Matsuoka, K., Mudie, P.J., Naudts, L., Pena-Marjarrez, J.L., Persson, A., Popescu, S.-M., Pespelova, V., Sangiorgi, F., Van der Meer, M.T.J., Vindk, A., Zonneveld, K.A.F., Vercauteren, D., Vlassenbroeck, J., Louwye, S., 2009. Process length variation in cysts of a dinoflagellate, Lingulodinium machaerophorum, in surface sediments: Investigating its potential as salinity proxy. Marine Micropaleontology 70, 54–69.

Mertens, K.N., Verhoeven, K., Verleye, T., Louwye, S., Amorim, A., Ribeiro, S., Deaf, A.S., Harding, I.C., Schepper, S.D., González, C., Kodrans-Nsiah, M., Vernal, A.D., Henry, M., Radi, T., Dybkjaer, K., Poulsen, N.E., Feist-Burkhardt, S., Chitolie, J., Heilmann-Clausen, C., Londeix, L., Turon, J.L., Marret, F., Matthiessen, J., McCarthy, F.M.G., Prasad, V., Pospelova, V., Hughes, J.E.K., Riding, J.B., Rochonp, A., Sangiorgi, F.,Welters, N., Sinclair, N., Thun, C., Soliman, A., Nieuwenhove, N.V., Vink, A., Young, M., 2009. Determining the absolute abundance of dinoflagellate cysts in recentmarine sediments: the Lycopodium marker-grain method put to the test. Review of Palaeobotany and Palynology 157, 238–252.

Mertens, K.N., Price, A.M., Pospelova, V., 2012. Determining the absolute abundance of dinoflagellate cysts in recent marine sediments II: Further tests of the Lycopodium marker-grain method. Review of Palaeobotany and Palynology 184, 74–81.

Mertens, K.N., Takano, Y., Head, M.J., Matsuoka, K., 2014. Living fossils in the Indo-Pacific warm pool: A refuge for thermophilic dinoflagellates during glaciations. Geology 42, 531–534.

Mertens, K.N., Carbonell-Moore, M.C., Vospelova, V., Head, M.J., Highfield, A., Schroeder, D., Gu, G., Andree, K.B., Fernandez, M., Yamaguchi, A., Takano, Y., Matsuoka, K., Nézan, E., Bilien, G., Okolodkov, Y., Koike, K., Hoppenrath, M., Pfaff, M., Pitcher, G., Al-Muftah, A., Rochon, A., Lim, P.T., Leaw, C.P., Lim, Z.F., Ellegaard, M., 2018. *Pentaplacodinium saltonense* gen. et sp. nov. (Dinophyceae) and its relationship to the cyst-defined genus *Operculodinium* and yessotoxin-producing *Protoceratium reticulatum*. Harmful Algae 71 57–77.

Mohamed, O., Piller, W.E., Egger, H., 2013. Dinoflagellate cysts and palynofacies across the Cretaceous/Palaeogene boundary at the Neritic Waidach Section (Eastern Alps, Austria). Review of Palaeobotany and Palynology 190, 85–103.

Montade, V., Nebout, N.C., Kissel, C., Mulsow, S., 2011. Pollen distribution in marine surface sediments from Chilean Patagonia. Marine Geology 282 (3–4), 161–168.

Montresor, M., Zingone, A., Sarno, D., 1998. Dinoflagellate cyst production at a coastal Mediterranean site. Journal of Plankton Research 20 (12), 2291–2312.

Moss, P.T., Kershaw, A.P., Grindrod, J., 2005. Pollen transport and deposition in riverine and marine environments within the humid tropics of northeastern Australia. Review of Palaeobotany and Palynology 134, 55–69.

Mudie, P.J., Harland, R., 1996. Chapter 21. Aquatic Quaternary. In: Jansonius, J., McGregor, D.C. (Eds.), Palynology: Principles and Applications. AASP Foundation, pp. 843–877.

Mudie, P.J., Rochon, A., 2001. Distribution of dinoflagellate cysts in the Canadian Arctic marine region. Jounal of Quaternary Science 16 (7), 603–620.

Mudie, P.J., Rochon, A., Aksu, A.E., Gillespie, H., 2002. Dinoflagellate cysts, freshwater algae and fungal spores as salinity indicators in Late Quaternary cores from Marmara and Black seas. Marine Geology 190, 203–231.

Nahm, W.-H., Kim, J.K., Kim, J.-Y., Yi, S., Lim, J., Kim, J.C., 2013. The Holocene climatic optimum in Korea: Evidence from wetland records. Palaeogeography, Palaeoclimatology, Palaeoecology 376, 163–171.

Naik, H., Chen, C.T.A., 2008. Biogeochemical cycling in the Taiwan Strait. Estuarine, Coastal and Shelf Science 78, 603–661.

Nakamura, A., Yokoyama, Y., Maemoku, H., Yagi, H., Okamura, M., Matsuoka, H., Miyake, N., Osada, T., Adhikari, D.P., Dangol, V., Ikehara, M., Miyairi, Y., Matsuzaki, H., 2016. Weak Monsoon event at 4.2 ka recorded in sediment from Lake Rara, the Himalayas. Quaternary International 397, 349–359.

Nan, F., Xue, H., Chai, F., Shi, L., Shi, M., Guo, P., 2011. Identification of different types of Kuroshio intrusion into the South China Sea. Ocean Dynamics 61, 1291–1304.

Narale, D.D., Anil, A.C., 2017. Spatial distribution of dinoflagellates from the tropical coastal waters of the South Andaman, India: Implications for coastal pollution monitoring. Marine Pollution Bulletin 115, 498–506.

Narale, D.D., Patil, J.S., Anil, A.C., 2013. Dinoflagellate cyst distribution in recent sediments along the south-east coast of India. Oceanologica 55, 979–1003.

Narale, D.D., Naidu, P.D., Anil, A.C., Godad, S.P., 2015. Evolution of productivity and monsoonal dynamics in the eastern Arabian Sea during the past 68ka using

dinoflagellate cyst records. Palaeogeography, Palaeoclimatology, Palaeoecology 435, 193–202.

Ndah, A.B., Becek, K., Dagar, L., 2016. A Review of Coastal Upwelling Research in the South China Sea: Challenges, Limitations and Prospects. International Journal of Earth and Atmospheric Science 3(4), 63–72.

Ndah, A.B., Dagar, L., Becek, K., 2017. Multi-temporal patterns of upwelling–downwelling dynamics in the South China Sea based on a 47-yeartime-series of the NOAA-ERD upwelling index. Regional Studies in Marine Science16, 225–239.

Ning, X., Chai, F., Xue, H., Chai, Y., Liu, C., Shi, J., 2004. Physical-biological oceanographic coupling influencing phytoplankton and primary production in the South China Sea. Journal of Geophysical Research 109, C10005.

Ogston, A.S., Allison, M.A., Mullarney, J.C., Nittrouer, C.A., 2017. Sediment- and hydro-dynamics of the Mekong Delta: From tidal river to continental shelf. Continental Shelf Research 147, 1–6.

Olde, K., Jarvis, Ian., David Uličný, D., Pearce, M.A., Trabucho-Alexandre, J., Čech, S., Gröcke, D.R., Laurin, J., Švábenická, L., Tocher, B.A., 2015. Geochemical and palynological sea-level proxies in hemipelagic sediments: A critical assessment from the Upper Cretaceous of the Czech Republic. Palaeogeography, Palaeoclimatology, Palaeoecology 435, 222 –243.

Oppo, D.W., Sun, Y., 2005. Amplitude and timing of sea-surface temperature change in the northern South China Sea: dynamic link to the east Asianmonsoon. Geology 33, 785–788.

Pan, X., Wong, G.T.F., Shiah, F., K., Ho, T.-Y., 2012. Enhancement of biological productivity by internal waves: observations in the summertime in the northern South China Sea. Journal of Oceanography 68, 427–437.

Pan, X.,Wong, G.T.F., Ho, T.-Y., Tai, J.-H., Liu, H., Liu, J., Shiah, S.-F., 2018. Remote sensing of surface [nitrite+nitrate] in river-influenced shelf-seas: The northern South China Sea Shelf-sea. Remote Sensing of Environment 210, 1–11.

Park, J.H., Farmer, D., 2013. Effects of Kuroshio intrusions on nonlinear internal waves in the South China Sea during winter. Journal of Geophysical Research: Oceans 118, 7081–7094.

Pelejero, C., Kienast, M., Wang, L., Grimalt, G.O., 1999. The flooding of Sundaland during the last deglaciation: imprints in hemipelagic sediments from the southern South China Sea. Earth and Planetary Science Letters 171, 661–671.

Penaud, A., Eynaud, F., Voelker, A., Kageyama, M., Marret, F., Turon, J.L., Blamart, D., Mulder, T., Rossignol, L., 2010. Assessment of sea surface temperature changes in the Gulf of Cadiz during the last 30ka: implications for glacial changes in the regional hydrography. Biogeosciences 8, 2295–2316.

Peros, M.C., Gajewski, K., 2008. Testing the reliability of pollen-based diversity estimates. Journal of Paleolimnology 40, 357–368.

Poliakova, A., Zonneveld, K.A.F., Herbeck, L., Jennerjahn, T.C., Permana, H., Behling, B. 2016. High resolution multi-proxy reconstruction of environmental changes in coastal waters of the Java Sea, Indonesia, during the late Holocene. Palynology 297–310.

Poliakova, A., Zonneveld, K.A.F., Kwiatkowski, C., Suryoko, M.A., Behling, H., 2017. Marine environment, vegetation and land use changes during the late Holocene in South Kalimantan and East Java reconstructed based on pollen and organic-walled dinoflagellate cysts analysis. Review of Palaeobotany and Palynology 238, 105–121.

Pospelova, V., Head, M.J., 2002. *Islandinium brevispinosum* sp. nov. (Dinoflagellata), a new organic-walled dinoflagellate cyst from modern estuarine sediments of New England (USA). Journal of Phycology 38, 593–601.

Pospelova, V., Kim, S.J., 2010. Dinoflagellate cysts in recent sediments from the aquaculture sites of southern South Korea. Marine Micropaleontology 76, 37–51.

Pospelova, V., Chmura, G.L. Boothman, W.S., and Latimer, J.S., 2002. Dinoflagellate cyst records and human disturbance in two neighboring estuaries, New Bedford Harbor and Apponagansett Bay, Massachusetts (USA). The Science of the Total Environment 298, 81-102.

Pospelova, V., Chmura, G.L., Walker, H.A., 2004. Environmental factors influencing the spatial distribution of dinoflagellate cyst assemblages in shallow lagoons of southern New England (USA). Review of Palaeobotany and Palynology 128, 7–34.

Pospelova, V., Chmura, G. L., Boothman, W. S., Latimer, J.S., 2005. Spatial distribution of modern dinoflagellate cysts in polluted estuarine sediments from Buzzards Bay (Massachusetts, USA) embayments. Marine Ecology Progress Series 292, 23–40.

Pospelova, V., Pedersen, T.F., de Vernal, A., 2006. Dinoflagellate cysts as indicators of climatic and oceanographic changes during the past 40 kyr in the Santa Barbara Basin, southern California. Paleoceanography 21, 1–16.

Pospelova, V., de Vernal, A., Pedersen, T.F., 2008. Distribution of dinoflagellate cysts in surface sediments from the northeastern Pacific Ocean (43–25° N) in relation to sea-surface temperature, salinity, productivity and coastal upwelling. Marine Micropaleontology 68, 21–48.

Pospelova, V., Esenkulova, S., Johannessen, S.C., O'Brien, M.C., Macdonald, R.W., 2010. Organic-walled dinoflagellate cyst production, composition and flux from 1996 to 1998 in the central Strait of Georgia (BC, Canada): A sediment trap study. Marine Micropaleontology 75, 17–37.

Pospelova, V., Price, A., Pedersen, T.F., 2015. Palynological evidence for late Quaternary climate and marine primary productivity changes along the California margin. Paleoceanography 30, 877–894.

Pospelova, V., Zonneveld, K.A.F., Heikkilä, M., Bringué, M., Price, A., Esenkulova, S., Matsuoka, K., 2018. Seasonal, annual, and inter-annual Spiniferites cyst production: a review of sediment trap studies. Palynology https://doi.org/10.1080/01916122. 2018.1465 738.

Price, A.M., Pospelova, V., 2011. High-resolution sediment trap study of organic-walled dinoflagellate cyst production and biogenic silica flux in Saanich Inlet (BC, Canada). Marine Micropaleontology 80, 18-43.

Price, A.M., Mertens, K.N., Pospelova, V., Pedersen, T.F., Ganeshram, R.S., 2013. Late Quaternary climatic and oceanographic changes in the Northeast Pacific as recorded by dinoflagellate cysts from Guaymas Basin, Gulf of California (Mexico). Paleoceanography 28, 1–13.

Price, A.M., Gurdebeke, P.R., Mertens, K.N., Pospelova, V., 2016. Determining the absolute abundance of dinoflagellate cysts in recent marine sediments III: Identifying the source of Lycopodium loss during palynological processing and further testing of the Lycopodium marker-grain method. Review of Palaeobotany and Palynology 226, 78–90.

Qi, Y., Ying, H., Lei, Z., Kulis, D.M., Anderson, D.M., 1996. Dinoflagellate cysts from recent marine sediments of the South and East China Seas. Asian Marine Biology 13, 87–103.

Qiu, Y., Li, L., Chen, C.T.A., Guo, X.G., Jing, C.S., 2011. Currents in the Taiwan Strait as observed by surface drifters. Journal of Oceanography 67, 395–404.

Qu, T. 2000. Upper-layer circulation in the South China Sea. Journal of Physical oceanography 30, 1450–1460.

Qu, T., 2002. Evidence for water exchange between the South China Sea and the Pacific Ocean through the Luzon Strait. Acta Oceanologcal Sinica 21, 75–185.

Radi, T., de Vernal, A., 2004. Dinocyst distribution in surface sediments from the northeastern Pacific margin (40–60°N) in relation to hydrographic conditions, productivity and upwelling. Review of Palaeobotany and Palynology 128, 169–193.

Radi, T., Pospelova, V., de Vernal, A., Barrie, J.V., 2007. Dinoflagellate cysts as indicators of water quality and productivity in British Columbia estuarine environments. Marine Micropaleontology 62, 269–297.

Reimer, P.J., Baillie,M.G.L., Bard, E., Bayliss, A., Beck, J.W., Blackwell, P.G., Bronk Ramsey, C., Buck, C.E., Burr, G.S., Edwards, R.L., Friedrich, M., Grootes, P.M., Guilderson, T.P., Hajdas, I., Heaton, T.J., Hogg, A.G., Hughen, K.A., Kaiser, K.F., Kromer, B., McCormac, F.G., Manning, S.W., Reimer, R.W., Richards, D.A., Southon, J.R., Talamo, S., Turney, C.S.M., van der Plicht, J., Weyhenmeyer, C.E., 2009. Intcal09 and marine09 radiocarbon age calibration curves, 0–50,000 years cal BP. Radiocarbon 51, 1111–1150.

Ribeiro, S., Moros, M., Ellegaard, M., Kuijpers, A., 2012. Climate variability in West Greenland during the past 1500 years: evidence from a high-resolution marine palynological record from Disko Bay. Boreas 41, 68–83.

Ribeiro, S., Amorim, A., Abrantes, F., Ellegaard, M., 2016. Environmental change in the Western Iberia Upwelling Ecosystem since the preindustrial period revealed by dinoflagellate cyst records. The Holocene 26, 874–889.

Richerol, T., Rochon, A., Blasco, S., Scott, D.B., Bennett, R.J., 2008. Distribution of dinoflagellate cysts in surface sediments of the Mackenzie Shelf and Amundsen Gulf, Beaufort Sea (Canada). Journal of Marine Systems 74, 825–839.

Rochon, A., de Vernal, A, Sejrup, H.P., Haflidason, H., 1998. Palynological Evidence of Climatic and Oceanographic Changes in the North Sea during the Last Deglaciation. Quaternary Research 49 (2), 197–207.

Rochon, A., de Vernal, A., Turon, J.-L., Matthiessen, J., Head, M.J., 1999. Distribution of recent dinoflagellate cysts in surface sediments from the North Atlantic Ocean and adjacent areas in relation to sea-surface parameters. American Association of Stratigraphic Palynologists, Contributions Series 35, pp. 146-152.

Ruddiman, W.F. 2008. Earth's Climate Past and Future, Second Edition. Freeman and Company, New York, pp. 138–142.

Schettler, G., Rein, B., Negendank, J.F.W., 1999. Geochemical evidence for Holocene palaeodischarge variations in lacustrine records from the Westeifel Volcanic Field, Germany: Schalkenmehrener Maar and Meerfelder Maar. The Holocene 9, 381-400.

Schwendemann, A.,Wang, G.,Mertz, M., Mcwilliams, R.T., Thatcher, S., Osborn, J.M., 2007. Aerodynamics of saccate pollen and its implications for wind pollination. American Journal of Botany 94 (8), 1371–1381.

Shao, L., Li, X.,Wei, G., Liu, Y., Fang, D., 2001. Provenance of a prominent sediment drift on the northern slope of the South China Sea. Science of China D 44, 919–925.

Shao, L., Li, X.J., Geng, J.H., Pang, X., Lei, Y.C., Qiao, P.J., Wang, L.L., Wang, H.B., 2007. Deep water bottom current deposition in the northern South China Sea. Science of China (Series D) 50, 1060–1066.

Shaw, P.-T., 1991. The seasonal variation of the intrusion of the Philippine sea water into the South China Sea. Journal of Geography Research 96, 821–827.

Shaw, P.-T., 1996. Winter upwelling off Luzon in the northeastern South China. Journal of Geophysical Research 101, 16435–16448.

Sheue, C.-R., Yang, Y.-P., Kuo-Huang, L.L., 2000. Structural variation of the needles of Pinus taiwanensis Hay. along an elevational gradient. Taiwan. Journal of Forest Science 15, 337–349.

Sheue, C.R., Yang, Y.P., Kuo-Huang, L.L., 2003. Altitudinal variation of resin ducts in Pinus taiwanensis Hayata (Pinaceae) needles. Botanical Bulletin- Academia Sinica Taipei 44, 305–313.

Shi, G., Jacques, F.M.B., Li, H., 2014. Winged fruits of Shorea (Dipterocarpaceae) from the Miocene of Southeast China: Evidence for the northward extension of dipterocarps during the Mid-Miocene Climatic Optimum. Review of Palaeobotany and Palynology 200, 97–107.

Shin, H.H., Yoon, Y.H., Kim, Y.O., Matsuoka, K., 2011. Dinoflagellate Cysts in Surface Sediments from Southern Coast of Korea. Estuaries and Coasts 34, 712–725.

Shin, H.H., Park, J.S., Kim, Y.-O., Baek, S.H., Yang, D., Yoon, H., 2012. Dinoflagellate cyst production and flux in Gamak Bay, Korea: A sediment trap study. Marine Micropaleontology 94–95, 72–79.

Shumilovskikh, L.S., Seeliger, M., Feuser, S., Novenko, E., Schlütz, F., Pint, A., Pirson, F., Brückner, H., 2016. The harbour of Elaia: A palynological archive for human environmental interactions during the last 7500 years. Quaternary Science Reviews 149, 167–187.

Song, B., Li, Z., Lu, H., Mao, Li, Saito, Y., Yi, S., Lim, J., Li, Z., Lu, A., Sha, L., Zhou, R., Zuo, X., Pospelova, V., 2017. Pollen record of the centennial climate changes during 9–7 cal ka BP in the Changjiang (Yangtze) River Delta plain. China. Quaternary Research 87, 275–287.

Steinke, S., Chiu, H.Y., Yu, P.S., Shen, C.C., Erlenkeuser, H., Löwemark, L. Chen, M.T., 2006. On the influence of sea level and monsoon climate on the southern South China Sea freshwater budget over the last 22,000 years. Quaternary Science Reviews 25, 1475–1488.

Steinke, S., Glatz, C., Mohtadi, M., Groeneveld, J., Li, Q., Jian, Z., 2011. Past dynamics of the East Asian monsoon: No inverse behaviour between the summer and winter monsoon during the Holocene. Global and Planetary Change 78, 170–177.

Stockmarr, J., 1971. Tablets with spores used in absolute pollen analysis. Pollen Spores 13, 616–621.

Su, J., Pohlmann, T., 2009. Wind and topography influence on an upwelling system at the eastern Hainan coast. Journal of Geophysical Research 114, C06017.

Su, J., Wang, J., Pohlmann, T., Xu, D.F., 2011. The influence of meteorological variation on the upwelling system off eastern Hainan during summer 2007–2008. Ocean Dynamics 61(6), 717–730.

Sun, X., Li, X., 1999. A pollen record of the last 37 ka in deep sea core 17940 from the northern slope of the South China Sea. Marine Geology 156, 227–244.

Sun, X., Li, X., Beug, H.J., 1999. Pollen distribution in hemipelagic surface sediments of the South China Sea and its relation to modern vegetation distribution. Marine Geology 156, 211–226.

Sun, X., Luo, Y., Huang, F., Tian, J., Wang, P., 2003. Deep-sea pollen from the South China Sea: Pleistocene indicators of East Asian monsoon. Marine Geology 201, 97–118.

Sun, Y., Kutzbach, J., An, Z., Clemens, S., Liu, Z., Liu, W., Liu, X., Shi, Z., Zheng, W., Liang, L., Yan, Y., Li, Y. 2015. Astronomical and glacial forcing of East Asian summer monsoon variability. Quaternary Science Reviews 115, 132–142.

Tanabe, S., Satio, Y.,Vu, Q.l., Hanebuth, T.J.J., Ngo, Q.L., 2006. Holocene evolution of the Song Hong (Red River) delta system, northern Vietnam. Sedimentary Geology 197, 29–61.

Tang, D.L., Kawamura, H., Dien, T.V., Lee, M.A., 2004. Offshore phytoplankton biomass increase and its oceanographic causes in the South China Sea. Marine Ecology Progress Series 268, 31–41.

ter Braak, C.J.F., Šmilauer, P., 2002. CANOCO reference nanual and Canodraw for Windows user's guide. Software for Canonical Community Ordination (Version 4.5). Microcomputer Power, Ithaca, New York, p. 500.

Thompson P.R., Shackleton, N.J., 1980. North Pacific palaeoceanography: late Quaternary coiling variations of planktonic foraminifer *Neogloboquadrina pachyderma.* Nature 287, 829–833.

Tong, J.A., You, Y., Müller, R.D., Seton, M., 2009. Climate model sensitivity to atmospheric CO_2 concentrations for the middle Miocene. Global and Planetary Change 67, 129–140.

Traverse, A., 2007. Paleopalynology. 2th Ed. Springer Press, Dordrecht, pp. 1–2.

Uddandam, P.R., Prasad, V., Rai, J., 2017. Dinoflagellate cyst distribution in sediments of western Bay of Bengal: Role of sea surface conditions. Palaeogeography, Palaeoclimatology, Palaeoecology 483, 31–48.

Urrego, L.E., Bernal, G., Polanía, J., 2009. Comparison of pollen distribution patterns in surface sediments of a Colombian Caribbean mangrove with geomorphology and vegetation. Review of Palaeobotany and Palynology 156, 358–375.

van der Knaap,W.O., 2009. Estimating pollen diversity from pollen accumulation rates: a method to assess taxonomic richness in the landscape. The Holocene 19, 159–163.

van Waveren, I.M., 1989. Palynofacies analysis of surface sediments from the northeastern Banda Sea (Indonesia). Netherlands Journal of Sea Research 24 (4), 501–509.

Verleye, T.J., Pospelova, V., Mertens, K.N., Louwye, S., 2011. The geographical distribution and (palaeo) ecology of Selenopemphix undulata sp. nov., a new late Quaternary dinoflagellate cyst from the Pacific Ocean. Marine Micropaleontology 78, 65–83.

Versteegh, G.J.M., Blokker, G., 2004. Resistant macromolecules of extant and fossil microalgae. Phycological Research 52, 325–339.

Wall, D., Dale, B., Lohmann, G.P., Smith, W.K., 1977. Environmental and climatic distribution of dinoflagellate cysts in modern marine sediments from regions in North and South-Atlantic Oceans and adjacent Seas. Marine Micropaleontology 2, 121-200.

Wang, B., Wu, Z., Li, J., Liu, J., Chang, C.P., Ding, Y., Wu, G. 2008. How to measure the strength of the East Asian summer monsoon. Journal of Climate 21, 4449–4463.

Wang, H., Wang, Y., Qiu, Y., Peng, X., Liu, Y., 2008. Geomorphology and its control of deep water slope of the margin of the South China Sea. Acta Oceanologica Sinca 30, 70–79.

Wang, J., Chern, C.-S., 1988. On the Kuroshio branch in the Taiwan Strait during wintertime. Progressive Oceanography 21, 469–491.

Wang, L., Sarnthein, et al., 1999. East Asian monsoon climate during the Late Pleistocene: high resolution sediment records from the South China Sea. Marine Geology 156, 245–284.

Wang, L., Sarnthein, M., Erlenkeuser, H., Grootes, P.M., Grimalt, J.O., Pelejero, C., Linck, G., 1999. Holocene variations in Asian monsoon moisture: a bidecadal sediment record from the South China Sea. Geophysical Research Letters 26, 2889–2892.

Wang, L., Li, J., Lu, H., Gu, Z., Rioual, P., Hao, Q., Mackay, A.W., Jiang, W., Cai, B., Xu, B., Han, J., Chu, G., 2012. The East Asian winter monsoon over the last 15,000 years: its links to high-latitudes and tropical climate systems and complex correlation to the summer monsoon. Quaternary Science Reviews 32, 131–142.

Wang, P., Li, Qu., 2009. The South China Sea: paleoceanography and sedimentology. Springer Press, pp. 1–6.

Wang, P., Clemens, S., Beaufort, L., Braconnot, P., Ganssen, G., Jian, Z., Kershaw, P., Sarnthein, M., 2005. Evolution and variability of the Asian monsoon system: state of the art and outstanding issues. Quaternary Science Review 24, 595–629.

Wang, P., Wang, B., Cheng, H., Fasullo, J., Guo, Z. T., Kiefer, T., Liu, Z.Y., 2014. The global monsoon across timescales: coherent variability of regional monsoons. Climate of the Past 10, 2007–2052.

Wang, R.-M., You, C.-F., Chu, H.-Y., Hung, J.-J., 2009. Seasonal variability of dissolved major and trace elements in the Gaoping (Kaoping) River Estuary, Southwestern Taiwan. Journal of Marine System 76, 444–456.

Wang, Y., Cheng, H., Edwards, R.L., He, Y., Kong, X., An, Z., Wu, J., Kelly, M.J., Dykoski, A., Li, X., 2005. The Holocene Asian monsoon: links to solar changes and North Atlantic climate. Science 308, 854–857.

Wang, Z., Matsuoka, K., Qi, Y., Chen, J., 2004a. Dinoflagellate cyst in recent sediments from Chinese coastal waters. Marine Ecology 25, 289–311.

Wang, Z., Matsuoka, K., Qi, Y., Chen, J., Lu, S., 2004b. Dinoflagellate cyst records in recent sediments from Daya Bay, South China Sea. Phycological Research 52, 396–407.

Wang, Z., Mu, D., Li, Y., Cao, Y., Zhang, Y., 2011. Recent eutrophication and human disturbance in Daya Bay, the South China Sea: Dinoflagellate cyst and geochemical evidence. Estuarine, Coastal and Shelf Science 92, 403–414.

Wejnert, K.E., Pride, C.J., Thunell, R.C., 2010. The oxygen isotope composition of planktonic foraminifera from the Guaymas Basin, Gulf of California: seasonal, annual, and interspecies variability. Marine Micropaleontology 74, 29-37.

Wong, G.T.F., Hung, C.-C., Gong, G.-C., 2004. Dissolved iodines pecies in the East China Sea—a complementary tracer for upwelling Water on the shelf. Continental Shelf Research 24, 1465–1484.

Wong, G.T.F., Tseng, C.-M., Wen, L.-S., Chung, S.-W., 2007. Nutrient dynamics and N-anomaly at the SEATS station. Deep-Sea Research II 54, 1528–1545.

Wong, G.T.F., Ku, T.-L., Liu, H., 2015. The oceanography of the Northern south China Sea Shelf-Sea (NoSoCS) and its adjacent Waters—overview and Highlights. Deep-Sea Research II 117, 3–9.

Woodson, C.B., Eerkes-Medrano, D.I., Flores-Morales, A., Foley, M.M., Henkel, S.K., Hessing-Lewis, M., Jacinto, D., Needles, L., Nishi-zaki, M.T., O'Leary, J., Ostrander, C.E., Pespeni, M., Schwager, K.B., Tyburczy, J.A., Weersing, K.A., Kirincich, A.R., Barth, J.A., McManus, M.A., Washburn, L., 2007. Local diurnal upwelling driven by sea breezes in northern Monterey Bay. Continental Shelf Research 27, 2289–2302.

Wu, C.-R., 2013. Interannual modulation of the Pacific Decadal Oscillation (PDO) on the low-latitude western North Pacific. Progress in Oceanography 110, 49–58.

Wu, C.-R., Hsin, Y.-C., 2012. The forcing mechanism leading to the Kuroshio intrusion into the South China Sea. Journal of Geophysical Research. http://dx.doi.org/10.1029/2012JC007 968.

Wu, G., Sun, S., 2000. Distribution of dinoflagellate cysts in surface sediments from the South China Sea. Tropic Oceanography 19, 8–16 (in Chinese with English abstract).

Wu, Z. (Ed.), 1980. Flora of China. Science Press, Beijing, pp. 823–916 (in Chinese).

Wyrtki, K., 1961. Physical oceanography of the Southeast Asia waters: Scientific results of marine investigations of the South China Sea and the Gulf of Thailand 1959–1961. Scripps Institution of Oceanography NAGA Rep. 2, 195.

Xiao, J., Nakamura, T., Lu, H., Zhang, G., 2002. Holocene climate changes over the desert/loess transition of north-central China. Earth and Planetary Science Letters 197, 11–18.

Xie, S.-P., Xie, Q., Wang, D., Liu, W.T., 2003. Summer upwelling in the South China Sea and its role in regional climate variations. Journal of Geophysical Research 108, 32–61,

Xu, Q., Li, Y., Yang, X., Xiao, Y., Liang, W., Peng, Y., 2005. Source and distribution of pollen in the surface sediment of Daihai Lake, inner Mongolia. Quaternary International 136, 33–45.

Xue, H., Chai, F., Pettigrew, N., Xu, D., Shi, M., Xu, J., 2004. Kuroshio intrusion and the circulation in the South China Sea. Journal of Geophysical Research 109, C02017.

Yamanoi, T., 2003. Mangrove plants and their pollen morphology in Southeast Asia. Monograph of the Mizunami Fossil Museum. 9, pp. 129–213 (in Japanese with Englis abstract).

Yan, J., 1997. Climatological characteristics on the onset of southwest monsoon in the South China Sea. Acta Meteorologica Sinica 55(2), 174–186.

Yan, Y.W., Ling, Z., Chen, C.L., 2015. Winter coastal upwelling off northwest Borneo in the South China Sea. Acta Oceanologcal Sinica 34(1), 3–10.

Yancheva, G., Nowaczyk, N., Mingram, J., Dulski, P., Schettler, G., Negendank, J., Liu, J., Sigman, D., Peterson, L., Haug, H., 2007. Influence of the intertropical convergence zone on the EAM. Nature 445, 74–77.

Yi, S., Saito, Y., Zhao, Q., Wang, P., 2003. Vegetation and climate changes in the Changjiang (Yangtze River) Delta, China, during the past 13,000 years inferred from pollen records. Quaternary Science Reviews 22, 1501–1519.

Yin, K.D., Song, X., Sun, J., Wu, M.C.S., 2004. Potential P limitation leads to excess N in the Pearl River estuarine coastal plume. Continental Shelf Research 16, 1895–1907.

Yu, K., Zhao, J., Wei, G., Cheng, X., Wang, P. 2005. Mid–late Holocene monsoon climate retrieved from seasonal Sr/Ca and $\delta^{18}O$ records of *Porites lutea* corals at Leizhou Peninsula, northern coast of South China Sea. Global and Planetary Change 47, 301–316.

Yu, T.O., Morozova, T.V., 2013. Dinoflagellate cysts in recent marine sediments of the western coast of the Bering Sea. Russian Journal of Marine Biology 39 (1), 15–29.

Yuan, D., 2002. A numerical study of the South China Sea deep circulation and its relation to the Luzon Strait transport. Acta Oceanologica Sinica 21, 187–202.

Yuan, D., Han, W., Hu, D., 2006. Surface Kuroshio path in the Luzon Strait area derived from satellite remote sensing data. Journal of Geophysical Research 111, C11007.

Yuan, D.L., 2002. A numerical study of the South China Sea deep circulation and its relation to the Luzon Strait transport. Acta Oceanological Sinica 21, 187–202.

Yuan, Y.C., Zhao, J.P., Wang, H.Q., Lou, R.Y., Chen, H., Wang, K.S., 2002. Current measurements and spectral analyses in the upper 450 m and deep layers of the northeastern South China Sea. Science of China (Series D) 45, 1008–1027.

Yuan, Y.C., Bu, G.X., Liao, W.H., Lou, R.Y., Su, J.L., Wang, K.S., 2004. Diagnostic calculation of the upper-layer circulation in the South China Sea during the winter of 1998. Acta Oceanologcal Sinica 23(2), 187–199.

Zevenboom, D., Brinkhuis, H., and Visscher, H., 1994. Dinoflagellate cysts palaeoenvironmental analysis of the Oligocene/Miocene transition in northwest and central Italy: Giornale di Geologia 56, 155–169.

Zhang, D., Lu, L., 2007. Anti-correlation of summer/winter monsoons? Nature 450, 77–79.

Zhang, Y., Long, J., 2008. Sporopollen and algae research of core B106 in the northern South China Sea and its paleoenvironmental evolution. Frontiers of Earth Science in China 2, 157–161.

Zhang, Y., Peng, X., Zhao, J., 2011. High resolution palynological record and evolution of vegetation and climate in the low latitude of the South China Sea since 15 ka BP. Journal of Tropical Oceanography 30, 67–73 (in Chinese with English abstract).

Zhang, Y., Zhang, W., Wang, K., 2002. Studies on the relationship between sporo-pollen of surface sediments and vegetation of the continental margin in the northeastern South China Sea. Marine Science Bulletin 21, 26–36 (in Chinese with English abstract).

Zhang,W.,Mu, S.-S., Zhang, Y.-J., Chen, K.-M., 2012. Seasonal and interannual variations of flow discharge from Pearl River into sea. Water Science and Engineering 5 (4), 399–409.

Zhao, H., 1990. The evolution of the Pearl River Estuary. China Ocean Press, Beijing, pp. 1–357 (in Chinese).

Zhao, M., Huang, C.Y., Wang, C.C., Wei, G., 2006. A millennial-scale U37K′ sea-surface temperature record from the South China Sea (8°N) over the last 150 kyr: Monsoon and sea-level influence. Palaeogeography, Palaeoclimatology, Palaeoecology 236, 39–55.

Zhao, X., Dupont, L., Meadows, M.E., Wefer, G., 2016. Pollen distribution in the marine surface sediments of the mudbelt along the west coast of South Africa. Quaternary International 404, 44–56.

Zhao, X., Dupont, L., Schefuß, E., Bouimetarhan, I., Wefer, G., 2017. Palynological evidence for Holocene climatic and oceanographic changes off western South Africa. Quaternary Science Review 165, 88–101.

Zhao, Y., Morzadec-Kerfourn, M.T., 1992a. Kystes de Dinoflagellés, pollens et spores des sédiments quaternaires du Bassin abyssal de Mer de Chine du Sud: leur signification paléoenvironnementale. Review of Micropaleontology 35 (1), 77–88 (in French).

Zhao, Y., Morzadec-Kerfourn, M.T., 1992b. Late Pleistocene - Holocene dinoflagellate cysts of South China Sea. Acta Microbiologica Sinica 9 (3), 291–302 (in Chinese with English abstract).

Zhao,M., Huang, C.Y.,Wang, C.C.,Wei, G., 2006. Amillennial-scale U37K′ sea-surface temperature record from the South China Sea (8°N) over the last 150 kyr: monsoon and sea-level influence. Palaeogeography, Palaeoclimatology, Palaeoecology 236, 39–55.

Zheng, Z., Yang, S., Deng, Y., Huang, K., Wei, J., Berne, S., Suc, J.P., 2011. Pollen record of the past 60 ka BP in the Middle Okinawa Trough: Terrestrial provenance and reconstruction of the paleoenvironment. Palaeogeography, Palaeoclimatology, Palaeoecology 307, 285–300.

Zheng, Z., Huang, K., Deng, Y., Cao, L., Yu, S. 2013. A ~200 ka pollen record from Okinawa Trough: Paleoenvironmental reconstruction of glacial-interglacial cycles. Science China (Earth Sciences) 56, 1731–1747.

Zhou, H., Guan, H., Chi, B. 2007. Record of winter monsoon strength. Nature 450, 74–77.

Zong, Y., 2004. Mid-Holocene sea-level highstand along the Southeast Coast of China. Quaternary International 117, 55–67.

Zonneveld, K.A.F., Jurkschat, T., 1999. *Bitectatodinium spongium* (Zonneveld, 1997) Zonneveld et Jurkschat, comb. nov. from modern sediments and sediment trap samples of the Arabian Sea (northwestern Indian Ocean): taxonomy and ecological affinity. Review of Palaeobotany and Palynology 106, 153–169.

Zonneveld, K.A.F., Brummer, G.J.A., 2000. (Palaeo-)ecological significance, transport and preservation of organic-walled dinoflagellate cysts in the Somali Basin, NW Arabian Sea. Deep-Sea Research II 47, 2229–2256.

Zonneveld, K.A.F., Pospelova, V. 2015. A determination key for modern dinoflagellate cysts. Palynology 39(3), 387–409.

Zonneveld, K.A.F., Versteegh, G.J.M., de Lange, G.J., 1997. Preservation of organic-walled dinoflagellate cysts in different oxygen regimes: a 10,000 year natural experiment. Marine Micropaleontology 29, 393–405.

Zonneveld, K.A.F., Bockelmann, F., Holzwarth, U., 2007. Selective preservation of organic walled dinoflagellate cysts as a tool to quantify past net primary production and bottom water oxygen concentrations. Marine Geology 237, 109–126.

Zonneveld, K.A.F., Versteegh, G., Kodrans-Nsiah, M., 2008. Preservation and organic chemistry of late Cenozoic organic-walled dinoflagellate cysts: A review. Marine Micropaleontology 68, 179–197.

Zonneveld, K.A.F., Chen, L., Möbius, J., Mahmoud, M.S., 2009. Environmental significance of dinoflagellate cysts from the proximal part of the Po-river discharge plume (off Southern Italy, Eastern Mediterranean). Journal of Sea Research 62, 189–213.

Zonneveld, K.A.F., Versteegh, G.J.M., Kasten, S., Eglinton, T.I., Emeis, K.C., Huguet, C., Koch, B.P., de Lange, G.J., de Leeuw, J.W., Middelburg, J.J., Mollenhauer, G., Prahl, F.G., Rethemeyer, J.,Wakeham, S.G., 2010. Selective preservation of organic matter in marine environments; processes and impact on the sedimentary record. Biogeosciences 7, 483–511.

Zonneveld, K.A.F., Marret, F., Versteegh, G.J.M., Bogus, K., Bonnet, S., Bouimetarhan, I., Crouch, E., de Vernal, A., Elshanawany, R., Edwards, L., Esper, O., Forke, S., Grøsfjeld, K., Henry, M., Holzwarth, U., Kielt, J.F., Kim, S.Y., Ladouceur, S., Ledu, D., Chen, L., Limoges, A., Londeix, L., Lu, S.H., Mahmoud, M.S., Marino, G., Matsouka, K., Matthiessen, J., Mildenhal, D.C., Mudie, P., Neil, H.L., Pospelova, V., Qi, Y., Radi, T., Richerol, T., Rochon, A., Sangiorgi, F., Solignac, S., Turon, J.L., Verleye, T., Wang, Y., Wang, Z., Young, M., 2013. Atlas of modern dinoflagellate cyst distribution based on 2405 data points. Review of Palaeobotany and Palynology 191, 1–197.

Appendix A
Data of pollen and spores from the sediment trap samples.

Sample No.	Uvic-Code	*Cedrus*	Cupressaceae	Taxodiaceae	*Picea*	*Tsuga*	*Pinus*	*Dacrycarpus*	*Podocarpus*	*Dacrydium*	*Alnus*	*Quercus* (Evergreen)	*Quercus* (Deciduous)	*Juglans*	*Fagus*	*Ulmus*	*Tilia*	*Castanopsis*	*Carya*	*Ilex*	*Lonicera*	Sapindaceae	Elaeagnaceae	*Helicia*	*Altingia*	Rutaceae	*Clausena*	*Liquidambar*	Oleaceae	*Planchonella*	Theaceae	Dipterocarpaceae	Anacardiaceae
BP1-1	UVic2015-287		3				106			1	7	9		2		8			4			3				2			1				
BP1-2	UVic2015-288		1			1	119				2	10		2		3			7										1				
BP1-3	UVic2015-289						161		1		3	12				5		3								1		1	1				
BP1-4	UVic2015-290		2				200			1		6	2			8			2													1	
BP1-5	UVic2015-291		2				125					14	1			1										4		2					
BP1-6	UVic2015-292		2			1	100				7	14	1			1		1				1		1		2	1	1					1
BP1-7	UVic2015-293		2				175			1	6	36	4			2		3				1				3			3				
BP1-8	UVic2015-294		3			2	119			1	5	21	1	3		4					1					3							
BP1-9	UVic2015-295			1		5	170				3	32	1	3		10		1								1		1	2	1			
BP1-10	UVic2015-296		3			1	127				4	25		1		8		1								1		1	2				
BP1-11	UVic2015-297					6	96				3	23	2			3	1					1							1				
BP1-12	UVic2015-298		2			2	78				3	12	1			2		1										1				1	
BP3-1	UVic2015-299		1	3			52	2		1	18	2	6	3												1		2	1				
BP3-2	UVic2015-300		1	2	1	2	63			1	5	13	2															9	2				1
BP3-3	UVic2015-301		5				79		2		8	15	5	1				1				2				4		4	7				
BP3-4	UVic2015-302		2			1	65	2		1	16	17	6	3		1		3		3				1		12		3	3		2	1	
BP3-5	UVic2015-303				2		62				15	14		1		2		2	1	3		2				3		3	1				
BP3-6	UVic2015-304	1	2				54		1		4	6	1	2		5		1	1							1		3	1			2	
BP3-7	UVic2015-305		1	1	1		43			1	6	10	1	3		4		1	1			2				2		4				1	
BP3-8	UVic2015-306		1			2	64		2	2	13	15	1	6		3		1	2							2		10	4				1
BP3-9	UVic2015-307				2		75		2		5	6				2			2	1	1	1				3		5	2				
BP3-10	UVic2015-308		1			2	57				5	10	1	1		5						1		1		1				1		1	
BP3-11	UVic2015-309		1		1		91	5	1	1	19	22	9	5	3	1			2	1		2	1		1	3		12	2				
BP3-12	UVic2015-310		2		1	1	53				6	9	5			3				3						2		1	1				

Sample No.	*Rhus*	Araliaceae	Meliaceae	*Myrica*	Hamamelidaceae	*Euphorbia*	*Claoxylon*	*Mallotus*	*Alchornea*	Apocynaceae	Myrtaceae	*Acacia*	*Eucalyptus*	Elaeocarpaceae	Myristicaceae	Berberidaceae	Lauraceae	Palmae	*Arenga*	*Phyllanthus*	Loranthaceae	*Dipsacales*	*Figus*	Moraceae	*Rhizophora* -a	*Rhizophora* -b	*Rhizophora mucronata*	*Pandanus*	Combretaceae	*Casuarina*	Poaceae	Daphniphyllaceae	Celastraceae	Rubiaceae	Brassicaceae	Acanthaceae
BP1-1	1		1	14		1		7															1	5						2	30			1		
BP1-2	3			31		2		1		3														7						1	29			2		
BP1-3	2			19		3		2																7	2					6	19			2	1	
BP1-4	2	1		39		2	5	4				1		1										10	1						9			1		
BP1-5	1			24		1		1															1	4							16					
BP1-6	2	1		32	1		2	1						3										3	1						17			1		
BP1-7	2	2		38		3		2				1											2	10							22					
BP1-8	2			34		3				1												1	1	1							16			2	1	
BP1-9	3	1		30		2	2			1		1		1									2	6	1	1					23					
BP1-10	4	1		18			1	1		3								1					2	4							26				1	
BP1-11	2	2		11		5	2	2				1		2										3	2						25			2		
BP1-12	1	1		14		2		1																3							22					
BP3-1				1		6		3		7	1				1	1	1	1		1			2								31		1	2		
BP3-2				2		3		1		3	1					1			3			1			1						36	1	1	2		1
BP3-3	1	3	1	1		1		3		3		1					1		2			1								1	37		1	3		
BP3-4	2	6			2	6		1		4		1		3		1		1	2	2					1			3	1		38			4		
BP3-5	4			2	3	3	3	4		1		1		1			1	1		3	1			3	1		2			1	33			3	1	
BP3-6	1	1		1	1		1	1	1			4	1	2		1			1	1	1			1	1			1	1		27		1	2		
BP3-7		1		3	1	1	3	2				1		1				1					1	2	3						28			5	2	
BP3-8	2	3		1		2		2		2							1		1					3						1	44		1	2		
BP3-9		1			1	4		2		1		1								1				1	1		1		1		19				1	
BP3-10	1			1		1		1												3					1						40				1	
BP3-11	2	1		3	8			7	1	3	2			3		2				1	1	2	1	2	4		1	1	1	2	64		2	5	3	
BP3-12						3		3										3	1		1										44			2	1	

Sample No.	Convolvulaceae	Cucurbitaceae	Verbenaceae	*Gmelina*	Valeriavaceae	Gesneriaceae	Fabaceae	Malpighiaceae	*Artemisia*	Compositae	*Aster*	Chenopodiaceae	Cyperaceae	*Typha*	*Thalictrum*	Potamogetonaceae	Polygonaceae	Aceaceae	*Lily*	*Nymphoides*	Lentibulariaceae	*Polypodiaceae* -Smooth	*Polypodiaceae* -Spine	*Polypodiaceae* -Boss	Gleicheniaceae	*Cyathea*	*Pteris*	*Lygodium*	*Lygodium microphyllum*	Osmundaceae	*Lycopodium*	*Hymenophyllum*	Parkeriaceae	*Pteridium*	*Cornopteris*	*Cibotium*
BP1-1									6	9		30	17									10		1	18	5						10	1		1	
BP1-2				4					2	8		25	9	1	2	1		1				14	1	3	9	5	2						2			
BP1-3									1	4		43	7		1							2	2	3	6	1	1					8	1		4	
BP1-4									2	4		27	7	1								3		3	16	3	2				1				1	
BP1-5									1	10		31	5									9		1	9	2	2	1				3	1		3	
BP1-6									7	16		27	15	2		1				1		6	2	2	12	3	3						1			
BP1-7			5				1		9	18		50	10						1			5		4	8	7		3				3	1		2	
BP1-8			2						16	7		25	10	4								11		5	17		2	5				7			1	
BP1-9			1			1			20	19		49						1				8	1	7	13	12	7	1				1	1		2	
BP1-10			1						12	10		29		2								2		5	18	7	6	1				5			1	
BP1-11						1			8	7		31	10	3								9	4	2	16	6	6	2				8	1			
BP1-12						2			4	3		19	5	1								6		5	14	8	3					6				
BP3-1			3		1				5	2	2	14	6	9		2		1				11	3	3	29	15		2		1	1	11	2	5		
BP3-2	1		2	1			1		4	8		25	11	2	3	5		2	5			29	3	11	26	9	1	7			2	19	2	4	1	
BP3-3				5					3	8		18	19	4		5	1		5			25	13	8	27	9		1				13	1	3	5	
BP3-4						3			18	7		24	28	7	1			1	2			29	11	6	25	9	5	5	1			19	1	2	6	
BP3-5		1	5						12	4		34	16	2	1			1	2			27	3	2	31	11	9	11			3	7			3	
BP3-6			6					1	8	8		30	20	7								20	5	9	35	8	5	5		1	3		6	4		1
BP3-7			3						8	7		17	9	6		2	1		2		1	18	2	1	28	9	11						2	1	4	
BP3-8				7		2			11	6		20	13	2		2	2					23	3	3	36	11	5			1		14			5	
BP3-9									6	2		13	9	4		1	1					23	6	6	31	16	4	2				21	1		4	
BP3-10			2						5	5		11	15	6	1			1	1			15	14	9	34	3	2	2			1	8	1		1	
BP3-11			3				2		21	3	4	32	43	5	5	14		4	4			36		26	35	17	6	3		3	2	18	8	2	4	
BP3-12			3						9	6		31	29	3								25	2	9	12	10	2	1			2	10	3		2	

Sample No.	Vittariaceae	Angiopteridaceae	*Ptyrogramma*	*Athyrium*	*Monogramma*	Hemionitidaceae	*Plagiogyria*	*Selaginella*	*trilete*	*Concentricystes*	*Zygnema*	Unidentified	Total pollen and spores	Exotic *Lycopodium* (18,584 grains/tablet)
BP1-1			6					1		1		8	333	8051
BP1-2			4		1	10		2		1		9	341	5361
BP1-3												1	336	6558
BP1-4			5		2	5		4				6	390	4081
BP1-5			1									9	285	7294
BP1-6			4			9						2	311	7632
BP1-7			3					1			1	12	462	13294
BP1-8			2							2		8	349	7468
BP1-9		1	3							2		18	473	5766
BP1-10			5		2					1		15	358	7776
BP1-11			1									9	319	12329
BP1-12			6		1					4		4	238	11546
BP3-1		1	1		4		1	2	3	1		8	300	9107
BP3-2		2			1			3	7			9	365	4326
BP3-3				1				1	5	3		8	384	3990
BP3-4		2			1			3	7	1		8	452	2913
BP3-5		1			1			1	3	7		10	391	3046
BP3-6			1					4	8	1		9	342	4913
BP3-7		1			1			3	11	3	2	9	299	2245
BP3-8	1		1		2			1	6	1		8	380	2932
BP3-9	1				1			4	2	5	1	10	316	5348
BP3-10		1	17		1				1	1		14	308	7370
BP3-11		4	1				2	8	1	2		20	643	7924
BP3-12			6		1			1	2		1	11	326	4234

Appendix B
Data of dinoflagellate cysts from the sediment trap samples.

Sample No.	Uvic-Code	empty or not	*Achomosphaera* spp.	*Bitectatodinium spongium*	*Cryodinium meridianum*	*Impagidinium strialatum*	*Impagidinium* spp.	*Lingulodinium hemicystum*	*Operculodinium centrocarpum*	*Operculodinium israellianum*	*Operculodinium longispinigerum*	*Operculodinium* cf. *janduchenei*	*Operculodinium* -type B (*O* . spp.)	*Operculodinium* spp.	Cyst of *Pentapharsodinium dalei*	*Polysphaeridium zoharyi*	*Spiniferites bentorii*	*Spiniferites delicates*	*Spiniferites hyperacanthus*	*Spiniferites mirabilis*	*Spiniferites ramosus*	*Spiniferites* spp.	*Spiniferites* -Type A (*S.* spp.)	*Spiniferites* -Type B (*S* . spp.)	*Spiniferites* -Type C (*S.* spp.)	*Spiniferites* -Type D (*S.* spp.)	*Spiniferites* -Type E(intergonal *S. bentorii*)	*Spiniferites* -Type F (S. membranaceus type)	Unknown auto-cysts	*Brigantedinium cariacoense*	*Brigantedinium irregulare*
BP1-1	UVic2015-287	empty cyst						2	4						4				1			1									5
		with cell content																			1	1									
BP1-2	UVic2015-288	empty cyst							1	1					1							1				1					2
		with cell content													2																
BP1-3	UVic2015-289	empty cyst							2												1	2			1					1	1
		with cell content													5															1	
BP1-4	UVic2015-290	empty cyst			1			1																							3
		with cell content													1																
BP1-5	UVic2015-291	empty cyst						1	3																			1		1	1
		with cell content																													
BP1-6	UVic2015-292	empty cyst						2	2	1						1															3
		with cell content							1						1																
BP1-7	UVic2015-293	empty cyst							1																						2
		with cell content																													
BP1-8	UVic2015-294	empty cyst																													
		with cell content							1																						
BP1-9	UVic2015-295	empty cyst				1			1																	1				2	2
		with cell content																				1								1	
BP1-10	UVic2015-296	empty cyst							1													1							2	1	
		with cell content														1															
BP1-11	UVic2015-297	empty cyst																		1										1	
		with cell content																													
BP1-12	UVic2015-298	empty cyst																		1											2
		with cell content																													

Sample No.	*Brigantedinium simplex*	*Brigantedinium* -Pale (thin wall)	*Brigantedinium* -type A	*Brigantedinium* spp.	*Dubridinium caperatum*	*Dubridinium cavatum*	*Echinidinium aculeatum*	*Echinidinium granulatum*	*Echinidinium transparantum*	*Echinidinium* spp.	*Echinidinium* -type A	*Echinidinium* -type E	Cyst of *Archaeperidinium minutum*	*Islandinium brevispinosum*	*Islandinium* spp.	*Lejeunecysta sabrina*	Cyst of *Protoperidinium oblongum*	Cyst of *Protoperidinium* spp.	*Quinquecuspis concreta*	*Selenopemphix nephroides*	*Selenopemphix quanta*	*Stelladinium reidii*	*Stelladinium* -type A (S. stellatum?)	Cyst of *Polykrikos sp.*	Unknown cysts	Exotic (Lycopodium) (18584/tablet)	Total empty or cell-content cysts	Total dinoflagellage cysts	Dry weight(g)
BP1-1	6	61	10	65		9	8	1		7	2		2					4			2					10378	194	291	0.6
		47	2	30			11										1	2			1	1					97		
BP1-2	2	105	12	63		11	4						1			2		9								5361	216	289	0.6
	1	63	1	3			1			1				1												73		
BP1-3	1	129	18	74	5	8	4			6								24			2					6558	279	372	0.6
		67	5	6	1		3							2				2			1						93		
BP1-4	2	122	13	77		19				5								39								6722	282	345	0.4
		47	1	6						3				3				2									63		
BP1-5	3	70	6	46	1	9				3							2	18								9488	165	189	0.5
		21		1		1	1																				24		
BP1-6	3	46	13	48		10				1								40	1							10444	171	193	0.5
		11	1	6			1							1													22		
BP1-7	7	76	4	63		15	2			1				2				30			2			1		13294	206	221	0.5
		7		4			1							1				2									15		
BP1-8		119	10	99		12	1		1	2								23		3		2				9542	272	302	0.6
		10		7			2		1	1					1		1	2		1		3					30		
BP1-9	3	57	6	143		17				3	1				1			27		1		3	5			5766	274	323	0.6
		14		19					1						8			1				2	2				49		
BP1-10	2	81	4	147		7				1								8		1	1		2			9007	259	312	0.6
		21		25			1								3							2					53		
BP1-11	1	38	6	118		4									1			9				1	1			12329	181	191	0.5
				4			2								4												10		
BP1-12	2	24	3	70		4	1			1	1							4			1					11546	114	125	0.4
		3		3			1		1						1			1									11		

Sample No.	Uvic-Code	empty or not	*Achomosphaera* spp.	*Bitectatodinium spongium*	*Cryodinium meridianum*	*Impagidinium strialatum*	*Impagidinium* spp.	*Lingulodinium hemicystum*	*Operculodinium centrocarpum*	*Operculodinium israelianum*	*Operculodinium longispinigerum*	*Operculodinium* cf. *janduchenei*	*Operculodinium* -type B (*O*. spp.)	*Operculodinium* spp.	Cyst of *Pentapharsodinium dalei*	*Polysphaeridium zoharyi*	*Spiniferites bentorii*	*Spiniferites delicates*	*Spiniferites hyperacanthus*	*Spiniferites mirabilis*	*Spiniferites ramosus*	*Spiniferites* spp.	*Spiniferites* -Type A (*S*. spp.)	*Spiniferites* -Type B (*S* . spp.)	*Spiniferites* -Type C (S. spp.)	*Spiniferites* -Type D (S. spp.)	*Spiniferites* -Type E(intergonal *S. bentorii*)	*Spiniferites* -Type F (S. membranaceus type)	Unknown auto-cysts	*Brigantedinium cariacoense*	*Brigantedinium irregulare*
BP3-1	UVic2015-299	empty cyst					5		6		1			1	3						1	3							2		
		with cell content							1																						
BP3-2	UVic2015-300	empty cyst					1	2	10	2					1		1	1	1	1	1	3		1	1	1					1
		with cell content							3						3						2	1		1							
BP3-3	UVic2015-301	empty cyst		1		1		4	11										1	1		1		1		2				2	
		with cell content							1																						
BP3-4	UVic2015-302	empty cyst			1			4	4							1			1							3					
		with cell content													2																
BP3-5	UVic2015-303	empty cyst		1					2						1				1			1									2
		with cell content																													
BP3-6	UVic2015-304	empty cyst							9	1			1					1	1		4	3				1				1	3
		with cell content							2												1										
BP3-7	UVic2015-305	empty cyst								2												1							1	1	2
		with cell content																													
BP3-8	UVic2015-306	empty cyst	1					2	3	1									1	2		2	1	2		1					2
		with cell content																			1										
BP3-9	UVic2015-307	empty cyst			1				5	1									1		1	3									6
		with cell content																	1		1					1					
BP3-10	UVic2015-308	empty cyst			1			3	3																						2
		with cell content																											1		
BP3-11	UVic2015-309	empty cyst						2	10									2			1	3					2				
		with cell content							3						1																
BP3-12	UVic2015-310	empty cyst			1	1		13	8			1			3		1		3	1	1	5			1				2	1	4
		with cell content							1																1						

Sample No.	*Brigantedinium simplex*	*Brigantedinium* -Pale (thin wall)	*Brigantedinium* -type A	*Brigantedinium* spp.	*Dubridinium caperatum*	*Dubridinium cavatum*	*Echinidinium aculeatum*	*Echinidinium granulatum*	*Echinidinium transparantum*	*Echinidinium* spp.	*Echinidinium* -type A	*Echinidinium* -type E	Cyst of *Archaeperidinium minutum*	*Islandinium brevispinosum*	*Islandinium* spp.	*Lejeunecysta sabrina*	Cyst of *Protoperidinium oblongum*	Cyst of *Protoperidinium* spp.	*Quinquecuspis concreta*	*Selenopemphix nephroides*	*Selenopemphix quanta*	*Stelladinium reidii*	*Stelladinium* -type A (S. stellatum?)	Cyst of *Polykrikos sp.*	Unknown cysts	Exotic (Lycopodium) (18584/tablet)	Total empty or cell-content cysts	Total dinoflagellage cysts	Dry weight(g)
BP3-1	11	40		58	1	6	1										1	1		2		1				9617	144	171	0.5
				26																							27		
BP3-2		93		95		11	2			3	3						1	12		3						4736	251	298	2.7
		36																				1					47		
BP3-3		142		75		10	1			2	1	1						4								3990	261	288	3.1
		25				1																					27		
BP3-4		104		132		4				3			1				2									2913	260	273	2.8
		11																									13		
BP3-5		125		94		5	3			1	1						3	7		1						3046	248	331	2.3
		79		2														2									83		
BP3-6		170	5	92		11					1						4	8	2	3		1			1	6543	323	396	2.6
		66				1	1			1									1								73		
BP3-7	9	108	13	42		8	1										5	11	1	2		1				2245	208	278	2.7
		68		1														1									70		
BP3-8	8	128	15	43		7										1	4	22	1	1	3				1	2932	252	306	2.1
		50		2	1																						54		
BP3-9	6	139	45	49	1	17				1	1							23	1	3	2	1			2	9962	309	358	1.4
		42		2														2									49		
BP3-10		45	11	38		4				1								7	1		1				2	9773	119	137	0.6
		17																									18		
BP3-11	12	192		83		6		1		6							1	2							2	7924	325	361	2.9
		32																									36		
BP3-12	5	101	47	50		13	2				1	1					1	8		1		1			2	9504	279	312	3.3
		29	1															1									33		

Appendix C
Data of dinoflagellate cysts from surface samples of this study.

Sample No.	Uvic code	Achomosphaera spp.	*Bitectatodinium spongium*	*Cryodinium* cf. *meridianum*	*Dapsilidinium pastielsii*	*Impagidinium aculeatum*	*Impagidinium pallidum* (*I.* spp.)	*Impagidinum plicatum* (*I.* spp.)	*Impagidinium paradoxum*	*Impagidinium patulum*	*Impagidinium sphaericum* (*I.* spp.)	*Impagidinium* cf. *sphaericum* (*I.* spp.)	*Impagidinium strialatum* (*I.* spp.)	*Impagidinium* spp.	*Impagidinium* spp. (<20 um)	*Lingulodinium hemicystum*	*Lingulodinium* spp.	*Nematosphaeropsis labyrinthus*	*Operculodinium centrocarpum*	*Operculodinium israelianum*	*Operculodinium* cf. *janducheneі*	*Operculodinium longispinigerum*	*Operculodinium* spp.	Cyst of *Pentapharsodinium dalei*	*Polysphaeridium zoharyi*	*Spiniferites bentorii*	*Spiniferites bulloideus* (*S.* spp.)	*Spiniferites delicates* (*S.* spp.)	*Spiniferites hyperacanthus*	*Spiniferites* cf. *ludhamensis (type C)*	*Spiniferites membranaceus*	*Spiniferites mirablis*	*Spiniferites pachyderma*	*Spiniferites ramosus*
79-48	UVic2017-1								1	1		1			2	17			44	4	3	11	2	1	16		2	1	31	6		22	0	29
08-CF2	UVic2017-2															16	1		14	1	1	2				1				1	1	5	0	9
08-CF10	UVic2017-5		1		1																	2			1				2			1	0	
08-E425 (CF6)	UVic2017-9					1		1	3	1	1					14			50	5	2	9			2				40	10	2	17	0	32
08-E501	UVic2017-10															5			10	1		1							12	4			0	10
08-E504	UVic2017-11				1	1		1								15	2		55	4		5			2				40	3		35	0	45
08-E524	UVic2017-13					2			1							12			43	9		9			7		1		49	8		22	0	18
08-E525	UVic2017-14								2							1		1	16			2			1				11			3	1	4
08-E605	UVic2017-15					1													2														0	
08-E702	UVic2017-16					1		2	1							5		1	3						1				2			2	0	
09-E108	UVic2017-17															1			1			1							2	1		1	1	1
09-E401	UVic2017-18																																0	
09-E420	UVic2017-19					1	1									3		1	4										5			2	1	3
09-E605	UVic2017-20			2		2		1								6		1	51	8		7			1				37	3		17	0	25
09-KJ14	UVic2017-22					1		1								2			4	1	3	1							11				0	1
09-KJ16	UVic2017-23					1	2	1		4			1			4		1	45	9	1	5				2			32	6		16	0	12
09-KJ21	UVic2017-24															1			4	3		2							8	1		4	0	1
09-KJ28	UVic2017-25																	1	3			1							6				0	1
09-Y01	UVic2017-26					4		1					3		1	4		1	32	1	1	3		1					44	2		12	0	6
09-Y07	UVic2017-27				2	1				1			2			1		1	13	11		7		1					7	1		5	0	2
D15-3	UVic2017-28												1			2			3	1		1							12	2		7	0	
D21-3	UVic2017-29															1			1	1		2							9	1		3	1	2
D22a-1	UVic2017-30			1												4			10	5		2				1			25	2		16	0	12
OR1-0182-3-B	UVic2017-31																																0	
OR1-0216-1-B	UVic2017-32																												4				0	
OR1-0299-1-B-1	UVic2017-48			1															5										4	1		1		1
OR1-0299-2-B-2	UVic2017-49															1			2							1			8			1		

Sample No.	*Spiniferites spinatus (S.spp.)*	*Spiniferites* spp.	*Spiniferites* -type A (*S.* spp.)	*Spiniferites* -Type B (*S.* spp.)	*Spiniferites* -type D (*S.* spp.)	*Tuberculodinium vancampoae*	Unknown auto-cysts	*Brigantedinium cariacoense*	*Brigantedinium irregulare*	*Brigantedinium simplex*	*Brigantedinium* -thin wall (*B.* spp.)	*Brigantedinium* spp.	*Brigantedinium* -type A (*B.* spp.)	*Dubridinium cavatum*	*Dubridinium caperatum*	*Echinidinium aculeatum*	*Echinidinium granulatum*	*Echinidinium transparantum*	*Echinidinium* spp.	*Echinidinium* -type A (*E.* spp.)	*Echinidinium* -type C (*E.* spp.)	*Echinidinium* -type E (*E.* spp.)	Cysts of *Protoperidinium oblongum*	Cysts of *Protoperidinium* spp.	*Quinquecuspis concreta*	*Selenopemphix nephroides*	*Selenopemphix quanta*	*Selenopemphix tholus*	*Stelladinium reidii*	*Trinovantedinium applanatum*	Unknown brown cysts	Total	Exotic *Lycopodium clavatum*	*Lycopodium* (9666 grains/tablet)	dry weight (g)
79-48		47	8	15	17	1	6		1		2	15										2		3		2	2		1	2	1	322	3509	1	1.3
08-CF2		8	1		2	1			2		7	24	4	3		1	2		2	3	2		2	14		3	1	1	2	1		141	3772	1	1.5
08-CF10		3	1						1		4	44	6	8						2				5					1		1	85	3668	1	0.9
08-E425 (CF6)	3	43	2	9	11						1	4				1										1						271	5136	1	1.3
08-E501		6		1	3		1			2	8	14	4						8	6			1	6		2	6			1		112	3279	1	1.8
08-E504	1	42	7	14	10	7					7	7							1				3	9					2	3		324	3069	1	1.6
08-E524	1	46	12	4	11	4						11								1			1	3		4	1					282	9418	2	3.7
08-E525		15	1			1	6					1							1													77	5865	1	1.3
08-E605		3				1																										10	668	1	1.3
08-E702		8																														31	5272	1	1.4
09-E108		2										3								2						1			1			18	4284	1	1.6
09-E401							1				1	18		3						1						1						25	4534	1	1.9
09-E420		15			1	2						1		1																		47	4620	1	1.2
09-E605		46	5	6	10	3				2	8	48	1	2					1	1				16		7	2					329	2782	1	1.8
09-KJ14		6	1			1																										38	4064	1	1.3
09-KJ16		28	2	5	7	3		2	3		26	111	3						1					15		9	7		1	1		376	5308	1	1.5
09-KJ21		5	1			2						1																				35	5555	1	1.2
09-KJ28		5				3													1											1		23	3545	1	1.2
09-Y01		13	1	7	7	6					1			1					2							1				1		166	4967	1	1.9
09-Y07		4		4	2					1	7	31	3	6	1	1			1				1	1		3	3					129	3975	1	1.3
D15-3		2		2						1	3	13	1	1				2	7		1			34		1	1					98	11319	1	0.7
D21-3		2		3	1	3				2	1	11							7					3			2			1		57	3705	1	2.4
D22a-1		26		3	4	2			1	2	10	20		1		1			33				3	24		4	8		1	3		225	3686	1	2.1
OR1-0182-3-B		4							1	1	19	36	3	3	2				1					13		2	1		1			87	3304	1	2.8
OR1-0216-1-B		2								3	42	61	9	3					2	1			3	11		1	2		2			146	5191	1	2.0
OR1-0299-1-B-1		1								2	14	62	4		4				6					5	1		2		1		1	117	4537	1	2.3
OR1-0299-2-B-2		1			1						24	27							5				1	5			1		1			79	3799	1	2.1

Sample No.	Uvic code	Achomosphaera spp.	*Bitectatodinium spongium*	*Cryodinium* cf. *meridianum*	*Dapsilidinium pastielsii*	*Impagidinium aculeatum*	*Impagidinium pallidum* (*I.* spp.)	*Impagidinum plicatum* (*I.* spp.)	*Impagidinium paradoxum*	*Impagidinium patulum*	*Impagidinium sphaericum* (*I.* spp.)	*Impagidinium* cf. *sphaericum* (*I.* spp.)	*Impagidinium strialatum* (*I.* spp.)	*Impagidinium* spp.	*Impagidinium* spp. (<20 um)	*Lingulodinium hemicystum*	*Lingulodinium* spp.	*Nematosphaeropsis labyrinthus*	*Operculodinium centrocarpum*	*Operculodinium israelianum*	*Operculodinium* cf. *janduchenei*	*Operculodinium longispinigerum*	*Operculodinium* spp.	Cyst of *Pentapharsodinium dalei*	*Polysphaeridium zoharyi*	*Spiniferites bentorii*	*Spiniferites bulloideus* (*S.* spp.)	*Spiniferites delicates* (*S.* spp.)	*Spiniferites hyperacanthus*	*Spiniferites* cf. *ludhamensis (type C)*	*Spiniferites membranaceus*	*Spiniferites mirablis*	*Spiniferites pachyderma*	*Spiniferites ramosus*
OR1-0311-56-B	UVic2017-50																				1												
OR1-0311-68-B	UVic2017-51									1									2										1				1
OR1-0311-80-B	UVic2017-52					1										3			20	1		3			2				24	1		10		5
OR1-0311-90-B	UVic2017-53		1													12		1	30	1		6			1				53	4		14		22
OR1-0455-10-B	UVic2017-55																																	
OR1-0455-15-B	UVic2017-56																			1									1					
OR1-0455-16-B	UVic2017-57	1																																
OR1-0455-17-B	UVic2017-58																																	
OR1-0455-19-B	UVic2017-59																																	
OR1-0455-1-B	UVic2017-60																												1					
OR1-0455-21-B	UVic2017-61																																	
OR1-0455-2-B	UVic2017-62								1	1									1						1				2	1				1
OR1-0455-6-B	UVic2017-63																																	
OR1-0455-7-B	UVic2017-64						1											1																
OR1-0455-9-B	UVic2017-65																			1									2					

Sample No.	*Spiniferites spinatus (S.spp.)*	*Spiniferites* spp.	*Spiniferites* -type A (*S.* spp.)	*Spiniferites* -Type B (*S.* spp.)	*Spiniferites* -type D (*S.* spp.)	*Tuberculodinium vancampoae*	Unknown auto-cysts	*Brigantedinium cariacoense*	*Brigantedinium irregulare*	*Brigantedinium simplex*	*Brigantedinium* -thin wall (*B.* spp.)	*Brigantedinium* spp.	*Brigantedinium* -type A (*B.* spp.)	*Dubridinium cavatum*	*Dubridinium caperatum*	*Echinidinium aculeatum*	*Echinidinium granulatum*	*Echinidinium transparantum*	*Echinidinium* spp.	*Echinidinium* -type A (*E.* spp.)	*Echinidinium* -type C (*E.* spp.)	*Echinidinium* -type E (*E.* spp.)	Cysts of *Protoperidinium oblongum*	Cysts of *Protoperidinium* spp.	*Quinquecuspis concreta*	*Selenopemphix nephroides*	*Selenopemphix quanta*	*Selenopemphix tholus*	*Stelladinium reidii*	*Trinovantedinium applanatum*	Unknown brown cysts	Total	Exotic *Lycopodium clavatum*	*Lycopodium* (9666 grains/tablet)	dry weight (g)
OR1-0311-56-B		2									1	2							1					1		1	2					11	2022	1	1.8
OR1-0311-68-B		3				1	1					3																				13	4153	1	2.1
OR1-0311-80-B	2	15			11						10	24	1	1					11				1	4		3	5		1			160	2629	1	1.5
OR1-0311-90-B		30	7	9	20	12					7	17		3					17					38	3	20	7					344	2663	1	2.1
OR1-0455-10-B												4																				4	3953	1	1.7
OR1-0455-15-B		2																														4	3232	1	1.4
OR1-0455-16-B																																1	3353	1	1.4
OR1-0455-17-B																																0	3955	1	1.7
OR1-0455-19-B																																0	3269	1	1.5
OR1-0455-1-B		2																	2													5	3788	1	1.9
OR1-0455-21-B																																0	5163	1	1.6
OR1-0455-2-B		1																					1									11	4946	1	1.6
OR1-0455-6-B											1	1												1		1	1					5	2353	1	1.5
OR1-0455-7-B		2																														8	3963	1	1.6
OR1-0455-9-B											2	5		1										3								14	3164	1	1.9

Appendix D
Data of pollen and spores from sediment core GLW31D.

Sample No.	UVic Lab. No.	Top depth (cm)	Bottom depth (cm)	*Cedrus*	Cupressaceae	Taxodiaceae	*Picea*	*Pinus*	*Dacrycarpus*	*Podocarpus*	*Dacrydium*	*Alnus*	*Celis*	*Quercus* (Evergreen)	*Quercus* (Deciduous)	*Juglans*	*Carpinus*	*Fagus*	*Salix*	*Ulmus*	*Tilia*	*Castanopsis*	*Carya*	*Ilex*	*Clerodendrum*	Icacinaceae	*Lonicera*	Sapindaceae	Elaeagnaceae	*Helicia*
GLW31D-1	UVic2014-67	0	2				2	124		1	1	2		1								2								
GLW31D-3	UVic2014-276	2	4		1		2	198			1	2		5		1				1		7		1						
GLW31D-5	UVic2014-69	4	6					165			2	6		3	1	1						1		1						
GLW31D-7	UVic2014-70	6	8					157				5		10	1							1	1							
GLW31D-9	UVic2014-71	8	10					170		4	5	5		5		1						1	2	1						
GLW31D-11	UVic2014-72	10	12					180			1	9		4	1	1						2								
GLW31D-13	UVic2014-73	12	14					161				6		12	2	2				1		3								
GLW31D-15	UVic2015-196	14	16	2				176		3	1			7	1	1						2								
GLW31D-17	UVic2014-75	16	18					170		1		7		11	5					1		3								
GLW31D-19	UVic2014-76	18	20					177		1		6		6	1					1		2	1	1						
GLW31D-21	UVic2015-197	20	22		1			206				7		7	4	1		1		2		1		1						
GLW31D-23	UVic2014-78	22	24				2	167	1		1	4		8	3		1	1						1						
GLW31D-25	UVic2014-79	24	26					205		1	3	3		9	1							1								
GLW31D-27	UVic2014-80	26	28					176			1	2	1	6	2			3				2	2							
GLW31D-29	UVic2014-81	28	30		1			178		1	1	3		14	1			1				3	1	1						
GLW31D-31	UVic2014-82	30	32					161				3	1	3	5	2							1							
GLW31D-33	UVic2014-83	32	34					150				3		12	2							3	1							
GLW31D-35	UVic2014-84	34	36				1	178		2	2	1		7	1			1				1		1						
GLW31D-37	UVic2014-85	36	38					156				4		8				1		2	1	3	1							
GLW31D-39	UVic2014-86	38	40		1			159				5		13	3					3		1								
GLW31D-41	UVic2015-198	40	42					188	1			1		5	1					0		1					2			
GLW31D-43	UVic2015-199	42	44					171		2	2	3		15																
GLW31D-45	UVic2014-89	44	46					214			1			2	1					1										
GLW31D-47	UVic2015-200	46	48					190	1	1		3		3	2					1		2		1						
GLW31D-49	UVic2014-91	48	50				1	165	1	1		1		7	4							1	2							
GLW31D-51	UVic2014-92	50	52					203	1		1	2		10								1								
GLW31D-53	UVic2014-93	52	54		2			160				3		8		1				2		2	1							
GLW31D-55	UVic2014-94	54	56					173			1	2		7	1							2	1							
GLW31D-57	UVic2014-95	56	58					191		1	1	1		5	1	3				1		1	2							

Sample No.	Passifloraceae	*Altingia*	Rutaceae	*Clausena*	*Liquidambar*	Magnoliaceae	Oleaceae	*Aglaia*	*Spathodea*	*Bombax*	Dipterocarpaceae	*Zanthoxylum*	Piperaceae	Anacardiaceae	*Rhus*	Araliaceae	Menispermaceae	Meliaceae	*Myrica*	Hamamelidaceae	*Euphorbia*	*Mallotus*	*Alchornea*	Apocynaceae	Myrtaceae	Samydaceae	*Eucalyptus*	Elaeocarpaceae	*Garcinia*	*Symplocos*	Rosiaceae	Sterculiaceae	Berberidaceae	Lauraceae
GLW31D-1			2													4				3														
GLW31D-3		1	2			2									1	1		1		1				2									1	
GLW31D-5			2		3									1			2		2		2												2	
GLW31D-7			2											4			2																	
GLW31D-9		3																	2											1				
GLW31D-11		1													3				2	1				1									1	
GLW31D-13		1	1				1							6					1															
GLW31D-15		2																		1														
GLW31D-17			1				2							1				1		1														
GLW31D-19					1									1						2	1													1	
GLW31D-21		1	4							2				1	1			1	3		1													
GLW31D-23					1					1								2	6	2										1				1	
GLW31D-25		2	1											1		4			5	2	2													
GLW31D-27		2			2			1						1	2				2	1	1			1						1			1	
GLW31D-29					2										1	1		3	1	2	1	1					1							
GLW31D-31					3		2								1				2	2													3	
GLW31D-33			2		2		1			1									1		1										1		1	
GLW31D-35		1			2		1							1		4			1	8														
GLW31D-37			2		1		1							1					1		1									1				
GLW31D-39			2		2									1					2		2													
GLW31D-41			1											1	1		1		4		1													
GLW31D-43		2																	2		1													
GLW31D-45		2																	1															
GLW31D-47					1										1				1		1									1		2		
GLW31D-49		2			3									1	1						3			1								2	1	
GLW31D-51			1		5																1													
GLW31D-53					2		2			1										2	1													
GLW31D-55		1	1		4									2	1					1	1									1				
GLW31D-57		1			1										2					2	1				1									

Sample No.	Palmae	*Arenga*	*Phyllanthus*	*Ardusua*	Loranthaceae	Moraceae	Clusiaceae	*Avicennia marina*	*Aegiceras corniculatum*	*Rhizophora* -a	*Rhizophora* -b	*Rhizophora mucronata*	*Excoecaria*	*Browlowia tersa*	*Pandanus*	Combretaceae	*Casuarina*	Poaceae	Cucurbitaceae	Solanaceae	Saururaceae	Celastraceae	*Manocelastrus*	*Rubiaceae*	*Coelospermum*	Balanophoraceae	Brassicaceae	Acanthaceae	Convolvulaceae	Verbenaceae	*Gmelina*	Malvaceae	Umbelliferae	Thymelaeaceae
GLW31D-1			2															8						2			2							
GLW31D-3									2									7						1			1			2				
GLW31D-5	3															1		6			1			1			1							2
GLW31D-7	1																	13						1										2
GLW31D-9													1					6						1					1					
GLW31D-11									2						2			7			1						1							1
GLW31D-13																		8						3										
GLW31D-15									1									4						6										
GLW31D-17						1												11			1			1										
GLW31D-19									1									3						4										1
GLW31D-21					1													7		2				1			1			2		1		
GLW31D-23									1									8						6										
GLW31D-25										1						1		7						4			1							
GLW31D-27						1			1	1								13			1			3			1							
GLW31D-29									1							1		8						1			2			1				1
GLW31D-31																1	1	7		1	2			4										2
GLW31D-33	1					1			1									6				1		4					2					
GLW31D-35																		5						4					2					
GLW31D-37	1					1				1						1		9						2			1		2					1
GLW31D-39	3					1												8		1				2						1				
GLW31D-41											1							11						1										
GLW31D-43						1			1					1				4						6										
GLW31D-45																		9										1						
GLW31D-47				1						1								7						1					2					
GLW31D-49	1																	14						2					1					
GLW31D-51			1															3																
GLW31D-53	1																	3						1										
GLW31D-55	1		1						2									5		1				4						2				
GLW31D-57										1							1	7						8				1		1				

Sample No.	Valeriavaceae	Nepenthaceae	*Peliosanthes*	Eriocaulaceae	Gesneriaceae	Caryophyllaceae	Fabaceae	*Plumbago*	*Artemisia*	Compositae	Chenopodiaceae	Cyperaceae	*Typha*	*Thalictrum*	Potamogetonaceae	Alismataceae	Iridaceae	Aceaceae	*Lily*	*Nymphoides*	Polypodiaceae-Smooth	Polypodiaceae-Boss	Gleicheniaceae	*Cyathea*	*Pteris*	*Lygodium*	Osmundaceae	*Lycopodium*	*Hymenophyllum*	Parkeriaceae	*Pteridium*	*Acrostichum*	*Cibotium*	Vittariaceae
GLW31D-1									3	1	1	9	3								19	2	135	24	5	1			1		6	1		
GLW31D-3									10		2	26	1		2	2				1	37	17	145	109	7			2	4		23	1		
GLW31D-5	1								5			16	1		1				1		26	26	119	32	5	3		2	4	1	17			3
GLW31D-7									2	1	3	16							1		7	10	92	42	8			3	7		22			3
GLW31D-9									6	1		20			2						17	6	79	34	3			2	1		10	1		
GLW31D-11									3	2		20			2		1		1		30	5	35	37	2	1		1	3		4			2
GLW31D-13	1								8	2	3	22									23	4	40	9	7	5		2	2		8			
GLW31D-15									5		1	7			3						20	7	35	23	14	3		1	4		9		1	
GLW31D-17							1		8			12		1	1			1			24	11	16	11		5	1	1	4		1			
GLW31D-19	1								9	3	1	11			1				1		17	2	20	4	3	7		1	1	1	2			3
GLW31D-21									4	3		9	1		3				1		4	1	4	15	4	5			3		5		2	4
GLW31D-23							1		5	3		14									24	6	24	12	3	2		1	2		1		1	1
GLW31D-25						1			4	1		6			1						12	4	14	10	3			1			2			1
GLW31D-27									5	2	1	22	1			2					4	4	5	13	5	2		1	2		1			
GLW31D-29									1	3		18	1		1				1		5	3	6	16	5	3		1						
GLW31D-31									4	3	2	16	1						1		31	10	24	14		9	1	2	2		3		1	4
GLW31D-33									7	1	1	19									16	10	17	10	3	2	3	1	8	1	2			3
GLW31D-35									4	3	3	10	1		3						24	8	19	11	8	4	1	2	1		2			2
GLW31D-37									6	1	1	16							1		21	8	18	16	4	2	2		3					4
GLW31D-39	1								1			29	1								27	6	14	13	4	2		1	2	1				
GLW31D-41									4	3		10									24	6	32	12	3	1	1	1	1	1				2
GLW31D-43									6	6		1	1								13	8	24	23	8	7	3	3	2		3			2
GLW31D-45										2		8									16	13	17	10	1	1			1		1			
GLW31D-47							1		5	3	1	8									22	6	23	7	6			1	2	2	1			1
GLW31D-49										1		22			1						19	4	20	7	4	2		1	1	1	1		1	1
GLW31D-51									4	2		5	1								21	11	22	18		1	1		1		1		1	
GLW31D-53									7	3		14	1		1						17	10	37	13	11	1		1	2		6			4
GLW31D-55									7	3	2	9	1		6	1					22	5	9	16	1	3	1		3		5			2
GLW31D-57									3	4		10	1						1		21	7	13	7	7	1	3		8		5			

Sample No.	Ophioglossaceae	Angiopteridaceae	*Ptyrogramma*	*Onychium*	*Athyrium*	*Dryopteris*	*Monogramma*	Hemionitidaceae	*Selaginella*	*Spiny spherea*	Unknown trilete	*Concentricystes*	*Zygnema*	Unidentified	Total	Exotra *Lycopodium* (18584 grains/tablet)	Dry weight(g)
GLW31D-1									2					1	370	699	3.7
GLW31D-3									1				2	5	641	473	3.3
GLW31D-5										5				2	479	750	4.1
GLW31D-7										1					418	777	4.2
GLW31D-9	1								2				1		395	563	4.5
GLW31D-11									1	1				4	376	667	4.2
GLW31D-13									1	3		1	1		350	1170	4.2
GLW31D-15												2			342	721	4.2
GLW31D-17							1		2			2		1	322	797	4.4
GLW31D-19												1		4	304	883	4.4
GLW31D-21									2	1		4		8	343	880	4.6
GLW31D-23									2	1				1	322	695	4.2
GLW31D-25									1			1		2	318	448	4.3
GLW31D-27									1	1					303	830	4.5
GLW31D-29									1			1		2	301	1038	3.9
GLW31D-31	1											4	1		341	955	4.4
GLW31D-33			1				1		3			1		7	314	797	4.4
GLW31D-35									3			1		5	339	1007	4.2
GLW31D-37												1		6	313	697	4.0
GLW31D-39									1	2		2		6	323	792	4.1
GLW31D-41										1				3	326	920	4.6
GLW31D-43									1			1		2	325	969	4.5
GLW31D-45			2						1					3	308	969	4.4
GLW31D-47		1	1							1		2		6	323	739	4.6
GLW31D-49		1	2							1				4	309	823	4.1
GLW31D-51									2			2		7	329	999	4.2
GLW31D-53									2	4		2		3	331	429	4.4
GLW31D-55		2	2						2		2	3		5	327	707	4.3
GLW31D-57		1							2	2				1	331	830	4.3

Sample No.	UVic Lab. No.	Top depth (cm)	Bottom depth (cm)	*Cedrus*	Cupressaceae	Taxodiaceae	*Picea*	*Pinus*	*Dacrycarpus*	*Podocarpus*	*Dacrydium*	*Alnus*	*Celis*	*Quercus* (Evergreen)	*Quercus* (Deciduous)	*Juglans*	*Carpinus*	*Fagus*	*Salex*	*Ulmus*	*Tilia*	*Castanopsis*	*Carya*	*Ilex*	*Clerodendrum*	Icacinaceae	*Lonicera*	Sapindaceae	Elaeagnaceae	*Helicia*
GLW31D-59	UVic2014-96	58	60					171	1	3	2	5		8	1							3	1							
GLW31D-61	UVic2014-97	60	62				1	182				2		4		1		1		1		1								
GLW31D-63	UVic2014-98	62	64				1	204			1			1		1						1								1
GLW31D-65	UVic2014-99	64	66		2			216			2	4		8	1	1						3								
GLW31D-67	UVic2014-100	66	68				1	189			1	3		6	2	1		2		2							1			
GLW31D-69	UVic2014-101	68	70		1		1	185			2	1		4	1							1	1							
GLW31D-71	UVic2014-102	70	72					163	1			2		8		1				1										
GLW31D-73	UVic2014-103	72	74		1			162			1	2		5	2					3		3		1						
GLW31D-75	UVic2014-104	74	76					186	1			4		13	1	1				1		8						1		
GLW31D-77	UVic2015-202	76	78		1			173		1	1			6									1							
GLW31D-79	UVic2014-106	78	80					184			2	2		8	1	1								1						
GLW31D-81	UVic2014-107	80	82					162			2	3		12	2					2		2								
GLW31D-83	UVic2014-108	82	84				3	189		1	1	1		6		1		1				3					1			
GLW31D-85	UVic2014-109	84	86					201	1		1			2	2															
GLW31D-87	UVic2014-110	86	88					164			1	1		8		1						1	1		1			1		
GLW31D-89	UVic2014-111	88	90		1			155	1			2		8	1	1						1		1						
GLW31D-91	UVic2014-112	90	92		1			185	2	1	3	2		6								5	1							1
GLW31D-93	UVic2014-113	92	94					184			3	1		4	1					1				1			1			
GLW31D-95	UVic2014-114	94	96				1	159	1		5	4		6	1							2	1							
GLW31D-97	UVic2014-115	96	98					178		1	3	1	1	12							1		1							
GLW31D-99	UVic2014-116	98	100				1	140	2		6	4		9		1						1	1				1			
GLW31D-101	UVic2014-117	100	102				1	178	2	2	4	1		6	2	1		1		2		4	1	1						
GLW31D-103	UVic2014-118	102	104	1			2	182		1	3			1						1				1						
GLW31D-105	UVic2014-119	104	106					184	1		1	4		12	4							5								
GLW31D-107	UVic2014-120	106	108		2			196	2	1	1	1		8	1	1				3		6	1	1						
GLW31D-109	UVic2014-121	108	110				2	175	2		1	4		5	2									1						
GLW31D-111	UVic2014-122	110	112		2			261				7	1	12	1	3				3		2	1							
GLW31D-113	UVic2014-123	112	114					175	2		3	2		2	1	2				1		3		1						
GLW31D-115	UVic2014-124	114	116					193			2	3		6						1		1	1							

Sample No.	Passifloraceae	*Altingia*	Rutaceae	*Clausena*	*Liquidambar*	Magnoliaceae	Oleaceae	*Aglaia*	*Spathodea*	*Bombax*	Dipterocarpaceae	*Zanthoxylum*	Piperaceae	Anacardiaceae	*Rhus*	Araliaceae	Menispermaceae	Meliaceae	*Myrica*	Hamamelidaceae	*Euphorbia*	*Mallotus*	*Alchornea*	Apocynaceae	Myrtaceae	Samydaceae	*Eucalyptus*	Elaeocarpaceae	*Garcinia*	*Symplocos*	Rosiaceae	Sterculiaceae	Berberidaceae	Lauraceae
GLW31D-59		1			1										2				3						1								1	
GLW31D-61		1	1		3									1	1				1	1													1	
GLW31D-63			1		2	1																												
GLW31D-65					1																												1	
GLW31D-67		1			2														1		2												1	
GLW31D-69			1		1																												1	
GLW31D-71		3			3										3				4	2	1	1											1	
GLW31D-73			1		2	1														3	1												2	
GLW31D-75			1		1		1											1	1		2													
GLW31D-77		1			2										2			1	1	2	1								1		1		1	
GLW31D-79		1			3								1						1	2	2													
GLW31D-81			2		2						2				1				1			1												
GLW31D-83		1			2								1						1	4														
GLW31D-85					5														2														2	
GLW31D-87					3								4						3	1													1	
GLW31D-89		6	1		7									2	1				3		1													
GLW31D-91		2	1		2	1										1				3	2			1										
GLW31D-93		2	1										1		4						1													
GLW31D-95		1	1		6								1		2				1	2	1													
GLW31D-97		1			7						1									1				1									1	
GLW31D-99	1	1	1		1		1									1		1	4														1	
GLW31D-101		2	1		2										4				2	1	1							1						
GLW31D-103					4	1																											2	
GLW31D-105		3																		3	1													
GLW31D-107		4	2	1	2											2			1	3	1			2	1	1						2	1
GLW31D-109		1	1		5		1						2		3					1			1										3	
GLW31D-111		2			3								2						1	1														
GLW31D-113		2	1		2								1		2	1			1	1	1													
GLW31D-115		2	2		1										5				1	1													1	

Sample No.	Palmae	*Arenga*	*Phyllanthus*	*Ardusua*	Loranthaceae	Moraceae	Clusiaceae	*Avicennia marina*	*Aegiceras corniculatum*	*Rhizophora* -a	*Rhizophora* -b	*Rhizophora mucronata*	*Excoecaria*	*Browlowia tersa*	*Pandanus*	Combretaceae	*Casuarina*	Poaceae	Cucurbitaceae	Solanaceae	Saururaceae	Celastraceae	*Manocelastrus*	*Rubiaceae*	*Coelospermum*	Balanophoraceae	Brassicaceae	Acanthaceae	Convolvulaceae	Verbenaceae	*Gmelina*	Malvaceae	Umbelliferae	Thymelaeaceae
GLW31D-59	1		1						3									5						7			1		1	1				
GLW31D-61																		6												2				
GLW31D-63									1									3						2						1				
GLW31D-65																1		10						4			1							
GLW31D-67																		7						1						1				1
GLW31D-69										2								9									1			5				
GLW31D-71	3					1				2								5									3							
GLW31D-73									3	1								14						2						1				
GLW31D-75	1								1	1				1				11						1										
GLW31D-77	2																	6						1			1	1		2				1
GLW31D-79	3				1							1			1	1		6			1			1						1				
GLW31D-81																1		12						1						1			1	1
GLW31D-83																		7						6			1			2				
GLW31D-85	1																	4						3				1		1				
GLW31D-87	2					1												8						2			1			2				
GLW31D-89										1								9						2			2			1				
GLW31D-91						1										1		7				1								3				
GLW31D-93	1																	7						1									1	
GLW31D-95								1		2	1					1		13				1							1	5				
GLW31D-97	2								1									5												2				
GLW31D-99	1								1								1	6						1			1			1	1			
GLW31D-101	1	1								1								7						2						2				3
GLW31D-103		2																11					2				1			1				
GLW31D-105																		4						1						1				
GLW31D-107				1						1		1						9			1			3										
GLW31D-109										1								5						5	1									
GLW31D-111	2	1	1												1	1		18						2	1		1							1
GLW31D-113			3														1	16						4						2				1
GLW31D-115	1								2									8						4			2							

Sample No.	Valeriavaceae	Nepenthaceae	*Peliosanthes*	Eriocaulaceae	Gesneriaceae	Caryophyllaceae	Fabaceae	*Plumbago*	*Artemisia*	Compositae	Chenopodiaceae	Cyperaceae	*Typha*	*Thalictrum*	Potamogetonaceae	Alismataceae	Iridaceae	Aceaceae	*Lily*	*Nymphoides*	Polypodiaceae-Smooth	Polypodiaceae-Boss	Gleicheniaceae	*Cyathea*	*Pteris*	*Lygodium*	Osmundaceae	*Lycopodium*	*Hymenophyllum*	Parkeriaceae	*Pteridium*	*Acrostichum*	*Cibotium*	Vittariaceae
GLW31D-59									7		1	53			11				1		15	6	13	11	4	3		2	8					
GLW31D-61									2	2		12			1						24	6	14	10	8		6	2	2		10	1		2
GLW31D-63					1					1	1	14			1						26	15	10	7	12	3			2		3	1		2
GLW31D-65									3		1	11	2		2			1			14	3	12	5	4	2	3							2
GLW31D-67									4	1	1	9	1		2						27	12	7	13	4	5	1	3	1		1		1	4
GLW31D-69									2	1		16						1	2		21	10	11	12	1	2	3		2	1	5			2
GLW31D-71						1			2			10						1	2		26	10	3	17	5	1	1		2	1	2			
GLW31D-73									6	1	1	17	1		1			1	1		22	5	14	19	4	2	1		1		2			1
GLW31D-75					1				8		3	6	1		2				1		24	12	4	14	8	6			1					
GLW31D-77							2		3			11	1		1						26	3	22	17	2	5		2	3		4			
GLW31D-79		4							5			10	1					3	1		23	3	8	18	9	1		1	1		1			4
GLW31D-81			1	2					7	9		14		1	2			1			15	4	9	5	5	2	1	0	1		2		3	
GLW31D-83					2				4	3		24		1							27	5	8	11		1					1			1
GLW31D-85	1											16			1			1			19	4	2	23	9	1	2		6		2			
GLW31D-87									4	4		17	1					1			20	9	13	20	6	2	5		11		1			
GLW31D-89							1		4	3	1	18	4								18	3	7	16	1	2			3		4		2	2
GLW31D-91									7	3	2	9	2	1				1			20	4	8	20	4	1	1		1					
GLW31D-93									1	2		8						2			23	7	13	8	3		3	1	5				1	2
GLW31D-95									5	2	1	6	1								26	3	15	7	5	1	2		6	1	1		2	3
GLW31D-97									4	4	1	14	1		2	1		1			22	7	17	11	6		3	1	5	1				
GLW31D-99									7	2		12			1			1			35	5	16	7	4	5	4		3	1	2			2
GLW31D-101							1		5	1	1	23	1					5	2		24	12	10	20	14		1	1	4		2			2
GLW31D-103							2		7	1		17						3	2		43	3	10	17	7		2		4		1		2	
GLW31D-105									10	3	1	8				1					16	10	7	15	2	4			1				1	2
GLW31D-107	1								4			10	1					1			21	3	10	13		1			2		1		1	3
GLW31D-109							1		3			15	1		2			2			13	4	8	8	4	1	3		2		8			
GLW31D-111	2								12	4	2	26	2		1						27	7	14	5	11	6		1	6		3		3	
GLW31D-113	2						1		5		3	10	2		1			3			22	7	4	7	7	2			2		10	1	3	2
GLW31D-115									7	2	3	15	1					1			19	6	15	13	4	3		1	1				1	

Sample No.	Ophioglossaceae	Angiopteridaceae	*Ptyrogramma*	*Onychium*	*Athyrium*	*Dryopteris*	*Monogramma*	Hemionitidaceae	*Selaginella*	*Spiny spherea*	Unknown trilete	*Concentricystes*	*Zygnema*	Unidentified	Total	Exotra *Lycopodium* (18584 grains/tablet)	Dry weight(g)
GLW31D-59									3		1	3			366	797	4.1
GLW31D-61									1			1			315	1053	3.7
GLW31D-63			1						2					5	328	919	4.2
GLW31D-65												2		5	327	915	4.0
GLW31D-67			4									1		6	333	1149	4.0
GLW31D-69		1									1	1		5	315	1233	4.0
GLW31D-71		1	1							1		4		8	307	1038	4.3
GLW31D-73		1								4		1		5	322	986	4.1
GLW31D-75								1				2	1	5	339	1111	4.1
GLW31D-77									1	1	1	2	1	9	327	899	4.8
GLW31D-79										1			1	3	323	1255	3.9
GLW31D-81		1						1	2		1	1		7	308	1479	3.8
GLW31D-83									1			1		4	326	1283	3.7
GLW31D-85									1			2		9	325	1599	3.3
GLW31D-87												1	3	7	332	1429	3.7
GLW31D-89									2	5		3		5	311	1299	3.6
GLW31D-91												1		7	325	925	3.9
GLW31D-93		1			1				3	1		1	1	7	309	931	4.2
GLW31D-95									2		1	2		1	313	1127	4.1
GLW31D-97		1							3			2		6	333	1279	3.7
GLW31D-99		1				1							1	3	304	1269	4.1
GLW31D-101		1							4	6		4		14	395	1624	3.7
GLW31D-103		1							1			4		6	349	977	4.0
GLW31D-105												1	3	4	313	615	4.2
GLW31D-107		1	1							1		3	1	4	346	1167	4.1
GLW31D-109		1												9	307	833	4.4
GLW31D-111		3							3	6		4		6	485	1910	3.8
GLW31D-113							3	1	1	2		3	2	7	344	1090	3.7
GLW31D-115		2							1			1		8	341	1237	3.5

Sample No.	UVic Lab. No.	Top depth (cm)	Bottom depth (cm)	*Cedrus*	Cupressaceae	Taxodiaceae	*Picea*	*Pinus*	*Dacrycarpus*	*Podocarpus*	*Dacrydium*	*Alnus*	*Celis*	*Quercus* (Evergreen)	*Quercus* (Deciduous)	*Juglans*	*Carpinus*	*Fagus*	*Salex*	*Ulmus*	*Tilia*	*Castanopsis*	*Carya*	*Ilex*	*Clerodendrum*	Icacinaceae	*Lonicera*	Sapindaceae	Elaeagnaceae	*Helicia*
GLW31D-117	UVic2014-125	116	118					150	2		3		1	6	2	2				1		13					1			
GLW31D-119	UVic2014-126	118	120					174		1		2		8								2								
GLW31D-121	UVic2014-127	120	122					182	1	2	3	8		11								3								
GLW31D-123	UVic2014-128	122	124			1	1	203	1		1	4		8	2							7	2	1						
GLW31D-125	UVic2014-129	124	126				1	158			1	2		5	2	1						1								
GLW31D-127	UVic2014-130	126	128					172	2		3	2		5							1	1	1	1						
GLW31D-129	UVic2014-131	128	130		1		1	161	1			4		5	2	1						3	1	1						
GLW31D-131	UVic2014-132	130	132				4	233		1	1			14	3							11								
GLW31D-133	UVic2014-133	132	134		3			154			3	5		5		5						4	1							
GLW31D-135	UVic2014-134	134	136		1			181	1			4		9						1		2	1							
GLW31D-137	UVic2014-135	136	138		4	1		206	1		1	1		8						1	2	1								
GLW31D-139	UVic2014-136	138	140		1			200	1		2	3		6	4	1						3					1			
GLW31D-141	UVic2014-137	140	142		1		1	197		1	6	5		7						1		4	1							
GLW31D-143	UVic2014-138	142	144					217			3			9	1	3				2		1		2			1			
GLW31D-145	UVic2014-139	144	146					195						11	3					1		8						2		
GLW31D-147	UVic2014-140	146	148		4			159			3	6		10						1		2								
GLW31D-149	UVic2014-141	148	150			1		223	2			5		7		2				1		1						1		
GLW31D-151	UVic2014-142	150	152					226				1		6	1					1		3	5	1						1
GLW31D-153	UVic2014-143	152	154		2			211	1		1			6		3				1		5				1				
GLW31D-155	UVic2014-144	154	156		3			192	1		8	2		13						1		5	1			1				
GLW31D-157	UVic2014-145	156	158		2			191			6	3		12	3	4				1		4		1						
GLW31D-159	UVic2014-146	158	160		1			243	3	1	4	1		13	2	2				2		3		1		1				
GLW31D-161	UVic2015-203	160	162		4	2		207	3	2		2		14	1					1		1		1				1		
GLW31D-163	UVic2014-148	162	164				1	198	4			2		11	2	1		1			1	1						1		
GLW31D-165	UVic2014-149	164	166		1		2	175		1	1	3		14	5					1		2	1	4						
GLW31D-167	UVic2014-150	166	168		1			212	1	5	4	3		12		8				1		2	1	1						
GLW31D-169	UVic2014-151	168	170		3		1	227	1		3	5		18		1				1		3	3	1						
GLW31D-171	UVic2014-152	170	172					242	2	3	3	4		23	1	2		1						2				1		
GLW31D-173	UVic2014-153	172	174					213		1	2	1		20	1	1		1			1	3		2						

Sample No.	Passifloraceae	*Altingia*	Rutaceae	*Clausena*	*Liquidambar*	Magnoliaceae	Oleaceae	*Aglaia*	*Spathodea*	*Bombax*	Dipterocarpaceae	*Zanthoxylum*	Piperaceae	Anacardiaceae	*Rhus*	Araliaceae	Menispermaceae	Meliaceae	*Myrica*	Hamamelidaceae	*Euphorbia*	*Mallotus*	*Alchornea*	Apocynaceae	Myrtaceae	Samydaceae	*Eucalyptus*	Elaeocarpaceae	*Garcinia*	*Symplocos*	Rosiaceae	Sterculiaceae	Berberidaceae	Lauraceae
GLW31D-117		1	2		3								1		2			1		3	2				1								3	
GLW31D-119	1	1			1									3	1				2	3														
GLW31D-121		1			6										2					3	1												1	
GLW31D-123		2			1										3				1		3												1	
GLW31D-125					1										4					4				1	1									
GLW31D-127		1	3		1								1		4				2	2	2				1									
GLW31D-129		1			1														2	1	3			1									1	
GLW31D-131		5	2		2								1	6	3				4	5	6			1	1									
GLW31D-133			3		2		2						2	1	2				2	4	10			4									1	
GLW31D-135					3								1	1					1	2	8			1									2	
GLW31D-137			1		5										2	1				1				1	1								2	
GLW31D-139					1										3				1	3													1	
GLW31D-141		8												5					1	4	2								1					
GLW31D-143		1	2		3		1		2				1		2			1	1	2	1												2	1
GLW31D-145					4		1								3					1	2							1					1	
GLW31D-147			2		7								2		2					3				3	1								3	10
GLW31D-149		1			1										3				1	2													3	
GLW31D-151		2	1		2															3	1												1	
GLW31D-153			1		4										2				3	1	2			1									2	
GLW31D-155					2										4				1	2	1			1										
GLW31D-157		2	2		2		2								2				1	1	1	1		3				1					5	
GLW31D-159					2		1								1	1					2			1										
GLW31D-161					2		1								1						3			1				1						
GLW31D-163					4										1						3			6										1
GLW31D-165		2			1	1	1		1					1		1		1	3	3				1										1
GLW31D-167			1												5				1	3	2			5				1						
GLW31D-169					3		1								3	1			2	1	3		1		1								1	
GLW31D-171			1		4		2								1				2	1	1			1										1
GLW31D-173					1									3	2				3	3	3			1				1					1	1

Sample No.	Palmae	*Arenga*	*Phyllanthus*	*Ardusua*	Loranthaceae	Moraceae	Clusiaceae	*Avicennia marina*	*Aegiceras corniculatum*	*Rhizophora* -a	*Rhizophora* -b	*Rhizophora mucronata*	*Excoecaria*	*Browlowia tersa*	*Pandanus*	Combretaceae	*Casuarina*	Poaceae	Cucurbitaceae	Solanaceae	Saururaceae	Celastraceae	*Manocelastrus*	*Rubiaceae*	*Coelospermum*	Balanophoraceae	Brassicaceae	Acanthaceae	Convolvulaceae	Verbenaceae	*Gmelina*	Malvaceae	Umbelliferae	Thymelaeaceae
GLW31D-117			2													1		7						3			1			2				
GLW31D-119	3								2				1					9				1		3						1				1
GLW31D-121	1															1		9						1						4				
GLW31D-123	2									3								9						3			1			1				
GLW31D-125	1		1							2					2	1		12						1						1				
GLW31D-127		1							4									16			1			9										
GLW31D-129			1												1			8						4			1			1				
GLW31D-131	4	2							1							1		12						4			1	2	1	5				
GLW31D-133		2								2								8			1			2						1				1
GLW31D-135																		7			2			4						1				2
GLW31D-137	1					1										1		10			1			2						2				2
GLW31D-139		1																10			1			4						8				
GLW31D-141	1																	7						1			3		1	1				
GLW31D-143	2					1			2							3		12						4			4			4				
GLW31D-145									1							1		5			1			4			1			1				
GLW31D-147						2				2			3					13						3			1			2				
GLW31D-149																1		16						2						4				
GLW31D-151																		2				1		3						2				
GLW31D-153						1												10						7			1			3				
GLW31D-155					1													6						3			1			3				1
GLW31D-157						1	1			1								19			2			1			1			1				
GLW31D-159										2						1		6			2							2						
GLW31D-161																		7						1						5				
GLW31D-163																1		10			1	1		1			2	1		6				
GLW31D-165									4								1	19				1		4			1	1						
GLW31D-167	2		1		2	2										1		15						3						5				2
GLW31D-169	1					1					1						1	16						4						2				
GLW31D-171											1					1		17			1			2			2				1			
GLW31D-173									1		2							26						1				1			2			1

Sample No.	Valeriavaceae	Nepenthaceae	*Peliosanthes*	Eriocaulaceae	Gesneriaceae	Caryophyllaceae	Fabaceae	*Plumbago*	*Artemisia*	Compositae	Chenopodiaceae	Cyperaceae	*Typha*	*Thalictrum*	Potamogetonaceae	Alismataceae	Iridaceae	Aceaceae	*Lily*	*Nymphoides*	Polypodiaceae-Smooth	Polypodiaceae-Boss	Gleicheniaceae	*Cyathea*	*Pteris*	*Lygodium*	Osmundaceae	*Lycopodium*	*Hymenophyllum*	Parkeriaceae	*Pteridium*	*Acrostichum*	*Cibotium*	Vittariaceae
GLW31D-117					2				4			20						1			16	3	15	9	7	1	3	1	3		10		2	
GLW31D-119									11	1		20	2				1	1			12	8	7	13	3	4			2		4		1	
GLW31D-121									4	3	1	15			1						18	3	14	5	7	2	1				2		6	2
GLW31D-123									6	1	1	12	1	2							11	4	16	4	6	3	1	2			3		4	2
GLW31D-125									6			7	2	1	2			1			20	6	12	14	2	2	4		5	1	2		4	
GLW31D-127									3	2	1	17	2					3			8	3	5	9	6		1	1	2	1	1		2	
GLW31D-129							1		4	1	3	11	1					2			16	6	11	6	2	2	4	1	3		1		5	1
GLW31D-131	1								10	3	2	20	4					3			27	11	14	18	5	6	2	1	3	1	3		2	1
GLW31D-133	1								6	3	8	11	3		1			2			22	6	11	8	5		3	2	2	1	4		1	3
GLW31D-135	2								9		1	21						2			32	4	23	12			5	1	1	1	2		5	2
GLW31D-137				1					6	2		19	3		1			2			15	11	8	7	1		1	1	1				1	1
GLW31D-139				1					4	2	4	13						3			11	12	16	10	2		4	2			1		2	3
GLW31D-141									8	1	1	9	1								9	2	10	19	1	2			4		2		3	
GLW31D-143							2		9	5		21	2		2			3			10	3	16	15			3	1			4		1	
GLW31D-145	2						1			5	7	14	1		3			9	4		17	3	7	10	2	1	2		2		3	1	2	
GLW31D-147							1		8	2	2	19	7					2			23	8	9	5	1							1	5	
GLW31D-149									5	2		11	2		2			1	1		16	7	4	6	4	2								
GLW31D-151					1				7			5			1			2			15	2	4	17	8								1	3
GLW31D-153									10	3		25	1					1			18	10	5	5	5	3			1	1	9		1	
GLW31D-155							1		3	2	3	16	3					2			18	7	2	12	3				3		2		1	2
GLW31D-157							1		12	5		22	2					1			14	8	10	4	3	2	3		6				3	
GLW31D-159									8	1	2	15	1					1	3		20	7	26	3	2	1	4		2		1	1		
GLW31D-161									8	4		13	3								20	5	11	9	6	6	3				4		3	2
GLW31D-163							1		6		1	21	4					1			18	4	9	7	7	1			1	1				1
GLW31D-165					1				9	3	1	30	2					3			14	1	13	6	1	1	1		1		10			4
GLW31D-167	1								12	3		22	4					1			12	2	15	8	1		1		1				1	
GLW31D-169									8	2	1	20	8								14	4	8	10	4	1	4	1	1		2		2	
GLW31D-171							1		9	1	2	9	4								22	5	12	14	2	1	5						1	2
GLW31D-173									8		2	21	4						3		23	5	16	9	4	8	2		1		2			2

Sample No.	Ophioglossaceae	Angiopteridaceae	*Ptyrogramma*	*Onychium*	*Athyrium*	*Dryopteris*	*Monogramma*	Hemionitidaceae	*Selaginella*	*Spiny spherea*	Unknown trilete	*Concentricystes*	*Zygnema*	Unidentified	Total	Exotra *Lycopodium* (18584 grains/tablet)	Dry weight(g)
GLW31D-117							1		1			2	1	8	326	1163	3.9
GLW31D-119	1	1										1		7	320	1059	4.1
GLW31D-121							1		2			3	1	11	342	1105	3.9
GLW31D-123									3					6	349	807	3.9
GLW31D-125							1		1	2		1	1	4	304	894	4.3
GLW31D-127		1					1		2	2		1		3	313	747	4.2
GLW31D-129		4						1				3	1	10	307	689	4.0
GLW31D-131		1							2	3		7	3	8	497	1370	3.9
GLW31D-133		2							2	11		1	1	5	355	854	4.0
GLW31D-135		2							1	2		2	1	7	373	979	4.2
GLW31D-137		2							2	4		4		7	360	868	3.9
GLW31D-139									2	4		2		6	359	929	4.0
GLW31D-141									1			2	1	4	339	565	3.9
GLW31D-143							1			8		3	2	7	409	661	4.1
GLW31D-145									1	4		3		4	355	723	4.3
GLW31D-147							1					2		3	343	542	4.1
GLW31D-149							1		2			2		5	350	687	4.1
GLW31D-151												2	3	1	335	672	4.2
GLW31D-153		1							3			3		2	376	748	4.1
GLW31D-155												2	1	6	342	887	4.0
GLW31D-157		1	1				1		1			7		8	392	785	4.0
GLW31D-159		1	1						1			3		11	413	635	4.3
GLW31D-161									2			2		6	368	737	4.2
GLW31D-163									5			4	2	7	362	775	4.1
GLW31D-165												1	1	2	363	667	4.3
GLW31D-167									2			1	2	10	401	604	4.1
GLW31D-169		1							2			2	1	9	415	729	4.1
GLW31D-171		1		1					3			3	1	9	431	598	4.3
GLW31D-173												1		11	421	774	4.1

Sample No.	UVic Lab. No.	Top depth (cm)	Bottom depth (cm)	*Cedrus*	Cupressaceae	Taxodiaceae	*Picea*	*Pinus*	*Dacrycarpus*	*Podocarpus*	*Dacrydium*	*Alnus*	*Celis*	*Quercus* (Evergreen)	*Quercus* (Deciduous)	*Juglans*	*Carpinus*	*Fagus*	*Salex*	*Ulmus*	*Tilia*	*Castanopsis*	*Carya*	*Ilex*	*Clerodendrum*	Icacinaceae	*Lonicera*	Sapindaceae	Elaeagnaceae	*Helicia*
GLW31D-175	UVic2014-154	174	176					155		1	3	5		12	5	3		1				4	3				1			
GLW31D-177	UVic2014-155	176	178		1			202				3		17	2			2		2				1						
GLW31D-179	UVic2014-156	178	180					166	2	2				7	4					1		1							1	
GLW31D-181	UVic2014-157	180	182			1		223	2			2		10	1					2		1							1	
GLW31D-183	UVic2014-158	182	184		2			272	3	1	1	4		11	1	4				1		2		1						
GLW31D-185	UVic2014-159	184	186		1			203		2	1			14		1						14		1						
GLW31D-187	UVic2014-160	186	188		1			186	2	1	1	6		5	1	2														
GLW31D-189	UVic2014-161	188	190		1		1	185	4		2	9		7						1		2	1							
GLW31D-191	UVic2014-162	190	192				2	201			1	10		9		2		1				3	2	1						
GLW31D-193	UVic2014-163	192	194					186		8	5	3		5	5					1		1	1							
GLW31D-195	UVic2014-164	194	196				1	214	4		2	3		7		1				1										
GLW31D-197	UVic2014-278	196	198		4			233	4		4	7		6						1		3		1		1				1
GLW31D-199	UVic2014-166	198	200		4			179				2		12	1	1				1			1							
GLW31D-201	UVic2014-167	200	202		4		1	185	2	1	6	6		7	1	1				2		3	1					1		
GLW31D-203	UVic2014-168	202	204					186	1	1		8		12	2					3		3		2						
GLW31D-205	UVic2014-169	204	206		1		2	226	1	7	4	1		8						2		2	1							
GLW31D-207	UVic2014-170	206	208		2	1		189			1	4	1	10	1					1	1	2								
GLW31D-209	UVic2014-171	208	210		1			220	3		2	2		5	2	1				1		1	1							
GLW31D-211	UVic2014-172	210	212		1			243		1	1	4		14	1	2				1		1	1							
GLW31D-213	UVic2014-173	212	214					218		4		5		14		1				3										
GLW31D-215	UVic2014-174	214	216		2			181	2	3	2	2		20	3	1						1								
GLW31D-217	UVic2014-175	216	218		1			218	1	3	1	2		8	1	1				2		5								
GLW31D-219	UVic2014-176	218	220		3			194	2			14		9	1	1				3		2								
GLW31D-221	UVic2014-177	220	222		3			192	1	3		6		19	2	2				1		2								
GLW31D-223-225	UVic2014-179	222	226		4		3	202		5	5			8	3	2		1		1										
GLW31D-227	UVic2014-180	226	228	1	4			204	2	1	3	5		16	1					2		3								
GLW31D-229	UVic2014-181	228	230		1			174		1	5	3		7	4	1				1		1								
GLW31D-231	UVic2014-182	230	232		7			195			3	5		14		1						2		1						1
GLW31D-233	UVic2014-183	232	234		5		1	178		2	3	5	1	8	8	2				2		3					2			

Sample No.	Passifloraceae	*Altingia*	Rutaceae	*Clausena*	*Liquidambar*	Magnoliaceae	Oleaceae	*Aglaia*	*Spathodea*	*Bombax*	Dipterocarpaceae	*Zanthoxylum*	Piperaceae	Anacardiaceae	*Rhus*	Araliaceae	Menispermaceae	Meliaceae	*Myrica*	Hamamelidaceae	*Euphorbia*	*Mallotus*	*Alchornea*	Apocynaceae	Myrtaceae	Samydaceae	*Eucalyptus*	Elaeocarpaceae	*Garcinia*	*Symplocos*	Rosiaceae	Sterculiaceae	Berberidaceae	Lauraceae
GLW31D-175			1											2		3				2														
GLW31D-177		1	1											1	1				2		1			1	1									
GLW31D-179					1		1									1					1			3										1
GLW31D-181													1		1				1		2			1	1				2				1	
GLW31D-183			1		6									2				1	2	5	2			6	1								2	2
GLW31D-185		1												1					1	3														
GLW31D-187		1			3										5	1				3	3			2				1					2	
GLW31D-189			4		3		3								2	1			1	2					1									
GLW31D-191			1		1									1	4					3	1			2										
GLW31D-193		4												3					2	3														
GLW31D-195															2					1	2			2									2	
GLW31D-197					2		1								5					3	3							1						
GLW31D-199		4			1							1	1		2			1	2	1				1										
GLW31D-201			2		2	1	3						2		3				3	1	1												2	
GLW31D-203			3		2								3		3				6	3	1							4					3	
GLW31D-205		1											1	1					1	3	1													
GLW31D-207			2		2											1			2		1	1						1						
GLW31D-209		2			2								1	2	2				2														1	
GLW31D-211			1		2	1	1								3				1	3	1													
GLW31D-213			1		4										1				2	1													7	
GLW31D-215		5					1							8	1				2	2														
GLW31D-217		3	2		4										5	1			2	2	1				1								1	
GLW31D-219		1	2		2		1							2	3				5	3	2			2									4	
GLW31D-221			2		6									1	2					2			1										4	
GLW31D-223-225		1			2	1						1		1	2					2				1									1	
GLW31D-227			1		2		1								2					5	1												1	
GLW31D-229			1		2				1			1		1	1	2			3	1					1									
GLW31D-231			1		2											2		1	2	3				2									1	
GLW31D-233		4	1										1	1	3				1	6	1	1		2									1	

Sample No.	Palmae	*Arenga*	*Phyllanthus*	*Ardusua*	Loranthaceae	Moraceae	Clusiaceae	*Avicennia marina*	*Aegiceras corniculatum*	*Rhizophora* -a	*Rhizophora* -b	*Rhizophora mucronata*	*Excoecaria*	*Browlowia tersa*	*Pandanus*	Combretaceae	*Casuarina*	Poaceae	Cucurbitaceae	Solanaceae	Saururaceae	Celastraceae	*Manocelastrus*	*Rubiaceae*	*Coelospermum*	Balanophoraceae	Brassicaceae	Acanthaceae	Convolvulaceae	Verbenaceae	*Gmelina*	Malvaceae	Umbelliferae	Thymelaeaceae
GLW31D-175									1							1		5						4			2		1	2				
GLW31D-177						1												24						1						2				
GLW31D-179																		14						5						5				
GLW31D-181	2									2								20				1		3						4				
GLW31D-183										1						1		18				4		5			1		2	1				1
GLW31D-185																		7						6						2				1
GLW31D-187																		16						4					1	4				2
GLW31D-189									1	1								14						4						4				2
GLW31D-191						1					1						1	7									2	1		6				1
GLW31D-193	1		1						1									4						7			1			2				
GLW31D-195					2	1			1							2	1	21				2		1						3				
GLW31D-197			1			1										2		14						1		1	3			3				
GLW31D-199																		19			1			10						1				
GLW31D-201					3					1								19				2		7			1			5				
GLW31D-203						1			3	3						1	1	19				1		2			1			3				
GLW31D-205	1																	4						3						2				
GLW31D-207																		22						4			2							
GLW31D-209						1											1	11						2						2				1
GLW31D-211																	1	25						5			1							
GLW31D-213						1					1					1		8				1		4						2				
GLW31D-215										1						2		8	1					5			1							
GLW31D-217																		14				1								2				
GLW31D-219			1				1											14										1						
GLW31D-221											1					1		23						2						2				2
GLW31D-223-225						1												8				1		5			2	1						
GLW31D-227	3															2		14												3				
GLW31D-229									1									8						6						1				1
GLW31D-231	1					1				1							2	31						3						3				
GLW31D-233	1								1								1	19	1					10			1							

Sample No.	Valeriavaceae	Nepenthaceae	*Peliosanthes*	Eriocaulaceae	Gesneriaceae	Caryophyllaceae	Fabaceae	*Plumbago*	*Artemisia*	Compositae	Chenopodiaceae	Cyperaceae	*Typha*	*Thalictrum*	Potamogetonaceae	Alismataceae	Iridaceae	Aceaceae	*Lily*	*Nymphoides*	Polypodiaceae-Smooth	Polypodiaceae-Boss	Gleicheniaceae	*Cyathea*	*Pteris*	*Lygodium*	Osmundaceae	*Lycopodium*	*Hymenophyllum*	Parkeriaceae	*Pteridium*	*Acrostichum*	*Cibotium*	Vittariaceae
GLW31D-175									7	3	1	22	4		1						14	2	6	7	5	4	1							
GLW31D-177									22			11	9								16	2	11	6	3	3			4		1	1		1
GLW31D-179							2		11	1	2	27	6								17	6	4	4		1			6		10		1	
GLW31D-181									3	3	1	29	4								23	2	14	7	8	2	5		2	1		1	2	
GLW31D-183									8		2	18	5		1						23	6	14	7	1	5	6	1	3					1
GLW31D-185									4	1	2	10	3		2						8	1	7	6	1	2								
GLW31D-187									4		1	21	2					1			10	1	9	10	5	1	5	1		1	2			2
GLW31D-189									8	3	1	11	4		1						11	5	7	9		1	2	2	3		2			1
GLW31D-191					7				11			13	5								10	4	9	2	1		2	1	1		1			3
GLW31D-193									7	1		13	1			1					10		6	6	4	2			1		1			
GLW31D-195									3	2	2	20	2					1			13	6	6	2		2	1	1			1			
GLW31D-197	1						2		10	3		19									13	12	8	4	1		3	2		1	1	1	1	2
GLW31D-199									7	5		19	1						2		6	2	8	4			1		3		1		1	1
GLW31D-201	1						1		25	3	4	15	3		6		2	1	4		24	4	8	2		1	2		1		1			
GLW31D-203	1						2		17	2	1	19	2		3				2		21	9	5	10	3		1	1	1	1	2		1	
GLW31D-205	1								5	2		10									7	2	1	6	3	2			1		2			
GLW31D-207									10	1	1	15			4				1		18	3	6	8	1		1		1		2			
GLW31D-209									17	1	1	27									14	8	13	3	1		2							
GLW31D-211									16	1	1	20	1					1			21	7	7	5	3	1	3							
GLW31D-213							2		19	7	1	18	3	2				1			21	3	1	4		3	1	1		2				
GLW31D-215									13			19	1		1						16	2	2				1		1		1			2
GLW31D-217					1	1	1		18	5	1	22	3					1			20	6	19	7	3		1	2		1	1			1
GLW31D-219							1		18	2	1	31									13	6	9	3	3		2		1	1	4			1
GLW31D-221					1				24	4	2	20			1						18	2	1	5	2		1		2	1	1		3	1
GLW31D-223-225									9	5	1	16	2		1						11	6	8	3	2						2			3
GLW31D-227									20	3		27	1		2			1			26	5	7	10	3	1	7		1	2	1			
GLW31D-229									16	5	1	18	1					1			17	2	6	5	4	1	3	1			1			1
GLW31D-231							1		12	5	1	16	2								20	7	6	4	3		6		3	1			1	
GLW31D-233							2		23	5	1	26	1				1				23	5	5	17	4	2	3		1				1	

Sample No.	Ophioglossaceae	Angiopteridaceae	*Ptyrogramma*	*Onychium*	*Athyrium*	*Dryopteris*	*Monogramma*	Hemionitidaceae	*Selaginella*	*Spiny spherea*	Unknown trilete	*Concentricystes*	*Zygnema*	Unidentified	Total	Exotra *Lycopodium* (18584 grains/tablet)	Dry weight(g)
GLW31D-175	2								1			2	1	5	305	521	4.5
GLW31D-177									4			3		6	370	592	4.1
GLW31D-179		1										3	1	11	330	561	4.2
GLW31D-181		1					1					3	1	7	405	608	4.2
GLW31D-183												2		10	480	682	4.2
GLW31D-185														2	308	507	4.3
GLW31D-187		1					1		2			1		5	339	640	4.3
GLW31D-189							2					2		7	338	606	4.1
GLW31D-191									1					15	351	467	4.3
GLW31D-193									1					2	300	418	4.2
GLW31D-195							1		3			3		9	354	585	4.5
GLW31D-197		1	2						1			2	1	15	412	635	4.4
GLW31D-199										5		2		10	324	491	4.2
GLW31D-201			1						2			3		15	408	644	4.4
GLW31D-203			1										1	8	395	570	4.5
GLW31D-205												2	1	3	321	414	4.4
GLW31D-207		1											1	11	336	655	4.7
GLW31D-209			1						2					4	363	676	4.1
GLW31D-211		1							2			3		7	415	820	4.6
GLW31D-213									3			1		7	379	709	4.7
GLW31D-215									1			4		7	325	593	4.2
GLW31D-217			1						4			3	1	12	417	916	4.5
GLW31D-219			1									1		7	378	621	4.6
GLW31D-221									1				1	8	379	802	4.6
GLW31D-223-225									2			1	1	5	342	570	4.4
GLW31D-227									1			1		4	400	830	4.2
GLW31D-229									2			5		3	322	613	4.3
GLW31D-231									2			3		9	387	816	4.2
GLW31D-233												1	2	3	402	738	4.3

Appendix E
Data of dinoflatellate cysts from the sediment core GLW31D.

Sample No.	Uvic Lab. No.	Top depth (cm)	Bottom depth (cm)	*Achomosphaera* spp.	*Bitectatodinium spongium*	*Bitectatodinium tepikiense*	*Cryodinium meridianum*	Cyst of *Gymnodinium catenatum*	Cyst of *Alexandrium* spp.	*Dapsilidinium pastielsii*	*Filisphaera filifera* (to unknown)	*Impagidinium aculeatum*	*Impagidinium pallidum*	*Impagidinium plicatum* (I. spp.)	*Impagidinium paradoxum*	*Impagidinium patulum*	*Impagidinium sphaericum*	*Impagidinium striatum*	*Impagidinium* spp. (<20 µm)	*Impagidinium velorum* (*I.* spp.)	*Impagidinium* spp.	*Lingulodinium hemicystum*	*Melitasphaeridium choanephorum*	*Nematosphaeropsis labyrinthus*	*Operculodinium centrocarpum*	*Operculodinium israelianum*	*Operculodinium* cf. *janduchenei*	*Operculodinium longispinigerum*	*Operculodinium placitum* (*O.* spp.)	*Operculodinium giganteum* (*O.* spp.)
GLW31D-1	UVic2014-67	0	2			1	1	1								1		1				15			16	2	3	4		
GLW31D-3	UVic2014-68,276	2	4				6					4		1		1		1	3			18		1	49	16	3	4		
GLW31D-5	UVic2014-69	4	6									1										16			27	3	1	1		
GLW31D-7	UVic2014-70	6	8		2											2			1			17			18	9	1	3		
GLW31D-9	UVic2014-71	8	10		2										2		1	4	1		2	8		1	24	2	1	3		
GLW31D-11	UVic2014-72	10	12	3			2		1	1									2		1	20	2		32	4	2	2		
GLW31D-13	UVic2014-73	12	14	1	2					3						1		3	1			18	3		36	5	4	5		
GLW31D-15	UVic2015-196	14	16		3							1				2		1	2	1	3	17		1	34	3	2	1		
GLW31D-17	UVic2014-75	16	18	4	2							2	1			2		1			1	13	1		32	1	1	5		
GLW31D-19	UVic2014-76	18	20	6	1					4		2	1						3			18	1		28	4		1		
GLW31D-23	UVic2014-78	22	24		1					2		2						1	2		1	11			24	2	2	4		
GLW31D-25	UVic2014-79	24	26									1				1		1				5			22	1	2	3		
GLW31D-27	UVic2014-80	26	28	2					1			1						3	1		1	5			31	2	2	5		
GLW31D-31	UVic2014-82	30	32		1					2								1				11			32	4	1	1		
GLW31D-35	UVic2014-84	34	36		1					3		1						2	1			10	1		19	2		2		
GLW31D-43	UVic2015-199	42	44			1				3									2		4	12			32	2		1		
GLW31D-51	UVic2014-92	50	52	1						3			1			1		4	2		2	29		1	29	1		5	1	
GLW31D-59	UVic2014-96	58	60	1											1		1	1	2	1	1	20		1	29	2		1		
GLW31D-65	UVic2014-99	64	66	1	2	1				6						2	1	1	2	1		15			36	4		1		
GLW31D-75	UVic2014-104	74	76							24			3				1				4	20			41	6	2	4		
GLW31D-83	UVic2014-108	82	84							59	1			1	1			1	3	1		20			43	1	2	3		
GLW31D-91	UVic2014-112	90	92		1					28			1			3	1	2	4		1	11		1	35	1		6		
GLW31D-105	UVic2014-119	104	106		1					1		1						6	2		1	16			44			2		
GLW31D-115	UVic2014-124	114	116											1	2	2		10	2	1	1	12			28	2	1	2		
GLW31D-119	UVic2014-126	118	120									1		3	3	5		6	2	2		7		1	33			1		

Sample No.	*Operculodinium* -type A (O. spp.)	*Operculodinium* -type B (O. spp.)	*Operculodinium* -type C (O. spp.)	Cyst of *Pentapharsodinium dalei*	*Polysphaeridium subtile* (to *P. zoharyi*)	*Polysphaeridium zoharyi*	*Polysphaeridium* -type A (to *P. zoharyi*)	*Spiniferites belerius* (*S.*spp.)	*Spiniferites bentorii* (*S.spp.*)	*Spiniferites bulloideus* (*S.* spp.)	*Spiniferites delicatus* (*S.* spp.)	*Spiniferites hainanensis* (*S.* spp.)	*Spiniferites hyperacanthus*	*Spiniferites mirabilis*	*Spiniferites multisphaerus* (*S.* spp.)	*Spiniferites pacificus* (*S.* spp.)	*Spiniferites pachydermus* (*S.* spp.)	*Spiniferites ramosus*	*Spiniferites scabratus* (*S.* spp.)	*Spiniferites spinatus* (*S.* spp.)	*Spiniferites* spp.	*Spiniferites* -Type A	*Spiniferites* -Type B	*Spiniferites* -Type C	*Spiniferites* -Type D	*Tectatodinium pellitum*	*Tuberculodinium vancampoae*	Unknown auto-cysts	*Brigantedinium cariacoense*	*Brigantedinium irregulare*	*Brigantedinium simplex*	*Brigantedinium* -thin wall	*Brigantedinium* -type A (large achaeopyle)	*Brigantedinium* spp.
GLW31D-1	1	1		3	8	8	5			1	2	2	5	11				7			11	1	1	5	2		0	3				9	26		43
GLW31D-3				3		22			3			7	27	9				14			27		8		1		0		2		12	19	9	123
GLW31D-5				3		14							23	2				6			15	2	4	1	1		0				2	12	4	127
GLW31D-7						10							29	6				6			16	5	2	8			0		1	1	3	20		107
GLW31D-9		2		3	9	3	4					2	11	12				16		1	19	2	1	3	10	1	1				5	18		52
GLW31D-11				4		28		4	1		4		14	11	2			10		1	40		1	1	4		3		3	1	2	14	6	32
GLW31D-13				3		20		2	2				28	12		3	1	12			43			3	1		1		2		4	10	6	28
GLW31D-15		1	1		4					1		1	19	20				16			14		1	3	17		1		1			15		81
GLW31D-17						19		2			2		15	7				10			26	2	3	1	13		2		2		4	28		35
GLW31D-19				2		8		3	3		3		15	21		2		20			30	1	2	2	6		0		7		3	17		46
GLW31D-23				2		12		3			1		11	5		2		5			33		3	1			1		9		7	38	1	94
GLW31D-25			4	2		8	3						1	22				19			29			2	4		1				6	26		71
GLW31D-27						9		3			3		5	3				9			28		2	1	6		1		3		6	38	2	107
GLW31D-31						17		4					14	13		5		19			23	1	1	3	4		1		3		4	26	1	57
GLW31D-35				8	9	3	8				1	1	12	9				20			44	2	4	4	7		4				8	16		32
GLW31D-43				2	2	12	6						18	16				17			24	1		2	12		1	1			8	29		31
GLW31D-51			2	1	4	11	5						13	30				21			36	3	2	3	17		0				1	11		30
GLW31D-59				20	3	4	8				1	1	21	13				21	1		35	3	4	4	10		0	1			4	22		53
GLW31D-65				1	1	2	7					1	10	16				21			35	1	2	3	6		0					19		59
GLW31D-75					5	5	7			1			17	8				27			11	3	2	4	4		0	1			9	32		51
GLW31D-83				15	5	8	6						9	14				12		1	43	2	1	7	9		1	4			5	25		19
GLW31D-91					1	10	4					2	6	16				4			21	1	2	1	1		0				1	21		59
GLW31D-105				5	6	9	5			4	1	1	8	17				14			40	1	1		1		0	1			1	20		54
GLW31D-115		1		12	2	5	1						21	11				14			33	3	1	1	7		0	3			11	23		47
GLW31D-119				8	3	2	1			1			16	12				10			51		1		4		0	6			10	27		45

Sample No.	*Dubridinium cavatum*	*Dubridinium caperatum*	*Echinidinium aculeatum*	*Echinidinium granulatum*	*Echinidinium transparantum*	*Echinidinium* spp.	*Echinidinium*-type A	*Echinidinium*-type C	*Echinidinium*-type E	*Islandinium* spp.	*Lejeunecysta sabrina*	*Lejeunecysta* spp.	Cyst of *Protoperidinium oblongum*	Cyst of *Protoperidinium*-type A (cyst of *P*. spp.)	Cyst of *Protoperidinium* spp.	*Quinquecuspis concreta*	*Selenopemphix alticincta*	*Selenopemphix biconicum*	*Selenopemphix nephroides*	*Selenopemphix quanta*	*Selenopemphix undulata*	*Selenopemphix* spp.	*Stelladinium abie*	*Stelladinium reidii*	*Stelladinium*-type A	*Trinovantedinium applanatum*	Football (to Unknown)	Unknown cysts	Exotic (Lycopodium)	Total dinoflagellate cysts	Dry weight (g)
GLW31D-1	20	3	1			14	6	1			1	1	6	2	55		1		8	2				1		3			1260	325	3.7
GLW31D-3	11					15				5	0		6		23				8	3				4		1			1753	469	6.5
GLW31D-5	2	2				14	2	1			0		2		16				13					4					2718	321	4.1
GLW31D-7	5	2			1	10	4			2	0		6		25	2			8	2		2		2		5			2171	343	4.2
GLW31D-9	6	3	1			10	2		1		0		1		61		1		8	2						1			1168	323	4.5
GLW31D-11	4	2			3	7					0		1		25	2		2	4	3						2	2		1717	315	4.2
GLW31D-13	3	1	1	1		13					0				24				3	4				1		1			2932	315	4.2
GLW31D-15	3		2			1	2	1			3		4		19		2		3	2				2					1658	311	4.2
GLW31D-17	4		1		2	13					1		7		30	2			2	6							2		1591	307	4.4
GLW31D-19	7	4			1	7					0		5		25				1							6	3		1981	319	4.4
GLW31D-23	8	3		1		11					1		2		21	2		2	3	1						1			1744	336	4.2
GLW31D-25	4	1	5			27	2				4		2		37		1		7	1				4		1			1512	330	4.3
GLW31D-27	5	2				5					1		3		27	2			8					2		2			2352	337	4.5
GLW31D-31	6	2				2					1		2		30	2			5	6				3		4	1		2285	313	4.4
GLW31D-35	8		3			11	1	4	1		0		2		26					3						7		1	1588	301	4.2
GLW31D-43	2	1	3			18					0		2		42				2	1						8			1318	318	4.1
GLW31D-51	2					12					0				38				2	2				1		4		3	1158	334	4.2
GLW31D-59	3	9	1			6	7		2		0		1		26		1		3							5		1	1782	355	4.1
GLW31D-65	8		2			20	4				0		1		13							1				3			1148	309	4.0
GLW31D-75	2		2			17	4				0				18		1		3			1		2		1		2	1334	345	4.1
GLW31D-83	1		8			7	7	1	2		0		2		22				1					1					1836	374	3.7
GLW31D-91	2		7			18	7	4			0				14		2		4					1		1			1194	305	3.9
GLW31D-105	2		3			19	2				0				21		1		1	1						4		1	593	318	4.2
GLW31D-115	7		1			19		3	2		1		1		47	2				1						2			1582	346	3.5
GLW31D-119	3		1			24	2				0		1		41	1				2									1394	336	4.1

Sample No.	Uvic Lab. No.	Top depth (cm)	Bottom depth (cm)	*Achomosphaera* spp.	*Bitectatodinium spongium*	*Bitectatodinium tepikiense*	*Cryodinium meridianum*	Cyst of *Gymnodinium catenatum*	Cyst of *Alexandrium* spp.	*Dapsilidinium pastielsii*	*Filisphaera filifera* (to unknown)	*Impagidinium aculeatum*	*Impagidinium pallidum*	*Impagidinium plicatum* (I. spp.)	*Impagidinium paradoxum*	*Impagidinium patulum*	*Impagidinium sphaericum*	*Impagidinium striatum*	*Impagidinium* spp. (<20 µm)	*Impagidinium velorum* (*I.* spp.)	*Impagidinium* spp.	*Lingulodinium hemicystum*	*Melitasphaeridium choanephorum*	*Nematosphaeropsis labyrinthus*	*Operculodinium centrocarpum*	*Operculodinium israelianum*	*Operculodinium* cf. *janduchenei*	*Operculodinium longispinigerum*	*Operculodinium placitum* (*O.* spp.)	*Operculodinium giganteum* (*O.* spp.)
GLW31D-127	UVic2014-130	126	128	5			1								2	2	1	5	1		1	12		1	37	2		3		
GLW31D-129	UVic2014-131	128	130	9								1				4		3	3		3	15			44	3		3		
GLW31D-131	UVic2014-132	130	132			1						3	1	1		5		6	1			7		1	26	1		2		
GLW31D-135	UVic2014-134	134	136				2						1		2	6		5	4			11		1	41	1	1	1		
GLW31D-137	UVic2014-135	136	138		1		1	8				2				1		3				6		1	32	2	1	4		
GLW31D-139	UVic2014-136	138	140			2	2	7								2		1	5			13	1		31	2	1			
GLW31D-141	UVic2014-137	140	142									2			3	4		5	4		1	4			21	3		2		
GLW31D-143	UVic2014-138	142	144			1	9					1				1		2	5			5		1	24	5	1	1		
GLW31D-145	UVic2014-139	144	146			2		3		1						2		3	1			5			17	1		1		
GLW31D-147	UVic2014-140	146	148		1			10										3	2			6		1	15	2		2		
GLW31D-149	UVic2014-141	148	150					4								3	1	3	1		2	11	1	2	19	3		2		
GLW31D-151	UVic2014-142	150	152												2	2		2	1			9			40	3		1		
GLW31D-153	UVic2014-143	152	154					10		1						1		2	4			13			32	1	3	1		
GLW31D-155	UVic2014-144	154	156					7										1	3			9			25	1	1			
GLW31D-157	UVic2014-145	156	158				1	4						1				1	1			6			21	2		2		
GLW31D-159	UVic2014-146	158	160			2	1	4				1						2	6		2	9			27	1	1			
GLW31D-161	UVic2015-203	160	162			2		6						2		1		1			2	7	1		27	2				
GLW31D-163	UVic2014-148	162	164		1			4										1	4			4			15	2	1	2		
GLW31D-165	UVic2014-149	164	166		1									3		3						5			31			2		
GLW31D-167	UVic2014-150	166	168		1	1	1	8						2		2		2	2		2	6			35	3		3		
GLW31D-169	UVic2014-151	168	170		2	4	1	4								6		1	6			6			23	1				
GLW31D-171	UVic2014-152	170	172			2	4	3								2		1	1			5			21	4	1			
GLW31D-173	UVic2014-153	172	174	1	1	3						2		3		3			2		1	8			28	2				
GLW31D-175	UVic2015-154	174	176		2										4	3		1	3			4	1		32	6		2		
GLW31D-177	UVic2014-155	176	178		1		1							1		2	1	1	3	1	1	1	1		35	1		2		

Sample No.	*Operculodinium*-type A (O. spp.)	*Operculodinium*-type B (O. spp.)	*Operculodinium*-type C (O. spp.)	Cyst of *Pentapharsodinium dalei*	*Polysphaeridium subtile* (to *P. zoharyi*)	*Polysphaeridium zoharyi*	*Polysphaeridium*-type A (to *P. zoharyi*)	*Spiniferites belerius* (*S*.spp.)	*Spiniferites bentorii* (*S.spp.*)	*Spiniferites bulloideus* (*S*. spp.)	*Spiniferites delicates* (*S*. spp.)	*Spiniferites hainanensis* (*S*. spp.)	*Spiniferites hyperacanthus*	*Spiniferites mirabilis*	*Spiniferites mutisphaerus* (*S*. spp.)	*Spiniferites pacificus* (*S*. spp.)	*Spiniferites pachydermus* (*S*. spp.)	*Spiniferites ramosus*	*Spiniferites scabratus* (*S*. spp.)	*Spiniferites spinatus* (*S*. spp.)	*Spiniferites* spp.	*Spiniferites*-Type A	*Spiniferites*-Type B	*Spiniferites*-Type C	*Spiniferites*-Type D	*Tectatodinium pellitum*	*Tuberculodinium vancampoae*	Unknown auto-cysts	*Brigantedinium cariacoense*	*Brigantedinium irregular*	*Brigantedinium simplex*	*Brigantedinium*-thin wall	*Brigantedinium*-type A (large achaeopyle)	*Brigantedinium* spp.
GLW31D-127				3		7			1	1	1		41	7		6		10		1	27	1	1	1	9	1	2		5	1	7	27	2	35
GLW31D-129				4		9			4	4	2		28	2				20		1	42	1	1	1	3		1		3	1	3	10		49
GLW31D-131				2	1	3	1			1			7	7				13			30	1	3	1	6		0	1			1	31		73
GLW31D-135				4		6		1	3		8		42	3		6		8			52	1	2	2	1		0		3	1	3	2	2	43
GLW31D-137		2		7		9			3				24	19				12			28	5	4	2	9		0			3	1	32	2	50
GLW31D-139		4		8		2							25					14			32	2	8	1	8		0		1	3	4	39	8	54
GLW31D-141				2		3	4			1	2		9	26				21			28		4	1	8		0	2			6	52		53
GLW31D-143		2		2		3			2				15	5				8			21				1		1		5	3	10	44	3	65
GLW31D-145		9		3		6			1				14	12				4			41	1	2	1	4		1		3	5	10	19	4	89
GLW31D-147		5				7							8	5				8			40			1	1		3		2	4	13	55	4	73
GLW31D-149		3		4		6			2				22	13				13			47	3	4	1	4		0		1		7	13	4	72
GLW31D-151				2	1	4	3				1	2	25	18				14			33	2	2	1	10		3	4			2	27		49
GLW31D-153		3		9		3							25	11	2			14			44	1	3	1	6		1		1		11	25	6	44
GLW31D-155		3		6		5			1				24	12				4		1	37	2	2	1	6		0		1	2	11	47	12	60
GLW31D-157		8		2		3			2				16	9	9						34	3	2	4	5		0		1		11	32	10	63
GLW31D-159		4		3		3			1				11	8	6						28		2	2	1		0		6		11	23	14	106
GLW31D-161		12				3							12	14	1			10			34	1	2	1	1		1		3		9	41	8	91
GLW31D-163		9		4		2			4				26	15				6			20	4		1	7		0		3		10	34	10	76
GLW31D-165				2		3	1					8	6	20				2			27	7	2		5		0	1			28	33		75
GLW31D-167		19		3		2							23	13				9			17	6	4	3	6		0		1	1	15	60	8	82
GLW31D-169		12		3		1							21	6				10			22	3	8	1	6		2		3		7	48	4	61
GLW31D-171		4											19	20				8			38	1	4	3	9		1		2		11	73	11	46
GLW31D-173		8		3		2							15	11				8			17	1	4	1	1		2		2	1	18	61	18	40
GLW31D-175				4									12	9				23			26	4		1	7		0				41	13		55
GLW31D-177				1		3							24	3	1			6			18	1	2	1	2		5		2		8	51	10	73

Sample No.	*Dubridinium cavatum*	*Dubridinium caperatum*	*Echinidinium aculeatum*	*Echinidinium granulatum*	*Echinidinium transparantum*	*Echinidinium* spp.	*Echinidinium*-type A	*Echinidinium*-type C	*Echinidinium*-type E	*Islandinium* spp.	*Lejeunecysta sabrina*	*Lejeunecysta* spp.	Cyst of *Protoperidinium oblongum*	Cyst of *Protoperidinium*-type A (cyst of *P*. spp.)	Cyst of *Protoperidinium* spp.	*Quinquecuspis concreta*	*Selenopemphix alticincta*	*Selenopemphix biconicum*	*Selenopemphix nephroides*	*Selenopemphix quanta*	*Selenopemphix undulata*	*Selenopemphix* spp.	*Stelladinium abie*	*Stelladinium reidii*	*Stelladinium*-type A	*Trinovantedinium applanatum*	Football (to Unknown)	Unknown cysts	Exotic (Lycopodium)	Total dinoflagellate cysts	Dry weight (g)
GLW31D-127	9	2	1			12					0				19				2	3				1					1415	319	4.2
GLW31D-129	5	2	2			10					0		1		15					3						1			1727	316	4.0
GLW31D-131	7		3			14	1	1			0				36				1	1						2			1302	303	3.9
GLW31D-135	6					6					0				15				3	3						2			1856	304	4.2
GLW31D-137	10					15		1			0				15					1									982	316	3.9
GLW31D-139	11	2	1	12	1						0			1	6					1									1236	315	4.0
GLW31D-141	4					17	1		2		0				18				1	1						1		2	1283	318	3.9
GLW31D-143	21	3	1		1	14		1			0		1	1	9				1					1		1			882	301	4.1
GLW31D-145	16		1			14					0		4		9				4	3				3					858	319	4.3
GLW31D-147	13	1	3			12					0		4		21	1			1	3				3					956	333	4.1
GLW31D-149	8		1			11					0				11				2	4				1	1	2			933	312	4.1
GLW31D-151	3		2			14	1				0		2		30		1		2	2								1	1221	321	4.2
GLW31D-153						19					0				27				2	1									976	327	4.1
GLW31D-155	12	1		1	2	10					0				7				2	3			2	1					1032	325	4.0
GLW31D-157	13	2				20	2	1			0		1		18				3	1				1		1			946	316	4.0
GLW31D-159	9	3	5			22	2	1			1				14	2			2	2				1					896	349	4.3
GLW31D-161	9	3				12					0				10	2			4	5		1		2					1084	343	4.3
GLW31D-163	9	1	1		2	13			1		0		2		11	2			3	2									996	312	4.1
GLW31D-165	10		1			13		1			0		6	1	43	1			4	3						1			1257	349	4.3
GLW31D-167	7		2			17	4			1	0		1		25	2			2	2	1					1			967	405	4.1
GLW31D-169	13	2			2	20					0		1		12				5	2				1					954	330	4.1
GLW31D-171	7	1	4		1	20					0		1		13				5	3				2		1			778	352	4.3
GLW31D-173	5	3				12	2				0		1		35				1	4						2			1020	332	4.1
GLW31D-175	6		2			5	2	3	1		0		1		26				2					1		1		1	1248	304	4.5
GLW31D-177	7	1				7	2			1	0				24				5	5				1					1288	316	4.1

Sample No.	Uvic Lab. No.	Top depth (cm)	Bottom depth (cm)	*Achomosphaera* spp.	*Bitectatodinium spongium*	*Bitectatodinium tepikiense*	*Cryodinium meridianum*	Cyst of *Gymnodinium catenatum*	Cyst of *Alexandrium* spp.	*Dapsilidinium pastielsii*	*Filisphaera filifera* (to unknown)	*Impagidinium aculeatum*	*Impagidinium pallidum*	*Impagidinium plicatum* (I. spp.)	*Impagidinium paradoxum*	*Impagidinium patulum*	*Impagidinium sphaericum*	*Impagidinium strialatum*	*Impagidinium* spp. (<20 µm)	*Impagidinium velorum* (*I.* spp.)	*Impagidinium* spp.	*Lingulodinium hemicystum*	*Melitasphaeridium choanephorum*	*Nematosphaeropsis labyrinthus*	*Operculodinium centrocarpum*	*Operculodinium israelianum*	*Operculodinium* cf. *janduchenei*	*Operculodinium longispinigerum*	*Operculodinium placitum* (*O.* spp.)	*Operculodinium giganteum* (*O.* spp.)
GLW31D-179	UVic2014-156	178	180		1	1	1									2		9	1		1	4			20		1	2	2	1
GLW31D-181	UVic2014-157	180	182				1			1						2		4	4		1	3			25	1	1	3	5	
GLW31D-183	UVic2014-158	182	184		1					4		1				4		8	4	1	1	0		1	30	1		2		
GLW31D-185	UVic2014-159	184	186	2	1					1						9		8	1			7		2	37	1		1		
GLW31D-187	UVic2014-160	186	188			1										8		3	3			10		1	31	1	1	1		
GLW31D-189	UVic2014-161	188	190		1		2							1		11		3	6			6			31	1		3		
GLW31D-191	UVic2014-162	190	192		2	1						1	3			14		4	7			2		1	33	4	1			
GLW31D-193	UVic2014-163	192	194	3	1								2			13		13	1			10			31	1		1		
GLW31D-195	UVic2014-164	194	196			1	1									6		2	7	1		7			30	4				
GLW31D-197	UVic2014-278	196	198				1									13		1	4			6			32	1	1	3		
GLW31D-199	UVic2014-166	198	200		2		1									11		7	7			4			30					
GLW31D-201	UVic2014-167	200	202		2		1									11		3	8			2			23			2		
GLW31D-205	UVic2014-169	204	206		2							1	1	1	4	21		8			2	5			23			1		
GLW31D-215	UVic2014-174	214	216		1										1	8	1	4	2			11			53		1	1		
GLW31D-219	UVic2014-176	218	220		2	2	1					4				10		2	3			6			68	2				
GLW31D-221	UVic2014-177	220	222			3	2					1				11			5	1		7			77	4	1			
GLW31D-223	UVic2014-178	222	224			1	1					1				13		4	7			7			41	3				
GLW31D-225	UVic2014-179	224	226	2									1	1	2	18		3	7		2	8	1		62		1			
GLW31D-227	UVic2014-180	226	228		3	1	1							1		9		5	2		1	5			30	6		1		
GLW31D-229	UVic2014-181	228	230		1							1	1	1		10	1	8	6		3	8			48		3			
GLW31D-231	UVic2014-182	230	232	2												6		2	1		1	7			28	4		3		
GLW31D-233	UVic2014-183	232	234			1								1		10		5	3		1	6			42		4			

Sample No.	*Operculodinium* -type A (O. spp.)	*Operculodinium* -type B (O. spp.)	*Operculodinium* -type C (O. spp.)	Cyst of *Pentapharsodinium dalei*	*Polysphaeridium subtile* (to *P. zoharyi*)	*Polysphaeridium zoharyi*	*Polysphaeridium* -type A (to *P. zoharyi*)	*Spiniferites belerius* (*S*.spp.)	*Spiniferites bentorii* (*S.spp.*)	*Spiniferites bulloideus* (*S.* spp.)	*Spiniferites delicatus* (*S* . spp.)	*Spiniferites hainanensis* (*S* . spp.)	*Spiniferites hyperacanthus*	*Spiniferites mirabilis*	*Spiniferites multisphaerus* (*S* . spp.)	*Spiniferites pacificus* (*S.* spp.)	*Spiniferites pachydermus* (*S.* spp.)	*Spiniferites ramosus*	*Spiniferites scabratus* (*S* . spp.)	*Spiniferites spinatus* (*S.* spp.)	*Spiniferites* spp.	*Spiniferites* -Type A	*Spiniferites* -Type B	*Spiniferites* -Type C	*Spiniferites* -Type D	*Tectatodinium pellitum*	*Tuberculodinium vancampoae*	Unknown auto-cysts	*Brigantedinium cariacoense*	*Brigantedinium irregulare*	*Brigantedinium simplex*	*Brigantedinium* -thin wall	*Brigantedinium* -type A (large achaeopyle)	*Brigantedinium* spp.
GLW31D-179		3		2		1			1		1		9	4				6			24		2		10		1		3		10	52	12	99
GLW31D-181				2		1							13	9				11			16	5	2		10		0		8		13	62	10	70
GLW31D-183		4		1		4							17	8				8			19	1	2	1	10		0		3	1	11	59	7	58
GLW31D-185			1	3	3	5	2					2	7	9				16			25	3	1	2			2				5	26		83
GLW31D-187		2		3		3					1		24	3				8			24	3	3	4	3		1		2		7	43	6	70
GLW31D-189		2		3		1			1				32	15				14			17	4	11		5		0		3		8	36	2	58
GLW31D-191		11		7		5			1				10	6				11			10			2	3		3			3	10	61	17	55
GLW31D-193				2	1	3	3			1		1	9	11				16	1		30	8		2			0	1				15		93
GLW31D-195		3		5		1			1				18	6				5			9	1	6	1	8		0		2	2	7	76	3	54
GLW31D-197				3		2							31	7				5			7	1	4	1	10		1		2	1	7	42	4	78
GLW31D-199				3		1							23	3				4			6	1	1	3	1		1	1	5		15	82		59
GLW31D-201				3		4							15	3				1			8		3	1	1		1				15	67	5	86
GLW31D-205				1	2	3	1						5	6				10			20	1					0	3			2	3		181
GLW31D-215				2		4	1						5	16				8			29	2	1	1	3		0				35	10		135
GLW31D-219		2		1		6							8	7				6			11	3	3	4	2		1		3	2	18	54	7	65
GLW31D-221		2		1		2			1				11	6				2			9			3	2		2			1	16	46	10	53
GLW31D-223		2		4		6						30		14				8			18	2	2	4	2		0			3	15	51	8	88
GLW31D-225				6	2	5	7						9	10				7			35		2		4		3	2			19	4		100
GLW31D-227		1				5							12	7				2			11		1	4			1			1	9	54	4	115
GLW31D-229				2	7	5	4						5	7				6			11		1	1	1		0	5			7	10		114
GLW31D-231				1		1							12	3				5	1		12	1	1	1			2		2	1	9	52	14	94
GLW31D-233				8	3	5					3	1	6	9				7			29		1	1	3		1	2			14	8		109

Sample No.	*Dubridinium cavatum*	*Dubridinium caperatum*	*Echinidinium aculeatum*	*Echinidinium granulatum*	*Echinidinium transparantum*	*Echinidinium* spp.	*Echinidinium* -type A	*Echinidinium* -type C	*Echinidinium* -type E	*Islandinium* spp.	*Lejeunecysta sabrina*	*Lejeunecysta* spp.	Cyst of *Protoperidinium oblongum*	Cyst of *Protoperidinium* -type A (cyst of *P* . spp.)	Cyst of *Protoperidinium* spp.	*Quinquecuspis concreta*	*Selenopemphix alticincta*	*Selenopemphix biconicum*	*Selenopemphix nephroides*	*Selenopemphix quanta*	*Selenopemphix undulata*	*Selenopemphix* spp.	*Stelladinium abie*	*Stelladinium reidii*	*Stelladinium* -type A	*Trinovantedinium applanatum*	Football (to Unknown)	Unknown cysts	Exotic (Lycopodium)	Total dinoflagellate cysts	Dry weight (g)
GLW31D-179	13	4	2			10					0		3		27	3			2	3				1		1			971	355	4.2
GLW31D-181	15					7	2				0		2		19	1			3	3				1		1			1033	337	4.2
GLW31D-183	9		2			8	2				0		1		19	2			1	3						3			795	322	4.2
GLW31D-185	15		1			5	2		1		0		3		35				3	2						1			1047	333	4.3
GLW31D-187	9					9				1	1				12				2	2				1		1			1528	308	4.3
GLW31D-189	8		1			5				2	0				21	2	1		3		1								1411	321	4.1
GLW31D-191	6		1			6		1		1	0		4		17	1			4	2						3			746	334	4.3
GLW31D-193	8		1			6	4		1		0				24				5	1						2			1035	325	4.2
GLW31D-195	12		2			15				2	0		1		36	4			5		2					3			810	349	4.5
GLW31D-197	10		2			13				2	0				12				5	1						2			812	315	2.9
GLW31D-199	11					12				3	0				24	2			4	1									840	328	4.2
GLW31D-201	16		7			7					0				25	3			4							4			818	331	4.4
GLW31D-205	2	1	2			11	5				2				30	2								1					755	363	4.4
GLW31D-215	4		6			5	1				0		3		33				1										543	388	4.2
GLW31D-219	20	4	2			17					0				13	2			5	1				1					687	368	4.6
GLW31D-221	12		2							7	1				32	2			2					1		2			579	340	4.6
GLW31D-223	10					10				4	0				19				4	1	1			1		1			832	386	4.2
GLW31D-225	7		3			12	3				0		1		28		1		2							2		1	891	383	4.4
GLW31D-227	10		2			6					0		2		20				2	2						1			809	337	4.2
GLW31D-229	7	4	3			6	3	1			0				14	1	2		1			1						3	720	323	4.3
GLW31D-231	20		1			17				1	0				24				1	2	1			1		1			809	335	4.2
GLW31D-233	11	6	2			9	1		3		0				24				2	1				1		1			771	344	4.3